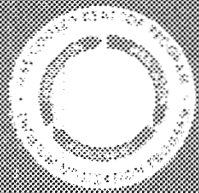




3 4456 0449213 6

cy.1



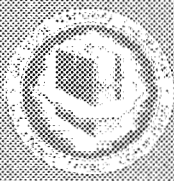
# GAS-COOLED REACTOR AND THORIUM UTILIZATION PROGRAMS

## ANNUAL PROGRESS REPORT

*Period Ending September 30, 1971*

OAK RIDGE NATIONAL LABORATORY  
CENTRAL RESEARCH LIBRARY  
DOCUMENT COLLECTION  
**LIBRARY LOAN COPY**

DO NOT TRANSFER TO ANOTHER PERSON  
If you wish someone else to see this  
document, send an email with document  
and the library will arrange a loan.



**OAK RIDGE NATIONAL LABORATORY**  
OPERATED BY UNION CARBIDE CORPORATION • FOR THE U.S. ATOMIC ENERGY COMMISSION

Printed in the United States of America. Available from  
National Technical Information Service  
U.S. Department of Commerce  
5285 Port Royal Road, Springfield, Virginia 22151  
Price: Printed Copy \$3.00; Microfiche \$0.95

This report was prepared as an account of work sponsored by the United States Government. Neither the United States nor the United States Atomic Energy Commission, nor any of their employees, nor any of their contractors, subcontractors, or their employees, makes any warranty, express or implied, or assumes any legal liability or responsibility for the accuracy, completeness or usefulness of any information, apparatus, product or process disclosed, or represents that its use would not infringe privately owned rights.

ORNL-4760  
UC-80 – Reactor Technology

Contract No. W-7405-eng-26

**GAS-COOLED REACTOR AND THORIUM UTILIZATION PROGRAMS**  
**ANNUAL PROGRESS REPORT**  
**For Period Ending September 30, 1971**

P. R. Kasten, Program Director  
J. H. Coobs, Associate Director  
A. L. Lotts, Associate Director

JANUARY 1973

OAK RIDGE NATIONAL LABORATORY  
Oak Ridge, Tennessee 37830  
operated by  
UNION CARBIDE CORPORATION  
for the  
U.S. ATOMIC ENERGY COMMISSION

LOCKHEED MARTIN ENERGY RESEARCH LIBRARIES



3 4456 0449213 6



# Contents

---

FOREWORD .....	vii
SUMMARY .....	ix
<b>PART I. THORIUM UTILIZATION PROGRAM</b>	
1. HEAD-END REPROCESSING DEVELOPMENT .....	1
1.1 Burner Feed Preparation .....	2
1.1.1 Comminution Studies with Resin-Bonded Fuel .....	2
1.1.2 Comminution of Pitch-Bonded Fuel .....	2
1.1.3 Comminution by Intercalation .....	2
1.2 Burner Technology – Cold Engineering .....	4
1.2.1 Fluidized-Bed Burning Tests with Pitch-Bonded Fuel .....	4
1.2.2 Fluidized-Bed Burning Rates .....	4
1.3 Head-End Reprocessing Studies – Hot Cells .....	5
1.3.1 Irradiated Compacts from the Dragon Project .....	5
1.3.2 Crushing Studies with Dragon Compacts .....	5
1.3.3 Head-End Studies of Unirradiated Dragon Compact 14719, Fuel Type 19M (Triso $UC_{10}$ –Triso $ThC_2$ ) .....	5
1.3.4 Head-End Studies of an Unnumbered Irradiated Dragon Compact, Fuel Type 19M (Triso $UC_{10}$ –Triso $ThC_2$ ) .....	7
1.3.5 Head-End Studies of Unirradiated Compact 22396, Type 2M4 (Biso Oxide) .....	13
1.3.6 Head-End Studies of Irradiated Compact 22365, Type 2M4 (Biso Oxide) .....	13
1.3.7 Head-End Studies of a Synthetic Mixture – Triso $UC_{20}$ –Biso (5Th/U) $C_{2,4}$ [a Possible 1100-MW(e) Makeup Fuel Type] .....	18
1.4 Off-Gas Handling and Decontamination .....	20
1.4.1 Solubility of Krypton in Liquid $CO_2$ .....	22
1.4.2 Krypton Solubility in Hot Carbonate Solution .....	23
1.5 Waste Treatment and Disposal .....	24
1.5.1 Identification of Waste Streams .....	24
1.5.2 Disposal of Waste Streams .....	24

2. FUEL MICROSPHERE PREPARATION DEVELOPMENT .....	29
2.1 Sol Preparation .....	29
2.1.1 UO <sub>2</sub> Sol Preparation .....	29
2.1.2 ThO <sub>2</sub> -UO <sub>3</sub> Sol Preparation .....	30
2.2 Sol-Gel Microsphere Preparation .....	31
2.2.1 Application of Ion Exchange to the Recycle of 2EH .....	31
2.2.2 Formation of UO <sub>2</sub> Spheres .....	32
2.2.3 Preparation of Microspheres in Nonfluidized-Bed Columns .....	33
2.2.4 Development of Prototype Equipment for TURF .....	34
2.2.5 Preparation of Test Materials .....	40
2.3 Resin-Based Microsphere Development .....	40
2.3.1 Laboratory Studies .....	40
2.3.2 Engineering Studies .....	43
2.3.3 Uranium Loading of Sulfonate Resins .....	44
3. FUEL FABRICATION PROCESS DEVELOPMENT .....	45
3.1 Microsphere Coating .....	45
3.1.1 Particle Coating .....	45
3.1.2 Particle Inspection .....	50
3.1.3 Particle Handling .....	51
3.2 Fuel Stick Fabrication .....	52
3.2.1 Particle Blending and Loading .....	52
3.2.2 Preparation and Characterization of Matrix .....	53
3.2.3 Fuel Stick Molding .....	53
3.2.4 Carbonization and Annealing .....	54
3.2.5 Stick Inspection .....	54
3.2.6 Fuel Stick Molding Machine .....	55
4. HTGR FUEL RECYCLE PILOT PLANTS .....	56
4.1 Head-End Pilot Plant Demonstration .....	56
4.1.1 Design of Processing Equipment .....	56
4.1.2 Design of Waste Treatment and Disposal Equipment .....	57
4.1.3 Design of Materials Handling Equipment and Facilities .....	59
4.2 Acid-Thorex Pilot Plant Demonstration .....	59
4.2.1 Design of Processing Equipment .....	60
4.2.2 Design of Waste Treatment and Disposal Equipment .....	60
4.2.3 Design of Materials Handling Equipment and Facilities .....	60
4.3 Refabrication Pilot Plant Demonstration .....	60
4.3.1 Design of Processing Equipment .....	60
4.3.2 Design of Waste Treatment and Disposal Equipment .....	62
4.3.3 Design of Materials Handling Equipment and Facilities .....	62
4.4 Thorium-Uranium Recycle Facility .....	62
5. RECYCLE FUELS IRRADIATION AND EVALUATION .....	65
5.1 Recycle Test Elements .....	65
5.2 Capsule Tests .....	67

6. COMMERCIAL RECYCLE PLANT STUDIES .....	69
6.1 Reactor Physics Studies .....	69
6.2 Fuel Value of $^{233}\text{U}$ in HTGRs .....	70
6.2.1 Characteristics of HTGR Design .....	70
6.2.2 Ground Rules and Assumptions .....	71
6.2.3 Procedure for Determining Value of Fuel Mixtures Containing $^{233}\text{U}$ .....	72
6.3 Evaluation of Plutonium Use in HTGRs .....	73
6.3.1 Ground Rules and Study Basis .....	73
6.3.2 Results of the Study .....	75
6.3.3 Conclusions .....	77
6.4 HTGR Fabrication Economics .....	77
<b>PART II. HTGR DEVELOPMENT PROGRAM</b>	
7. PRESTRESSED CONCRETE PRESSURE VESSEL DEVELOPMENT .....	79
7.1 PCRV Thermal Cylinder Test .....	79
7.1.1 Calibration of Instrumentation .....	81
7.1.2 Assembly of the Test Mold .....	81
7.1.3 Fabrication of Temperature and Pressure Control Systems .....	83
7.1.4 Casting of Thermal Cylinder and Companion Specimens .....	83
7.1.5 Testing Program .....	83
7.1.6 Analysis of Thermal Cylinder .....	91
7.2 Subcontract Studies .....	91
7.2.1 Structural Behavior of Prestressed-Concrete Reactor Vessels .....	91
7.2.2 Concrete Triaxial Creep Tests at the University of Texas .....	95
7.2.3 Concrete Moisture Migration Study and Multiaxial Creep Tests .....	95
8. HTGR FUEL ELEMENT DEVELOPMENT .....	96
8.1 Resin Particle Development .....	96
8.1.1 Kernel Fabrication .....	96
8.1.2 Carbonization and Thermal Stability .....	98
8.1.3 Particle Design .....	100
8.1.4 Irradiation Testing .....	100
8.2 Coating Development .....	100
8.2.1 $\text{PuO}_2$ Coating Development .....	100
8.2.2 Coating Properties .....	102
8.2.3 Particle Design .....	102
8.2.4 Optical Anisotropy Factor (OPTAF) Studies .....	102
8.3 Bonded Fuel Development .....	108
8.3.1 Fabrication by Intrusion Bonding .....	108
8.3.2 Fabrication by Slurry Blending and Warm Molding .....	109
8.3.3 Thermal Conductivity and Electrical Resistivity .....	111
8.4 Fuel Migration Studies .....	112
8.5 Design and Preparation of Irradiation Experiments .....	113
8.5.1 HRB-2 Experiment .....	114
8.5.2 HRB-3 Experiment .....	114
8.5.3 P13-N Experiment .....	115
8.5.4 Sweep Capsule Irradiation in ORR .....	116
8.5.5 Target Capsule Experiments in HFIR .....	116

8.6 Examination and Evaluation of Irradiation Experiments .....	118
8.6.1 Development of Bonding Materials for HTGR Fuel Elements .....	118
8.6.2 HRB-1 Experiment .....	120
8.6.3 HRB-2 Examination .....	121
8.6.4 Postirradiation Examination of Capsule HT-8 .....	121
8.6.5 Target Capsules HT-7 and HT-9 .....	124
<b>9. IRRADIATION EXPERIMENTS .....</b>	<b>126</b>
9.1 HFIR Irradiations .....	126
9.1.1 Removable Beryllium Facility Irradiation Tests .....	126
9.1.2 Target Irradiation Tests .....	134
9.2 ORR Irradiations .....	136
9.3 Analysis of Irradiation Conditions .....	137
9.3.1 Dosimeter Data from HT and HRB Capsules .....	137
9.3.2 HFIR Dosimetry Experiment .....	137
<b>10. IRRADIATION EXPERIMENT ANALYSIS AND FISSION PRODUCT TRANSPORT .....</b>	<b>139</b>
10.1 Fission Product Release from Bonded Beds .....	139
10.2 Fission Product Transport Through Particle Coatings .....	140
10.3 Results and Analysis of Fission Product Loop Tests .....	143
<b>PART III. GAS-COOLED FAST BREEDER REACTOR PROGRAM</b>	
<b>11. GCFBR IRRADIATION EXPERIMENTS .....</b>	<b>149</b>
11.1 Irradiation of GCFBR-ORR Capsule GB-9 .....	149
11.1.1 Effluent Sweep Line Activity .....	152
11.1.2 Steady-State Fission-Gas Release vs Burnup .....	152
11.1.3 Fission-Gas Release during Slow Pressure Cycling .....	152
11.1.4 Correlation of Effluent Sweep Line Activity Data and Sweep-Gas Sample Data .....	156
11.1.5 Fission-Gas Release vs Charcoal Trap Temperature .....	157
11.1.6 Fission-Gas Release vs Fuel Rod Power Temperature .....	159
11.1.7 Decay Heating in Charcoal Trap .....	162
11.1.8 Iodine Deposition in Charcoal Trap .....	162
11.1.9 Neutron Radiography .....	162
11.1.10 Fission-Gas Release vs Sweep Pressure .....	163
11.2 Design of GCFBR-ORR Capsule GB-10 .....	163
11.3 Analysis of Irradiation Conditions .....	164
<b>12. GCFBR FUEL FABRICATION .....</b>	<b>166</b>
12.1 Replacement Fuel for the F-1 Irradiation Experiment .....	166
12.2 Fuel for GB-10 Capsule .....	166
<b>PART IV. ASSOCIATED USAEC EXCHANGE PROGRAMS</b>	
<b>13. EXCHANGE PROGRAMS .....</b>	<b>169</b>
13.1 USAEC/Dragon HTGR Exchange .....	169
13.2 USAEC/KFA Exchange Arrangement .....	169
<b>ORGANIZATION CHART .....</b>	<b>171</b>

## Foreword

---

The Gas-Cooled Reactor and Thorium Utilization Programs are being carried out at the Oak Ridge National Laboratory under sponsorship of the U.S. Atomic Energy Commission. These programs contribute to the development of high-temperature gas-cooled reactors (HTGRs), fuel-recycle technology for HTGRs, and gas-cooled fast breeder reactors (GCFBRs). The major effort is in HTGR technology, with emphasis on fuel and fuel recycle development, and includes irradiation testing, fission product behavior, and fuel performance studies. Work is also carried out on the performance of prestressed concrete reactor vessels (PCRV) under possible reactor conditions. Work in GCFBR development emphasizes fission product behavior in vented fuel elements and involves irradiation testing of a vented fuel element concept under various flow conditions. Close coordination is maintained with Gulf General Atomic (GGA) relative to their efforts in the design and development of gas-cooled reactors and in HTGR fuel-recycle development.

Major incentives for developing HTGRs are the prospects for economically attractive power production, the conservation of low-cost uranium ore reserves, the potential for obtaining low environmental impact at a diversity of plant sites, and the potential for high-temperature process heat applications. The good neutron economy and fuel performance permit high burnup and associated low fuel-cycle costs. The high-temperature capability of the graphite core structure facilitates reactor plant operation at high thermodynamic efficiency, and thus requirements for heat dissipation to the environment are low. Excellent fission product retention by the coated fuel particles leads to coolant circuits with low radioactivity levels. Further, the high exposures attainable with HTGR fuels

permit the development of economic fuel recycling. At the same time, the development of fuel-recycle technology is important to the commercial acceptance of HTGRs as economic power producers.

The fuel-recycle effort is part of the national HTGR fuel-recycle development program being carried out by the USAEC at ORNL, GGA, and the Idaho Chemical Processing Plant. The objective of the fuel-recycle program is to develop the pertinent technology so that commercial plants for reprocessing and refabrication of HTGR fuels can be built and operated economically. The operations to be considered take place between the discharge of spent fuel elements from the reactor and the return of refabricated fuel elements to the reactor; these include fuel shipping, storage, fuel recovery and purification, refabrication, and waste management. The work involves fuel reprocessing development, fuel refabrication development, irradiation testing of refabricated fuels, and fuel-recycle systems analyses involving the economics associated with various processes and equipment. The program at ORNL includes development of head-end processing methods for irradiated fuels and associated off-gas cleanup technology, production of microspheres containing recycle fuel, microsphere coating technology, recycle-fuel-element fabrication technology, associated equipment and process development, recycle-fuel irradiations, and fuel-recycle systems analyses.

HTGR fuel development work at ORNL is largely concerned with evaluating, understanding, and improving fuel performance, and includes study of the behavior of certain fission products. Coated-particle fuel studies involve irradiation testing, with emphasis on demonstration of satisfactory fuel and materials performance at the required fuel burnup and fast-neutron

fluences. In these tests, the High-Flux Isotope Reactor (HFIR) has proved to be highly useful as an irradiation facility. A small effort has been placed on development of fuels having higher temperature capabilities; successful development would have important implications relative to helium-turbine and/or process-heat HTGRs.

In work on PCRVs, a thermal cylinder experiment has been initiated which studies the time-dependent stress-strain behavior of a simulated segment of a PCRV vessel. The prestressing, pressure, and thermal-gradient conditions are those expected under HTGR design conditions; experimental results will be compared with those from theoretical calculations.

The helium-cooled GCFBR offers a high breeding ratio, a doubling time of about ten years, a core conversion ratio of approximately 1.0, and a small reactivity change from loss of coolant. The high core conversion ratio makes possible extended operating periods without refueling and results in low reactivity

swings during fuel exposure. The fuel performance requirements for this reactor are basically similar to those for the liquid-metal-cooled fast breeder reactor (LMFBR), and thus the program draws heavily on the fuel development of the LMFBR. ORNL fuel work for the GCFBR now principally involves irradiation testing of fuel pins. Irradiation test results for a vented fuel element were obtained during this report period, with encouraging results.

Work on gas-cooled reactors is also being performed in Europe, with significant efforts being carried out on the HTGR concept by the Dragon Project and by Germany. Associated information pertaining to HTGR research and development work is obtained through the USAEC/Dragon HTGR Agreement and the USAEC/KFA Exchange Arrangement. These exchange programs involve information on fuel development, performance and testing, and reprocessing.

## Summary

### PART I. THORIUM UTILIZATION PROGRAM

#### 1. Head-End Reprocessing Development

**1.1 Burner feed preparation.** A promising approach to removing fuel element graphite from HTGR fuel materials (U and Th) involves breaking the elements into small pieces by crushing and burning them in a bed containing fluidized alumina ( $Al_2O_3$ ) particles as a heat transfer medium. Crushing studies of fuel with several of the kinds of bonding materials proposed for holding fuel particles in sticks have shown that pitch-bonded and resin-bonded fuel sticks may both be crushed in a hammer mill to an acceptable size with acceptably low coated-fuel-particle breakage. The resin-bonded fuel sticks contained Triso-coated  $ThC_2$  and  $UC_2$  particles. Under the most severe conditions tested ( $3/8$ -in. grate spacing in the hammer mill), 3.4% of the fissile particles ( $UC_2$ ) and 17% of the fertile particles ( $ThC_2$ ) were broken. The pitch-bonded fuel sticks contained both Biso-coated and Triso-coated  $ThC_2$ . Hammer milling with a grate space of  $\sim 3/8$  in. resulted in  $<1\%$  breakage of Triso-coated particles, but extensive Biso-coated particle breakage was observed. A cursory test of intercalation with 90%  $HNO_3$  as a means of separating bulk graphite from fuel particles led to the conclusion that this method was unreliable because of extremely wide variability of attack by the  $HNO_3$ , depending on the stick fabrication conditions.

**1.2 Burner technology — cold engineering.** Use of  $\sim 3/8$ -in. crushed pitch-bonded fuel rods combined with similarly crushed graphite in fluidized-bed burner studies gave results indicating that Biso- and Triso-coated  $ThC_2$  material performs essentially the same as Triso-Triso-coated material tested earlier. The Biso-

coated  $ThC_2$  was converted to a fine  $ThO_2$  powder. The burning rate was 16.3 kg of carbon per square foot of burner cross section per hour. A test run at a rate of 47.5 kg of carbon gave similar results, indicating that in this range there is no effect of increased particle breakage from higher burning rates.

**1.3 Head-end reprocessing studies — hot cells.** Hot-cell studies of head-end reprocessing operations are being carried out using irradiated compacts and unirradiated controls obtained from the Dragon project. The compacts listed below were worked with during this report period.

Compact No.	Fuel type <sup>a</sup>	Composition	Kernel size ( $\mu$ )	Comments
14719	19M	Triso $UC_{10}$ Triso $ThC_2$	500 900	Unirradiated
Unnumbered	19M	Triso $UC_{10}$ Triso $ThC_2$	500 900	Irradiated <sup>b</sup>
22396	2M4	Biso (10Th,U) $O_2$	500	Unirradiated
22365	2M4	Biso (10Th,U) $O_2$	500	Irradiated <sup>b</sup>
14397 <sup>c</sup>	18M	Triso $UC_{20}$	500	Unirradiated
14158 <sup>c</sup>	38M	Biso (5Th,U) $C_{2.4}$	500	Unirradiated

<sup>a</sup>These are designations given the compacts by the Dragon Project.

<sup>b</sup>The burnups were nominally about 0.07 FIMA (fissions per initial heavy metal atom) with a fast-neutron fluence of  $2.5 \times 10^{21}$ .

<sup>c</sup>These two compacts were combined after crushing to simulate a mixed Biso-Triso fuel.

Crushing studies were carried out first using a jaw crusher set at  $5/8$ -in. jaw settings followed by crushing with jaws set at  $\sim 1/8$  in. In general, about half of the

material from each crushed compact was in the size range -4 to +9 mesh, about a fourth was in the range -9 to +20, and the remainder was smaller than 20 mesh.

Particle breakage was greater with the irradiated 19M-type fuel than with the unirradiated, but wide differences between samples make a meaningful quantitative comparison difficult. Roughly speaking, however, breakage was about twice as extensive with irradiated fuel, averaging about 18% for the irradiated fissile particle. Only about one-third as many fissile as fertile particles were broken in both irradiated and unirradiated fuel.

Approximately 7% of the  $^{85}\text{Kr}$  was released from the irradiated 19M-type fuel during the initial burning, and <1% of the  $^{85}\text{Kr}$  was released during leaching of the burner product. Most of the  $^{85}\text{Kr}$  (~85%) was associated with the fissile particle, and the majority of this (83.7% of the total) was released during the grinding and preburn roast.

Only 82 to 85% of the thorium and uranium was found in the +60-mesh fraction after the 2M4 fuel was crushed, burned, and sieved. This indicates that more durable oxide kernels are required if particle separation based on size is to be used for Biso-coated oxide particles.

With the composite prepared from compact types 18M and 38M, a rather unexpected result was the finding of 3 to 10% of the (oxidized) carbide particle in the fissile (+35-mesh) fraction. The oxidation apparently occurred without completely disintegrating the carbide particle to a fine ash.

**1.4 Off-gas handling and decontamination.** Burning HTGR fuel blocks as a step in recovering fuel values will lead to large amounts of  $\text{CO}_2$  contaminated with relatively very small amounts of radioactive isotopes. The principal goal of our present studies is to develop a practical means of removing  $^{85}\text{Kr}$  from the  $\text{CO}_2$  so that the  $\text{CO}_2$  may be released. Four methods have been identified from the large number considered as holding promise of reaching that goal: (1) stagewise absorption of krypton in liquid  $\text{CO}_2$ , (2) controlled solidification of  $\text{CO}_2$ , (3) simple distillation of liquid  $\text{CO}_2$ , and (4) hot potassium carbonate sorption of  $\text{CO}_2$ .

For the scale of the hot recycle demonstration proposed to be carried out (9.7 Fort St. Vrain fuel elements per day), the approximate expected concentrations of several important fission products are as follows, if whole element burning is assumed and the elements are exposed for six years in the reactor and cooled 150 days:

Fission product	Concentration (ppm)
$^{85}\text{Kr}$	0.23
Kr (total)	2.5
Xe (total)	9.7
$^3\text{H}$	$4.0 \times 10^{-3}$
Iodine (total)	0.5

Laboratory studies and theoretical calculations are under way to determine more accurately the separation factor for the krypton-liquid  $\text{CO}_2$  system to aid in design and evaluation of engineering experiments. Separation factors appear to range from 11 to 18 at  $-60^\circ\text{C}$  to 1.8 to 4 at  $30^\circ\text{C}$ .

The solubility of krypton in hot potassium carbonate solutions has been estimated to be about 0.02 ml of krypton (at 1 atm) per milliliter of carbonate solution at  $120^\circ\text{C}$ , suggesting that one or more stripping stages would be required to remove krypton to a level of 1% or less of its original concentration.

**1.5 Waste treatment and disposal.** Detailed chemical flowsheets showing the compositions and flow rates of all process streams from the HTGR fuel recycle plant proposed for TURF have been prepared. These flowsheets and mass flows indicate magnitude of the waste disposal problem which must be dealt with during TURF operations.

## 2. Fuel Microsphere Preparation Development

**2.1 Sol preparation.** Engineering development of the CUSP process for preparing  $\text{UO}_2$  sol was continued during this report period. Several equipment improvements and simplifications were made and are being incorporated into the design of equipment for preparing 1-kg batches of enriched  $\text{UO}_2$  sol.

We have continued to operate the solvent extraction system to prepare  $\text{ThO}_2\text{-UO}_3$  sol at the rate of 1 kg of oxide per hour for use in preparing spheres for use in fabrication studies. One hundred kilograms of  $\text{ThO}_2\text{-UO}_3$  sol having a Th/U ratio of 3 was prepared successfully using rates up to 1.5 kg of oxide per hour, but attempts to go to 2 kg/hr were unsuccessful because of formation of interfacial crud. We were pleased with the fact that the present solvent extraction equipment could be successfully pushed well beyond its design throughput of 1 kg/hr before encountering any problems.

**2.2 Sol-gel microsphere preparation.** Use of ion exchange to remove nitric and formic acids from the 2-ethyl-1-hexanol sphere-forming fluid is a recent process improvement. The acids are extracted from sols during the sphere-forming operation and accumulate to

the point that they interfere with the operation. This work is essentially completed, and a report has been issued (ORNL-TM-3226).

Urania spheres have been prepared from about a hundred different CUSP sols. We have been able to correlate sphere formation behavior with changes in sol preparation; however, more work is necessary on drying and firing operations before the appearance of the fired oxide sphere can be related to preparation variables. Certain factors, such as the type and extent of sphere-forming alcohol cleanup, entrainment of organic material in the sols during preparation, sol viscosity, sol conductivity, and  $U^{IV}/U^{VI}$  ratio, are important to the successful preparation of product oxide spheres.

We have emphasized preparation of 150- to 200- $\mu$ -diam  $UO_2$  spheres in recent work. Spheres in this range have been an important type fuel in considerations of future HTGRs. Spheres smaller than about 200  $\mu$  may be made advantageously in a nonfluidized column filled with alcohol containing no surfactants. This greatly simplifies alcohol recycle. A demonstration run to prepare about 50 kg of 150- to 200- $\mu$ -diam spheres will be made in this system using the nonfluidized column during the next report period.

Processes and equipment have been satisfactorily demonstrated for preparing  $ThO-UO_2$  spheres in the size and composition ranges required for HTGR recycle fuel and at a capacity of 10 to 12 kg of oxide per day, the scale of the proposed hot process demonstration in TURF. The necessity of operating equipment remotely in TURF has led us into developing means whereby the sphere-forming operation may be viewed remotely. For this purpose we have developed a gel sphere removal system which brings the spheres into a viewing chamber. A dual-objective periscope is used to inspect the gel spheres for conformance to size and shape specifications. A particle size analyzer is also being evaluated as an on-stream analyzer of gel spheres.

A wide variety of types of sols and microspheres has been prepared for use in other parts of the fuel recycle program.  $ThO_2$ ,  $ThO_2-UO_3$ , and  $UO_2$  sols have been prepared in kilogram amounts, and kilograms of spheres of these sols have been made from them. Both natural and enriched uranium have been used.

In addition to the above more or less routine preparations, we have prepared  $PuO_2$  and  $ThO_2-PuO_2$  microspheres for use in a test element by Gulf General Atomic. These microspheres were produced using  $PuO_2$  sols prepared by a flowsheet that was developed for use in preparing LMFBR test fuel. Sphere forming was carried out in the same manner and with the same type of equipment used in our urania and thoria sol work.

**2.3 Resin-based microsphere development.** Uranium-loaded resin beads are being considered for use in HTGRs. Such beads can be treated to produce a carbonized product with a wide range of uranium contents in the range of interest for use as HTGR fuel. We are developing processes to optimize fuel loading and to permit ready engineering scaleup. Two approaches to resin loading are being studied. One involves loading resin columns by passing uranyl nitrate solution up or down a set of columns in series. The other involves batch equilibration of resin with  $UO_3$  in a warm dilute solution of uranyl nitrate. The former appears suitable for loading strong-acid resins, and the latter for loading weak-acid resins. The advantage of weak-acid resins over strong is that the weak-acid resins contain no sulfur, whereas the strong do, having a sulfonic acid functional group. For our purposes Amberlite IRC-72 is by far the best of the weak-acid resins we have studied so far. It loads more rapidly and has a much better percentage of spherical crack-free beads than the other resins. Dowex 50W-X8 appears to be an adequate resin of the strong-acid type. It is the type used in preparation of four 100-g quantities of resin loaded with  $^{235}U$  for use in irradiation tests.

### 3. Fuel Fabrication Process Development

The objective of the fuel fabrication process development is to provide a basis for the design and operation of the remote refabrication line to be installed in the Thorium-Uranium Recycle Facility (TURF) to demonstrate the recycle of HTGR fuel. This fabrication line will accept bare fissile microspheres and perform the necessary fabrication and inspection operations for production of graphite-based fuel elements on a pilot scale. The principal activities of the process development during this period have been particle coating and inspection and fuel stick fabrication.

**3.1 Microsphere coating.** Although additional equipment modification will be required for fully remote operation, the prototype remote coater presently being used for the engineering development is a highly automated, versatile, reliable system with a 5-in.-diam coating chamber. It is equipped for coating with both pyrolytic carbon and silicon carbide. Several modifications were made to the coating system during the year to improve reliability in applying pyrolytic carbon coatings and to obtain the capability for coating with silicon carbide. The prototype remote coater and a second 5-in.-diam coater have been used to investigate the effect of various process parameters on the quality of coatings produced.

Additional work has been done to obtain more efficient methods of particle inspection. In particular, a particle size analyzer has been developed to the stage that it now appears that the instrument is capable of counting and measuring particle diameters at the rate of several hundred particles per minute with sufficient accuracy for process control of particle coating thickness. Although we had previously developed various pieces of equipment for storing, classifying, blending, and sampling  $^{233}\text{U}$ -bearing particles, this equipment has never been tested in an integrated fashion; therefore we have assembled a test stand to be used for determining stability and accuracy of material inventory monitors, long-term performance of individual components, and operating parameters for pneumatic transfer.

**3.2 Fuel stick fabrication.** Another development in the refabrication technology included assessment of various means for fabricating fuel sticks. Emphasis is now being placed on the slug-injection technique, which is based on the use of hot (150–190°C) precast matrix injected under pressure into a mold containing coated particles. This method has shown great promise in the bench-scale work. Currently a prototype fuel stick molding machine, based on the slug-injection technique and capable of producing 500 fuel sticks per day, is being designed. Processes for carbonizing and annealing fuel sticks have been studied to determine the effect of various processing parameters and matrix material on dimensional stability and matrix structure. Additionally, techniques are being developed for various inspections required for the fuel sticks, namely, to characterize the matrix, the fuel loading, the dimensions, and the uranium and thorium contamination coming from both surface contamination and broken coatings.

#### 4. HTGR Fuel Recycle Pilot Plants

The HTGR fuel recycle development program is to culminate in a demonstration of recycle technology in pilot-scale equipment. ORNL has been concerned with the conceptual design of the three pilot plants that are required for the demonstration: the head-end pilot plant, the Acid-Thorex pilot plant, and the refabrication pilot plant.

**4.1 Head-end pilot plant demonstration.** The conceptual design of the head-end pilot plant was based on use of the Thorium-Uranium Recycle Facility (TURF) and portions of the Molten-Salt Reactor Experiment (MSRE) facility for interim fuel handling and storage. The plant is sized to have a fuel reprocessing rate of about ten Fort St. Vrain Reactor (FSVR) fuel elements

per day, which is about 10% of the requirement for a 1-ton/day reprocessing plant. Seven major processing systems were considered in the design: burner feed preparation, burning, burner ash handling, classified ash treatment, scrap recycle, off-gas handling and decontamination, and process services.

**4.2 Acid-Thorex pilot plant demonstration.** Our conceptual design of the pilot plant for acid-Thorex processing was prepared on the basis that the hot demonstration task would be carried out in facilities at ORNL. The plant would utilize existing equipment and facilities at Building 3019, with additions and modifications as required to perform the necessary operations. The design is based on a capacity of approximately 6 kg of heavy metal per day, which is the present nominal capacity of the facility. Primary attention in the design of processing equipment was given to equipment items in the feed preparation and the off-gas handling and decontamination systems, where the greatest unknowns were judged to exist.

**4.3 Refabrication pilot plant demonstration.** We commenced the conceptual design of the pilot plant for demonstrating refabrication technology. The design basis is a plant that will have a fuel refabrication rate of about two recycle fuel elements per day. The conceptual design is to include processing equipment, waste treatment and disposal equipment, and equipment and facilities for handling the various materials required in the pilot plant.

**4.4 Thorium-Uranium Fuel Cycle Facility.** Work was carried out to maintain TURF in operational readiness and for conduct of the HTGR fuel recycle program. Work included repair and improvement of equipment, preparation of operating instructions, and routine maintenance.

#### 5. Recycle Fuels Irradiation and Evaluation

The irradiations in the HTGR recycle program have two main objectives: (1) to provide irradiated fuel for head-end processing studies and (2) to proof-test the products of the process development program. The total program involves capsule irradiation tests in the ETR, pilot-scale irradiations in the Peach Bottom reactor, and a series of tests that will eventually include testing of remotely fabricated recycle test elements (RTE) in the Fort St. Vrain reactor.

**5.1 Recycle test elements.** Six RTEs have been operating as planned in the Peach Bottom reactor since July 14, 1970. In April of 1971, after 252 days of operation, one element (RTE-7) was discharged, and an additional element was installed. RTE-7 is being

shipped to ORNL for disassembly, examination, and head-end reprocessing studies. Two of the remaining elements will be discharged after about 500 days of operation, and the remainder are scheduled to operate for 800 days or more, achieving fast-neutron exposures of approximately  $4 \times 10^{21}$  neutrons/cm<sup>2</sup> ( $E > 0.18$  MeV).

**5.2 Capsule tests.** For accelerated burnup rate tests, two capsules were prepared and are being irradiated in the ETR. Five fissile-fertile particle combinations are being irradiated at temperatures of 750, 950, 1050, and 1300°C up to fast-neutron fluences of  $8 \times 10^{21}$  neutrons/cm<sup>2</sup> ( $E > 0.18$  MeV). Four of these combinations are those of principal interest to the HTGR recycle development program, while the fifth contains a fissile particle consisting of a Biso-coated fueled strong-acid resin.

## 6. Commercial Recycle Plant Studies

Commercial recycle plant studies are being conducted to provide the requirements to be met by the fuel recycle development program. Emphasis has been on determining fuel cycle costs under various circumstances and on assessment of available alternatives for fabrication of HTGR fuels.

**6.1 Reactor physics studies.** Reactor design parameters which influence fuel cycle cost include fuel particle size, fuel stick size, fuel composition, and fuel isotopic assay. A number of revisions to existing computer codes and additional computer code development have been made, so that calculations performed will adequately represent the physics effects associated with these parameters.

**6.2 Fuel value of  $^{233}\text{U}$  in HTGRs.** The reactor fuel value of bred  $^{233}\text{U}$  contained in recycle uranium was determined by comparing its performance with that of  $^{235}\text{U}$ . The fuel value of fissile material contained in the recycle fuel was calculated by an "indifference value" approach similar to that used in other fuel value studies. A typical value obtained for bred fuel after repetitive HTGR recycle for 20 to 30 years was about \$16.5 per gram of  $^{233}\text{U}$ .

**6.3 Evaluation of plutonium use in HTGRs.** High-temperature gas-cooled reactors are generally proposed for operation on the thorium fuel cycle using highly enriched  $^{235}\text{U}$  as makeup fissile fuel with recycle of bred  $^{233}\text{U}$ ; however, plutonium can also be used as makeup fuel. A systems analysis study was performed to determine whether such plutonium use was advantageous to HTGR penetration of the nuclear power market. The results of the study show that (1) use of

the plutonium-makeup fuel cycle permits HTGRs to penetrate the power market much deeper than use of the  $^{235}\text{U}$ -makeup fuel cycle alone; (2) plutonium-makeup HTGRs are economically preferred over plutonium-fueled light-water reactors over the period of the study; (3) use of plutonium-makeup HTGRs has no significant influence on the introduction and use of fast breeder reactors; and (4) if fast breeder reactors produce excess fissile fuel, it appears economically desirable that such fuel be  $^{233}\text{U}$  for use in HTGRs.

**6.4 HTGR fabrication economics.** A study of HTGR fabrication economics has been initiated. To date a computer code for calculation of HTGR fuel fabrication costs has been partially developed.

## PART II. HTGR DEVELOPMENT PROGRAM

### 7. Prestressed Concrete Pressure Vessel Development

**7.1 PCRV thermal cylinder test.** The thermal cylinder experiment that was designed to study the time-dependent stress strain behavior of a simulated segment of a PCRV vessel has been assembled, cast, and placed under test. The special instrumentation procured and developed for this experiment has been calibrated, and its performance is being evaluated as a major test objective. Each of the regimes of loading, including prestressing, thermal gradient, and internal pressure, has been achieved as scheduled. Initial time-dependent stress analyses have been performed, and the experimental data obtained during the first six-month period of the test are being reduced for comparison with theoretical behavior.

**7.2 Subcontract studies.** The series of tests planned to systematically study the structural behavior of head regions in PCRVs has been completed. Twenty-three model vessels were built and tested to various stages of failure as a part of a project to develop analytical techniques to predict the overload capacity and failure mode of these structures.

The investigations on moisture movement in mass concrete and multiaxial creep studies have been completed, and summary reports have been prepared on one series of concrete creep experiments.

### 8. HTGR Fuel Element Development

The objectives of the fuel element development program are (1) to develop and demonstrate the performance of reference and alternate design coated particles and fuel sticks to full HTGR fluence and

burnup, (2) to develop alternate fabrication processes that have either improved performance or economics, and (3) to develop advanced fuels with higher temperature capability than reference materials. These objectives are achieved through fabrication development, irradiation testing, and theoretical studies.

**8.1 Resin particle development.** Work on fuel particles derived from ion exchange resins demonstrated the simplicity of fabrication and product reproducibility. Irradiation tests showed this excellent irradiation stability and also showed that a buffer coat as now defined is not required on resin kernels. Amoeba studies indicated the better amoeba resistance of particles derived from strong-acid resins.

**8.2 Coating development.** Our coating technology was used successfully in the preparation of Triso-coated  $\text{PuO}_2$  particles in a glove-box operation. Sufficient coated material for a test fuel element was produced in this small-scale operation. A Leitz microscope was adapted for measuring reflectance intensities of coatings with a plane-polarized light source and a microphotometer. The ratio of reflectance intensities is a means of measuring the coating anisotropy in terms of an optical anisotropy factor (OPTAF). The instrument is being checked with standard samples consisting of single crystals of graphite.

**8.3 Bonded fuel development.** Theoretical analyses showed that packing factors of particles much less than the ~62 vol % found in intrusion-bonded sticks could be used in HTGR fuel elements provided the kernel diameters of the fissile and fertile particles are larger. A slurry-blending process was developed for fabricating fuel sticks with less than 40 vol % coated particles.

**8.4 Fuel migration studies.** We developed a model to explain the failure of coated oxide fuel particles by the "amoeba effect." This model is based on the transport of carbon by the diffusion of  $\text{CO}_2$  and CO across a temperature gradient and the establishment of local equilibrium in the C-CO- $\text{CO}_2$  system. Results from model calculations yield pressures of CO and  $\text{CO}_2$  that are consistent with measured values and indicate that the SiC layer may chemically buffer the system during irradiation by the action of the SiC-SiO<sub>2</sub>-C equilibrium.

**8.5 Design and preparation of irradiation experiments.** Accelerated testing of HTGR fuels is carried out in two types of capsules in HFIR. The second in a series of instrumented and swept capsules was built and irradiated in the removable beryllium (HRB) facility, and a third capsule of this type is being prepared. A series of HFIR target capsules designed to study the fast-neutron effects on a series of Triso-coated particles

was built and irradiated. The tenth capsule in this series is still in test. In addition, specimens were furnished for irradiation testing in ORR sweep capsule C1-28 and in GGA experiment P13-N.

**8.6 Examination and evaluation of irradiation experiments.** Irradiation tests on bonded sticks fabricated by the conventional "intrusion" process showed that matrices containing a wide variety of carbonaceous filler materials will survive the full HTGR fluence successfully. Both ORNL fuel sticks made on a laboratory scale and GGA fuel sticks made on a preproduction scale were successfully irradiated to the full HTGR fluences and to burnups higher than the HTGR reference without coating failures. The shrinkage of the intrusion-bonded sticks, important from the heat transfer standpoint, is controlled by the densification of particle coatings. With Triso coatings or Biso coatings that have high-density outer layers ( $\rho \geq 2.0 \text{ g/cm}^3$ ), linear shrinkage of bonded sticks can be controlled to 2% or less.

Triso-type coatings were irradiated to the full HTGR fluences in HFIR target capsules. Results showed that isotropic coatings derived from propylene performed well if the densities were in the range 1.78 to 2.04  $\text{g/cm}^3$ . Some coatings with densities of 1.68 to 1.75  $\text{g/cm}^3$  failed because of mechanical interactions between the pyrolytic carbon and SiC coatings.

## 9. Irradiation Experiments

**9.1 HFIR irradiations.** Two types of irradiation facilities in the HFIR are used to test HTGR fuels. In the HFIR, HT capsules, which are small and uninstrumented, occupy a target position and permit rapid attainment of the desired exposure; HRB capsules, relatively large instrumented capsules with provisions for a gas sweep, are inserted in the HFIR removable beryllium reflector region. The fast-neutron flux in HRB positions is about 35% of that in the target capsules and requires about eight months to attain reference HTGR fast-neutron exposure.

Five HT capsules, the sixth through tenth, were built during this report period. Irradiation was completed on four of these, while the tenth is still in the reactor. These capsules are all similar in design, and irradiation specimens include graphite materials, bonded fuel sticks containing coated particles, and samples of loose coated particles. Some of the graphite specimens in the seventh and ninth capsule were examined after irradiation and then reinserted in the tenth capsule so as to permit stepwise determination of dimensional changes with

exposure. Irradiation temperatures in the capsules varied from 750 to 1100°C, and fast-neutron exposure varied from  $2.5 \times 10^{21}$  to  $9.6 \times 10^{21}$  neutrons/cm<sup>2</sup> ( $E > 0.18$  MeV), depending on the duration of the irradiation and the axial position within the capsule.

The second removable beryllium capsule, HRB-2, was irradiated during this period. The capsule contained both GGA and ORNL bonded fuel sticks with various types of kernels, coatings, and matrix materials. There were sixteen 0.412-in.-diam bonded fuel sticks, with a total bed length of 14 in., irradiated at a nominal temperature of 1200°C to a peak fast-neutron fluence of 7.9 neutrons/cm<sup>2</sup> ( $E > 0.18$  MeV). The combined release rates (R/B) for all the specimens were typically  $1.8 \times 10^{-5}$  for  $^{85m}\text{Kr}$ ,  $7 \times 10^{-6}$  for  $^{87}\text{Kr}$ ,  $8 \times 10^{-5}$  for  $^{133}\text{Xe}$ , and  $2 \times 10^{-5}$  for  $^{135}\text{Xe}$ . A third removable beryllium capsule is under construction.

**9.2 ORR irradiations.** A third type of irradiation capsule was built for the C-1 irradiation facility of ORR. This capsule was designed to study the performance of bonded specimens containing fueled carbonized ion exchange resin particles under severe temperature gradients and at temperatures up to 1500°C. In addition, the capsule contained 21 samples of different particle batches having various kernels and coating combinations. These samples will be subjected to postirradiation fission product release tests. The fission-gas release rate from this capsule was so high from the start of the irradiation that it was not possible to reach design temperatures within the operating limits of the capsule facility. The capsule was irradiated at low temperatures, less than 1000°C, to produce burnup of at least 5% heavy metal in the loose particles so as to make fission product release studies feasible.

**9.3 Analysis of irradiation conditions.** The analysis of irradiation test conditions in HFIR experiments has been complicated by difficulties in interpreting data from dosimeter wires due to transformations from the very high thermal-neutron flux and chemical reactions at the high temperatures. Consistent data were obtained on several experiments by correcting for depletion of active products and by encapsulating the dosimeters. Finally, we initiated a special dosimetry experiment designed to measure the time and spatial dependence of the neutron damage flux and spectrum in the HFIR. Fifteen capsules for short-term exposure in the central hydraulic tube and two one-cycle capsule experiments are being exposed and analyzed as part of this experiment. Results from the dosimeters will complement the data on flux and spectra calculated using diffusion and transport theory, and permit a complete mapping of damage spectra in the HFIR.

## 10. Irradiation Experiment Analysis and Fission Product Transport

**10.1 Fission product release from bonded beds.** The distribution of fission products in an irradiated bonded bed of pyrolytic-carbon-coated UO<sub>2</sub> particles after a 2500-hr anneal at 1250°C showed that a negligible amount of cesium and about 3% of the strontium were retained in the matrix. More than 30% of the cesium was found in the particle coatings, which indicates that cesium release from Biso-coated particles is controlled by the outer coating.

**10.2 Fission product transport through particle coatings.** Diffusion coefficients and an activation energy of 106 kcal/mole were determined for cesium, considering cesium transport in propylene-derived pyrocarbon at 1250°C. It was found that the activation energy for cesium diffusion and the diffusion coefficients for cesium and strontium in the pyrocarbon deposited from propylene were considerably higher than those obtained for pyrocarbon deposited from methane at 2000 to 2200°C. Cesium diffusion in the coated particle studies was not significantly affected by burnup or fast fluence.

**10.3 Results and analysis of fission product deposition (FPD) loop tests.** The experimental program on cesium transport and deposition was terminated with the completion of three additional loop runs. The analytical model previously presented for transverse flow of helium through the graphite was broadened to include the geometry of the Fort St. Vrain fuel element. A mathematical analysis based on the transverse flow mechanism shows that the thickness of the diametral gas gap between the fuel element and the graphite must be very small, for example, 0.002 in. or less, to have any appreciable effect on controlling the transverse flow transport of cesium through the graphite sleeve. The overall data obtained from the experiments performed in the high-temperature, pressurized-helium FPD loop correlate reasonably well with the transverse flow analysis.

## Part III. GAS-COOLED FAST BREEDER REACTOR PROGRAM

### 11. GCFBR Irradiation Experiments

In the joint ORNL-GGA irradiation testing program for the evaluation of (U,Pu)O<sub>2</sub>-fueled metal-clad fuel pins for the GCFBR, current emphasis is on the thermal- and fast-flux testing of fuel pins of the vented-and-pressure-equalized fuel rod concept, which is the reference fuel rod design for the GCFBR. The

fuel-cladding-interacting type of sealed fuel pin, tested previously in the program, is the backup concept for the GCFBR. The vented fuel rod is the present reference GCFBR fuel rod design because of its better performance potential and because information being developed in LMFBR fuel-pin-testing programs is more applicable to this design. The better performance potential results from the elimination of large pressure differentials across the cladding by venting the fuel rod interior to a pressure equalization system.

**11.1 Irradiation of GCFBR-ORR capsule GB-9.** Thermal-flux irradiation capsule GB-9, which contains a (U,Pu)O<sub>2</sub>-fueled stainless-steel-clad vented rod with a charcoal trap, has operated successfully in the ORR poolside facility to a burnup of 51,000 MWd per metric ton of heavy metal on the way toward a burnup goal of 75,000 MWd/metric ton. In this instrumented test, the release of fission products to and through the charcoal trap in the fuel rod is being monitored with the rod operating at a heat generation rate of 16 kW/ft, a maximum cladding outer surface temperature of 700°C, a charcoal trap temperature of 300°C, and cladding internal and external pressures of 1000 and 975 psig respectively. In addition to normal operation under these steady-state conditions, special tests have also been performed to determine fission-gas release dependence on charcoal trap temperature, fuel region temperature, and cladding internal pressure. Tests to obtain information on fission-gas release during pressure cycling and to determine fission product decay heating in the charcoal trap and iodine deposition in the trap have also been made. The steady-state fission-gas release rates measured as a function of time at normal operating conditions showed a general increase the first 10,000 MWd/metric ton burnup and since then have remained about constant. The charcoal trap performance in reducing the steady-state fission-gas release rates is close to original predictions. The results of the special tests have shown that (1) the fission-gas release from the rod is much more sensitive to temperature changes and to temperature profile changes over the fuel region of the rod than to temperature changes of the charcoal trap; (2) there is little or no fission product decay heating in the trap, indicating that volatile fission products are not migrating to the trap in appreciable quantities during steady-state operation; and (3) less than 1.5% of the steady-state <sup>133</sup>I and <sup>135</sup>I inventory generated in the fuel was found to be deposited in the charcoal trap.

**11.2 Design of GCFBR capsule GB-10.** Design of the next capsule experiment in the series of GCFBR fuel

rod irradiation tests in the ORR poolside facility has been completed, and fabrication of the capsule is scheduled for completion by April 1, 1972. This experiment, designated capsule GB-10, will be similar to the capsule GB-9 experiment. Capsule GB-10 has been designed with increased capability to measure fission product release and transport, including release from the oxide fuel matrix. The planned operating conditions for capsule GB-10 are the same as those for capsule GB-9.

**11.3 Analysis of irradiation conditions.** An improved technique for predicting fission-heat-generation rates and detailed radial power distributions in the fuel of GCFBR thermal-flux capsules was implemented during the preirradiation analysis of capsule GB-10. Calculations of this type are required, to determine the power asymmetry across the fuel pellets and the effect of this asymmetry on the readings of thermocouples used to monitor the fuel rod temperature during irradiation. The improved calculational technique consists in coupling a full core diffusion theory calculation (CITATION program) to a detailed two-dimensional transport theory calculation of a subregion containing the capsule (DOT program) through appropriate boundary conditions. The coupling is achieved with a program which digests CITATION neutron flux output and calculates appropriate boundary conditions for the subregion DOT calculation.

## 12. GCFBR Fuel Fabrication

The fuel for GCFBR capsule GB-10 and for the EBR-II F-1 series replacement pins is being fabricated. Pellets of two types, 88% dense solid pellets and 92% dense annular pellets, were made from sol-gel-derived (U,Pu)O<sub>2</sub> powder for the F-1 pins. The (U,Pu)O<sub>2</sub> powder for fabrication of the GB-10 pellets is being prepared.

## PART IV. ASSOCIATED USAEC EXCHANGE PROGRAMS

### 13. Exchange Programs

The USAEC/Dragon HTGR Agreement and the USAEC/KFA Exchange Arrangement concern HTGR research and development and also involve exchange of reports and visits of personnel. Under the Dragon Exchange Agreement, selected ORNL fuel compacts irradiated in the Dragon Reactor were returned to

ORNL for postirradiation examination and use in head-end reprocessing studies. Under the KFA Exchange Arrangement, reactor physics calculations for

the AVR were performed using an ORNL calculational program; also, discussions were held relative to personnel exchange in the field of fuel reprocessing.



# Part I. Thorium Utilization Program

---

## 1. Head-End Reprocessing Development

C. L. Fitzgerald	K. J. Notz
R. W. Glass	J. W. Snider
P. A. Haas	V. C. A. Vaughen
R. S. Lowrie	D. C. Watkins
A. B. Meservey	M. E. Whatley

Demonstration of all important process steps and obtaining information for use in the design of commercial HTGR fuel recycle plants in a timely manner are goals of the National HTGR Fuel Recycle Development Program Plan.<sup>1</sup> This chapter describes the work on head-end reprocessing development, which covers two important areas: (1) recovery of fuel from the irradiated HTGR fuel elements and (2) disposal of radioactive wastes generated in the recovery operations. One important aspect of fuel recovery is discussed in Sect. 4.2 (Acid-Thorex Pilot Plant Demonstration) rather than here, because no development work is being conducted at present and only a minimal amount is expected to be required. Thus this recovery step has been considered to be primarily a pilot-plant demonstration rather than a development effort.

The head-end problems being studied are dictated by the nature of the HTGR fuel elements. These elements are mainly graphite in the form of large hexagonal blocks containing fuel and coolant channels and have been described in many reports (e.g., ORNL-4702). The basic problem in fuel recovery is that of recovering

$^{233}\text{U}$  in good yield and relatively free from carbon and  $^{235,236}\text{U}$ . The  $^{233}\text{U}$  is formed from  $^{232}\text{Th}$ , and the mixture of isotopes  $^{235,236}\text{U}$  is formed from  $^{235}\text{U}$  present in the fabricated element.

Although there are a variety of possible methods for fuel recovery from the elements, we have chosen to study only those that appear certain in principle to work. Thus we are not relying on any methods that require no distortion of the fuel elements under radiation or that require a specific or selective reactivity of the graphite with chemical reagents. We believe that simple burning of the elements affords the certainty we require. We have not yet decided whether there is an advantage in simple physical separation of a large fraction of the graphite before burning. It seems that about as many problems are added as are avoided. Important work in this area is being carried out by Gulf General Atomic (GGA), and close collaboration is maintained between them and ORNL. The work at GGA stresses fluidized-bed burning and physical removal of part of the carbon before burning; the work at ORNL, which has been on fluidized-bed burning, is being redirected to stress burning the entire fuel element.

The problem of head-end off-gas cleanup is very important in these studies. The novel problem we face

---

1. Oak Ridge National Laboratory and Gulf General Atomic, *National HTGR Fuel Recycle Development Program Plan*, ORNL-4702 (August 1971).

is that of removing relatively very small amounts of fission products from CO<sub>2</sub>. Although we believe we can remove the principal offenders, <sup>85</sup>Kr, <sup>129</sup>I, <sup>3</sup>H, and perhaps Xe, to acceptable levels by one or more of the methods discussed below, any requirement of a drastic reduction in the amounts of other nuclides which can be released, such as the transuranium elements, would pose problems relative to meeting such release limits.

Finally, an overall look at the waste streams from a recycle plant has convinced us that, to the extent possible to predict, we have delineated practicable methods for waste disposal under present rules.

## 1.1 BURNER FEED PREPARATION

R. S. Lowrie

Of the several types of burners proposed for use in reprocessing HTGR fuel, all but the whole-block burner require comminution of the fuel element to reduce it to a size range suitable for burner feed. The fluidized-bed burner has been studied most so far. Fuel for it will be reduced to pieces about 1/4 in. or smaller. The method used to comminute the fuel element must keep the particle coating breakage to a minimum to reduce crossover of the <sup>235</sup>U and <sup>236</sup>U in the fissile particles to the bred <sup>233</sup>U in the fertile particles. Because of the importance of the comminution operations, we have been studying various approaches to this problem in collaboration with GGA.

### 1.1.1 Comminution Studies with Resin-Bonded Fuel

Two unirradiated graphite fuel samples containing resin-bonded Triso-coated<sup>2</sup> ThC<sub>2</sub> and UC<sub>2</sub> particles were crushed in the hammer mill using 3/4- and 3/8-in. grate spacings to determine the size distributions and particle coating breakages (Table 1.1).

Fuel particles or pieces of the fuel rod were found in all +60-mesh or larger size fractions from both tests. Particle coating breakage was determined by leaching the product with Thorex dissolvent (13 M HNO<sub>3</sub>; 0.04 M F<sup>-</sup>; 0.1 M Al<sup>3+</sup>). Coatings were broken on 1.6% of the fertile and 0.8% of the fissile particles in the product when the hammer mill grate spacing was 3/4 in., and on 17% of the fertile and 3.4% of the fissile particles when the spacing was 3/8 in. In the present head-end reprocessing flowsheet, all the fertile material will be recovered; so the 17% breakage of fertile particle coatings may not be significant. The 3.4% loss (cross-

Table 1.1. Size distribution of the product obtained by crushing HTGR fuel in a hammer mill

Mesh size of powder produced	Hammer mill product (wt %)	
	3/4-in. grate spacing	3/8-in. grate spacing
+ 3/4 in.	0.8	
- 3/4 + 3/8 in.	19.7	0.2
- 3/8 in. +4 mesh	27.00	14.6
-4 mesh +12 mesh	14.80	20.1
-12 +30 mesh	19.30	30.0
-30 +45 mesh	9.3	13.0
-45 +60 mesh	2.5	4.7
-60 +80 mesh	1.3	3.3
-80 mesh	5.6	13.6

over) of fissile material due to broken particle coatings is well below the 10% crossover considered permissible.<sup>3</sup>

### 1.1.2 Comminution of Pitch-Bonded Fuel

Several unirradiated pitch-bonded fuel rods containing Biso- and Triso-coated ThC<sub>2</sub> particles were received from GGA. Uncrushed samples of these rods were placed in a boat and burned at 759°C for 16 hr. Examination of the residue showed that the Biso-coated ThC<sub>2</sub> kernels did not oxidize to a fine powder but remained in the form of chunks, and less than 1% of the Triso-coated particles were broken. Two rods were crushed in the hammer mill, one with the grate set to pass - 3/4-in. material and the other with the grate set to pass - 3/8-in. material. Microscopic examination of crushed material from both rods showed that <1% of the Triso-coated particles were broken during crushing. However, many of the Biso coatings were broken, particularly in the material in the product from the hammer mill having a grate spacing of 3/8 in. The very strong odor of acetylene around the crusher suggests the need to crush carbide fuel in an inert atmosphere.

### 1.1.3 Comminution by Intercalation

K. J. Notz

A possible method for the selective disintegration of fuel sticks and graphite blocks is intercalation. Differences are known to exist between fuel blocks, fuel-stick

2. Particles were made and coated by GGA.

3. Chem. Technol. Div. Annu. Progr. Rep. May 31, 1970, ORNL-4572, p. 85.

matrix material, and fuel particle coatings with regard to their graphitic properties; thus one would expect differences in the rates and/or degree of penetration of these materials by intercalating agents. The block graphite is well crystallized, with crystal planes oriented longitudinally in the extruded blocks. The fuel sticks consist of microspheres bonded together by a carbonized matrix which is more isotropic and less well-crystallized than the block. The coated particles should be less reactive than either matrix or block because of their highly dense, impervious coating of pyrolytic graphite. Earlier work by Ferris et al.<sup>4</sup> showed that 90% HNO<sub>3</sub> quickly disintegrated graphite but did not affect

coated particles. Consequently, this reagent was tested on several types of fuel sticks and on H-327 graphite.

Table 1.2 summarizes the results obtained with block graphite and two types of fuel sticks for 20 min exposure to 90% HNO<sub>3</sub> at room temperature. Longer exposures had no further effect. Only a minor amount of chemical oxidation occurred (as evidenced by brown fumes of NO<sub>2</sub>); mainly on block graphite. Although the coated particles appeared to be unaffected by this treatment, the kernels of those particles whose coatings were broken either in the manufacture of the fuel stick or during their exposure in the reactor would be attacked by the reagent.

The block graphite disintegrated quickly into pieces about 1 × 1/2 × 1/2 in. These pieces were very friable and could be broken apart with very gentle pressure. Fuel sticks of the Fort St. Vrain (FSVR) type (made by

4. L. M. Ferris, A. H. Kibbey, and M. J. Bradley, *Processes for Recovery of Uranium and Thorium from Graphite-Base Fuel Elements, Part II*, ORNL-3186 (Nov. 16, 1961).

Table 1.2. Disintegration of graphite and fuel sticks with fuming nitric acid

Conditions: 20 min exposure to a large excess of 90% HNO<sub>3</sub> at room temperature; occasional stirring, followed by a water wash and drying at 110° C

Great Lakes H-327 block graphite				
Mesh size range of powder produced	Weight percent in mesh size range			
	Sample 1	Sample 2		
+10	66	70		
10--20	26	21		
--20	8	9		
FSVR type fuel sticks -- no disintegration; apparently unaffected				
Experimental slurry-molded fuel sticks				
Mesh size range of powder produced	Weight percent in mesh size range			Description of powder
	JH-102-3, 41 vol % microspheres	JH-112-2, 44 vol % microspheres	JH-101-1, 21 vol % microspheres	
+10	13	7	56	Large pieces of matrix; some beads trapped internally
10--20	19	23	11	Large pieces of matrix; some beads trapped internally
20--30	58	56	29	Mostly microspheres
30--45	7	4	2	About half beads and half matrix pieces
--45	3	9	2	Matrix pieces only

slug injection of carbon-loaded pitch and annealed to 1400°C) were not affected, even after 18 hr exposure. Thus fuel elements made of these two materials could, in principle, be separated. On the other hand, the experimental sticks made by molding a solvent-containing slurry (and also annealed at 1400°C) disintegrated quite readily. Since intercalation is so dependent on details of fuel preparation, particle removal from the block graphite by this method does not appear promising.

## 1.2 BURNER TECHNOLOGY—COLD ENGINEERING

R. S. Lowrie

The fuel burner for which the technology is most advanced and which appears at present to be the most likely to be used is the fluidized-bed burner. The tests reported below were carried out in a 2-in.-diam fluidized-bed burner. Fluidized alumina served as a heat transfer medium to carry heat from the burning carbon to the cool surfaces in the burner.

### 1.2.1 Fluidized-Bed Burning Tests with Pitch-Bonded Fuel

The  $\frac{3}{8}$ -in. crushed pitch-bonded fuel rod (see sect. 1.1.3) material was combined with graphite (crushed in the hammer mill to pass  $\frac{3}{8}$ -in. grate spacing) at a 1:4 ratio and the mixture burned in the fluidized-bed burner. Operating conditions are listed below:

Pressure	3 psig
Superficial gas velocity	1.25 fps
Burning rate of carbon <sup>a</sup>	16.3 kg ft <sup>-2</sup> hr <sup>-1</sup>
Heat transfer medium	90–120 mesh alumina
Reagent gas composition	70% oxygen, 30% diluent
Wall temperature	750° ± 25°C

<sup>a</sup>The area given here is the cross-sectional area of the burner.

No operating problems were encountered; buildup of fine particles on the filters was similar to that obtained with Triso-Triso fuel. Oxygen utilization was >99%, and the CO concentration in the off-gas was <1%. Microscopic examination of the burner residue indicated that the breakage of Triso-coated particles was low and that the Bisco-coated ThC<sub>2</sub> particles had been converted to a fine ThO<sub>2</sub> powder associated with the alumina (–90 mesh). Leaching tests of two samples riffled from the burner residue show 4.0% breakage in one and 1.3% breakage in the other sample, for an average value of 2.6% of the Triso-coated particles broken in the crushing and burning steps. Some of this

material was also burned with the fluidized-bed burner operating at a much higher carbon burning rate (47.5 kg ft<sup>-2</sup> hr<sup>-1</sup>, 22 psig, 1.75 fps superficial velocity). Breakage of the Triso coatings, based on microscopic examination of the residue, appeared to be similar to that obtained with the lower carbon burning rate.

### 1.2.2 Fluidized-Bed Burning Rates

Tests were carried out in the fluidized-bed burner using crushed graphite (material passing a  $\frac{3}{8}$ -in. grate spacing in the hammer mill) to determine the maximum burning rate as a function of oxygen partial pressure and superficial gas velocity. Norton RR-grade alumina (–90 +120 mesh) was used as the heat transfer medium. The reagent gas composition was held constant at 70% oxygen–30% diluent since previous work indicated that, with 100% oxygen, fertile particle coating breakage increased and sintering of the bed occurred.<sup>5</sup> Burner wall temperature was held at 750 ± 25°C. Increasing the pressure from 3 to 18 psig while holding the superficial gas velocity constant at 1.25 fps increased the carbon burning rate from 16.3 to 30.1 kg ft<sup>-2</sup> hr<sup>-1</sup> (see Table 1.3). A further increase in pressure to 22 psig caused a

Table 1.3. Fluidized-bed burning rates

Superficial gas velocity (fps)	Burning pressure (psig)	Oxygen flow rate (std liters/min)	Burning rate of carbon (kg ft <sup>-2</sup> hr <sup>-1</sup> )
1.25	3	11.0	16.3
1.25	12	17.0	24.5
1.25	18	20.4	30.1
1.25	22	22.9	<i>a</i>
1.75	3	15.5	22.8
1.75	12	23.5	34.6
1.75	18	28.5	42.0
1.75	22	32.2	47.5

<sup>a</sup>Hole burned in wall of the burner.

hole to burn through the wall of the burner. Repeating these tests with a superficial velocity of 1.75 fps increased the burning rate from 22.8 to 47.5 kg ft<sup>-2</sup> hr<sup>-1</sup> as the burner pressure increased from 3 to 22 psig. These values can be used to obtain an idea of the size of the primary burners required for a demonstration of the size proposed for the demonstration run of 9.7 FSVR

5. Chem. Technol. Div. Annu. Progr. Rep. May 31, 1970, ORNL-4572, p. 90.

fuel elements per day, which is equivalent to  $\sim 41$  kg  $\text{ft}^{-2} \text{hr}^{-1}$ . The burner size could be decreased from the  $22\frac{1}{2}$  in. diameter required for a superficial velocity of 1.25 fps at 3 psig to  $12\frac{5}{8}$  in. if a superficial velocity of 1.75 fps at 22 psig were used.

### 1.3 HEAD-END REPROCESSING STUDIES -- HOT CELLS

V. C. A. Vaughen    C. L. Fitzgerald

A very important part of our head-end reprocessing development work is that involving hot-cell studies of irradiated fuel samples. In these studies we can determine whether results obtained during cold engineering studies are valid for material that has been irradiated. We are particularly interested in particle breakage before and during reprocessing. We are also very much concerned with behavior of the fission products during reprocessing, especially those which find their way into off-gas streams.

#### 1.3.1 Irradiated Compacts from the Dragon Project

A second set of irradiated fuel compacts and unirradiated controls was obtained from the Dragon project. Table 1.4 lists the fuel compacts that were received. Unirradiated compacts of fuel types 2M4, 19M, 18M, and 38M have been studied. Experimental work on irradiated compacts of fuel types 2M4 and 19M was completed, and the data are being analyzed. Preliminary results of these studies are presented below.

The processing flowsheets used in these small-scale studies are dependent on the fuel type. As seen in Table 1.4, fuel type 2M4 is a Biso-coated mixed-oxide fuel of the reference recycle type; however, it is not sol-gel derived. The reference flowsheet for this fuel is crush-burn-leach. It is of interest to determine if the oxide kernels retain their integrity adequately to be separated from the alumina according to size, because recycle of the alumina to the burner without leaching would be advantageous. If this fuel is to be recycled in such a way that the  $^{236}\text{U}$  is always kept separated from the  $^{233}\text{U}$ , the fertile oxide kernel must retain its integrity through the burning step so that it can be separated from the alumina and fissile particle ashes ( $\text{U}_3\text{O}_8$ ) by a procedure based on size difference. It is virtually certain that the Biso-coated fissile particles will convert to powdered  $\text{U}_3\text{O}_8$ .

Fuel types 18M (Triso  $\text{UC}_{20}$ ) and 38M [Biso ( $\text{U}/5\text{Th})\text{C}_{2.4}$ ] were mixed to simulate a reference B block makeup fuel. In this concept, the Triso coating preserves the fissile ( $^{235}\text{U}$ ) particle through the burning

step, so that crossover of uranium between the fuel types is minimized.

Fuel type 19M consists of a mixture of small Triso-coated  $\text{UC}_{10}$  and larger Triso-coated  $\text{ThC}_2$ . Since both particles are Triso coated, a postburning particle separation based on size can yield three fractions: fertile, fissile, and alumina (plus broken particle ash). An unirradiated compact of this type has been studied, and results are reported below. Preliminary results of studies on the irradiated compact are also given.

#### 1.3.2 Crushing Studies with Dragon Compacts

In each head-end flowsheet, the preliminary step is size reduction to provide suitable feed for a burner. Typically, one compact of each fuel type was available. For these cases, half a compact (napkin ring) was saved for an archive sample; the remaining half was crushed and sieved to determine the product size distribution for correlation with breakage results.

The half-compacts were crushed by the standard procedure (first by the  $\frac{5}{8}$ -in. jaw opening and then by the  $\frac{1}{8}$ -in. jaw opening). Since sawing has been found to break all particles contacted by the saw, the weighed fines were usually combined with the crusher product before sieving. However, the saw fines (a total of 5.9% of the compact) from compact 22365, containing irradiated Biso-coated oxide (2M4), were sieved separately to obtain an estimate of their size distribution. Table 1.5 shows the size distribution of these fines as well as the results for the crusher-product-fines combinations for the other compacts.

Two general observations can be made from the early crushing results: (1) The particle loadings are lower (i.e., the burnable carbon content is greater) than was the case in compacts received previously. The results show a steadily decreasing weight with decreasing size (similar to the results of crushing pure graphite), without a large weight of loose whole particles in the +42-mesh size fraction. (2) There is evidence of some differences in crushing behavior due to fuel type (e.g., Triso vs Biso) and level of irradiation, but these are not large. Additional confirmatory experiments are needed to determine the relationship.

#### 1.3.3 Head-End Studies of Unirradiated Dragon Compact 14719, Fuel Type 19M (Triso $\text{UC}_{10}$ -- Triso $\text{ThC}_2$ )

Fuel type 19M is an experimental fuel from the Dragon Project Metallurgical Series I. The fissile particle kernel is fully enriched  $\text{UC}_{10}$ , 60 to 70% of theoretical

Table 1.4. Irradiated Dragon compacts<sup>a</sup> received for ORNL head-end studies

Experimental fuel No.	Th/U atom ratio (93% <sup>235</sup> U)	Kernel composition	Kernel diameter (μm)	Type of coating	Thickness of coatings (μm)	Comments
2M4	10	(U,Th)O <sub>2</sub>	500	Biso	130	Simulates ( <sup>233</sup> U,Th)O <sub>2</sub> reference (Biso) recycle particle for 1100-MW(e) HTGR; will be compared with ORNL sol-gel recycle particle
2M7	10	(U,Th)O <sub>2</sub>	500	Triso	160	Simulates ( <sup>233</sup> U,Th)O <sub>2</sub> alternate (Triso) recycle particle for 1100-MW(e) HTGR
2M10	10	(U,Th)C <sub>2</sub>	500	Triso	150	Suitable for comparison of carbides vs oxides in head-end studies; simulates FSVR fertile-fissile particle
3M	10	(U,Th)C <sub>2</sub>	900	Triso	50/30/80	Large kernel size; can be mixed with other fuels for particle separation studies of Triso-Triso and Triso-Biso mixes (18M and ORNL sol-gel Biso-coated fuels)
18M		UC <sub>20</sub>	500	Triso	25/30/70	Simulates fissile ( <sup>235</sup> U) particles; will be used in particle separation studies
19M		ThC <sub>2</sub> UC <sub>10</sub>	900 500	Triso Triso	25/30/70 25/30/70	Simulates FSVR fuel particles; will be used in particle separation studies
38M	5	(U,Th)C <sub>2</sub>	500	Biso	40/80	1100-MW(e) HTGR simulated fertile-fissile particle with accelerated burnup; could be mixed with UC <sub>10</sub> Triso-coated particles (which are presently available) for separation studies
ORNL sol-gel <sup>b</sup>	3, 4, 5	(U,Th)O <sub>2</sub>	290	Biso		1100-MW(e) reference recycle fuel (fertile)

<sup>a</sup>Exposed to a burnup of about 7% FIMA and  $2.5 \times 10^{21}$  fast fluence.

<sup>b</sup>12 to 18% FIMA; not yet received.

Table 1.5. Crushing and sieving results

Type	Comments	Percent by weight on screens						Total handling loss (%)
		+4	-4 +9	-9 +20	-20 +42	-42 +100	-100	
19M	Triso-Triso <sup>a</sup>	3.4	48.7	27.3	11.0	4.4	5.3	0.9
19M	Triso-Triso <sup>b</sup>	4.5	58.0	25.3	6.9	3.1	2.2	0.4
2M4	Biso-oxide <sup>a</sup>	0.7	45.6	38.7	9.6	2.6	2.9	0.1
2M4	Biso-oxide <sup>b</sup>	4.7	53.9	26.9	8.7	2.6	3.2	0.5
18M	Triso UC <sub>20</sub> <sup>a</sup>	13.8	40.4	18.1	14.1	6.4	7.1	2.2
38M	Biso (U,Th)C <sub>2,4</sub> <sup>a</sup>	0.4	45.5	40.0	8.4	2.7	3.0	0.4
2M4	Biso-oxide sawdust <sup>c</sup>	0	0	0	21.1	34.8	44.1	4.1

<sup>a</sup>Unirradiated; standardized procedure for the laboratory crusher was used.

<sup>b</sup>Irradiated; standardized procedure for the hot-cell crusher was used.

<sup>c</sup>About 6% of compact.

density, 422 to 600  $\mu\text{m}$  (509  $\mu\text{m}$ , av) in diameter, with PyC/SiC/PyC coatings of 18/31/63  $\mu\text{m}$  respectively. The fertile particle kernel is 850- to 1200- $\mu\text{m}$ -diam ThC<sub>2</sub>, 60 to 70% of theoretical density, with PyC/SiC/PyC coatings of 30/29/56  $\mu\text{m}$  respectively.

Compact 14719 was weighed and sawed into two rings. One became an archive sample, while the other was used in further studies (Fig. 1.1). The sawdust was burned and leached to determine particle breakage. (The thorium and uranium carbide kernels exposed by breakage are readily soluble.) One ring was crushed by the standard procedure and sieved (Table 1.5), and then each sieve fraction was divided into duplicate samples. Overall handling losses were <1%. Each sample was mixed with about 2 g of Al<sub>2</sub>O<sub>3</sub> per gram of fuel and was burned in a fluidized-bed burner at 750°C using a superficial gas velocity of 1 to 1.5 fps. Burning proceeded over a 4- to 8-hr period with oxygen-nitrogen mixtures. About 90% of the fuel weight charged was lost during burning. Sample R-1 contained some unburned carbon. The burner product was screened, and then the screened fractions were inspected and combined to give three fractions: whole SiC-coated ThC<sub>2</sub> particles, whole SiC-coated UC<sub>10</sub> particles, and alumina plus broken particles of both kinds. Since there were very few whole SiC-coated particles, only the alumina was processed further. The weights, expressed in grams, of leached uranium and thorium were converted to equivalent weights of SiC-coated particles by dividing by the factors 0.44 and 0.75 respectively.

Particle breakages, based on the calculated total weight of coated particles, are given in Fig. 1.2. Although a small sample burned in a ceramic dish and

leached indicated that about 2% of the fissile and about 5% of the fertile particles were broken in the uncrushed fuel, breakages of about 6 to 9% of the fissile particles and about 20 to 24% of the fertile particles were found in crushed fuel.

#### 1.3.4 Head-End Studies of an Unnumbered Irradiated Dragon Compact, Fuel Type 19M (Triso UC<sub>10</sub>-Triso ThC<sub>2</sub>)

This type 19M compact was weighed and rough-crushed with the jaw crusher wide open. One larger piece was selected and passed through the crusher again to give metallography, graphite disintegration, and archive samples (Fig. 1.3). The remainder of the compact was crushed in the jaw crusher (shimmed to  $\frac{3}{16}$ -in. jaw opening) and split into two replicate samples using the standard procedure. One replicate was burned in a fluidized-bed burner with about 2 g of Al<sub>2</sub>O<sub>3</sub> per gram of crushed fuel as the fluidizing medium, while the other was burned in a quiescent manner on top of a bed of about 5 g of Al<sub>2</sub>O<sub>3</sub>. Considerable difficulty was experienced with the fluidized-bed burning operation. The oxygen flow rate was varied from 100 to 400 cc/min, while the nitrogen flow was held constant at 1000 cc/min. The lower oxygen flow rates gave intermittent burning, while the higher rates gave temperature excursions up to 1025°C. Most of the burning was accomplished at 900 to 950°C. We think that the burner fuel support plate may have been cracked. The quiescent burning was a smooth operation, with a burning rate of about 1.4 g of carbon per hour; a small amount of unidentified gray residue was

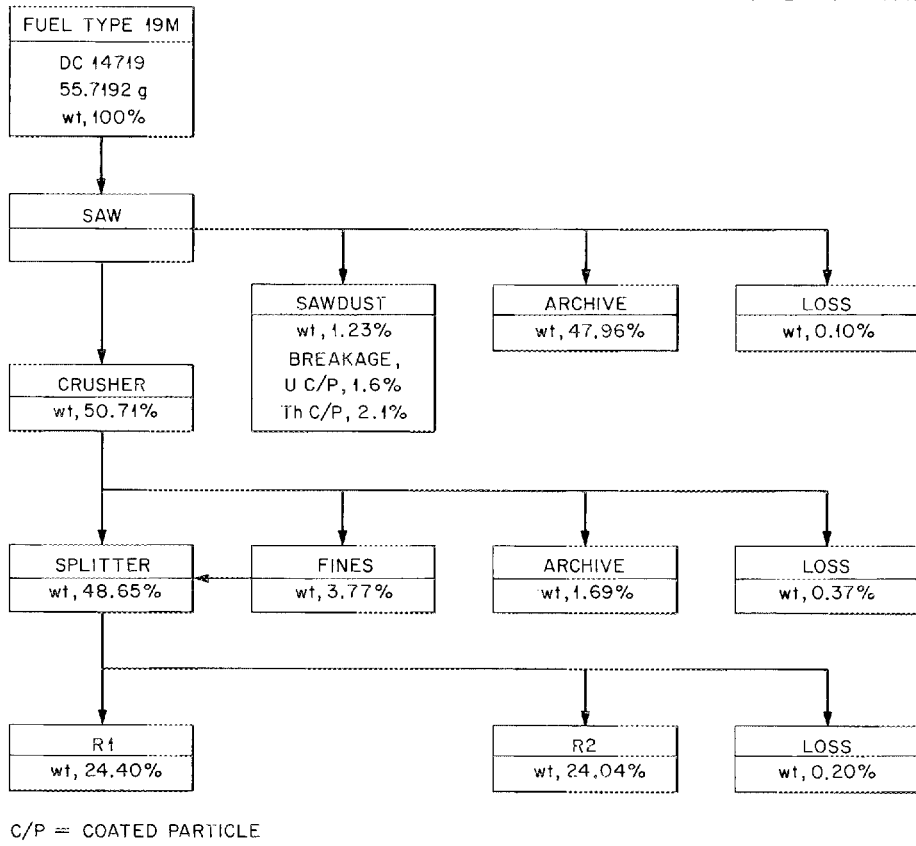


Fig. 1.1. Results of sawing, crushing, and sieving unradiated Dragon compact 14719, type 19M.

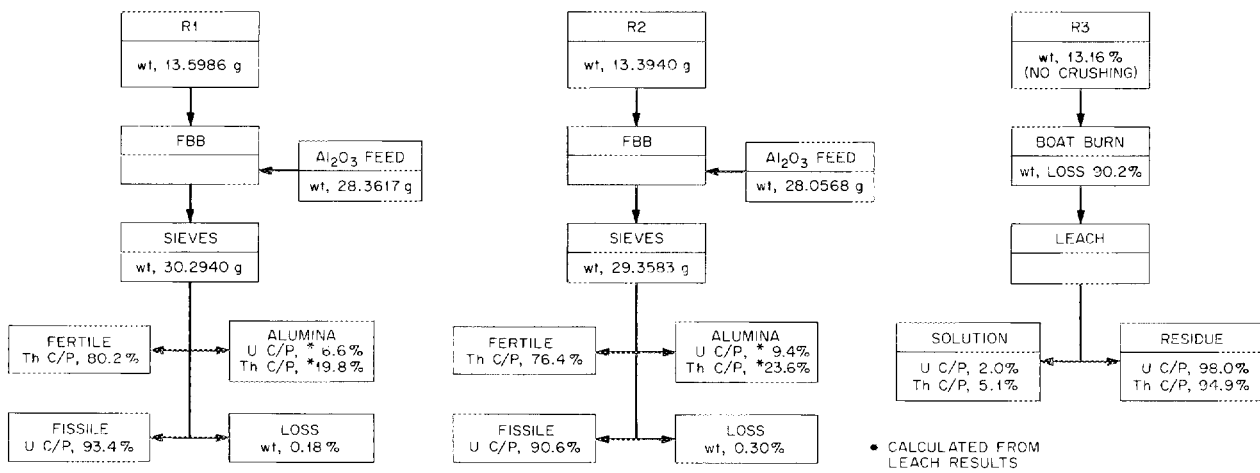


Fig. 1.2. Results of fluidized-bed burning, sieving, and leaching steps with Dragon compact 14719, type 19M.

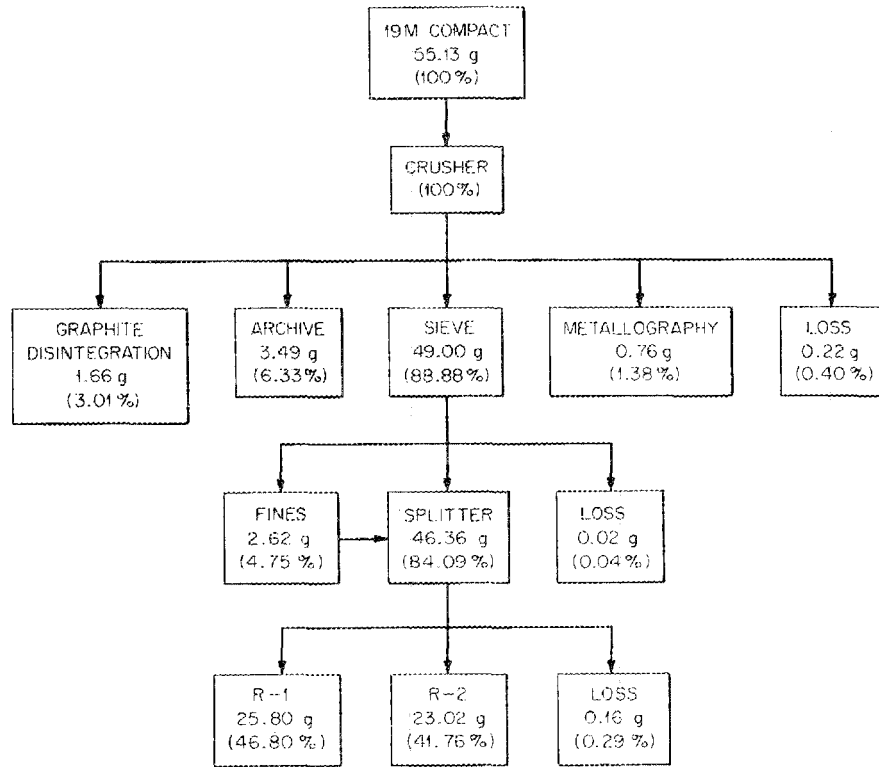


Fig. 1.3. Triso  $UC_{10}$ -Triso  $ThC_2$ : crushing and splitting of unnumbered irradiated Dragon compact, type 19M.

found while examining the burner product. The burner products were screened to separate fertile, fissile, and alumina fractions. The fertile and fissile particles for R-2 were recombined and leached to determine the nature of the gray residue. About 1% of the total uranium, 5% of the thorium, and 3% of the fission products were found in this leach. After leaching, the fertile and fissile particles were separated, and the standard procedure for Triso-coated particles was resumed for both replicates. This procedure involves (for both fertile and fissile particles) grinding, burning, and two Thorex leaches. Although the data have not been completely analyzed, there are some preliminary data available. Flow diagrams for the various operations are shown in Figs. 1.3 and 1.4, and Tables 1.6 and 1.7 present quantitative information from the burner operations.

The increased breakage experienced with fraction R-1 (presumably due to excessive burning temperatures) compared with R-2 is easily seen. The numbers reflect some inconsistency between the totals of each fraction. Therefore a third fraction (from a second 19M com-

compact) is being processed in a quiescent burner to resolve some of the questions.

The isotopic uranium concentrations were determined (Table 1.8). Assuming that the only source of  $^{233}U$  is the irradiated thorium in the fertile particle and that there is no separation of  $^{233}U$  from  $^{232}Th$  in the head-end steps, it is possible to use the ratio  $^{233}U/^{232}Th$  to test for internal consistency of the data. It is immediately obvious that this ratio for the +20 fraction from R-2 is out of line with the other values. Excluding this point, the range of this ratio for the remaining five samples of both runs is  $0.0273 \pm 0.0074$  (95% confidence, Student's  $t$  distribution). Since the total thorium recovered in R-2 is low, we assumed that the thorium value for the R-2 +20 fraction was low and calculated a new value using the average ratio and the  $^{233}U$  value for this sample. The calculated thorium value is 0.4214 g (vs 0.1056 measured). The total calculated yield of thorium for R-2 is thus 0.6098 g (vs 0.2940 g). Based on the fraction of thorium found in the +20-mesh sample, breakages of fertile particles for R-1 and R-2 are 79 and

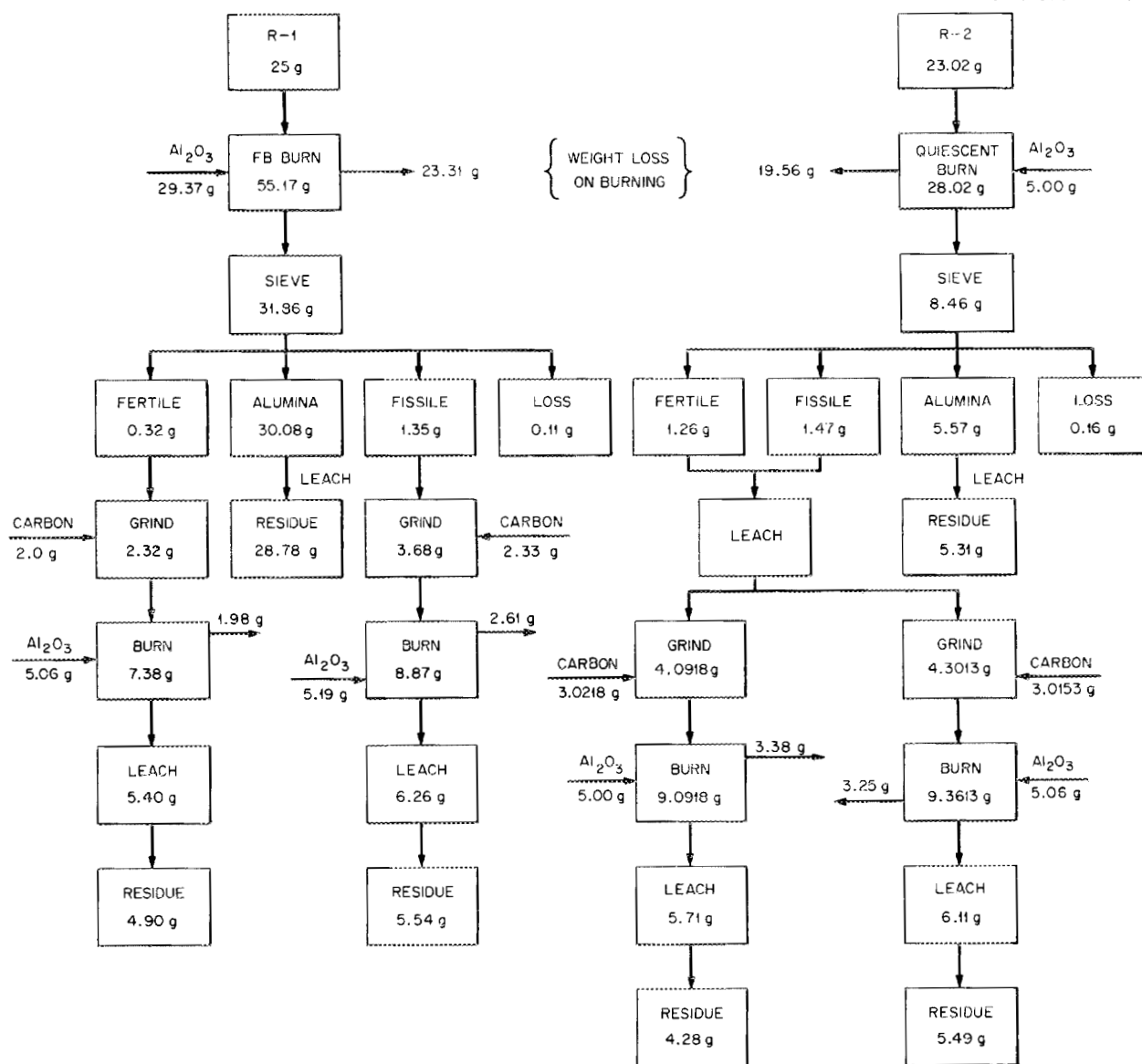


Fig. 1.4. Triso  $UC_{10}$ -Triso  $ThC_2$ : burning, sieving, and leaching of unnumbered irradiated Dragon compact, type 19M.

31%. Breakages of fissile particles based on the  $^{235}U$  content of the +42-mesh fraction (without correcting for  $^{235}U$  from  $^{232}Th$ ) for R-1 and R-2 are 24 and 13%. We conclude that the particle breakage was significantly increased under the conditions of fluidized-bed burning. (The temperature of burning was difficult to control with this sample.)

Crossovers of  $^{235}U$  to the  $^{233}U$  product (+20-mesh fraction plus -42-mesh fraction) for R-1 and R-2 were

24 and 13%, respectively, and of  $^{233}U$  to the  $^{235}U$  stream (+42-mesh fraction), 14 and 7% respectively. This latter crossover (7%) is surprising in that the +20- and the +42-mesh fractions from the first screening of R-2 were leached before grinding to avoid having broken fertile particles contribute to the fissile particle inventory. We must conclude that some of the SiC-coated fertile particles were smaller than 20 mesh, since the +20-mesh screen did not appear to be defective.

Table 1.6. Burner results for an irradiated Dragon compact, type 19M

	R-1	R-2	Calculated values, British data
Weight of fuel fed, g	25.80	23.02	
Weight of Al <sub>2</sub> O <sub>3</sub> fed, g	29.37	5.00	
Weight of burner product, g	31.86	8.46	
Percent weight loss on burning <sup>a</sup>	90.3	85.0	90.9 <sup>b</sup>
Percent +20-mesh fertile particles <sup>a</sup>	1.24	5.47	3.23
Percent +42-mesh fissile particles <sup>a</sup>	5.23	6.39	5.83
Percent fines <sup>c</sup>	102.4	111.4	

<sup>a</sup>Based on the weight of crushed fuel fed to the burner.

<sup>b</sup>Assumes no broken particles.

<sup>c</sup>Based on the weight of alumina fed to the burner; i.e., a fuel-free basis.

Table 1.7. Summary of weight material balances for an irradiated Dragon compact, type 19M

	R-1	R-2	Grand total
UC <sub>10</sub> , g	0.5023	0.6378	1.1401
ThC <sub>2</sub> , g	0.5779	0.3244	0.9023
Burnable carbon, calculated, g	23.4522	20.9252	44.3774
Burnable carbon, measured, g	23.31	19.56	42.87
Al <sub>2</sub> O <sub>3</sub> weight, g	39.4567	15.08	54.5367
Al <sub>2</sub> O <sub>3</sub> material balance, %	99.6	100.1	99.7
Sample weight, g	25.80	23.02	48.82
Overall material balance, %	97.6	93.8	96.2

**Fission product distributions and yields.** The fission product distributions are given in Table 1.9. Comparing ratios of fission products in the various fractions with similar thorium and uranium ratios, it was found that the <sup>95</sup>Zr and <sup>95</sup>Nb and (for R-2) the <sup>106</sup>Ru ratios were anomalous. The distribution of the others (<sup>134</sup>Cs, <sup>137</sup>Cs, <sup>144</sup>Ce, and <sup>106</sup>Ru for R-1) was similar to the distribution of the <sup>235</sup>U.

**Off-gas studies.** Krypton release data were obtained from all steps of the static bed burning run (R-2) (see Table 1.10). We found  $3.047 \times 10^{11}$  dis/min total. About 7% of the total <sup>85</sup>Kr was released in the first burning, presumably from unhydrolyzed broken particles. About 0.6% was recovered from the burner product ash (-42 mesh) during leaching, and 0.13% was recovered when the combined sieve products (+20 and +42 mesh) were leached. About 7.5% of the <sup>85</sup>Kr was

associated with the unbroken fertile particles (+20 mesh), and most of this (4.9%) was released in the crushing and roasting steps prior to the second burning. The remainder (84.6%) was associated with the fissile particles (+42 mesh). The majority of this (83.7%) was released in the grinding and preburn roast. In both cases  $\leq 0.1\%$  of the <sup>85</sup>Kr was left with the ashes.

The off-gas for the initial burning was analyzed for <sup>14</sup>C content. A 250-cc sample of the burner gas composite gave  $1.6 \times 10^5$  dis/min of <sup>14</sup>C, which corresponds to  $1.6 \times 10^6$  dis/min per gram of carbon burned. Based on the burnable carbon in an average FSVR fuel element, this gives 5.7 Ci/metric ton (U + Th). This value is about halfway between the yields calculated for 1 and 10 ppm N<sub>2</sub> impurity in the carbon charged to the reactor.

**Table 1.8. Isotopic uranium distribution in fluidized-bed burner product fractions**

Irradiated Dragon compact, type 19M

	Grams recovered				Percent	
	+20	+42	-42	Total	Measured	Calculated
<b>Sample R-1</b>						
U total	0.0075	0.2418	0.0846	0.3339	100	100
<sup>233</sup> U	0.0038	0.0022	0.0100	0.0160	4.79	4.0
<sup>234</sup> U	0.0005	0.0041	0.0023	0.0069	2.07	1.7
<sup>235</sup> U	0.0014	0.1389	0.0433	0.1836	54.99	50.4
<sup>236</sup> U	0.0004	0.0658	0.0169	0.0831	24.89	33.3
<sup>238</sup> U	0.0014	0.0307	0.0121	0.0442	13.24	10.7
Th total	0.1091	0.1037	0.3109	0.5237	100	
<b>Sample R-2</b>						
U total	0.0330	0.3451	0.0412	0.4242 <sup>a</sup>	100	100
<sup>233</sup> U	0.0115	0.0011	0.0032	0.0162 <sup>a</sup>	3.82	4.0
<sup>234</sup> U	0.0016	0.0057	0.0007	0.0081 <sup>a</sup>	1.91	1.7
<sup>235</sup> U	0.0100	0.1975	0.0175	0.2271 <sup>a</sup>	53.54	50.4
<sup>236</sup> U	0.0039	0.0956	0.0045	0.1045 <sup>a</sup>	24.63	33.3
<sup>238</sup> U	0.0060	0.0452	0.0153	0.0683 <sup>a</sup>	16.10	10.7
Th total	0.1056	0.0491	0.1042	0.2940 <sup>a</sup>	100	

<sup>a</sup>Includes 0.0049 g uranium and 0.0351 g thorium recovered from the first burning screen product (+20- and +42-mesh beads) by leaching.

**Table 1.9. Fission product distribution in fluidized-bed burner product crusher fractions for an irradiated Dragon compact, type 19M**

Fraction	Fission product (dis/min)						Gross gamma (counts/min)
	<sup>95</sup> Zr	<sup>95</sup> Nb	<sup>106</sup> Ru	<sup>134</sup> Cs	<sup>137</sup> Cs	<sup>144</sup> Ce	
<b>Sample R-1</b>							
+20	$1.66 \times 10^9$	$3.20 \times 10^9$	$8.28 \times 10^9$	$2.17 \times 10^{10}$	$3.10 \times 10^{10}$	$8.75 \times 10^{10}$	$1.90 \times 10^{10}$
+42	$2.79 \times 10^{10}$	$3.65 \times 10^{10}$	$2.63 \times 10^{11}$	$9.57 \times 10^{11}$	$1.11 \times 10^{12}$	$2.98 \times 10^{12}$	$6.20 \times 10^{11}$
-42	$3.33 \times 10^{10}$	$6.21 \times 10^{10}$	$1.22 \times 10^{11}$	$3.95 \times 10^{11}$	$4.11 \times 10^{11}$	$1.49 \times 10^{12}$	$3.03 \times 10^{11}$
Total	$6.29 \times 10^{10}$	$1.02 \times 10^{11}$	$3.93 \times 10^{11}$	$1.37 \times 10^{12}$	$1.55 \times 10^{12}$	$4.56 \times 10^{12}$	$9.42 \times 10^{11}$
<b>Sample R-2</b>							
+20	$1.32 \times 10^{11}$	$3.04 \times 10^{11}$	$6.84 \times 10^{10}$	$1.52 \times 10^{11}$	$1.89 \times 10^{11}$	$2.21 \times 10^{11}$	$2.01 \times 10^{11}$
+42	$1.72 \times 10^{10}$	$1.14 \times 10^{10}$	$8.52 \times 10^{10}$	$1.11 \times 10^{12}$	$1.30 \times 10^{12}$	$2.55 \times 10^{12}$	$2.61 \times 10^{11}$
-42	$2.86 \times 10^9$	$1.43 \times 10^{10}$	$2.36 \times 10^{10}$	$1.34 \times 10^{11}$	$1.64 \times 10^{11}$	$2.75 \times 10^{11}$	$8.99 \times 10^{10}$
Total	$1.52 \times 10^{11}$	$3.30 \times 10^{11}$	$1.77 \times 10^{11}$	$1.40 \times 10^{12}$	$1.65 \times 10^{12}$	$3.05 \times 10^{12}$	$5.52 \times 10^{11}$

Table 1.10.  $^{85}\text{Kr}$  release during processing of R-2 fraction of an irradiated 19M Dragon compact

Operation	Percent of total $^{85}\text{Kr}$ release <sup>a</sup>
Initial burning	7.22
Residue leach (-42 mesh)	0.57
Fuel leach (+20 and +42 mesh)	0.13
+20-mesh fertile grinding	3.77
Ground particle roasting	1.13
Ground particle burning	2.50
Ground, burned particle leaching	0.06
+42-mesh fissile grinding	75.48
Ground particle roasting	8.20
Ground particle burning	0.82
Ground, burned particle leaching	0.10

<sup>a</sup>Total  $^{85}\text{Kr}$  recovered =  $3.047 \times 10^{11}$  dis/min.

### 1.3.5 Head-End Studies on Unirradiated Compact 22396, Type 2M4 (Biso Oxide)

This experimental fuel is from the Dragon Project Metallurgical Series II. The kernel is  $(10\text{Th/U})\text{O}_2$ , 60 to 70% of theoretical density, 422 to 600  $\mu\text{m}$  in diameter (523  $\mu\text{m}$ , av), and has two pyrolytic carbon coatings (40/80  $\mu\text{m}$ ). The density of the outer coating is 2.0 g/cc, with a Bacon anisotropy factor of 1.18. The compact contained 14% coated particles by volume.

This type of fuel is similar to the reference recycle fuel proposed for commercial 1100-MW(e) reactors. Although separation of  $^{233}\text{U}$  from  $^{235}(^{236})\text{U}$  is not required for the recycle fuel blocks, this type of particle might also be used with a Triso- or a Biso-coated  $\text{UO}_2$  fissile particle (which would convert to  $\text{U}_3\text{O}_8$  powder on burning) in makeup fuel blocks. Consequently, separation by sieving was tested on the burner product before leaching.

The compact was sawed in half, and the saw fines were collected, weighed, and added to the crusher product before sieving. One half of the compact was crushed by the standard procedure to give the fractions shown in Table 1.5. The crushed material was sieved, and each sieve fraction  $\geq 42$  mesh was divided into two samples (Fig. 1.5). Each of the samples was composited with one sample from the other sieve fractions to produce duplicate samples of crushed fuel. The crusher fines ( $< 42$  mesh) were burned and leached. Crusher breakage was about 1.2%, and handling losses were less than 1%.

Each of the duplicate samples was burned in a fluidized bed at 750°C, as before. The burner product

was sieved into a series of sizes, inspected, and composited into +60- and -60-mesh fractions (Fig. 1.6). The fractions were leached, and 82 to 85% of the fuel was found in the +60-mesh fraction and 15 to 17.5% in the -60-mesh fraction. This result indicated that oxide kernels more durable than those in this compact would be required if particle separation based on size is required for Biso-coated oxide particles. The burn-leach process is suitable for this unirradiated recycle type of fuel if particle separation is not required. Overall losses to insoluble residues were 0.05% of the uranium and 0.21% of the thorium.

### 1.3.6 Head-End Studies of Irradiated Compact 22365, Type 2M4 (Biso Oxide)

Compact 22365 was sawed and split as shown in Fig. 1.7. A half-compact napkin ring was used for crush-burn-leach studies. The archive half compact was sectioned to provide a sample for graphite disintegration study of the coated particle integrity. The relatively large amount of sawdust was due to difficulties in hand sawing in the hot cell, and a number of X-Acto saw blades were worn out without much progress. Final cutting was done with a commercial hacksaw blade. The recovered sawdust was sieved and added to the corresponding sieve fractions from the crushed half compact before splitting and burning of R-1 and R-2 fractions.

The half compact was fed vertically into the jaw crusher at  $\frac{5}{8}$ -in. opening, and the product was passed through the crusher again at  $\frac{3}{16}$ -in. jaw opening. The crusher product was sieved. Results are shown in Fig. 1.8. After sieving, the +42-mesh fraction from the sawdust and the intermediate sieve fractions (+9 to +42) were split into two replicate samples, R-1 and R-2, for burn-leach studies. The +4-mesh fraction was retained for future studies, and the  $\pm 100$  fractions (sawdust plus crusher fines) were leached for combined breakage. Handling losses were less than 1% in these steps.

The leaches and residues were analyzed and summed without material balance corrections. We felt that uncertainties in assigning losses to inert materials and/or to heavy metals were too great to risk introducing significant errors by arbitrary corrections to these high-burnup samples (58% fissions per initial fissile atom).

The weight material balance summary data are presented in Table 1.11. Fission product weights were estimated from a computer printout of the Dragon irradiation ( $1.375 \times$  uranium output weight = fission

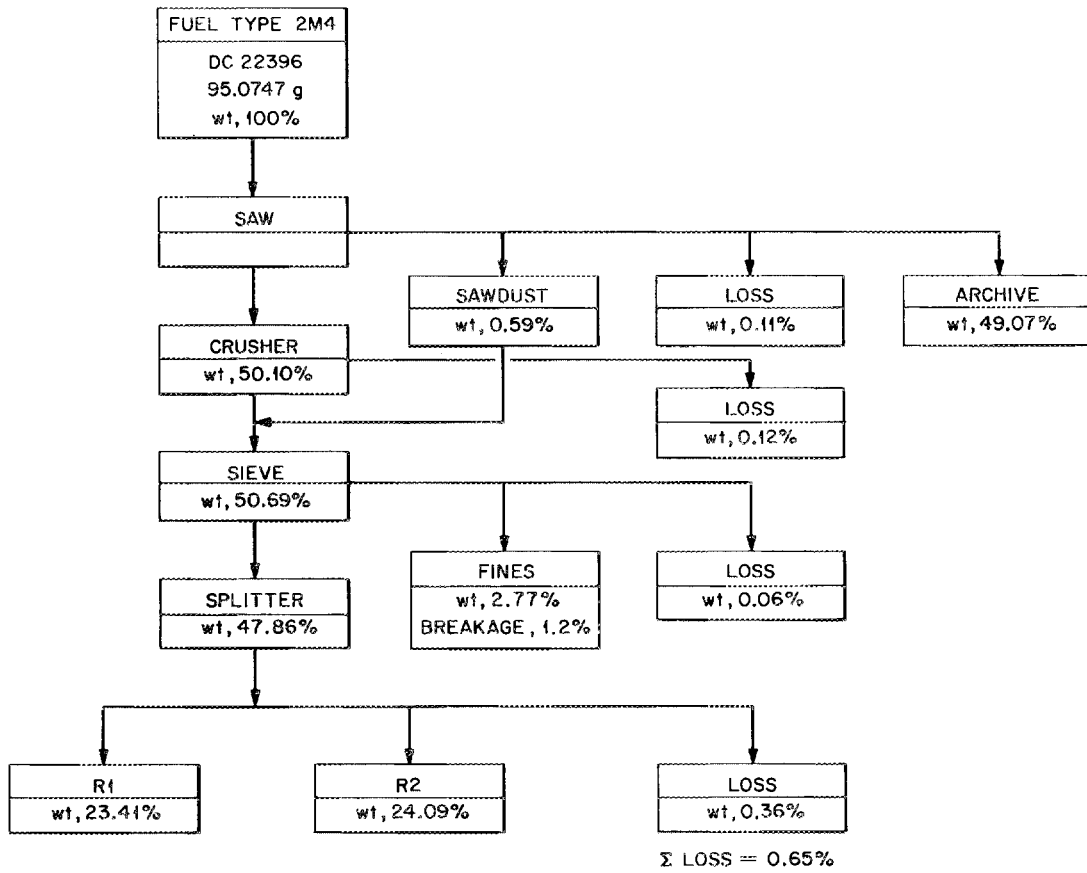


Fig. 1.5. Results of crushing and dividing Dragon compact 22396, type 2M4.

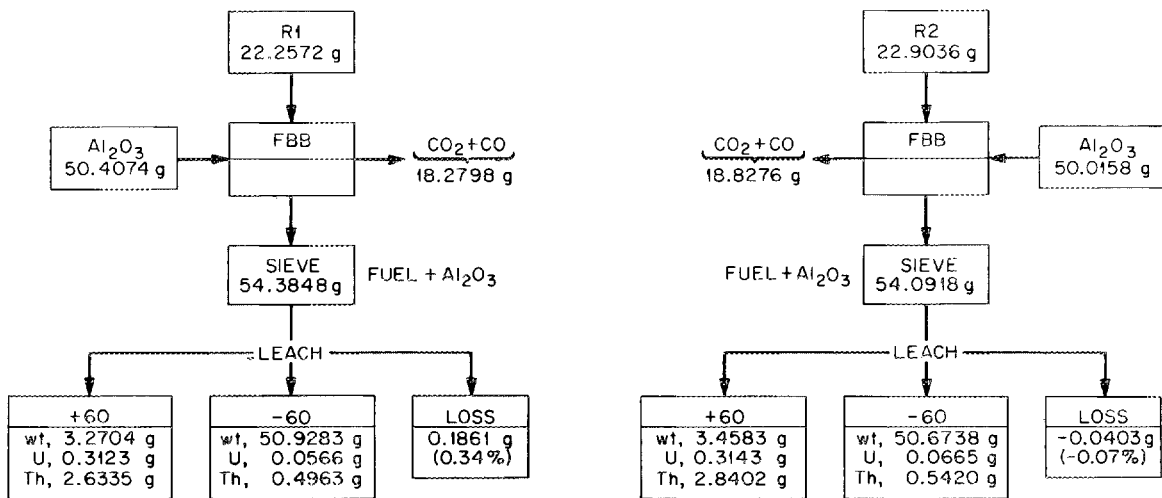


Fig. 1.6. Results of fluidized-bed burning, sieving, and leaching steps with unirradiated Dragon compact 22396, type 2M4.

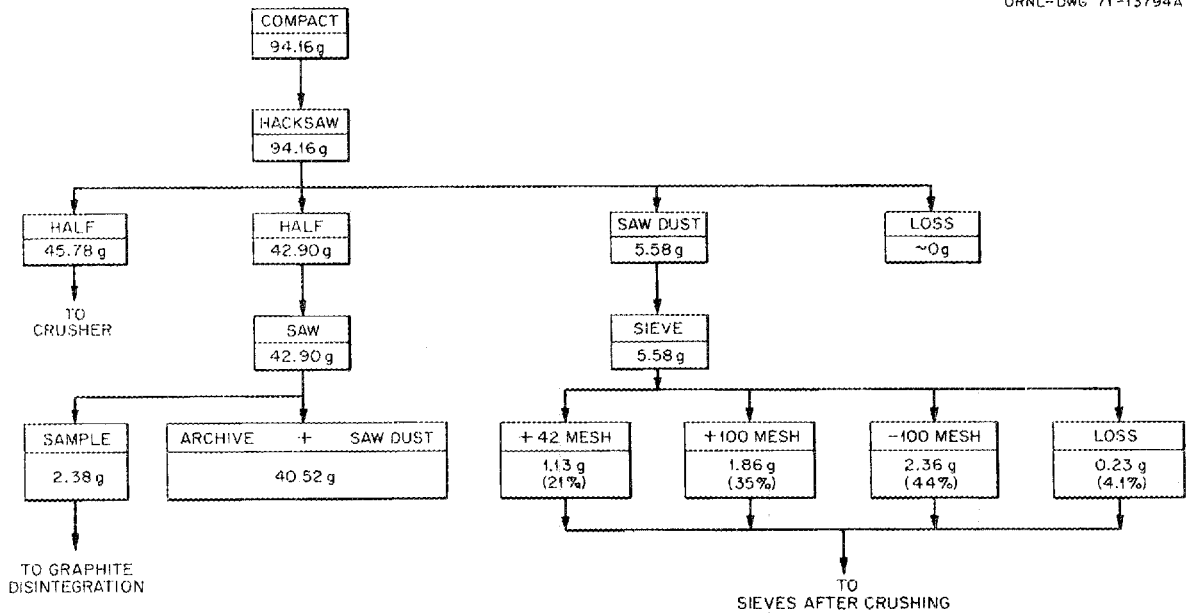


Fig. 1.7. Sawing of compact 22365: irradiated Biso oxide, type 2M4.

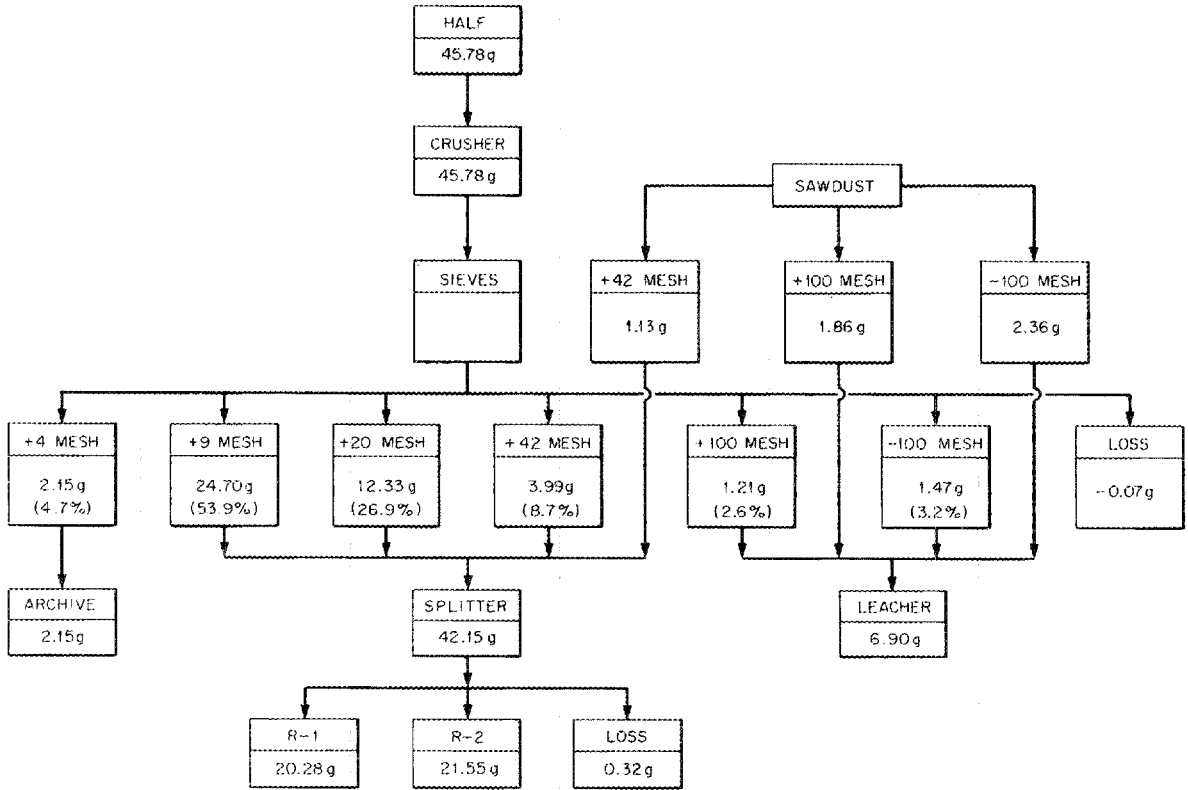


Fig. 1.8. Crushing and sieving of compact 22365: irradiated Biso oxide, type 2M4.

Table 1.11. Summary of weight material balances for compact 22365, Biso oxide

Initial compact weight, 94.16 g					
	R-1	R-2	Crusher + saw fines	Graphite disintegration	Grand total
UO <sub>2</sub> , g	0.2882	0.3212	0.1343 <sup>a</sup>	0.0109 <sup>a</sup>	0.7546
ThO <sub>2</sub> , g	3.4541 <sup>a</sup>	3.1010	0.5421 <sup>a</sup>	0.1010 <sup>a</sup>	7.2071
Fission products, <sup>b</sup> g	0.3493	0.3894	0.1628	0.1221	1.0236
Burnable carbon, g					
Calculated	16.53	17.56	5.62	1.94	
Measured	16.76	17.55	5.78 <sup>c</sup>	2.16	42.20
Al <sub>2</sub> O <sub>3</sub> weight, <sup>d</sup> g	29.20	5.00			34.20
Al <sub>2</sub> O <sub>3</sub> material balance, <sup>e</sup> %	94.1	92.2			93.8
Sample weight, <sup>d</sup> g	20.28	21.55	6.90	2.38	51.11
Sample material balance, <sup>e</sup> %	102.8	99.2	93.9	95.6	99.7

<sup>a</sup>Questionable values (see text).

<sup>b</sup>Calculated assuming that weight of fission products as oxides was  $1.375 \times$  weight of uranium recovered (based on analogy to computer run for this material).

<sup>c</sup>Residue weight only (leached, not burned).

<sup>d</sup>Feed weights as measured in hot cell.

<sup>e</sup>(Output/input)  $\times$  100.

product oxides). Matrix graphite and pyrolytic carbon (burnable carbon) were estimated by weight loss during burning and residues from graphite disintegration. A total of 82.5% by weight was found. The unirradiated compact analyzed 81.5% burnable carbon.

Material balances on total summed sample weights were 93.9 to 102.8%, and the grand total was 99.7%. Alumina material balances were 92 to 94% and could reflect some losses by solubility in Thorex reagent and in handling of the final residues.

We conclude that handling losses are within acceptable limits and the totals of the data are reasonable.

**Estimate of fraction of particle coatings broken in irradiation.** A graphite disintegration step was performed on a sawed, dust-free 2.38-g sample of compact. The two leaches (white fuming nitric acid followed by Thorex reagent) contained 0.0083 g of uranium and 0.0776 g of thorium. The bulky sludge residues were analyzed, with no meaningful results. It will probably be necessary to burn these routinely before analysis in the future. Assuming that the composition of the entire piece is the same as for R-2, the calculated total uranium and thorium values are 0.0312 and 0.302 g, respectively, for this sample. Thus the original particle breakage estimate is 26.7% based on uranium and 25.7% based on thorium.

**Breakage of particles due to sawing and crushing.** The saw fines (4.22 g) and the crusher fines (2.68 g) were

composed (6.90 g) and leached twice with Thorex reagent. Totals of 0.118 g of uranium and 0.473 g of thorium were found. The unburned residue was analyzed, with no meaningful results. With the same procedure as before, we calculated that the fines could have contained as much as 0.0906 g of uranium and 0.875 g of thorium. Particle breakage due to sawing and crushing is 130% based on uranium and 54.1% based on thorium. One must assume that the saw and crusher fines have the same composition as the compact.

**Uranium isotopic material balances.** The Dragon data indicated the compact contained 1.3514 g <sup>235</sup>U and 12.7 g <sup>232</sup>Th as loaded. The combined fractions R-1 and R-2 analyzed in parts totaled 41.83% of the weight of the compact. No corrections were applied, although the thorium value for R-1 is probably high. Mass spectrometer assay of the principal uranium products averaged 28.01% <sup>233</sup>U, 3.70% <sup>234</sup>U, 45.28% <sup>235</sup>U, 14.66% <sup>236</sup>U, and 8.34% <sup>238</sup>U. Input uranium assay was assumed to be typical of 93%-enriched uranium.

The material balances are given in Table 1.12. One test of the internal consistency of the data is the good agreement for the quantities of <sup>238</sup>U.

**Leaching studies.** The fractions of heavy metals and fission products in the leaches of the +60- and -60-mesh (alumina) fractions from the burner are given in Tables 1.13 and 1.14. These indicate that 10 to 20%

Table 1.12. Uranium isotopic material balances, compact 22365, Biso oxide (burnup 58% fissions per initial fissile atom)

Basis: 41.83% of total compact analyzed and summed

Isotope	Input <sup>a</sup> (g)	Output <sup>a</sup> (g)
<sup>233</sup> U	0	0.1505
<sup>234</sup> U	0.0045	0.0199
<sup>235</sup> U	0.5610	0.2433
<sup>236</sup> U	0	0.0788
<sup>238</sup> U	0.0423	0.0448
Total U	0.6078	0.5373
<sup>232</sup> Th	5.312	5.769 <sup>b</sup>

<sup>a</sup>Four decimal places are quoted for arithmetical consistency; precision is probably limited to ±5% of totals.

<sup>b</sup>Believed to be high.

Table 1.13. Heavy-metal distribution in the leached burner products of compact 22365, type 2M4, Biso oxide

	Sample R-1		Sample R-2	
	U	Th	U	Th
Total recovered, g	0.2541	3.0356 <sup>a</sup>	0.2832	2.7330
Percent <sup>b</sup> of total in:				
+60-mesh fraction				
Leach 1	79.6	94.8 <sup>a</sup>	89.2	89.6
Leach 2	0.6	1.0	0.7	0.7
Residue	0.03	0.001	NA <sup>c</sup>	NA <sup>c</sup>
Total	80.2	95.8	89.8	90.2
-60-mesh fraction				
Leach 1	18.9	3.8 <sup>a</sup>	10.2	9.6
Leach 2	0.8	0.4	0.1	0.1
Residue	0.08	0.04	0.06	0.02
Total	19.8	4.2	10.2	9.8

<sup>a</sup>Questionable value.

<sup>b</sup>Rounded to one decimal place.

<sup>c</sup>Not available.

Table 1.14. Fission product distribution in the leached burner products of compact 22365, type 2M4, Biso oxide, sample R-2

	Gross gamma	<sup>95</sup> Zr	<sup>95</sup> Nb	<sup>106</sup> Ru	<sup>134</sup> Cs	<sup>137</sup> Cs	<sup>144</sup> Cs
Recovered counts/min or dis/min (total)	$7.43 \times 10^{11}$	$2.13 \times 10^{11}$	$2.21 \times 10^{11}$	$1.96 \times 10^{11}$	$9.02 \times 10^{11}$	$1.20 \times 10^{12}$	$4.88 \times 10^{12}$
Percent <sup>a</sup> of total in:							
+60-mesh fraction							
Leach 1	82.0	86.4	50.2	43.4	84.6	85.0	88.9
Leach 2	2.0	1.3	18.2	4.5	0.8	0.7	0.6
Residue <sup>b</sup>							
Total	83.9	87.8	68.3	47.9	85.4	85.8	89.5
-60-mesh fraction							
Leach 1	12.8	11.5	17.1	6.5	13.6	13.4	10.2
Leach 2	0.7	0.5	7.7	2.3	0.2	0.2	0.2
Residue	2.5	0.2	7.2	43.2	0.7	0.6	0.02
Total	16.2	12.2	32.0	52.0	14.6	14.3	10.4

<sup>a</sup>Numbers are rounded; may not add precisely to 100%.

<sup>b</sup>Weight 0.15 g, not analyzed.

of the fuel materials were smaller than 60 mesh, similar to that found for the unirradiated compact. The thorium analyses for fraction R-1 are suspect. The combined residues contained less than about 0.1% of

the heavy metals and varying amounts of fission products. About 2.5% of the total gross gamma activity and about 43% of the total ruthenium activity were found in the alumina residue.

### 1.3.7 Head-End Studies of a Synthetic Mixture – Triso $UC_{20}$ -Biso $(5Th/U)C_{2.4}$ [a Possible 1100-MW(e) Makeup Fuel Type]

Compact 14397, Dragon Project Metallurgical Series II, containing type 18M fuel, has a kernel of  $UC_{20}$  that is 422 to 600  $\mu m$  in diameter and 60 to 70% of theoretical density. The standard Dragon Triso coating was used (PyC/SiC/PyC: 25/30/70  $\mu m$ ). Compact 14158 (Metallurgical Series II), containing type 38M fuel, has a kernel of  $(5Th/U)C_{2.4}$  that is 600  $\mu m$  in diameter and 60 to 70% of theoretical density. It has a two-layer PyC coating 121  $\mu m$  thick.

In a synthetic mixture made up of these two fuel types, the Biso  $(U,Th)C_2$  particle represents the  $^{233}U$  recycle particle. Briefly, head-end reprocessing consists of crushing, burning, and leaching. The unbroken Triso particles are recovered for storage by separation according to size after burning or after leaching. The Biso particles, which should burn to a fine oxide powder, would be recovered from the alumina by leaching.

The flowsheets for the crushing step and the results obtained are given in Figs. 1.9 and 1.10. The three middle-size fractions (+9, +20, +42) were each divided into two samples, which were combined between

compacts to give duplicate samples R-1 and R-2 for burn-leach testing. The fine fractions ( $-42$  mesh) were burned and leached to determine particle breakage during comminution operations. Less than 0.1% of the Triso  $UC_{20}$  and 4% of the Biso  $(5Th/U)C_{2.4}$  particles were found to be broken.

Samples R-1 and R-2 were burned in a fluidized bed with about 1 g of  $Al_2O_3$  per gram of fuel (Fig. 1.11). The burner product was sieved to recover a fissile fraction (Triso particle, +35 mesh), a fertile fraction ( $-35$  +60 mesh), and the alumina fraction ( $-60$  mesh). The three fractions were leached, and 3 to 11% of the leachable oxides (Th + U) were found in the fissile fraction, 52 to 58% in the fertile fraction, and the remaining 32 to 45% in the alumina fraction. Losses to the insoluble residue consisted of <0.1% of the heavy metals.

A rather unexpected result was the finding of 3 to 10% of the oxidized carbide particles in the fissile ( $+35$ -mesh) fraction. The oxidation apparently occurred without completely reducing the carbide particle to a fine ash. This occurrence makes leaching of the fissile fraction of this fuel mandatory. It may be necessary to determine whether failure of the particles to crumble

ORNL-DWG 71-6329

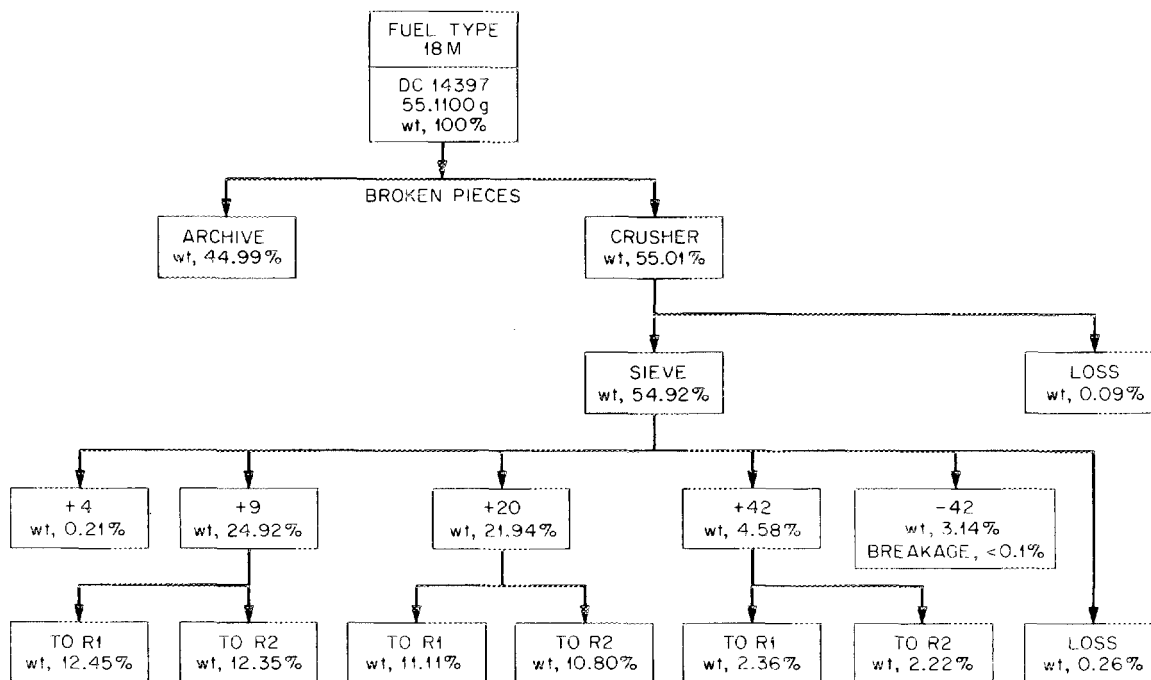


Fig. 1.9. Results of crushing and sieving unirradiated Dragon compact 14397, type 18M.

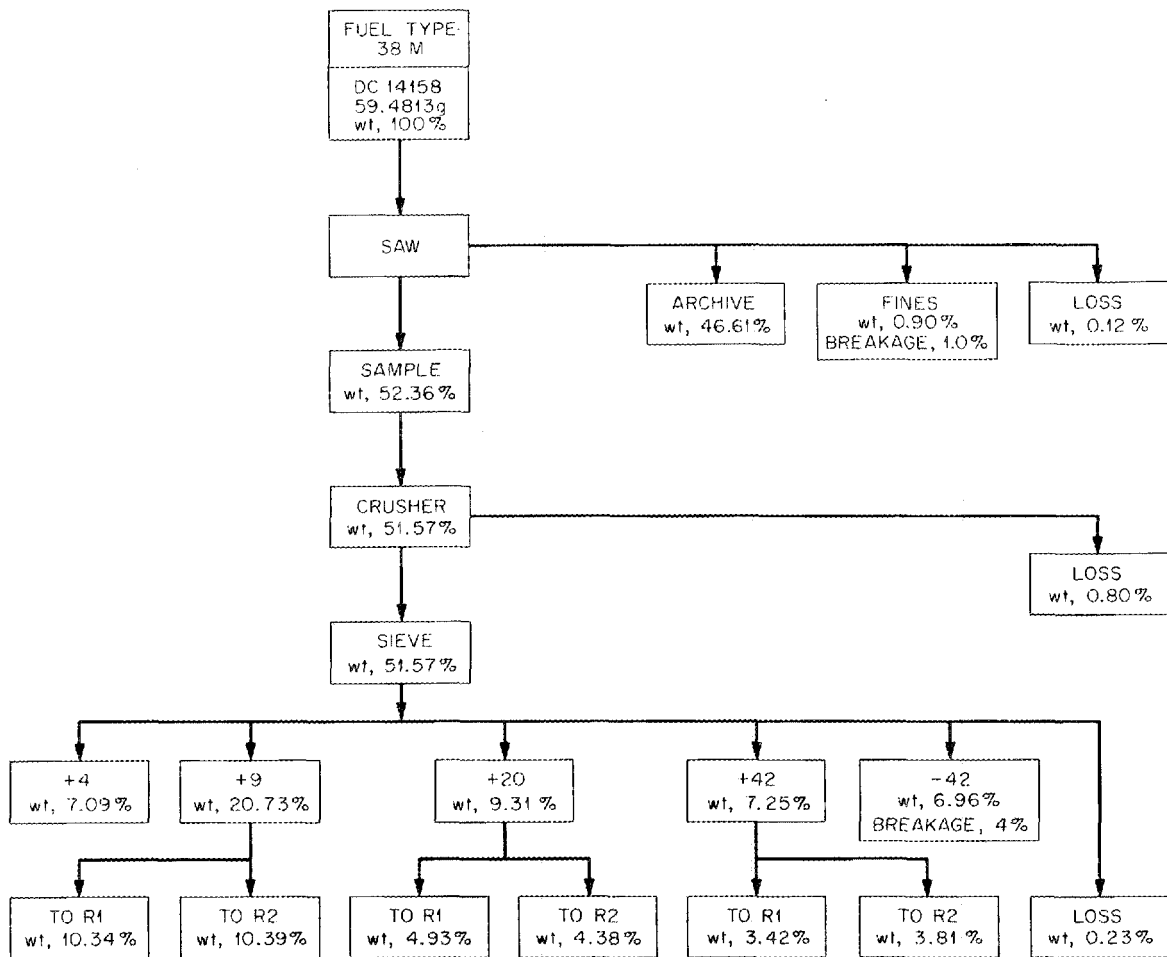


Fig. 1.10. Results of sawing, crushing, and sieving unirradiated Dragon compact 14158, type 38M.

during oxidation or agglomeration of ash particles in the fluidized bed led to this result. In experiments<sup>6</sup> with compacts irradiated in the Peach Bottom reactor, reuse of the alumina fraction was precluded by an accumulation of heavy metals in this fraction when the bed ash was sieved into an alumina (+120-mesh) fraction and a fines (-120-mesh) fraction. This accumulation was attributed to heavy-metal oxide sticking to the alumina particles. In light of the above result, this might have been due to incomplete powdering of the fuel kernel and separation of a third fraction (i.e.,

+80-mesh oxide). This question can only be answered by alumina recycle tests using irradiated Bisco-coated thorium-uranium carbides.

In the experiment as carried out, the sieved burner products were leached in three fractions. However, using the original sieve weight distribution, we calculated that, if the alumina had been screened to the size range of the original alumina (-80 +100 mesh), only about 10 to 15% of the heavy metals would have been found with the alumina. Thus it may be possible to recover 85 to 90% of the heavy metals by leaching only the small amounts of material present with +80- and -100-mesh fractions. By close-screening (-80 +100 mesh) the alumina, it may be possible to recycle the alumina fraction to the burner without leaching.

6. V. C. A. Vaughn et al., *Hot-Cell Evaluation of the Burn-Leach Method for Reprocessing Irradiated Graphite-Base HTGR Fuels*, ORNL-4120, p. 45 (February 1970).

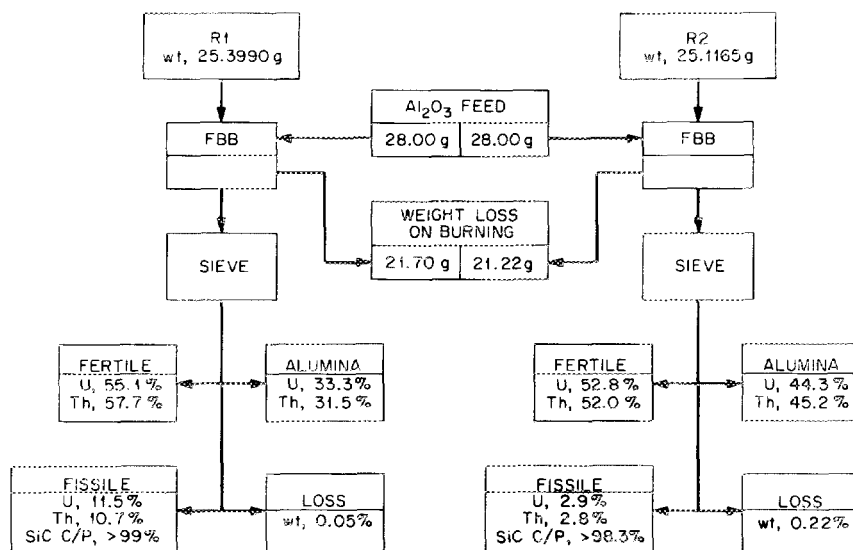


Fig. 1.11. Results of fluidized-bed burning, sieving, and leaching steps with unirradiated Dragon compacts 14397 and 14158, types 18M and 38M.

#### 1.4 OFF-GAS HANDLING AND DECONTAMINATION

P. A. Haas

The off-gas from burning irradiated HTGR graphite fuel elements will contain radioactive gases, which must be removed before discharge of the  $\text{CO}_2$  and other components to the environment. A literature search has been made to collect information on processes that might be used to effect a decontamination of the off-gas. These are reported in order to indicate the scope of study made and to point out those possibilities most deserving of experimental investigation.<sup>7</sup>

As presently envisioned, the head-end reprocessing of spent HTGR fuel elements will produce an off-gas rich in carbon dioxide and containing radioactive contaminants. Amounts of major off-gas constituents of special concern were estimated to obtain an idea of the magnitude of the off-gas problem at the scale of the TURF demonstration.<sup>8</sup> These are presented in Table 1.15. The ORIGEN code was used to calculate the

amount of contaminants, and these estimates are given in Table 1.16 for two fuel exposures. As planned, 9.7 FSVR fuel elements will be processed per day. It is assumed that the elements will have cooled no less than 150 days. Exposure for these elements will vary from one to six years. Burning the whole element would substantially increase the amount of off-gas to be treated as compared with partial element burning. Both burning methods are being considered since each offers advantages and holds uncertainties at the present stage of development. Thus, while it is not possible to state the exact composition of the off-gas from the proposed TURF demonstration, the estimates in Tables 1.15 and 1.16 indicate the magnitude of part of the decontamination problem to be solved.

The principal decontamination problem being considered at present is that of separating part-per-million concentrations of  $^{85}\text{Kr}$  from gas which is predominantly carbon dioxide, with smaller amounts of oxygen, nitrogen, and perhaps carbon monoxide. The target decontamination factor is  $10^2$ ; that is, at least 99% of the krypton must be collected in a concentrated form for storage. Several other fission products will probably require detailed attention.

Certain physical similarities of krypton and  $\text{CO}_2$  appear to preclude the practical use of several processes commonly employed or suggested for noble-gas separation. Specifically, membrane permeation, charcoal and

7. R. W. Glass, P. A. Haas, R. S. Lowrie, and M. E. Whatley, *HTGR Head-End Processing: A Preliminary Evaluation of Processes for Decontamination of Burner Off-Gas*, ORNL-TM-3527 (in preparation).

8. *National HTGR Fuel Recycle Development Program Plan*, ORNL-4702 (August 1971).

Table 1.15. Estimates<sup>a</sup> of the amounts of noncondensable head-end off-gas constituents based on the TURF demonstration scale

Major component	Partial (25%) element burning			Whole element burning		
	Lb/hr	Scfm	Vol %	Lb/hr	Scfm	Vol %
Carbon dioxide	212.5	28.9	89.7	494.2	67.2	89.7
Oxygen	13.0	2.4	7.5	30.4	5.7	7.5
Nitrogen <sup>b</sup>	4.2	0.9	2.8	9.8	2.1	2.8
Xenon <sup>c</sup>			26 ppm			61 ppm
Krypton <sup>c</sup>			6.8 ppm			16 ppm
Total	229.7	32.2	100	534.4	75.0	100

<sup>a</sup>Estimates are based on currently proposed processing of 9.7 FSVR fuel elements (150-day-cooled material) per 24-hr day.

<sup>b</sup>The nitrogen need not be present; changes in operating procedures can eliminate it.

<sup>c</sup>Xenon and krypton are given in ppm rather than vol % because of the relatively small amounts of them. It is assumed that the elements have been irradiated six years in the FSVR.

Table 1.16. Estimates of content of selected radioactive products of irradiation in the fuel based on processing 9.7 FSVR fuel elements per 24-hr day after 150 days cooling

Nuclide	Activity (Ci/day)	Type of radiation	Expected form <sup>a</sup> in the off-gas
<sup>134,137</sup> Cs	$8.5 \times 10^4$	Beta	Aerosol
<sup>144</sup> Ce	$8.3 \times 10^4$	Beta	Aerosol
<sup>89,90</sup> Sr	$4.4 \times 10^4$	Beta	Aerosol
<sup>85</sup> Kr	$5.5 \times 10^3$	Beta	Gas
<sup>238</sup> Pu	$1.0 \times 10^3$	Alpha	Aerosol
<sup>242,244</sup> Cm	670	Alpha	Aerosol
<sup>3</sup> H <sup>b</sup>	100	Beta	Vapor
<sup>129,131</sup> I	1.6	Beta	Vapor
<sup>14</sup> C <sup>b</sup>	0.2	Beta	Gas

<sup>a</sup>In all instances except <sup>85</sup>Kr, and perhaps <sup>129,131</sup>I, the elements listed are expected to be present as oxides. Of the oxides, only those of <sup>3</sup>H and <sup>14</sup>C will be gaseous; the others will be solid-gas aerosols.

<sup>b</sup>The amounts of these materials could be increased substantially by impurities in the graphite; thus the amount of <sup>3</sup>H would be tripled by the presence of 7 ppm Li and <sup>14</sup>C would be tripled by the presence of 75 ppm N<sub>2</sub>.

molecular sieve sorption, and selective physical sorption by a third component show little promise as separation processes for use in head-end reprocessing of HTGR fuel elements. Thermal diffusion, hot-metal trapping, and chemical reaction of the rare gases are not practical for the amounts and composition of burner off-gas expected.

Of the processing schemes reviewed, four seem to hold potential for effecting the desired separation. In no case can feasibility be assured by available information, but no available information precludes their consideration. A cursory look at the economics of these processes suggests that their costs will not be prohibitive but, within the prevailing uncertainties, provides no basis for selecting one over another. In order of current emphasis the four processes are:

1. stagewise absorption of krypton in liquid CO<sub>2</sub> (KALC),
2. controlled solidification of CO<sub>2</sub> (CSC),
3. simple distillation of liquid CO<sub>2</sub> (DLC),
4. hot potassium carbonate sorption of CO<sub>2</sub> (HPC).

The absorption of krypton in liquid CO<sub>2</sub> (KALC) flowsheet is the only one that accomplishes both

separation and requisite concentration of the krypton. It has the advantages that the krypton is separated from the carbon monoxide, nitrogen (if any), and almost all of the oxygen early in the process and that all process streams are fluid, operating well above the liquidus of CO<sub>2</sub>. The primary uncertainty in this process is in knowledge of the distribution coefficient for krypton between liquid CO<sub>2</sub> and gases at temperatures of interest. While its value is known with sufficient accuracy to establish the plausibility of the separation, the design of engineering experiments and process evaluation cannot proceed without the more precise values currently being obtained (see sect. 1.4.1). The experimental engineering program will be greatly accelerated through use of the modified Freon absorption pilot plant developed for study of reactor off-gas decontamination at K-25.<sup>9</sup> One Freon plant is being modified so it can be operated with liquid CO<sub>2</sub> to make large-scale tests of the feasibility of the KALC process.

The controlled solidification process (CSC) promises a very high separation factor between CO<sub>2</sub> and krypton in a single stage and may find use as a final concentration step after a process such as KALC. Controlled solidification has the disadvantage of requiring a batch-wise handling of the solid CO<sub>2</sub>. Validation of the expected high separation factor is necessary before extensive further work can be justified.

The simple distillation (DLC) process requires, for its evaluation, the same experimental information that is needed for evaluation of the KALC process. We would expect to use simple distillation only to supplement the other processes to enhance separations needed from nongaseous radioactive contaminants.

#### 1.4.1 Solubility of Krypton in Liquid CO<sub>2</sub>

A. B. Meservey    K. J. Notz

The solubility of krypton in liquid CO<sub>2</sub> is being determined as a part of the study on the use of liquid CO<sub>2</sub> to scrub krypton from the O<sub>2</sub>-N<sub>2</sub> fraction of the HTGR burner off-gases. Engineering design and evaluation of this process require a knowledge of the solubilities of the above gases in liquid CO<sub>2</sub>. Data have been published for O<sub>2</sub> and N<sub>2</sub>,<sup>10-14</sup> but nothing on krypton was in the open literature at the time our work was started.

9. M. J. Stephenson, J. R. Merriman, and D. I. Dunthorn, *Experimental Investigation of the Removal of Krypton and Xenon from Contaminated Gas Streams by Selective Absorption in Fluorocarbon Solvents: Phase I Completion Report*, K-1780 (Aug. 17, 1970).

Very recently, Laser and Beaujean, at KFA Jülich, published some data on the Kr-CO<sub>2</sub> system in a progress report;<sup>15</sup> these data are shown in Fig. 1.12, replotted as the gas/liquid separation factor (mole fraction ratio of krypton in gaseous and liquid phases divided by mole fraction ratio of CO<sub>2</sub> in gaseous and liquid phases). Also shown in Fig. 1.12 are some calculated solubilities and some of our preliminary data. The first calculations (curves A and B) were made on the basis of ideal behavior, that is, by using Raoult's law and Dalton's law. Since the temperature range of interest is above the critical temperature of krypton, it was necessary to extrapolate the vapor pressure line of krypton beyond the critical point; differences between functions used to make the extrapolations are responsible for the difference between these two curves. Davis<sup>16</sup> did a much more refined series of calculations following Hildebrand and Scott's real solution theory allowing for nonideality in the liquid phase (curve C) and in both phases (curve D).

Our preliminary data were obtained by a tracer method (<sup>85</sup>Kr) with equipment which gave problems in sampling and temperature control. We have, therefore, designed and built a system which will obviate sampling; the concentration of <sup>85</sup>Kr in gaseous and liquid phases of a temperature-equilibrated charge will be determined by counting in situ. This equipment (Fig. 1.13) is currently being shaken down and calibrated.

The range of values shown in Fig. 1.12 for the separation factors permits an estimate to be made of the equipment and conditions necessary for krypton

10. I. R. Krichevskii et al., "Liquid-Gas Equilibrium in the N<sub>2</sub>-CO<sub>2</sub> System under Elevated Pressures," *Khim. Prom.* 1962, 169-71.

11. G. H. Zenner and L. J. Dana, "Liquid-Vapor Equilibrium Compositions of CO<sub>2</sub>-N<sub>2</sub>-O<sub>2</sub> Mixtures," *Chem. Eng. Progr. Symp. Ser.* 59(44), 36-41 (1963).

12. N. K. Muirbrook and J. M. Prausnitz, "Multicomponent Vapor-Liquid Equilibria at High Pressures: Part I. Experimental Study of the N<sub>2</sub>-O<sub>2</sub>-CO<sub>2</sub> System at 0°C," *A.I.Ch.E. J.* 11(6), 1092-96 (1965).

13. G. Kaminishi and T. Toriumi, "Gas Equilibrium under High Pressures: VI. Vapor-Liquid Phase Equilibrium in the CO<sub>2</sub>-H<sub>2</sub>, CO<sub>2</sub>-N<sub>2</sub>, and CO<sub>2</sub>-O<sub>2</sub> Systems," *Kogyo Kagaku Zasshi* 69(2), 175-78 (1966).

14. A. Fredenslund and G. A. Sather, "Gas-Liquid Equilibrium of the O<sub>2</sub>-CO<sub>2</sub> System," *J. Chem. Eng. Data* 15(1), 17-22 (1970).

15. KFA Jülich, *Reprocessing of Thorium-Containing Nuclear Fuels, Progress Report for Second Half 1970*, pp. 67-71 (February 1971).

16. W. Davis, Jr., *Calculated Liquid-Vapor Equilibria in the Systems CO<sub>2</sub>-Xe and CO<sub>2</sub>-Kr at -55 to +5°C*, ORNL-TM-3622 (in press).

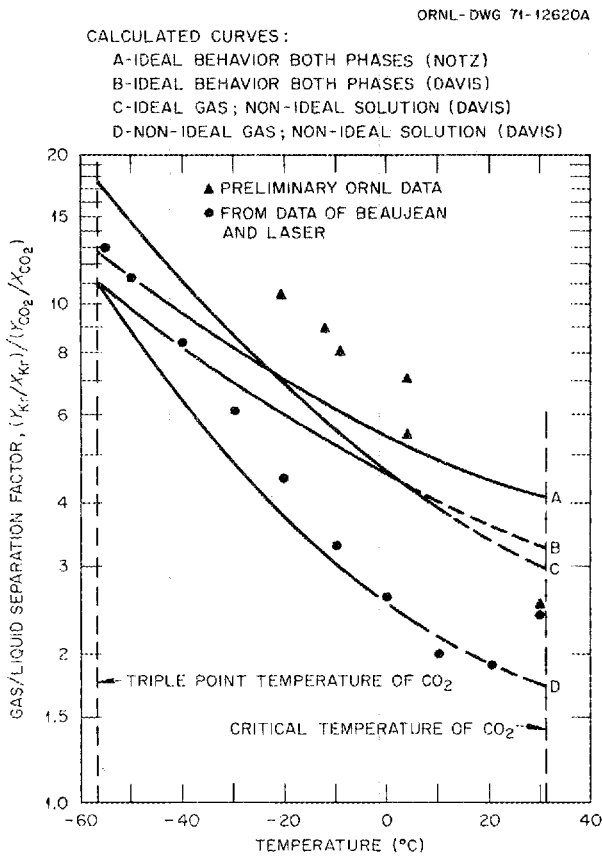


Fig. 1.12. Separation factors for the krypton-liquid CO<sub>2</sub> system.

scrubbing with CO<sub>2</sub>. However, more precise values will be needed in order to carry out a proper evaluation of pilot-scale work to be done on this process.

### 1.4.2 Krypton Solubility in Hot Carbonate Solution

K. J. Notz

One factor pertinent to the design and operation of the hot carbonate process for the separation of krypton from CO<sub>2</sub> is the solubility of krypton in the carbonate solution. The process customarily is operated under pressure during the absorption cycle, which will increase the amount of krypton dissolved. Furthermore, the solubility of the rare gases in water is reported to increase at higher temperatures.<sup>17,18</sup> However, a major factor acting to minimize the quantity of krypton that might be dissolved in hot carbonate solution is dilution by the O<sub>2</sub> (and N<sub>2</sub>), which comprises 7 to 10% of the total burner off-gas. By use of data on the room-temperature solubility of krypton in water,<sup>19</sup> it was estimated that 3% of the total krypton would carry

17. S. Glasstone, *Textbook of Physical Chemistry*, 2d ed., p. 696, Van Nostrand, 1954.  
 18. R. Battino and H. L. Clever, *Chem. Rev.* 1966, 395-463.  
 19. A. Seidell and W. F. Linke, *Solubilities of Inorganic and Metal-Organic Compounds*, vol. II, 4th ed., p. 341, American Chemical Society, 1965.

ORNL-DWG 71-12622A

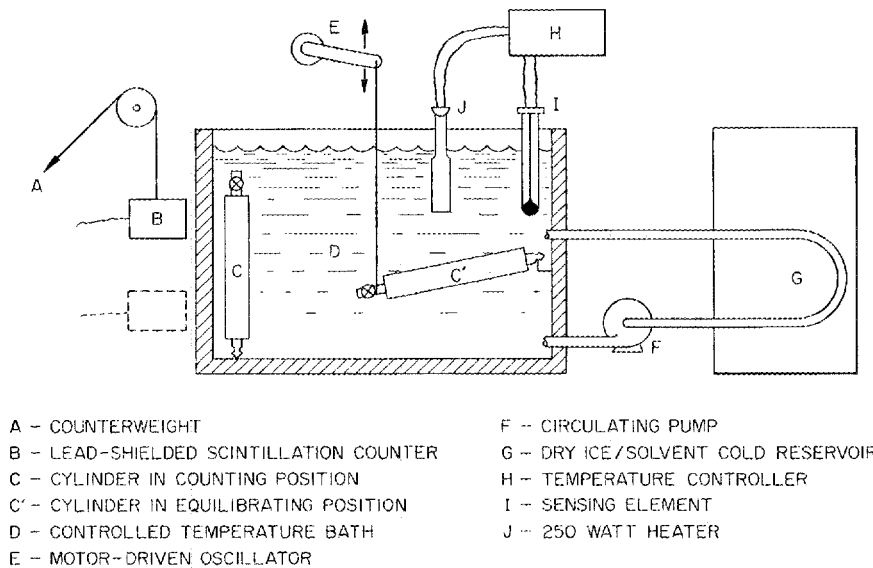


Fig. 1.13. Equipment for measuring solubility of krypton in liquid CO<sub>2</sub>.

over with the  $\text{CO}_2$ , an amount in excess of our tentative allowable decontamination factor of 100. Since both temperature and salting-out effects promised to be significant relative to krypton solubility, a thorough search of the literature was made. Pertinent data<sup>19-23</sup> are plotted in Fig. 1.14, where it is seen that the krypton solubility is at a minimum near  $100^\circ\text{C}$  but that the minimum is rather broad. Acid addition has very little effect, but there is an increasing effect as the alkalinity of the electrolyte increases; carbonate addition should produce an effect lying between those for  $\text{CaCl}_2$  and  $\text{NaOH}$ . Allowing for both of the above effects, the estimated solubility of krypton in 20% potassium carbonate solution at  $120^\circ\text{C}$  and under 20 atm total pressure ( $\text{Kr} + \text{O}_2 + \text{N}_2 + \text{CO} + \text{CO}_2$ ) is about 1% of the total present in the burner off-gas. This indicates that the carbonate process would require one or more stripping stages to recycle krypton (and a small amount of  $\text{CO}_2$ ) to assure  $\geq 99\%$  removal of krypton from the  $\text{CO}_2$ .

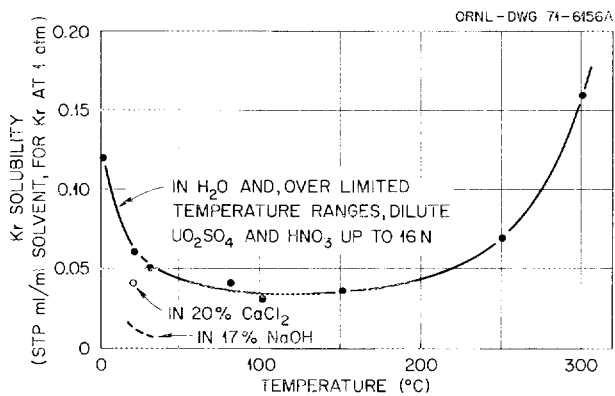


Fig. 1.14. Solubility of krypton in water and aqueous solutions.

## 1.5 WASTE TREATMENT AND DISPOSAL

R. S. Lowrie

Studies are being performed to define the problems involved in handling and disposing of the waste streams

20. J. A. M. van Liempt and W. von Wijn, *Rec. Trav. Chim.* **56**, 632 (1937).

21. T. J. Morrison and N. B. Johnstone, *J. Chem. Soc.* **1954**, 3441.

22. C. J. Anderson, R. A. Keeler, and S. J. Klach, *J. Chem. Eng. Data* **7**, 291 (1962).

23. *Chem. Technol. Div. Quart. Progr. Rep. Aug. 20, 1951*, ORNL-1141, p. 20 (Mar. 11, 1952).

generated during the hot demonstration of HTGR fuel reprocessing and refabrication facilities to be conducted at Oak Ridge National Laboratory under the National HTGR Recycle Development Program.<sup>24</sup> During these studies the waste streams generated by the Head-End, Acid-Thorex, and Refabrication facilities were identified, and processes and facilities necessary to prepare these wastes for disposal were determined.<sup>25</sup>

### 1.5.1 Identification of Waste Streams

Detailed chemical process flowsheets were prepared showing the compositions and flow rates of the process streams for the Head-End and Acid-Thorex pilot plants<sup>26</sup> and for the sol-preparation (Fig. 1.15) and microsphere-forming steps (Fig. 1.16) of the refabrication plants. Estimates were made of the composition and flow rates of entering and exiting streams in the particle coating, fuel stick preparation, and fuel element assembly steps. Calculations were based on the following assumptions.

1. Daily production capacity would be 12 kg of  $(\text{Th}-^{233}\text{U})\text{O}_2$  microspheres with a Th/U ratio of 4.25, with a product yield of 10 kg/day.
2. All the  $^{233}\text{U}$  needed would be recovered from irradiated FSVR fuel elements.
3. The thorium, uranium, and fission product concentrations and isotope compositions would be calculated using the ORIGEN code<sup>27</sup> for fertile and fissile particles in FSVR fuel discharged after 2 years of equivalent full-power operation and cooled 150 days.

The relationship between most of the entering streams and waste streams leaving the various process steps is shown in Fig. 1.17.

### 1.5.2 Disposal of Waste Streams

**Gaseous waste.** Gaseous wastes will be discharged to the atmosphere after suitable treatment to remove radioactive materials. These wastes are of two classes: (1) those containing both radioactive particulate matter

24. *National HTGR Fuel Recycle Development Program Plan*, prepared by ORNL and Gulf General Atomic, ORNL-4702 (August 1971).

25. R. S. Lowrie, *Study of the Waste Handling Requirements for the HTGR Fuel Recycle Development Program*, ORNL-TM-3597 (in preparation).

26. *GCR-TU Programs Semiannu. Progr. Rep. Sept. 30, 1970*, ORNL-4637, pp. 87-88 (July 1971).

27. *Ibid.*, p. 89.

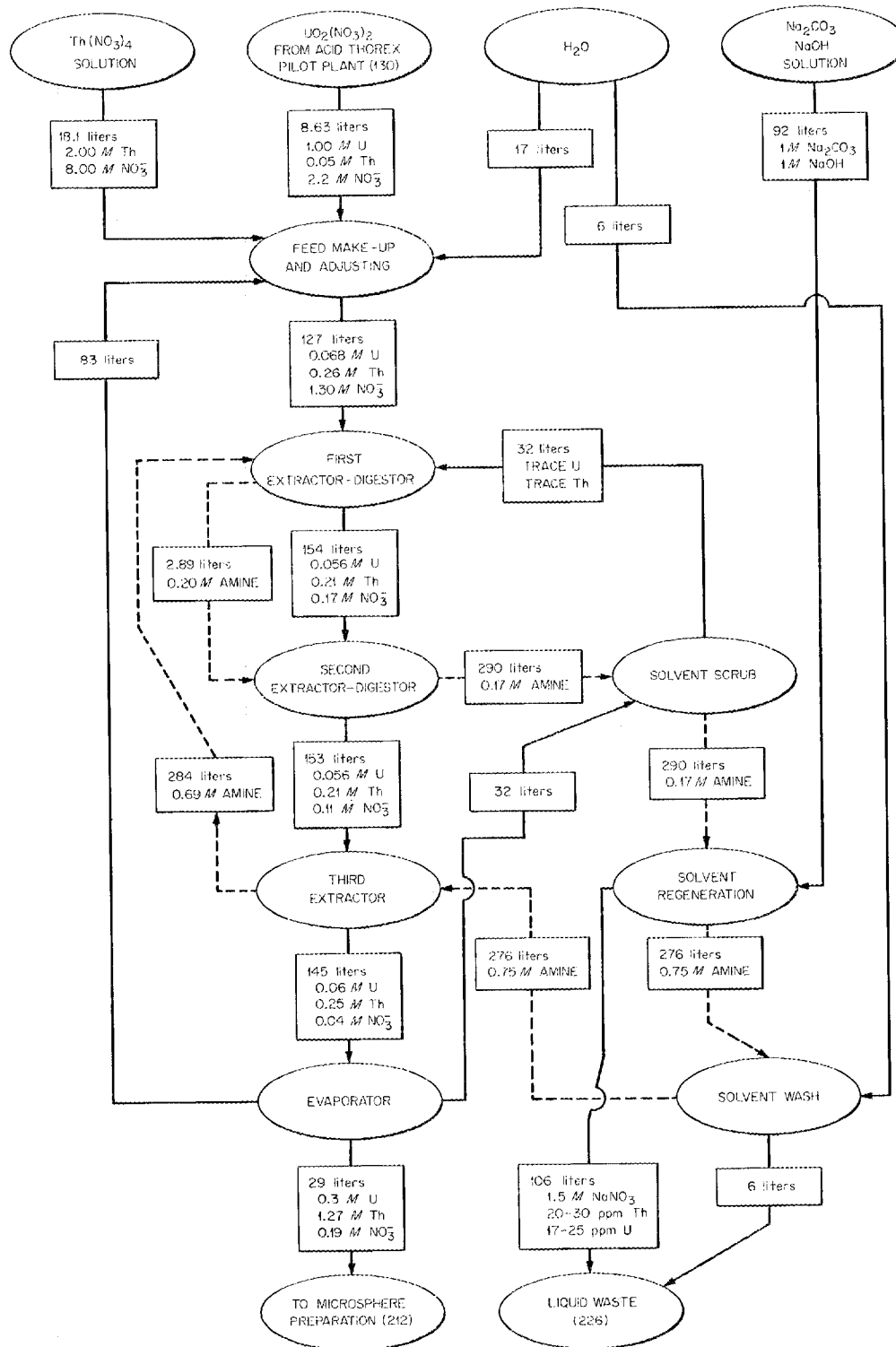


Fig. 1.15. Compositions and relative flows of ThO<sub>2</sub>-UO<sub>2</sub> sol preparation.

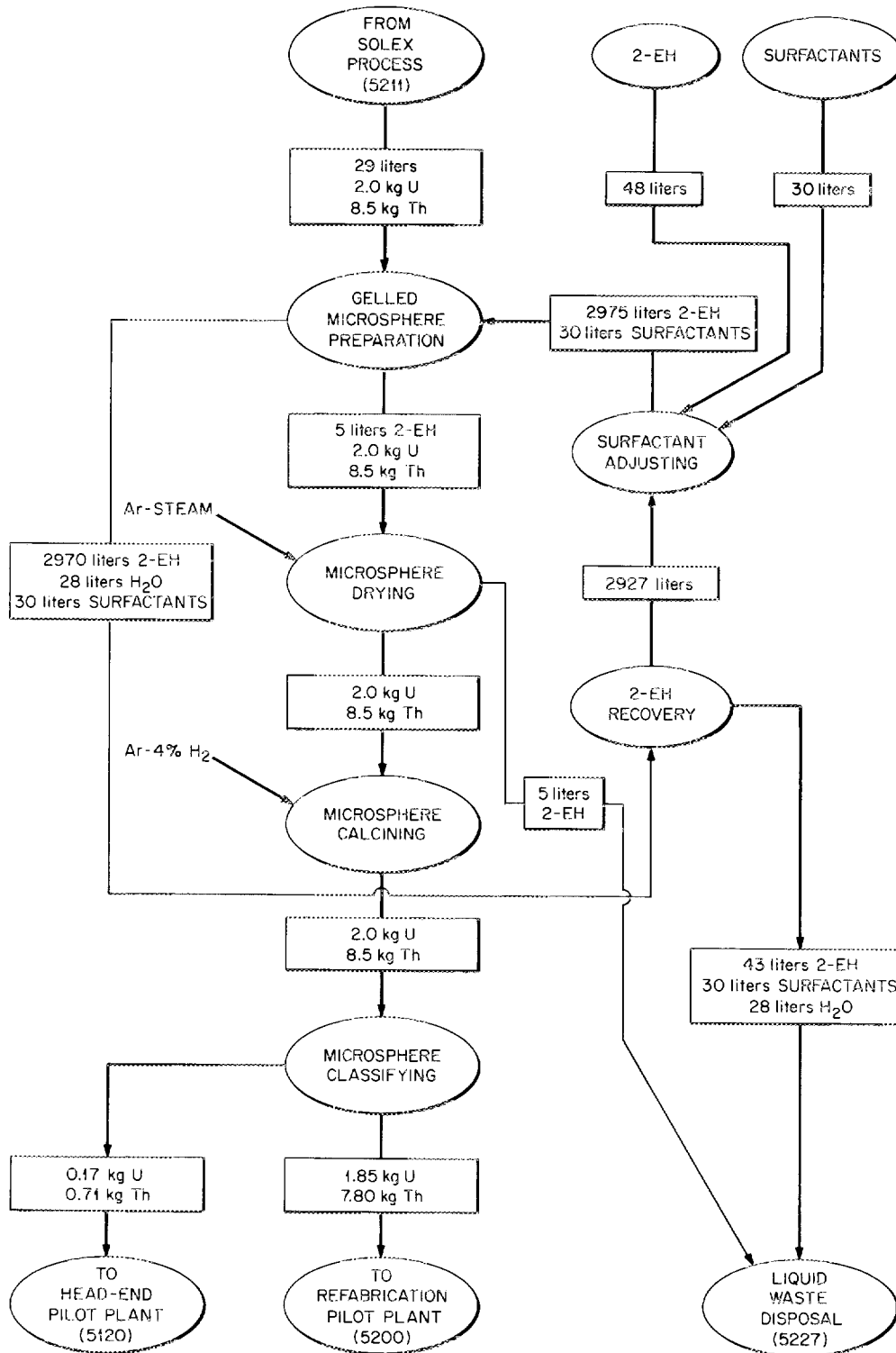
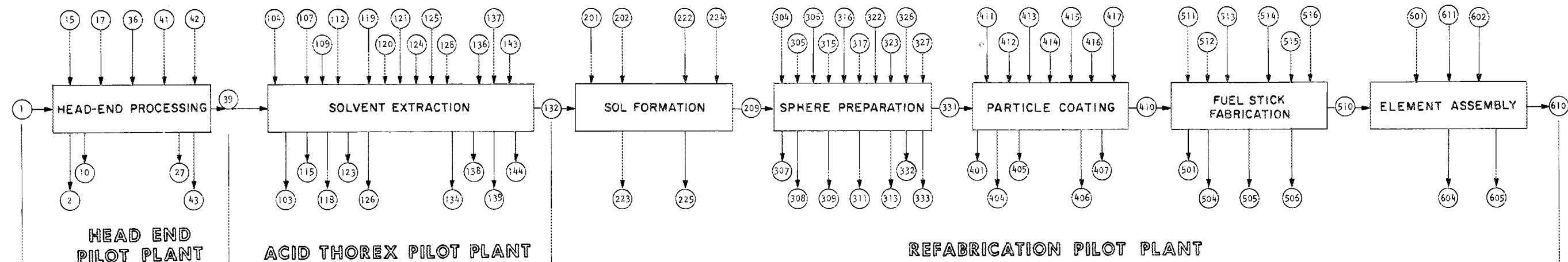


Fig. 1.16. Proposed microsphere-forming chemical flowsheet for the preparation of 10 kg/day of microspheres with a Th:U ratio of 4.



1 Canned Fuel Element (2 yr exposure)

39 Canned Fertile-Particle Burner Ash and  $Al_2O_3$  Fines132 Concentrate  $UO_2(NO_3)_2$  Solution

209 Concentrated Sol Product

331 Specification Spheres

410 Coated Microspheres

510 Specification Fuel Sticks

610 Recycle Fuel Element to FSVR

## (INPUTS)

- 15 Primary Burner Reagent Gas
- 17 Make-up  $Al_2O_3$
- 36 Fertile Particle Burner Reagent Gas
- 41 Cans for Fissile Particle Storage
- 42 Cans for Burner Ash and  $Al_2O_3$  Fines Shipment

## (DISCHARGES)

- 2 Empty Fuel Can
- 10 Canned Barren Graphite
- 27 Canned Fissile Particles
- 43 Combined Burner Off-Gas to Decontamination

## (INPUTS)

- 104 Acid to Leacher
- 107 Recycled U + Th As Oxides
- 109 Wash Water to Filter
- 112 Steam to Feed Adjustment Step
- 119 Scrub I-AS
- 120 Nitric Acid I-AX- $HNO_3$
- 121 Solvent I-AX 30% TBF in N-Dodecane
- 124  $HNO_3$  I-BX
- 125 Solvent Scrub I-BS
- 128 Uranium Strip I-CX
- 136  $Na_2CO_3$  Solvent Wash
- 137  $HNO_3$  Solvent Wash
- 143 Can for Dried Filter Cake

## (DISCHARGES)

- 103 Empty Cans
- 115 Condensate from Feed Adjustment
- 118 Off-Gas from Leacher
- 123 Raffinate I-AW
- 126 Thorium Product I-BT
- 134 Condensate from  $UO_2(NO_3)_2$  Evaporator
- 138  $HNO_3$  to Waste
- 139  $Na_2CO_3$  to Waste } from Solvent Cleanup
- 144 Canned Filter Cake to Waste Storage

## (INPUTS)

- 201  $Th(NO_3)_2 \cdot 4H_2O$
- 202 Water
- 204 Water
- 222 Solvent Regeneration Solution
- 224 Solvent Wash Water

## (DISCHARGES)

- 223 Spent Solvent Regeneration Solution
- 225 Waste Solvent Wash Water

## (INPUTS)

- 304 Ethyl Alcohol to Ion Exchange Column
- 305  $NH_4OH$  Solution to Ion Exchange Column
- 306 Waste Water to Ion Exchange Column
- 315 Make-up 2-Ethyl Hexanol
- 316 Span - 80
- 317 Ethomene S/15
- 322 Argon to Dryer
- 323 Steam to Dryer
- 326 Hydrogen to Furnace
- 327 Argon to Furnace

## (DISCHARGES)

- 307 Ethyl Alcohol from Ion Exchange Column
- 308  $NH_4OH$  Waste from Ion Exchange Column
- 309 Wash Water to Waste from Ion Exchange Column
- 311 Organic Waste from Solvent Cleanup
- 313 Aqueous Waste from Solvent Cleanup
- 332 Condensate
- 333 Combined Dryer-Furnace Off-Gas

## (INPUTS)

- 411 Argon to Purge System
- 412 Argon to Gas Distribution
- 413 Caustic
- 414 Hydrogen
- 415 Hydrocarbon Gases ( $C_2H_2$  &  $C_3H_6$ )
- 416 Silane
- 417 Graphite Cone

## (DISCHARGES)

- 401 Particle Coater Off-Gas
- 404 Caustic Solution from Particle Coater Off-Gas Scrubber
- 405 Graphite Cones
- 406 Compressed Soot
- 407 Carbon Chips

## (INPUTS)

- 511 Binder Materials
- 512 Fertile Particles
- 513 Argon for Carbonization Furnace
- 514 Argon for Heat Treatment Furnace
- 515 Water
- 516 Solvents

## (DISCHARGES)

- 501 Off-Gas from Carbonization Furnace
- 504 Waste Solvents (organic)
- 505 Waste Binder Materials
- 506 Waste Alumina

## (INPUTS)

- 601 Fuel Blocks
- 602 Fuel Hole Caps
- 611 Cement for Caps

## (DISCHARGES)

- 604 Reject Graphite Blocks (unfueled)
- 605 Carbon Scrap

Fig. 1.17. HTGR fuel-recycle summary process flowsheet.

and radioactive gases (e.g.,  $^3\text{H}$  and  $^{85}\text{Kr}$ ) and (2) those containing primarily particulate material. Methods for decontaminating gases in the first class, such as the burner off-gas, are discussed in Sect. 1.4.<sup>28</sup> Gases containing only particulate matter, such as those from the particle coater, will be filtered, scrubbed to remove acidic constituents (HCl), and, after dilution, released to the stack.

**Liquid waste.** Both aqueous and organic liquid wastes are generated in the fuel-recycle operations. Aqueous liquid wastes, such as the 1-AW stream from the acid-Thorex solvent extraction systems, would be pumped to hold tanks, monitored, and discharged to the ORNL Liquid Waste System. The small volume of alpha-contaminated liquid organic waste can be disposed of by burning in a fluidized-bed-type burner or it can be sorbed on a solid such as Microcel-E and sent to the waste disposal system in the form of a solid packed in drums.

**Solid waste.** Three waste streams [the fissile particle stream (27), the dried filter residue stream (144), and the barren graphite stream (10)] contain most of the solid waste generated in the fuel recycle operations. The fissile particle and filter residue streams will be canned<sup>26</sup> and sent to the ORNL Solid Waste Facility. The barren graphite from the screen-tumbling step will be combined with other graphite waste streams. Only two disposal methods for this combined stream appear feasible: burning in an auxiliary burner or removal from the cell and subsequent discard to the ORNL solid waste disposal system.

28. R. W. Glass, P. A. Haas, R. S. Lowrie, and M. E. Whatley, *HTGR Head-End Processing: A Preliminary Evaluation of Processes for Decontaminating Burner Off-Gas*, ORNL-TM-3527 (in preparation).

The ORIGEN code was used to study the amounts of  $^3\text{H}$  and  $^{14}\text{C}$  produced by irradiation of the light elements (impurities) present in the block graphite used in the FSVR fuel elements, since these materials would be released in the burner off-gas. For the base case, where only the graphite and boron were considered, 22 Ci of  $^3\text{H}$  and 2.6 Ci of  $^{14}\text{C}$  will be generated in the graphite associated with 1 metric ton of thorium (as charged to the reactor). As the nitrogen impurity was increased from 0 to 10 ppm, the  $^{14}\text{C}$  content increased from 2.6 to 7.9 Ci per metric ton of U + Th. Similarly, a very small concentration of lithium, 0.1 ppm, increased the  $^3\text{H}$  level from 22 to 289 Ci per metric ton of Th + U. Tritium in the burner off-gas will be present as  $\text{H}_2\text{O}$  and can be removed. The  $^{14}\text{C}$  will be present as  $\text{CO}_2$  and will pass through the off-gas decontamination step and be discharged to the atmosphere.

The loss of fertile and fissile particles to the barren graphite waste largely determines its activity level and hence the shielding required. Thus, if 0.1% of the fertile and fissile particles remain with the barren graphite, it would contain  $\sim 35$  Ci of mixed fission products per cubic foot (FSVR fuel, 2 year exposure, 150 day cooled) or  $\sim 250$  Ci in a 55-gal drum (22 in. OD, 33.5 in. high). Calculations were made to determine the amount of lead shielding necessary to reduce the dose rate to 2.5 mR/hr 6 ft from the drum.

Fission product (Ci per drum)	Lead shielding required (in.)
50	2.39
250	3.56
500	4.10

Based on the above values and assumptions, about 4 in. of lead shielding would be required on the solid waste carrier.

## 2. Fuel Microsphere Preparation Development

B. C. Finney   P. A. Haas   C. C. Haws   K. J. Notz

---

Sol-gel processes, which are well suited to the preparation of oxide fuel spheres, are being developed as an integral part of the HTGR fuel cycle. They can be adapted readily to remote operation to give high-density oxide spheres by use of three principal operations: (1) preparing an aqueous oxide sol; (2) dispersing the sol, as drops, into an organic fluid and then removing the water from these drops to give solid gel particles; and (3) firing at controlled conditions to remove volatiles, sintering to a high fuel density, and performing any necessary reductions or chemical conversions.

This program has been in progress for several years, and development is well advanced. By use of processes we have developed, spheres of  $\text{ThO}_2$ ,  $\text{UO}_2$ , and  $\text{ThO}_2\text{-UO}_2$  were produced for a variety of HTGR fuel test elements. Process and equipment development and design are in progress for refabrication of  $\text{ThO}_2\text{-}^{233}\text{UO}_2$  spheres in the Thorium-Uranium Recycle Facility (TURF). Flowsheets for demonstrating preparation of  $\text{UO}_2$  sols and spheres are being developed.

Coated particles made from ion exchange resins offer an attractive alternative to "fissile" particles specified for advanced HTGRs. Reference fissile particles consist of 100- $\mu$ -diam fully dense  $\text{UC}_2$  kernels coated with a 100- $\mu$ -thick buffer coating (density  $1.2 \pm 0.2 \text{ g/cm}^3$ ) and a composite outer coating consisting of 20  $\mu$  of pyrolytic carbon, 30  $\mu$  of SiC, and 30  $\mu$  of pyrolytic carbon. The density of the pyrolytic carbon in the outer coating is  $1.75 \pm 0.05 \text{ g/cm}^3$ . If we consider everything within the outer coating, the metal density is 1.57 g of uranium per cubic centimeter, and the porosity is 38%. An alternative particle consists of a

void-diluted kernel with a diameter of  $300 \pm 10 \mu$ , 38% porosity, and a uranium density of  $1.58 \text{ g/cm}^3$ . This kernel is made by contacting an ion exchange resin with uranyl nitrate until a uniform concentration of uranium is achieved throughout the sphere. The resin microspheres are then filtered and dried, after which the particles are carbonized by heating in helium in a fluidized bed. Studies are in progress both to improve the chemical flowsheets and to demonstrate the preparation and performance of "fissile" particles from ion exchange resins.

### 2.1 SOL PREPARATION

B. C. Finney

#### 2.1.1 $\text{UO}_2$ Sol Preparation

Engineering development of the CUSP process for preparing  $\text{UO}_2$  sol was continued. Considerable difficulty was encountered in maintaining the aqueous-solvent interface when preparing a 4-kg  $\text{UO}_2$  sol batch using the surge tank set off to the side.<sup>1</sup> A second extraction system, which included a 15-liter surge tank for the aqueous phase, a nitrate extraction column, and a solvent reservoir located directly over the surge tank, was added to the existing extraction unit, which has a sol capacity of 4 liters. Appropriate piping and valves were installed so that the two systems for sol preparation could use the same conductivity probe, heat

---

1. GCR--TU Programs Semiannu. Progr. Rep. Sept. 30, 1970, ORNL-4637, p. 102.

exchanger, circulation pump, and differential-pressure cell. One system has a 4-liter sol capacity (1 kg of  $\text{UO}_2$ ) and the other a 15-liter capacity (4 kg of  $\text{UO}_2$ ).

A Vanton Flexi-Liner pump with a Viton Flexi-Liner and Teflon body was evaluated as a possible replacement for the centrifugal pump used to circulate the aqueous phase, because the centrifugal pump has a tendency to cavitate during the crystallization and degassing phase of the sol preparation. Pumping is accomplished by a rotor mounted on an eccentric shaft that rotates within the liner, thus creating a progressive squeeze action on the fluid trapped between the liner and the body block. The pump will circulate gas-liquid mixtures without cavitation and will not emulsify mixtures of immiscible liquids. A pump of this type was installed in a loop and operated intermittently to pump  $\text{UO}_2$  sol for a total of 177 hr at  $60^\circ\text{C}$  with no operational difficulties; however, some difficulty was encountered in sol preparation which is attributed to the Viton-A Flexi-Liner. Apparently the Viton-A introduced a contaminant into the sol that masked the conductivity probe, resulting in low conductivity readings, and caused an interference in the uranium analysis. Therefore it is concluded that the Vanton pump with a Viton-A Flexi-Liner is unsatisfactory as an aqueous phase circulation pump.

Operation of the sol preparation equipment will be continued primarily to assist in the design of equipment to be installed in Building 3019 for preparing 1-kg batches of 93%-enriched  $\text{UO}_2$  sol and to provide sol for microsphere-forming studies.

### 2.1.2 $\text{ThO}_2\text{-UO}_3$ Sol Preparation

The amine solvent extraction system<sup>2</sup> was operated in continuing engineering demonstrations<sup>3</sup> to prepare 100 kg of  $\text{ThO}_2\text{-UO}_3$  sol for use in fuel fabrication studies and to fabricate prototype HTGR fuel elements for use in studies of spent power reactor fuel reprocessing. The sol was prepared by extraction of the nitrate from a  $0.27\text{ M Th}(\text{NO}_3)_4 - 0.09\text{ M UO}_2(\text{NO}_3)_2 - 1.3\text{ M NO}_3^-$  feed (Th/U atom ratio of 3) using 35% excess  $0.75\text{ M}$  Amberlite LA-2 in *n*-paraffin as the extractant and a countercurrent extraction flowsheet similar to that of the continuous sol preparation demonstration. The

equipment was operated for 6 to 7 hr each day at the rate of 1.0 kg of oxide per hour; no difficulty was encountered with the frequent startups and shutdowns.

Prior to this campaign, the volume of the digester that is located between the first and second extraction contactors was doubled; otherwise, the equipment was the same as that operated for 200 hr at a production rate of 0.5 kg of oxide per hour. An attempt to start up at a rate of 2.0 kg of oxide per hour was unsuccessful because of excessive interfacial crud and emulsions. Therefore the equipment was started up at a 0.5-kg/hr rate and, when steady state was attained, was increased to 1.0 kg/hr, at which operation was very satisfactory. After approximately 100 kg of  $\text{ThO}_2\text{-UO}_3$  as sol had been prepared at the 1.0-kg/hr rate, rates of 1.5 and 2.0 kg/hr were tested for short periods. Operation was normal at 1.5 kg/hr but became unsteady at 2.0 kg/hr, as indicated by fluctuations in the conductivity of the product sol leaving the third extraction contactor. Analyses of typical  $\text{ThO}_2\text{-UO}_3$  sols prepared by continuous amine solvent extraction in the engineering-scale equipment using a countercurrent flowsheet are presented in Table 2.1. The data indicate that the engineering-scale equipment designed for a rate of 10 kg of oxide per day can be successfully operated at 1.5 kg/hr (36 kg/day), but it would be necessary to carry out continuous operations for prolonged periods to verify this.

The sol prepared at the 1.0-kg/hr rate was divided into 40-liter batches and concentrated to  $1.5\text{ M}$  (Th + U) in the forced-circulation evaporator without difficulty.

The engineering-scale sol preparation equipment is located adjacent to the wall in a sheet-metal building that is inadequately heated. Two abnormal upsets in operation were encountered during the campaign due to severe cold weather, which caused the solvent to separate into two phases in the contactors and surge tank.

Immediately following an equipment malfunction caused by excessive cooling of the building in which the sol preparation equipment was located, off-specification sol was produced. Because of this, the two batches of sol involved were collected separately. Analyses of these sols are presented in Table 2.2. When attempts were made to concentrate the sols in the forced-circulation evaporator, both sols became very thick at  $\sim 1\text{ M}$  (Th + U) and gelled within three days. In comparing the first three sols in Table 2.1 with the off-specification sols, it can be noted that the acceptable sols have an  $\text{NO}_3^-$ /metal mole ratio of  $\leq 0.1$  and conductivities in the range 500 to 600 micromhos/cm at  $18^\circ\text{C}$ ; conductivities of

2. Chem. Technol. Div. Annu. Progr. Rep. May 31, 1969, ORNL-4422, pp. 156-59.

3. C. C. Haws, B. C. Finney, and W. D. Bond, *Engineering-Scale Demonstration of the Sol-Gel Process: Preparation of 100 kg of  $\text{ThO}_2\text{-UO}_2$  Microspheres at the Rate of 10 kg/day*, ORNL-4544 (May 1971).

Table 2.1. Analyses of ThO<sub>2</sub>-UO<sub>3</sub> sols prepared by amine solvent extraction using a countercurrent flowsheet

Sol production rate, kg of oxide per hour	0.5	1.0	1.5	2.0 <sup>a</sup>	0.5 <sup>b</sup>
Th, <i>M</i>	0.223	0.227	0.225	0.227	0.253
U, <i>M</i>	0.075	0.076	0.076	0.076	0.059
Th/U atom ratio	2.97	2.95	2.98	2.99	4.28
NO <sub>3</sub> <sup>-</sup> , <i>M</i>	0.026	0.029	0.031	0.036	0.038
NO <sub>3</sub> <sup>-</sup> /metal mole ratio	0.087	0.096	0.10	0.12	0.12
Conductivity, micromhos/cm at 18°C	518	559	578	853	546

<sup>a</sup>Operation at this rate was unsatisfactory, and the product was considered unacceptable.

<sup>b</sup>Data obtained in previous operation.

Table 2.2 Analyses of off-specification dilute ThO<sub>2</sub>-UO<sub>3</sub> sol

	Batch EV-43-25	Batch EV-43-26
Th, <i>M</i>	0.226	0.225
U, <i>M</i>	0.078	0.076
Th/U atom ratio	2.90	2.96
NO <sub>3</sub> <sup>-</sup> /metal mole ratio	0.082	0.077
Conductivity, micromhos/cm at 18°C	925	1040

the off-specification sols are from 900 to 1100 micromhos/cm at 18°C. It can also be noted that the last sol in Table 2.1 (Th/U ratio of 4.28) has a conductivity in the range for acceptable sols. This would indicate that, in order for a dilute ThO<sub>2</sub>-UO<sub>3</sub> sol (Th/U atom ratio of 3 or 4.25) prepared by the countercurrent flowsheet to be concentrated and remain stable, it should have a conductivity in the range of 500 to 600 micromhos/cm at 18°C.

## 2.2 SOL-GEL MICROSPHERE PREPARATION

B. C. Finney P. A. Haas C. C. Haws

The successful continuous formation of gel spheres requires control of the composition of the 2-ethyl-1-hexanol (2EH) fluidizing medium. The desired concentrations for surfactants, water, and nitrate fall in ranges having maximum and minimum values. Materials extracted from the sol or formed by degradation of surfactants or 2EH probably only have maximum limits, with zero as the desired lower limit. The water content can easily be controlled by simple distillation. The surfactants can be added to replace losses, although the control of the concentrations of these substances is difficult because convenient methods are not available

for their measurement. Most of our development studies involving large columns during this report period were concerned with procedures for recycling the 2EH without excessive accumulation of impurities.

### 2.2.1 Application of Ion Exchange to the Recycle of 2EH

The 2EH entering the still contains surfactants (Span 80, Ethomeen S/15), nitric acid, and perhaps formic acid. The nitric acid may be extracted from any of our sol droplets by the 2EH; formic acid is extracted from UO<sub>2</sub> sols.

Water accumulating in the 2EH during sol droplet gelation must be removed by distillation. As the distillation operation takes place, the nitric acid reacts with the surfactants (and perhaps the alcohol), and degradation products are formed. These degradation products and the formic acid prevent continuous long-term operation of the sphere-forming column. Small amounts of formic acid — for example, a concentration of only 0.005 *M* — cause clustering and coalescence and thus make fluidization impossible. The application of ion exchange to remove these acidic materials from 2EH before the feed stream of 2EH

enters the distillation operation was investigated and reported.<sup>4</sup> Conditions were determined for using Amberlite IRA-93 or Amberlyst A-21 anion exchange resins to remove the formic and nitric acids. Complete operating cycles were demonstrated in 1- and 4-in.-ID ion exchange columns of 24-in. lengths. Breakthrough of the formic acid was determined by measuring the pH of the 2EH effluent. The regeneration cycle was controlled by use of preset solution volumes. Detailed results and recommended operating cycles were reported.<sup>4</sup>

The application of ion exchange to remove nitric acid from the 2EH before it enters the still to remove H<sub>2</sub>O is a significant process improvement. Starting with pure 2EH, excellent ThO<sub>2</sub> spheres are easily prepared with Ethomeen S/15 as the only surfactant. The nitric acid extracted from the ThO<sub>2</sub> sol into the 2EH has two deleterious effects. First, the Ethomeen S/15 is less effective for preventing doublets and clustering as the pH of the 2EH decreases, and for this reason the addition of Span 80 may be necessary to prevent doublets and clustering. Second, the nitric acid reacts with both Ethomeen S/15 and Span 80 at 150°C in the still and destroys them; thus surfactant additions are necessary. By using ion exchange to remove the nitric acid, we eliminate the need for Span 80 and reduce the loss of Ethomeen S/15.

### 2.2.2 Formation of UO<sub>2</sub> Spheres

The large-column studies of microsphere forming from CUSP UO<sub>2</sub> sols have been concerned primarily with development and testing of procedures for treating the 2EH so that it may be continuously reused. At the beginning of most of these tests, the 2EH was adjusted to contain 0.3 or 0.4 vol % Span 80, 0.1 vol % Ethomeen S/15, and about 1.2 vol % water. New 2EH containing these amounts of additives gave good UO<sub>2</sub> gel spheres when the pH of the 2EH was in the range 3 to 5.7 and for 2EH temperatures up to 55°C. However, gel spheres large enough to produce high-density UO<sub>2</sub> spheres with diameters of 550 μ are difficult to dry and fire without cracking. If 2EH from the sphere-forming column is treated only by distillation to remove the water, it can be recycled only a short time because of the following changes in composition:

1. buildup of formic acid in the 2EH by extraction from the UO<sub>2</sub> sol, resulting in coalescence, clustering, and sticking;
2. loss of Span 80 and Ethomeen S/15 by reactions with nitrate in the still;

3. accumulation of surfactant degradation products, which contribute to cracking problems and to increased coalescence, clustering, and sticking.

It has been found that formic acid and nitric acid can be removed from 2EH by ion exchange. During the large-column studies with CUSP sols, 2EH from the forming column was passed through a column of ion exchange resin before it was distilled to remove water. This technique prevents the accumulation of excessive amounts of formic acid in the 2EH and eliminates the degradation of Ethomeen S/15 which takes place if nitric acid is allowed to remain in the 2EH during distillation. Continuous recycle of 2EH for more than 100 hr was demonstrated without difficulty from accumulations of formic acid or from loss of Ethomeen S/15. Unfortunately, Span 80 is lost during this treatment, probably by hydrolysis in the ion exchange column. Periodic additions can be made to replace the Span 80, but its degradation products accumulate in the 2EH. We now plan to limit the accumulation of Span 80 degradation products to tolerable levels by continuously bleeding off a small stream of the 2EH and replacing it with purified 2EH containing the appropriate amounts of surfactants. For each volume of sol feed, it is necessary to circulate about 100 volumes of 2EH through the ion-exchange-distillation loop in order to control the water concentration in the 2EH, but we expect that a much lower rate of continuous replacement of 2EH is required to control the concentrations of surfactants and surfactant degradation products. However, the waste stream will be large enough to warrant recovery and purification of 2EH for reuse.

Distillation is being considered for purifying waste 2EH so that it may be recycled to the sphere-forming column. When waste 2EH is distilled at temperatures ranging from 100 to 180°C (depending on the water content), both the 2EH and water can be recovered in the distillate while the surfactants and many of the degradation products remain in the still bottoms. By means of the azeotropic distillation method normally used, water can then be removed from the 2EH. It has been shown that 2EH recovered by this method contains essentially no surface-active materials. However, analyses by gas chromatography show that the recovered 2EH is only 99.4% pure, compared with 99.93% purity for the 2EH as received from the manufacturer. This amount of impurity is comparable

4. A. P. Luina, P. A. Haas, and C. C. Haws, Jr., *Application of Ion Exchange for Recycle of 2-Ethyl-1-hexanol to Sol-Gel Preparation of Spheres*, ORNL-TM-3226 (February 1971).

with or larger than the amounts of surfactants we add. Thus, it may have an important effect on sphere forming. The boiling point of the impurity is somewhat lower than the boiling point of 2EH, and experiments are in progress to remove the impurity by further distillation. Some of the 2EH recovered by this double-distillation method was used to form spheres from CUSP sols. Column operation was satisfactory, and good gel spheres were formed. These spheres cracked when they were fired, but this is not necessarily an indication that the purified 2EH was unsatisfactory since comparable samples prepared with new 2EH also showed excessive cracking. Continued development is required to perfect the distillation method of purification and to test the quality of the purified 2EH.

Urania spheres have been prepared from about a hundred different CUSP sols. We have been able to correlate the behavior of gel-sphere formation with changes in the method of sol preparation and with sol properties. However, drying and firing procedures have not been controlled, and results have not been reproducible enough to correlate sphere cracking with sol preparation methods and properties. The standard CUSP process consistently forms reproducible sols, so that the variations from sol to sol do not appreciably affect the sphere-forming behavior. If the sol viscosity, conductivity, U(IV)/U ratio, and the amount of entrained organic material, or "crud," are within normal ranges, sphere-forming behavior is almost always normal. Difficulties are usually encountered with thixotropic sols; therefore sols should have sufficient shelf life to remain fluid until they are formed into spheres. Since sols with large amounts of entrained organic material or crud, high or low conductivities, or low U(IV)/U ratios almost always caused difficulties in sphere forming, these variations in sol properties should be avoided.

### 2.2.3 Preparation of Microspheres in Nonfluidized-Bed Columns

Uranium dioxide microspheres of the order of 200  $\mu$  diameter may find application as fuel for future HTGRs. Thus, it is of interest to find improved ways of producing spheres in this size range. The preparation of sol-gel spheres by extraction of water into alcohols is simpler for nonfluidized- than for fluidized-bed operation. This mode of operation is practiced for spheres smaller than about 200  $\mu$ . The principal limitation on the nonfluidized preparation of spheres is that the sol drops introduced into a nonfluidized column must be small enough to gel before they settle to the bottom.

The maximum sphere diameter that can be produced is typically 200  $\mu$  or less. The column heights required are dependent on mass transfer and settling velocity. Mass transfer as a function of sol drop and organic liquid variables was investigated and correlated by Clinton;<sup>5</sup> the settling velocities may be calculated using Stokes' equation or a drag coefficient. Both the sol-drop size and the density vary with time. Thus, mass transfer and settling velocity also vary with time, and analytical solutions are not possible. However, the time and free-fall distance as a function of sol drop variables and alcohol variables can be conveniently calculated using a computer program. These and other general considerations and some results of nonfluidized column operation have been reported.<sup>6</sup>

Additional calculations were made with a computer program for mass transfer to determine the effects of varying the temperature of the 2EH. The conditions were selected to apply to a new 28-ft-high nonfluidized column with our usual  $\text{UO}_2$  or  $\text{ThO}_2$  sols. The calculated values are for a water concentration driving force,  $\Delta C$ , of 0.010 g/ml or 1.0 vol % water (i.e., the water concentration in the 2EH is 1 vol % less than saturation). The gelation times (Fig. 2.1) or the free-fall distances (Fig. 2.2) are inversely proportional to  $\Delta C$ ; therefore the values for other water concentrations can be easily calculated. For example, the times or distances for 1.8 vol %  $\text{H}_2\text{O}$  in the 2EH at 28°C ( $\Delta C + 0.005$ ) would be twice those shown for 1.3 vol %  $\text{H}_2\text{O}$  in the 2EH at 28°C ( $\Delta C + 0.010$ ). For the 28-ft (850-cm) column (Fig. 2.2), the sizes of the fired spheres shown increase from 180 to 280  $\mu$  for 2.5 M  $\text{ThO}_2$  sol and from 145 to 210  $\mu$  for 1.0 M  $\text{UO}_2$  sol as the 2EH temperature increases from 25 to 80°C. Whereas the rate of water extraction increases by a factor of 7 or 8, the allowable sphere size only increases by about 50% as the 2EH temperature increases from 25 to 80°C. This can be explained by the increase in settling velocity as the temperature increases. For the same column conditions the allowable initial sol drop sizes are generally about 5% larger for the 1 M  $\text{UO}_2$  sol as compared with those for the 2.5 M  $\text{ThO}_2$ ; however, the drops of the more dilute sol shrink to a smaller final size. Whereas the thoria sol, which is more concentrated, is closer to

5. S. D. Clinton, *Mass Transfer of Water from Single Thoria Sol Droplets Fluidized in 2-Ethyl-1-hexanol*, M.S. thesis, University of Tennessee, Knoxville (1968); also issued as ORNL-TM-2163 (June 1968).

6. P. A. Haas, "Preparation of Sol-Gel Spheres Smaller than 200 Microns without Fluidization," *Nucl. Technol.* **10**(3), 283-92 (1971).

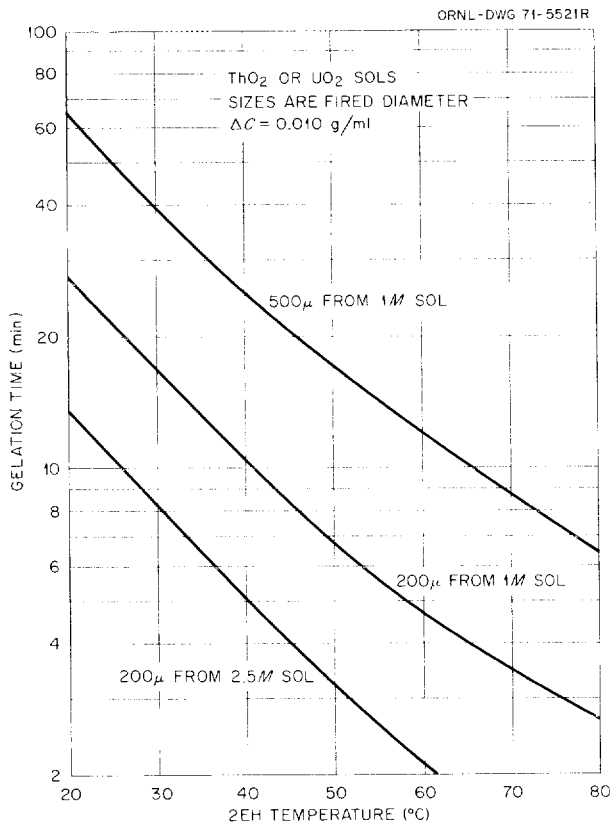


Fig. 2.1. Calculated gelation times vs 2EH temperature.

gelation, the higher density and the higher settling velocity for a ThO<sub>2</sub> sol drop as compared with those for a UO<sub>2</sub> sol drop of the same initial size result in a larger free-fall distance before gelation.

A new 28-ft-high (Fig. 2.3) nonfluidized column was operated with 2.5 M ThO<sub>2</sub> sol and 1 M UO<sub>2</sub> sol feed. Heated 2EH is supplied to the top of the column, and the temperature down the column decreases as heat is lost to the surroundings. This temperature gradient is favorable since it gives rapid extraction of water at the top, where the sol is fluid, and slower extraction at the bottom, where gelation occurs. Operation was satisfactory with sol drops having an initial diameter of 470 μ (yielding 190-μ-diam ThO<sub>2</sub> spheres after firing). This result agrees with the calculated allowable sol drop size (480 μ) for these conditions and a 2EH temperature of 35°C. For sol drops with an initial diameter of 520 μ, gelation was incomplete in 2EH at about 30°C, and the drops clumped in the transfer line. For an average 2EH temperature of about 45°C, the 520-μ drops were gelled without difficulty. Results with the 1 M UO<sub>2</sub> sol also

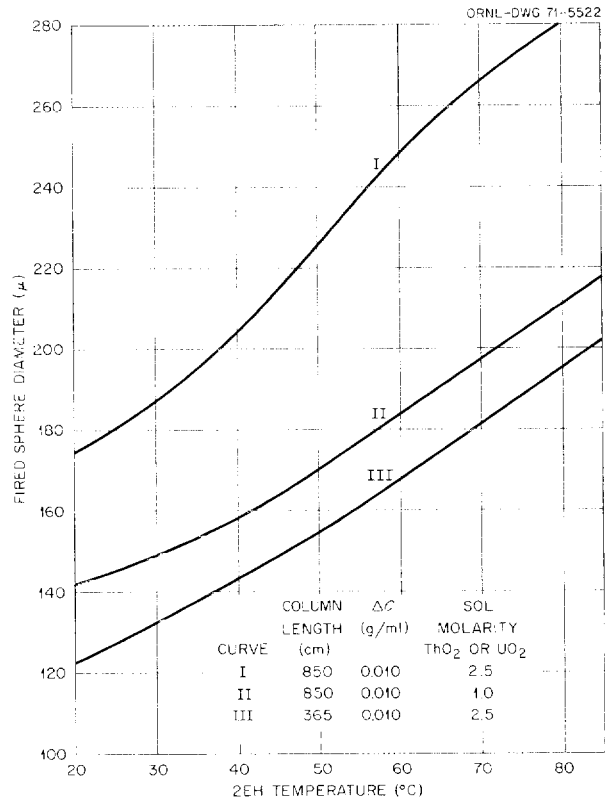


Fig. 2.2. Calculated fired sphere sizes for nonfluidized columns.

confirmed the allowable sol drop diameters predicted by mass transfer calculations.

We now plan to make a demonstration run to produce 150- to 200-μ fired UO<sub>2</sub> spheres using the nonfluidized column system. Gel sphere samples from this system have been dried and fired with none of the cracking which occurs for larger spheres from CUSP UO<sub>2</sub> sols in the fluidized column. Tests to optimize the recycle of the 2EH are in progress.

#### 2.2.4 Development of Prototype Equipment for TURF

The Thorium-Uranium Recycle Facility (TURF) will contain equipment to convert thorium nitrate and uranyl nitrate (<sup>233</sup>U) solutions to ThO<sub>2</sub>-UO<sub>3</sub> sols by solvent extraction, form them into ThO<sub>2</sub>-UO<sub>3</sub> gel spheres, and dry and fire them to produce ThO<sub>2</sub>-<sup>233</sup>UO<sub>2</sub> for subsequent fuel fabrication. The process and equipment for these operations have been demonstrated under conditions of direct operation at 10 kg of

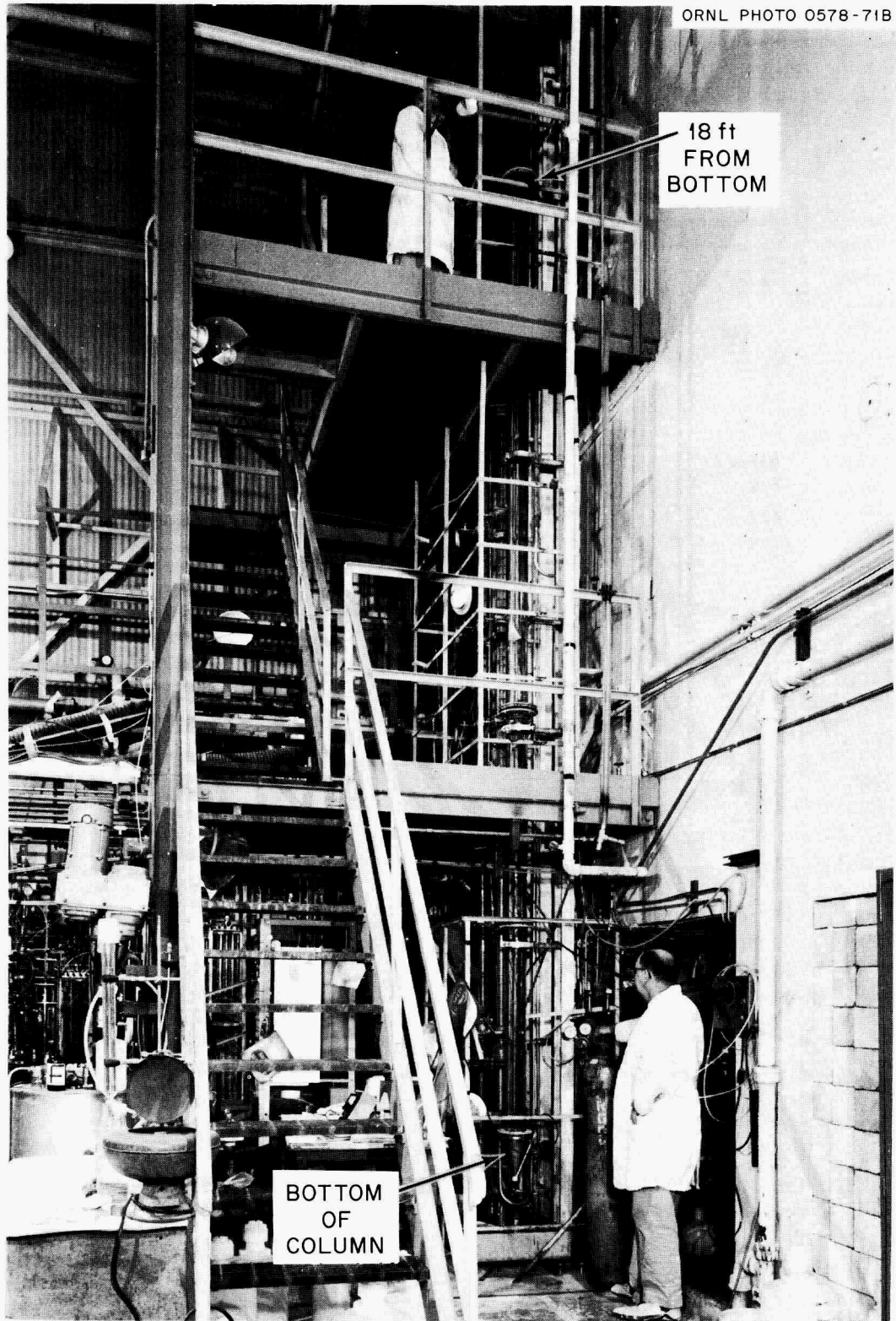


Fig. 2.3. Bottom 20 ft of 28-ft-high nonfluidized column for formation of sol-gel spheres.

oxide ( $\text{ThO}_2 + \text{UO}_2$ ) per day,<sup>3</sup> the design capacity of TURF. Additional development work is needed to demonstrate the capability for remote operation and provide design information for prototype equipment.

Sol is to be prepared by the Solex process,<sup>7-9</sup> and 350- $\mu$ -diam microspheres are to be prepared as dense oxide particles using microsphere-forming techniques discussed previously.<sup>10-13</sup> Flowsheets of the Solex (Fig. 2.4) and microsphere-forming (Fig. 2.5) processes based on TURF design throughput were prepared to determine the materials and waste handling problems to be expected in TURF.

Development of this equipment has now reached the point where the design of TURF prototypes can begin as soon as appropriate.

The solvent extraction equipment for preparing  $\text{ThO}_2\text{-UO}_3$  sol was demonstrated at capacities up to three times the capacity of TURF (see sect. 2.1).<sup>3</sup> The additional requirement that the equipment be remotely operable does not appear to pose difficulties. The equipment and processes are similar to those which have been repeatedly and successfully met for other applications of solvent extraction processes. Equipment for the formation of  $\text{ThO}_2\text{-UO}_3$  gel spheres was demonstrated at TURF design capacity with natural uranium.<sup>3</sup>

In microsphere preparation it is necessary to observe the operation of the sol disperser and to examine the beads leaving the column for shape, surface properties, integrity, and size. Cold operations present no problems; the disperser is directly observable, and samples of particles are taken from the bottom of the column and examined with a bench-mounted microscope. Since operation cannot be monitored in this fashion in hot work, we are working on substitute process control methods amenable to hot-cell operations.

A dual-objective periscope purchased for this work was mounted in the column cubicle in the Coated-

Particle Development Laboratory (CPDL) (Fig. 2.6). The nozzle was enclosed for observation in a flat-sided Lucite box and maintained well above the top of the column. The view of droplets leaving the multiple two-fluid-nozzle disperser was excellent. Lighting was simple, and the 1.9 magnification with a 4.5-in.-diam field (at 15 in.) appears to be a good choice for this leg of the periscope.

The determination of bead properties will involve not only optical examination but also the taking of a sample within the cell and the return of the sample to the process. This must be done in a fashion suitable for hot operations and without bead breakage. An arrangement that works by simply operating valves in proper sequence was suggested. The microspheres to be examined are carried by a stream of 2EH into (and out of) a viewing cell mounted opposite the 15X objective of the periscope. It was installed and operated repeatedly and is satisfactory for hot application. Several "bursts" of alcohol are necessary to clear all the beads from the viewing cell after examination, but this presents no problem.

Two different spacings (0.062 and 0.031 in.) between the windows of the viewing cell were checked. The larger spacing allowed about three layers of beads to collect in the cell, while a "staggered" single layer collected in the narrower space. Since we were preparing beads to be fired to  $350 \pm 50 \mu\text{m}$ , the shallower bed of beads is preferred because light passes through it more readily. An even narrower spacing could be used to get a single layer of beads, but the possibility of getting a doublet in the cell and its hanging there must be considered.

By use of a yellow light and back lighting, the beads are perfectly outlined for periscope examination. Internal cracks are visible, and detail of surface finish and profile is excellent. Front lighting is better for diameter measurements since the reticle is better outlined.

A great improvement over viewing alone would be the use of a Polaroid camera and its readily available prints, which would provide a permanent record. Therefore an attachment was provided for mounting a Polaroid camera to the eyepiece of the periscope. With the lens open ( $f/4.5$ ) and a shutter speed of 1 sec, we obtained a poorly exposed (yellow-back-lighted) color print of a sample of beads in the viewing cell. These are the practical limits of our present camera. Motion was also apparent. The slow speed of the color film and the low transmission of light through the periscope may provide insurmountable obstacles in taking color shots. Black-and-white pictures do not give as good results as the color prints, but they are certainly adequate.

7. *Chem. Technol. Div. Annu. Progr. Rep. May 31, 1968*, ORNL-4272, pp. 129-34.

8. *Chem. Technol. Div. Annu. Progr. Rep. May 31, 1967*, ORNL-4145, pp. 154-59.

9. *Chem. Technol. Div. Annu. Progr. Rep. May 31, 1969*, ORNL-4422, pp. 183-90.

10. *Chem. Technol. Div. Annu. Progr. Rep. May 31, 1970*, ORNL-4572, pp. 135-44.

11. *Chem. Technol. Div. Annu. Progr. Rep. May 31, 1968*, ORNL-4272, pp. 129-37.

12. *Chem. Technol. Div. Annu. Progr. Rep. May 31, 1967*, ORNL-4145, pp. 169-75.

13. *Chem. Technol. Div. Annu. Progr. Rep. May 31, 1966*, ORNL-3945, pp. 146-52.

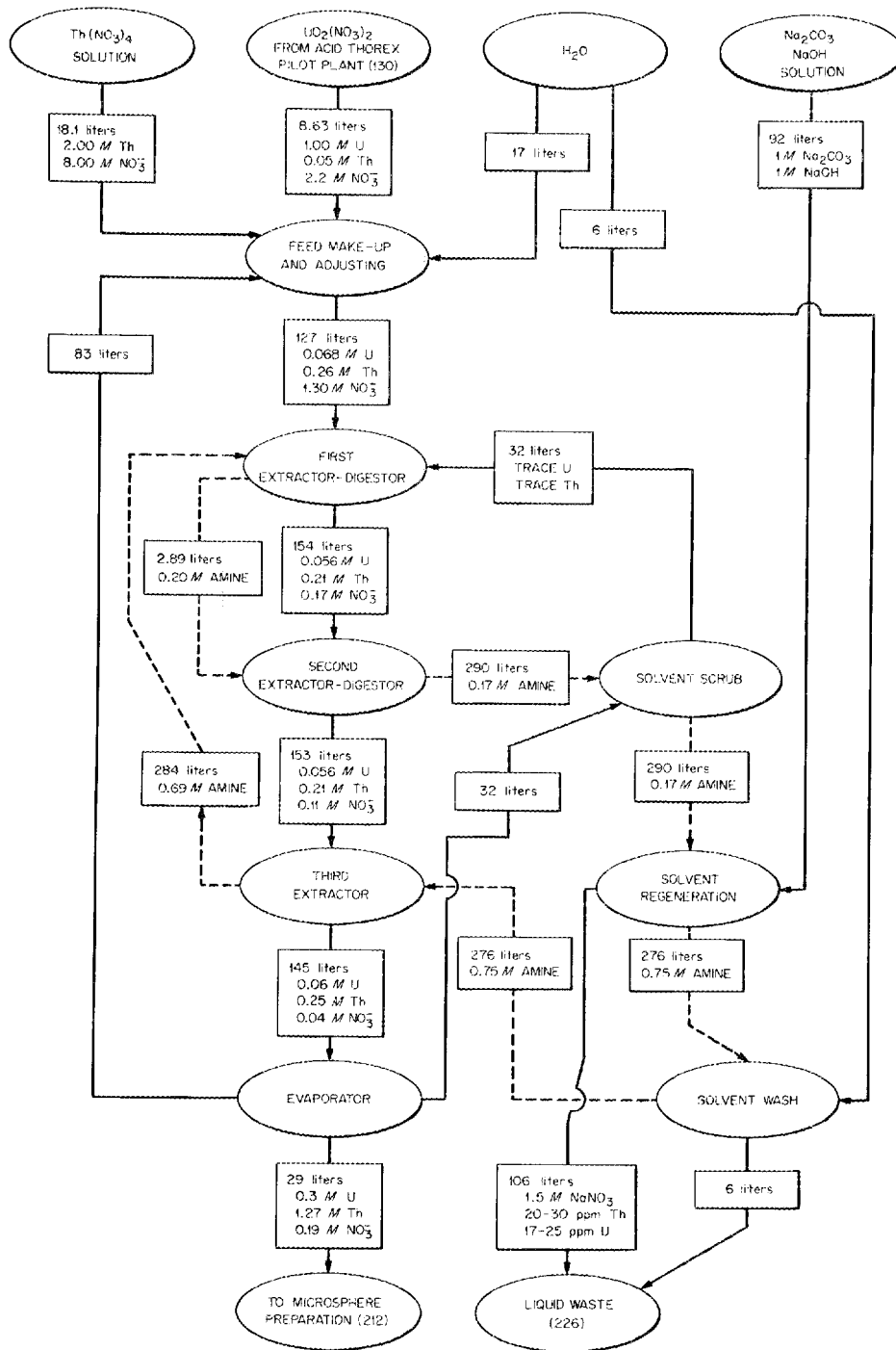


Fig. 2.4. Proposed chemical flowsheet for the preparation of sol for forming 10 kg of microspheres (Th/U ratio of 4.25) per day by the Solex process.

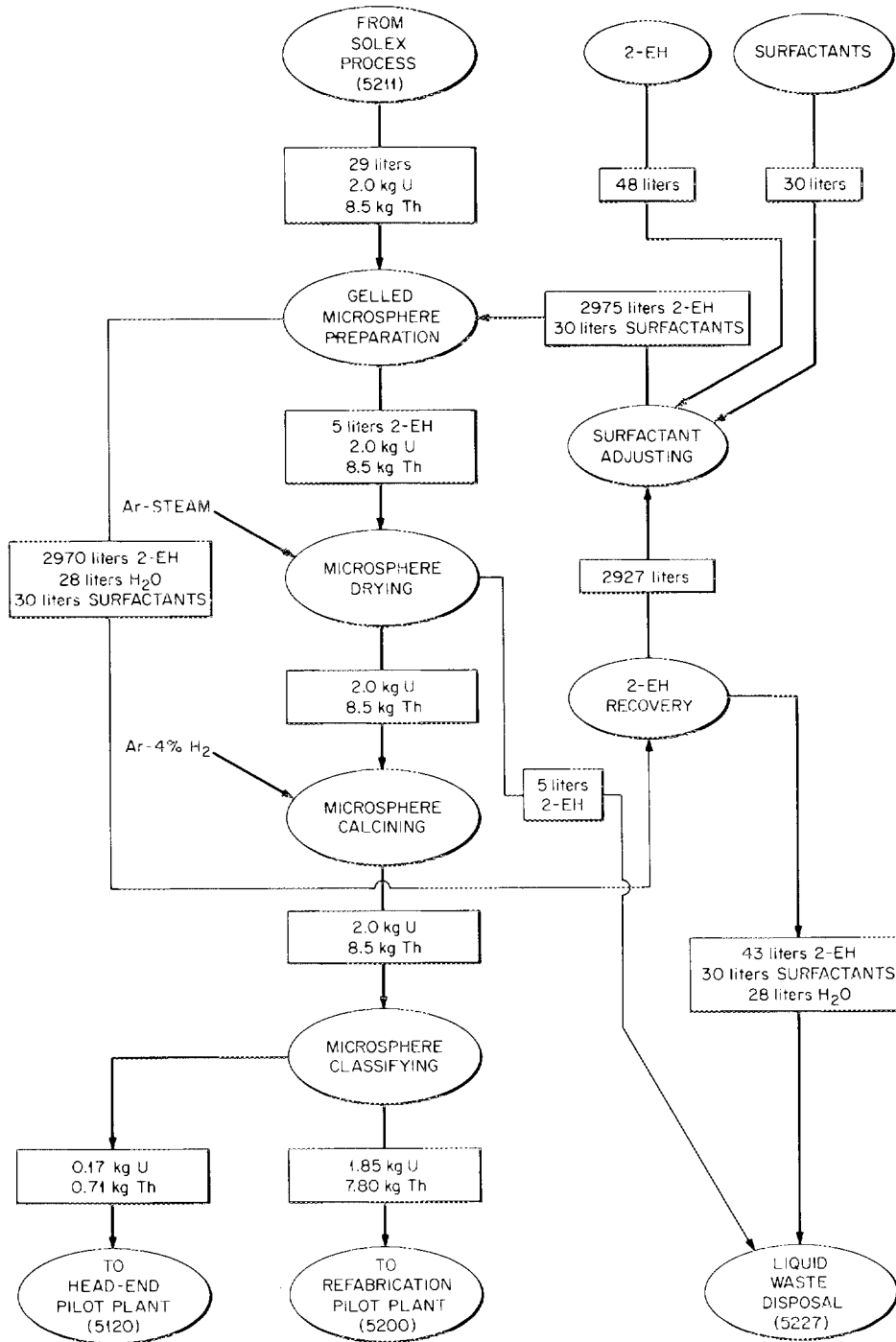


Fig. 2.5. Proposed chemical flowsheet for the preparation of 10 kg of ThO<sub>2</sub>-UO<sub>2</sub> microspheres (Th/U ratio of 4.25) per day.

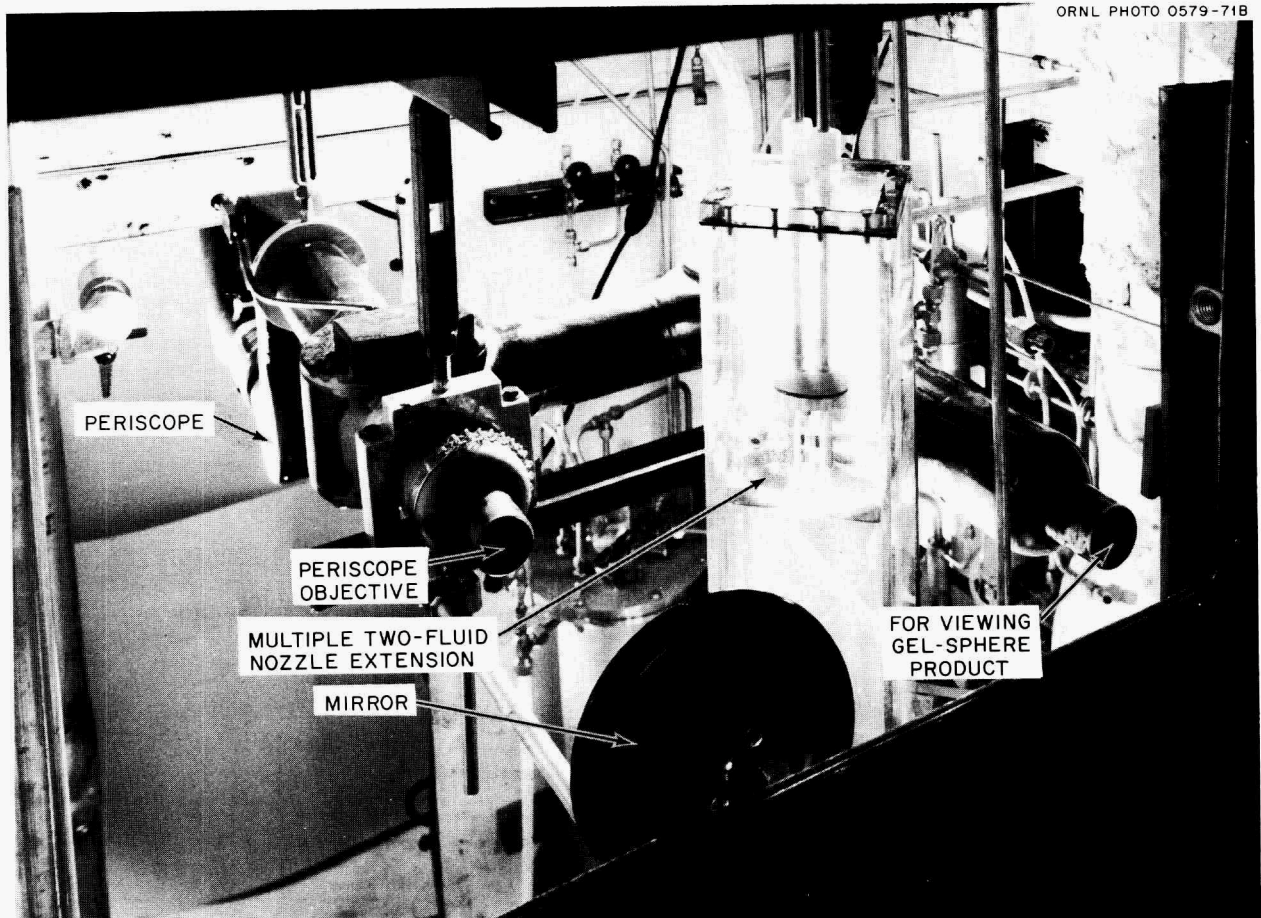


Fig. 2.6. Periscope installed in CPDL microsphere-preparation cubicle.

The periscope was mounted from the roof of the sheet metal and angle iron constructed enclosure. Motion was apparent to anyone standing on the operating gallery, a situation which cannot be corrected. Since all the work planned in the CPDL cubicle, with exception of the actual photography, has been completed, the periscope has been dismantled and moved to another location where motion can be eliminated. Only details of lighting and photographic techniques remain to be studied.

The Metals and Ceramics Division bought a particle size analyzer (HIAC) and had it reworked by the Instrumentation and Controls Division. This instrument (used while preparing spheres) uses a beam of visible light and measures the alteration of the beam by single particles passing through the beam. We discussed this device with both Metals and Ceramics and Instrumentation and Controls Division personnel, and it seems that it has good probability of serving us in a similar

application. In our service we will have the head filled with 2EH from the process stream, whereas M&C uses a gas. Parallel use for our purposes is believed to present only minor problems. Fresh 2EH has a flat absorption characteristic across the entire visible range of frequencies. Used 2EH and the "color" it contains absorb slightly more light in the blue range (4200–4900 Å) than the fresh alcohol does; however, they are essentially equal on out through the red region. Although we may be able to ignore this small difference, a compensating circuit is already built into the present equipment if needed. The sampling system already described for the periscope should also serve this equipment, but additional devices will be required to pass the particles through the light cell one at a time. The presentation of particles to the light cell in 2EH may be difficult.

We borrowed the HIAC from the M&C Division to scout our application, but so far have been unable to use it because of electronic problems. However, we

hope to have stable operation from the equipment and to begin testing soon.

Demonstration of drying and firing the gel beads will require additional equipment development. Drying is accomplished with a flowing stream of gas in a heated container. Critical requirements are (1) good contact between the gel spheres and the flowing gas and (2) smooth temperature changes carried out on a reasonable schedule without excessive temperature gradients. Although we have successfully met these requirements with rather primitive equipment, the need for remote operation, for conservation of cell space, and for criticality control imposes severe limitations on the design of equipment for use in TURF. We are in the process of selecting prototype designs.

### 2.2.5 Preparation of Test Materials

As in previous years, sol-gel oxide spheres were prepared for a number of National HTGR Fuel Recycle Program needs. In some cases, these needs have been satisfied by material produced as part of the sphere preparation development studies, but for the most part special preparations were necessary as follows:

1. additional (100 ± 30)-μ-diam UO<sub>2</sub> from UO<sub>2</sub> (93% <sup>235</sup>U) sol (this was additional material for the recycle test elements described previously);<sup>14</sup>
2. six kilograms of 400-μ-diam ThO<sub>2</sub> spheres for near-term test elements and capsules;
3. about 1600 g of 200-μ-diam UO<sub>2</sub> spheres from UO<sub>2</sub> (93% <sup>235</sup>U) sol for near-term test elements and capsules;
4. about 5000 g of 350-μ-diam ThO<sub>2</sub>-UO<sub>2</sub> spheres from a blend of UO<sub>2</sub> (93% <sup>235</sup>U) and ThO<sub>2</sub> sols (to give a sol having a Th/U atom ratio of 2.75) for use in near-term test elements and capsules;
5. about 100 kg of ThO<sub>2</sub>-UO<sub>3</sub> as sol (Th/U atom ratio, 3.0) from <sup>238</sup>U to be formed into 350-μ-diam spheres for fabrication development and for test elements to be used in head-end processing development;
6. about 40 kg of 400-μ-diam ThO<sub>2</sub> spheres for fabrication development and for test elements to be used in head-end processing development;
7. four samples totaling about 1000 g of ThO<sub>2</sub>-UO<sub>2</sub> with varying Th/U and <sup>235</sup>U/U ratios for Gulf General Atomic and ORNL irradiation specimens.

In addition to the above, plutonium-fueled spheres were prepared for Gulf General Atomic for their use in a special plutonium test element. A 500-g batch of

ThO<sub>2</sub>-PuO<sub>2</sub> (Th/U = 31) spheres 300 to 420 μ in diameter and two 175-g batches, one 63 to 125 μ in diameter and the other 150 to 250 μ, were prepared. These will be tested as replacements for the ThO<sub>2</sub>-<sup>235</sup>UO<sub>2</sub> and <sup>235</sup>UO<sub>2</sub> fuel particles presently under consideration as the reference HTGR nonrecycle fuel particles. The preparation of these fuel particles was straightforward. Sol-making techniques developed in connection with LMFBR fuel particle preparation studies were used to prepare PuO<sub>2</sub> sols. Standard sol-gel process sphere-forming techniques were used. The only problem encountered was a high iron content in the spheres, which probably resulted from corrosion of an equipment piece that had been in service for several years. The iron content was reduced to an acceptable low level by high-temperature treatment with hydrogen.

## 2.3 RESIN-BASED MICROSPHERE DEVELOPMENT

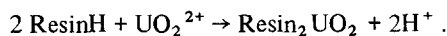
### 2.3.1 Laboratory Studies

K. J. Notz    C. W. Greene

Uranium-loaded resin beads, which are subsequently carbonized, are being developed for possible use as fissile particles in HTGRs. It has been shown previously at ORNL that strong-acid resins can be loaded to a uranium content of about 50 wt %, after carbonizing,<sup>15</sup> by contacting them with concentrated uranyl nitrate solution. This procedure required a large excess of uranium and a minimum contact time (at ambient temperature) of 2 hr.<sup>15</sup> Currently we are developing chemical flowsheets that will optimize the loading process and also be suitable for engineering scaleup.

Our first objective in column loading was to improve the efficiency of uranium utilization with sulfonate resins. To correlate data on this basis we defined the "efficiency ratio" as the number of milliequivalents of uranyl nitrate required for full loading per milliequivalent of resin bed capacity. In the earlier work an efficiency ratio of 5 to 7 had been realized (i.e., a 400 to 600% excess of uranyl nitrate was required to achieve full loading). Our objective was to attain an efficiency ratio close to unity.

The use of dilute uranyl nitrate solutions gave a large improvement in efficiency. The loading reaction, starting with the acid form of the resin, may be written as:



14. *Chem. Technol. Div. Annu. Progr. Rep. May 31, 1970, ORNL-4572, pp. 142-44.*

15. *GCR-TU Programs Semiannu. Progr. Rep. Sept. 30, 1970, ORNL-4637, pp. 3-7.*

Since hydrogen ion is a product of the reaction, decreased acidity will favor the forward reaction, and the hydrolytic acidity of uranyl nitrate solutions decreases with decreasing concentration. Also, from the expression for the equilibrium constant,

$$K = \frac{[R_2UO_2][H^+]^2}{[RH]^2[UO_2^{2+}]}$$

it can be seen that in order to maximize the ratio  $R_2UO_2/RH$  the ratio  $H^+/UO_2^{2+}$  must be minimized, which can be aided by going to lower solution concentration because  $[H^+]$  enters as the square. Figure 2.7 illustrates the advantage of using dilute uranyl nitrate for improved uranium utilization. The efficiency ratios are plotted vs the pH of the column effluents, thus providing a convenient way to follow these reactions by means of the evolved  $H^+$ . When the reaction is complete, the pH levels off at the value for the feed solution. These data are for 50 ml of 20–50 mesh Dowex 50W-X8 resin contained in a column 1.4 cm in diameter and 33 cm long. It can be seen that major improvement results by going to about 0.1 M uranyl nitrate. Although an even lower concentration does give some further improvement in efficiency, this is offset by the larger volume of solution that is required.

A second objective was to control the solution flow rate. The summary data shown in Fig. 2.8 were obtained with the same resin and the same sized column as the data in Fig. 2.7. Although the maximum efficiency is obtained at the slowest flow rate, an intermediate flow rate of 5 to 10 ml/min gives the optimum performance since a very slow flow requires excessive time. A flow of 5 to 10 ml/min is equivalent to 6 to 12 bed volumes per hour, or 3.3 to 6.6 ml  $\text{min}^{-1} \text{cm}^{-2}$ . Two physical factors related to flow rate are channeling and density streamers, both of which become significant at flow rates of 3 ml/min or less but can be alleviated by flowing the uranyl nitrate solution upward. However, at flows of 5 ml/min or greater, downward flow presents no problems.

A third factor investigated was the effective column length. Proper control of column length permits effectively 100% efficiency in uranium utilization; that is, no uranium need ever be recycled. If the column is long enough, the upper part of the resin bed can be fully loaded before any uranium breaks through. For strong-acid resins and the optimum concentration and flow rate given earlier, a threefold increase in column length accomplishes this. A simple way of doing this is to connect three "standard" columns in series. The first will then be fully loaded before any uranium breaks through the third. At this point (determined via pH

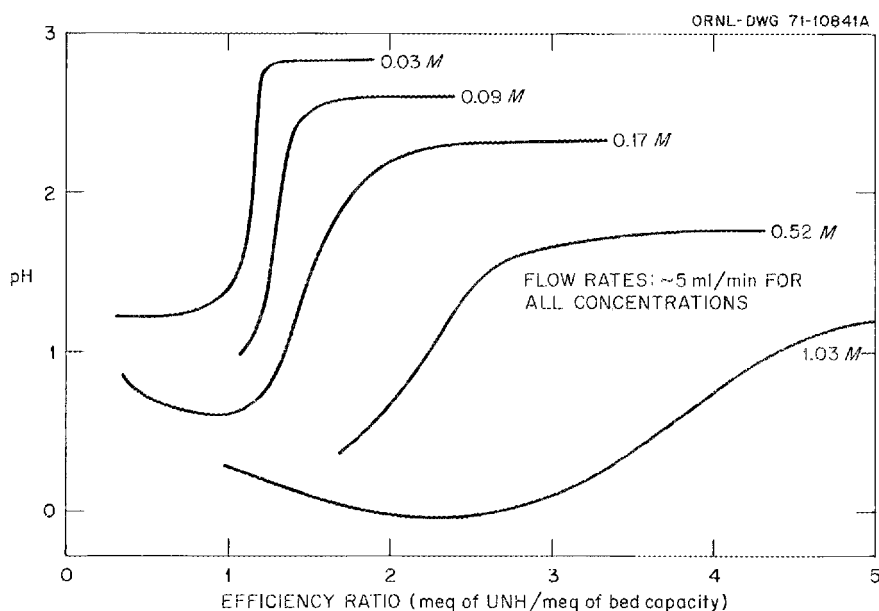


Fig. 2.7. Effect of uranyl nitrate concentration on ion exchange resin loading efficiency.

measurement) the first column is removed and a fresh column placed in the third position. This procedure can be continued indefinitely. (A more elegant way of accomplishing the same thing on a continuous basis is to move the resin countercurrently by means of a Higgins-type contactor.) A three-column line was set up, after scaling up by a factor of 5 (Fig. 2.9), and has

been used as described above to produce about 800 g (after calcination) of uranium-loaded resin beads. These products are described in Sect. 2.3.3.

Full loading of resin beads requires diffusion of uranyl ion to the center of each bead. From the flow rate runs it was possible to estimate a minimum diffusion time of 1.1 hr for 20--50 mesh beads at 25°C

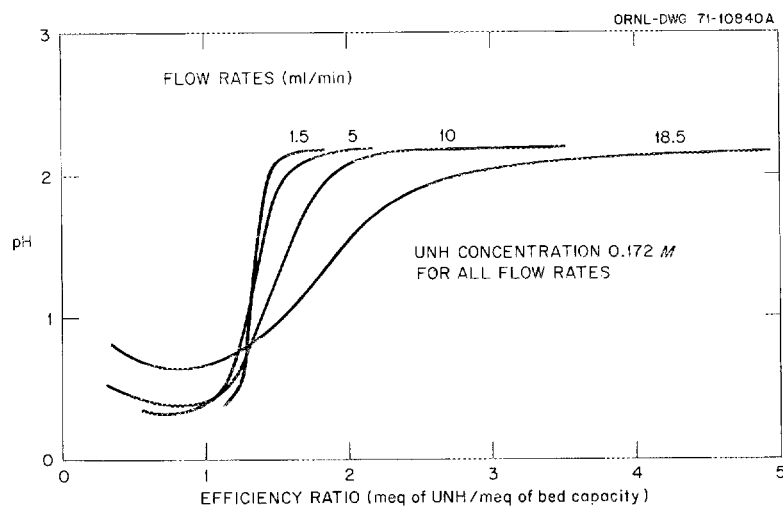


Fig. 2.8. Effect of flow rate on ion exchange resin loading efficiency.

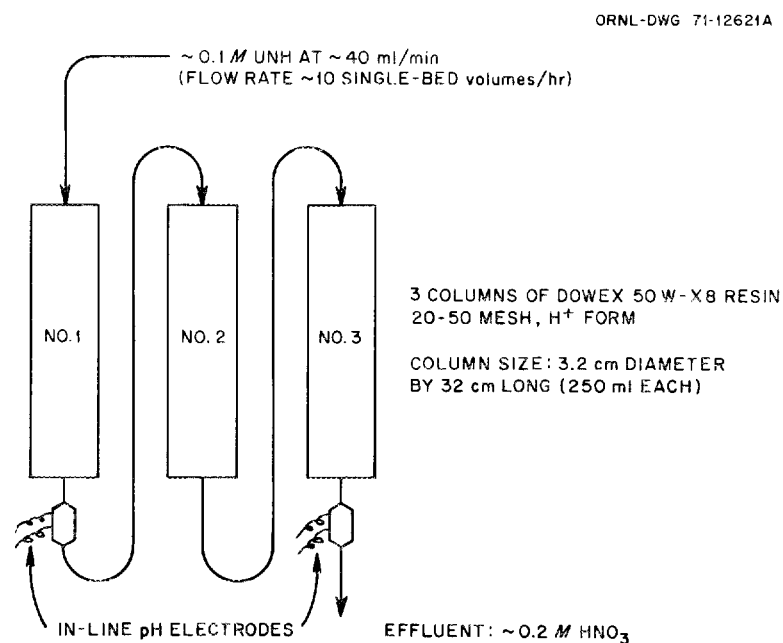


Fig. 2.9. Flowsheet for laboratory-scale multiple column loading of strong-acid resin beads.

and 0.17 *M* uranyl nitrate. Increasing the temperature would increase the diffusion rate. Observation of breakthrough volumes indicates that about 75% of the uranium required for full loading loads in about 15 min. This corresponds to 37% penetration along the radius of an "average" sized sphere, in reasonable agreement with the minimum diffusion time.

A total of about 20 samples were loaded using Dowex 50W-X8 or the corresponding Bio-Rad resin. After calcination, the uranium contents varied between 46.3 and 48.8 wt % (av 47.2). This corresponds to 96.7 and 104.3 wt % (av 100.3) of the theoretical capacity, as determined by titration with standard NaOH. Starting with 100 ml of resin in the acid form loaded into a column by the usual fluidizing method, the following volumes (and weights) were noted: under loading solution downflow, 98 ml; after uranium loading, 93 to 96 ml; after air drying, 50 ml (65 g); after calcination at 1100°C, 26 ml (46 g).

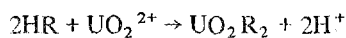
### 2.3.2 Engineering Studies

P. A. Haas

A procedure with important advantages for engineering scaleup for loading ion exchange resins with uranium is to react the cation exchange resin in the hydrogen form with  $\text{UO}_3$  using a small amount of a uranyl salt solution as a transfer medium. The overall reaction, where HR represents the resin, is



This reaction is the sum of



and



The  $\text{UO}_3$  powder readily dissolves in uranyl nitrate solutions to give acid-deficient uranyl nitrate solutions with  $\text{U}/\text{NO}_3^-$  mole ratios up to 0.65 at high uranium concentrations. The simplest method of loading resins using this concept is to agitate the resin and the  $\text{UO}_3$  in the uranyl salt solution until all the  $\text{UO}_3$  is dissolved. The advantages of this method of loading, compared with the usual procedure of flowing uranyl nitrate solution through a bed of resin, are given below.

1. The desired amount of  $\text{UO}_3$  and ion exchange resin can be reacted leaving the same uranyl salt

concentration as the starting solution. Thus there is no partially depleted uranium solution for waste recovery.

2. Agitation of the resin particles promotes rapid loading and minimizes the possibility of nonuniform loading as compared with a fixed bed of resin.

3. Uranyl nitrate solutions with  $\text{NO}_3^-/\text{U}$  mole ratios of less than 2 (acid deficient) and/or with high uranium concentrations can be efficiently used if required for loading weakly acidic cation exchange resins of the type R-COOH.

4. The concentration of the loading solution can be kept near optimum throughout without any displacement flow.

5. A final uniform solution concentration can be selected by mixing the correct amounts of  $\text{UO}_3$ , resin, and uranyl salt solution without any need to monitor flow rates or concentrations.

6.  $\text{UO}_3$  is more desirable as a feed material than uranyl nitrate, particularly with respect to convenient and safe shipping and storage.

The above advantages can be illustrated by the following examples.

*Example I.* The following were combined in a 250-ml beaker and warmed to 70°C with stirring: 8 meq of uranyl nitrate, 77 meq of  $\text{UO}_3$  (based on 2 equiv/mole), 39.5 cc of Dowex 50-8X resin, and  $\text{H}_2\text{O}$  to give 70 cc total volume. Within 15 min after mixing, the solution was clear, free of  $\text{UO}_3$  slurry, and had a pH of 2.1. This shows complete loading of strong-acid resin in 15 min, leaving only uranium solution which could be used to load the next batch without any recovery treatments.

*Example II.* The following were agitated and warmed in a 250-ml beaker: 200 meq of uranyl nitrate, 48.5 cc of Amberlite IRC-50 resin, 165 meq of  $\text{UO}_3$  (based on 2 equiv/mole) added in four increments, and  $\text{H}_2\text{O}$  to give about 150 ml total volume. After 3.1 hr, there was 76 cc of clear solution (loss of volume was evaporation of  $\text{H}_2\text{O}$ ) containing 182 meq of uranium. This shows complete loading of a weak-acid resin which was only loaded to 70% or less with difficulty using uranyl nitrate solutions flowing through a fixed bed.

Tests are being continued to improve the loading of weak cation exchange resins by using  $\text{UO}_3$  with a small amount of uranyl nitrate solution as a transfer medium. A sample of Amberlite IRC-72 had a much better combination of properties than the previously tested weak-acid resins. Of the previously tested weak-acid resins, Amberlite IRC-50 is irregular in shape, with few spheres, while Amberlite IRC-84 and Duolite CC-3 require over 50 hr at 80°C to load and show cracking and crazing when the  $\text{UO}_2^{2+}$  loading exceeds 50% of

capacity. The Amberlite IRC-72 is essentially all spheres before and after loading and showed the following loading behavior.

*Example III.* 212 cc of Amberlite IRC-72 was treated with dilute  $\text{HNO}_3$  and washed to give about 110 cc of resin in the acid form (literature lists 85% swelling for  $\text{H}^+$  to  $\text{Na}^+$  conversion). The resin in water was warmed to  $70^\circ\text{C}$ , and 365 meq of uranium as  $\text{UO}_3$  and 78 meq of uranium as  $\text{UO}_2(\text{NO}_3)_2$  were added. After 1 hr at  $70^\circ\text{C}$ , the  $\text{UO}_3$  was all dissolved and solution pH was 2.85, indicating a loading of about 3.3 meq of uranium per milliliter of resin in the acid form (85% loading). Finally, the resin was washed and air dried at room temperature to give crack-free spheres of 43.3 wt % uranium. The appearance and loading behavior of Duolite CC-3 resin are identical to those of Amberlite

IRC-84; both load slowly at  $80^\circ\text{C}$  and begin to show crazing and cracking at about 50 hr and 1.8 meq of uranium per milliliter of resin in the acid form.

Typical results for resins tested using the  $\text{UO}_3$  loading procedure are given in Table 2.3.

### 2.3.3 Uranium Loading of Sulfonate Resins

K. J. Notz C. W. Greene

Preparation of 100-g quantities of sulfonate resin beads loaded with enriched uranium for use in irradiation tests is being done on a routine basis using the column flowsheet described in Section 2.3.1 and outlined in Fig. 2.7. Table 2.4 lists the products that have been made so far.

Table 2.3. Results of resin loading experiments

Resin	Acid type	Uranium concentration		
		Milliequivalents per milliliter of wet resin	Weight percent, dried at $25^\circ\text{C}$	Weight percent, carbonized
Dowex 50W-X8	Strong	2.0	31.0	
Amberlite IR-120	Strong	1.95	29.7	49.1
Amberlite IRC-50	Weak	3.0	37.0	67.9
Duolite CC-3	Weak	2.0		
Amberlite IRC-84	Weak	2.0	27.7	60.7
Amberlite IRC-72	Weak	3.3	43.3	67.4

Table 2.4. Production of  $^{235}\text{U}$ -containing resin-based microspheres<sup>a</sup>

Desired enrichment (%)	7.2-7.5	7.2-7.5	20	30
Quantity of wet resin (acid form) (ml)	750	500	250	250
1100°C calcined products				
Yield (g)	347	232	113.2	113.6
Isotopic enrichment (at. % $^{235}\text{U}$ )	7.32	7.32	20.3	30.0
Total U (wt %)	47.2	46.9	47.7	46.6
Carbon (wt %)	36.6		36.4	35.9
Sulfur (wt %)	11.4		9.9	10.4

<sup>a</sup>Resin is Dowex 50W-X8, 20--50 mesh.

## 3. Fuel Fabrication Process Development

J. D. Sease

---

Our objective is to develop equipment and processes necessary for the design and operation of the remote refabrication line to be installed in TURF to demonstrate the recycle of HTGR fuel. The line will accept bare fissile microspheres, coat them with the proper pyrolytic carbon coatings, blend them with the fertile particles, and form them into sticks which will be carbonized, annealed, and assembled into the graphite fuel elements. The inspection and quality assurance procedures that will be required for each step are an integral part of the process development.

### 3.1 MICROSPHERE COATING

W. J. Lackey    W. H. Pechin  
C. F. Sanders    F. C. Davis  
F. J. Furman<sup>1</sup>

The particle coating task includes particle inspection and particle handling in addition to the coating operation. The particles must be sampled and inspected, they must be classified to the proper size range and shape separated, and provisions must be made for particle transfer and storage and for the blending of coated particles from a number of coater runs to produce a single homogeneous batch from which the sticks can be prepared.

#### 3.1.1 Particle Coating

Particle coating equipment and processes are being developed for the preparation of the proposed HTGR

recycle fuel particles described in Table 3.1. The fissile particles are to be coated remotely at the rate of about 10 kg of heavy metal per day. Particles of these types were successfully produced in 1- to 2-kg batches in the 5-in.-diam prototype remotely operated coating furnace; however, our principal effort this year was modification of the equipment. Although additional equipment modification will be required for fully remote operation, the coater is currently a highly automated, versatile, and reliable system.

The particles to be coated are levitated by injection of gas into the apex of a 5-in.-diam cone. For deposition of carbon coatings the coating gas is either acetylene or propylene; helium may be used as a diluent. For deposition of SiC the coating gas is a mixture of methyltrichlorosilane ( $\text{CH}_3\text{SiCl}_3$ ) and hydrogen. An external view of the coating furnace is shown in Fig. 3.1, and a sectional view is shown in Fig. 3.2. The control panel is shown in Fig. 3.3, and the entire system is diagrammed in Fig. 3.4. Important features of the coating system, described previously,<sup>2</sup> are given below.

1. Modular design is used to facilitate in-cell maintenance.
2. The total heat capacity of the furnace is low to permit accurate temperature control during rapid change in conditions in the coating region and to allow rapid cooldown to facilitate particle unloading and routine maintenance.

---

1. Currently attending the University of Miami, Fla.

2. R. B. Pratt and S. E. Bolt, *Status and Progress Report for Thorium Fuel Cycle Development for Period Ending December 31, 1966*, ORNL-4275, pp. 61-78.

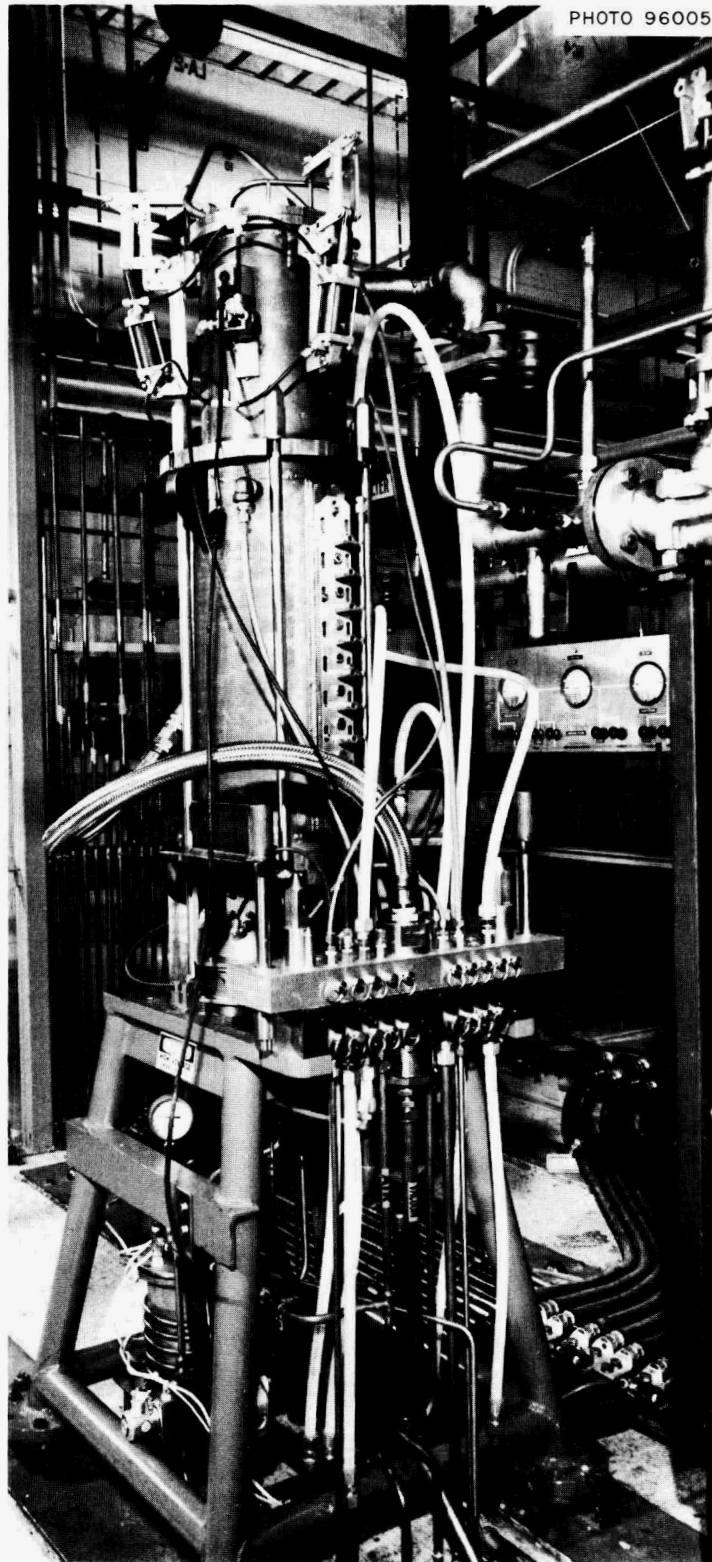


Fig. 3.1. Prototype remote fluidized-bed coating furnace.

Table 3.1. HTGR recycle fuel particles

	Fissile particle	Fertile particle
Kernel composition	(Th-20% U)O <sub>2</sub>	ThO <sub>2</sub>
Kernel diameter, $\mu\text{m}$	350	400
Buffer carbon thickness, $\mu\text{m}$	80	50
Outer pyrolytic carbon thickness, $\mu\text{m}$	120	70
Total particle diameter, $\mu\text{m}$	750	640

ORNL-DWG 67-2691R

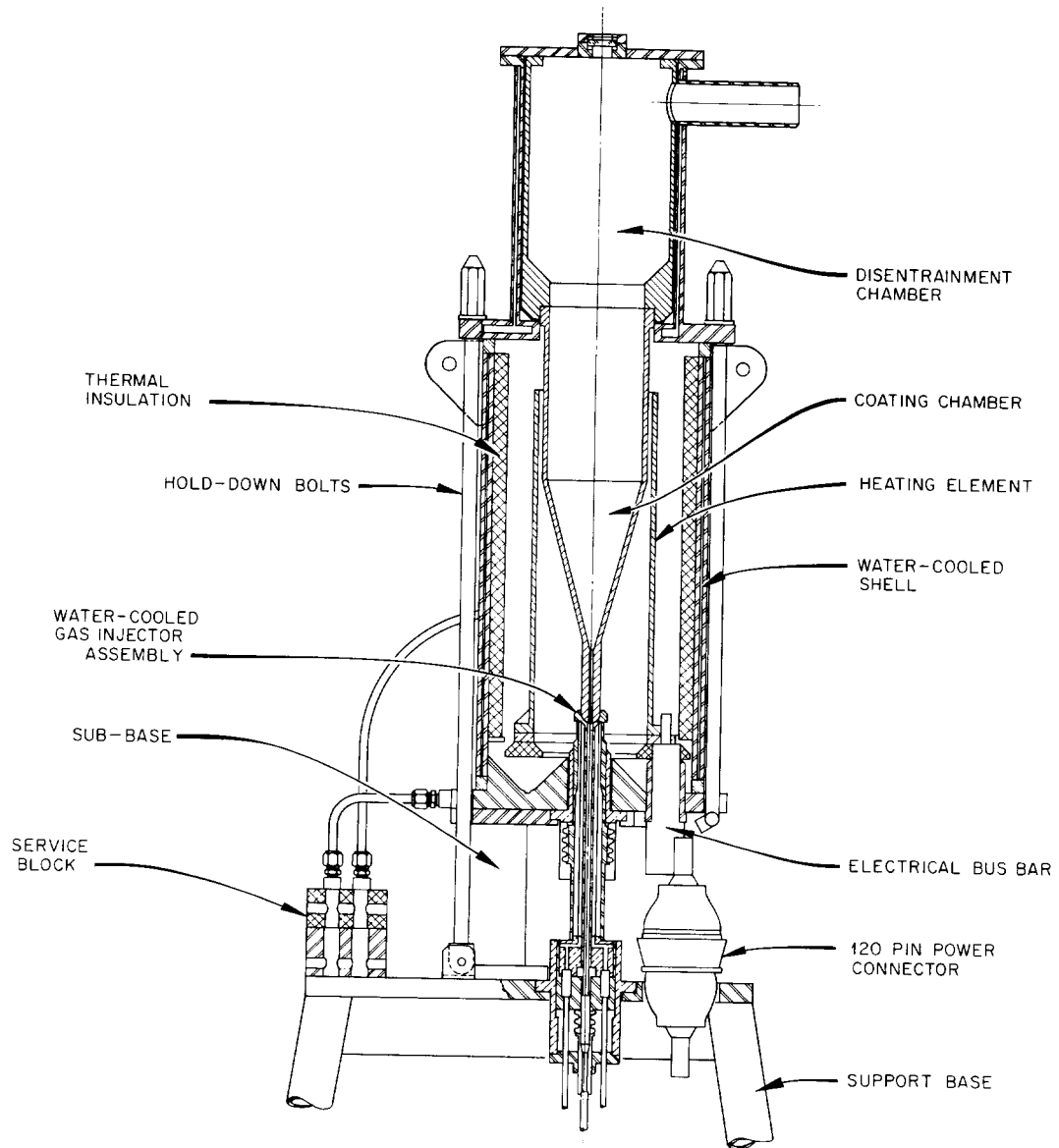


Fig. 3.2. Arrangement of prototype remote coater.

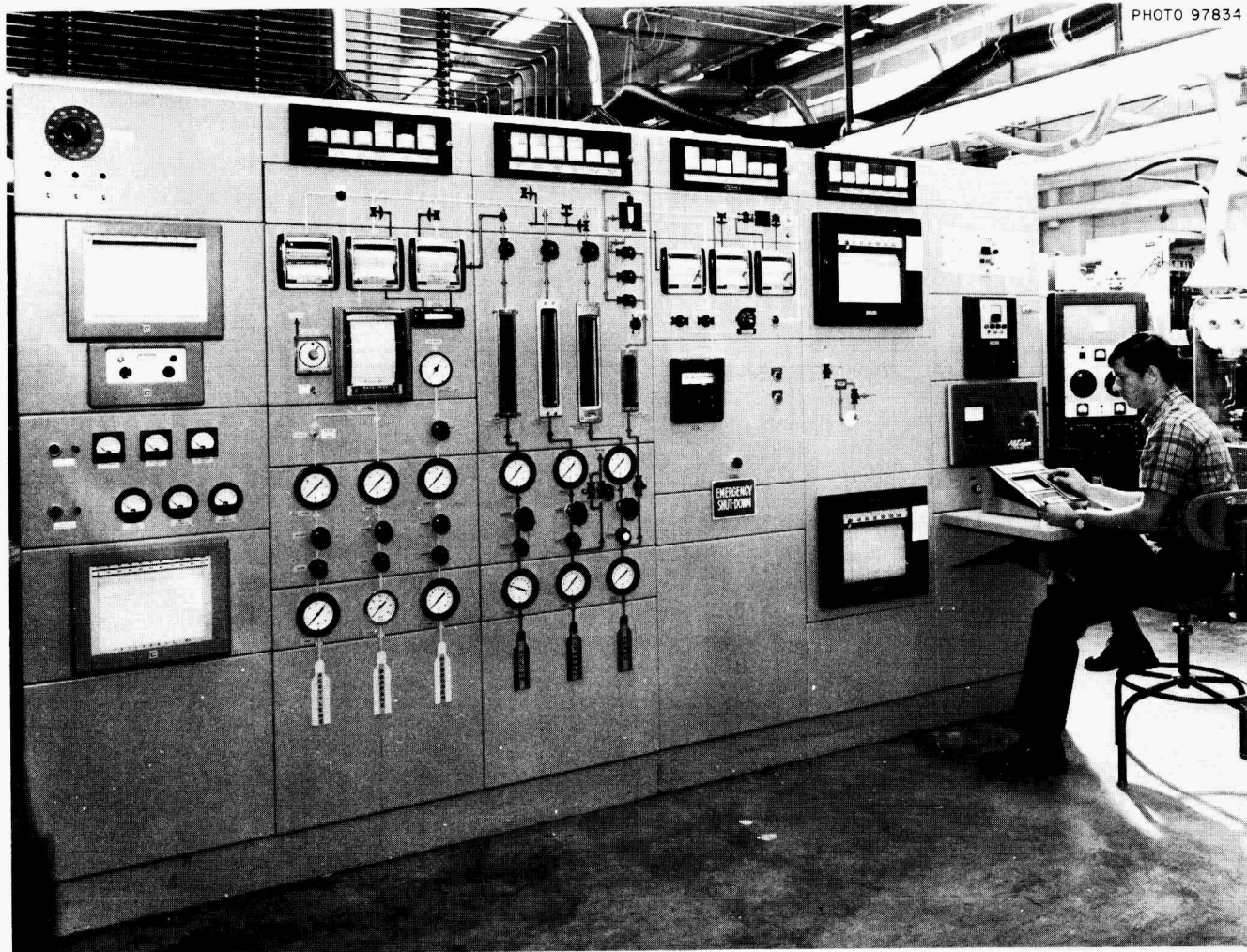


Fig. 3.3. Control panel for prototype remote coater.

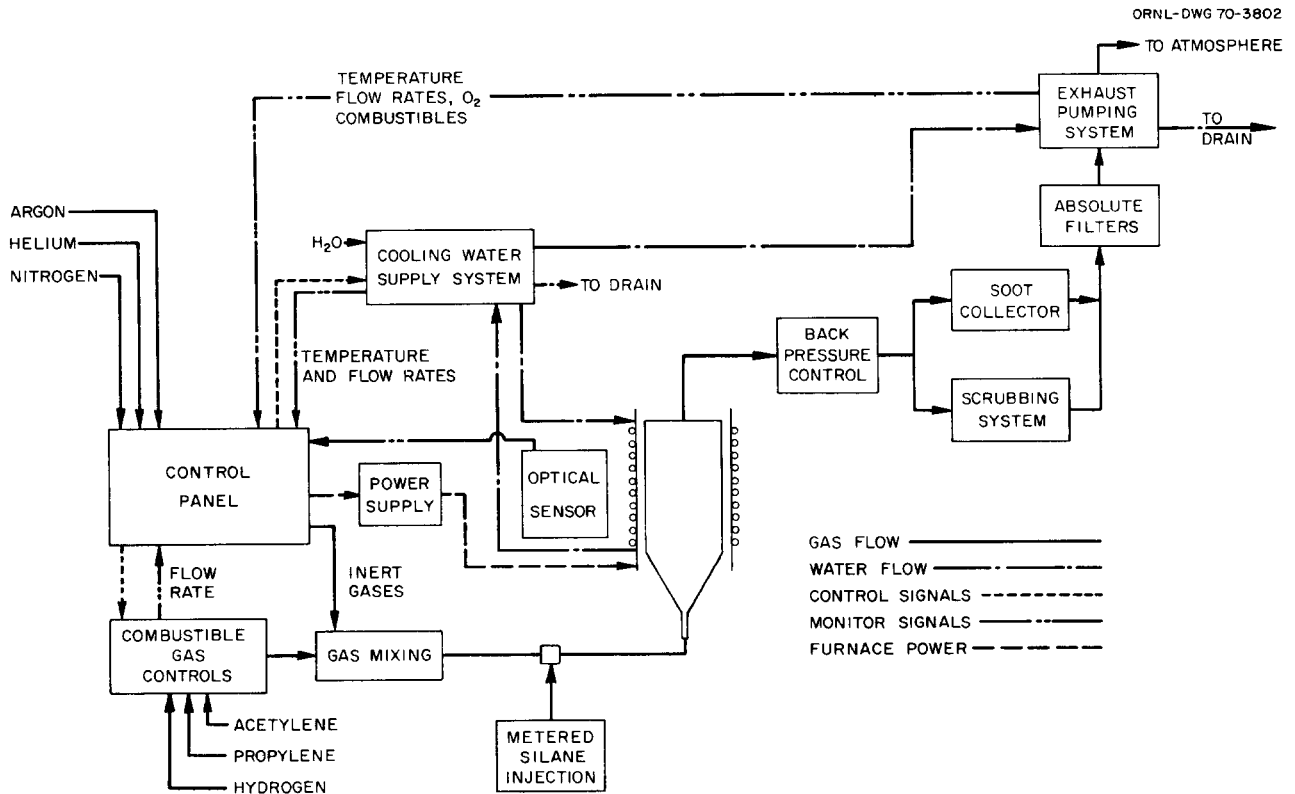


Fig. 3.4. Block diagram of prototype coating system.

3. Exhaust pump allows variation of the furnace pressure if desired and permits absolute filtration of exhaust gas.
4. The flow of combustible gases is controlled without routing these gases to the remote control panel.
5. The hydrocarbon and diluent flow rate can be programmed to maintain a constant gas flux throughout the coating run.
6. Numerous temperature, pressure, flow, and combustible gas monitors are interlocked within the system to protect both the operator and the equipment.
7. Hydrogen chloride produced during deposition of SiC coatings is removed from the effluent gas via a caustic scrubber.

Equipment modifications successfully completed included alteration of the furnace electrodes to permit tighter clamping of the heating element assembly to minimize thermal and electrical resistance, fabrication of more rigid molybdenum heat shields, installation of a particle transfer system, and installation of a critically

safe geometry soot filter. With the particle transfer system we demonstrated that particles that had been separated from the soot and soot balls that form during deposition of carbon coatings could be pneumatically transferred in a  $\frac{3}{8}$ -in.-diam stainless steel tube that was 160 ft long and at points elevated as much as 17 ft above the tube inlet and exit. Transfer of uncleaned particles occasionally led to blockage of the transfer line. To alleviate this problem a grizzly-bar-type separator was designed for installation on the unloading port of the coating furnace. The new soot filter performed satisfactorily, but cleaning of the filter, which is required after about 10 to 15 coating runs, proved too time consuming. Thus a filter designed to be more easily cleaned and requiring cleaning less often is being fabricated.

Several equipment modifications were made in order to prepare SiC coatings. A heat exchanger was installed in the furnace effluent gas line on the inlet side of the gas scrubber used to remove HCl from the effluent. We were unsuccessful in using a metering pump to introduce silane into the gas inlet line of the coating furnace, but a simplified system that consists of using an

overpressure of argon to force silane out of a volumetrically calibrated glass reservoir through a metering valve worked properly. With this system we successfully deposited SiC coatings with a density of 3.21 g/cm<sup>3</sup> for the first time in the prototype coater.

While equipment modifications to the prototype coater were in progress, a second 5-in.-diam coater was used to investigate the effect of propylene gas flow rate and temperature on the density and extent of faceting of isotropic carbon coatings. The large influence that gas flux and temperature have on coating density is shown in Fig. 3.5. Although the evidence was not conclusive, there appeared to be a correlation between coating density and the extent of faceting; increased faceting was observed for the higher density coatings. Similar studies will be performed using the prototype coater to determine the effects that temperature, time, coating gas flow rate and composition, particle size, and furnace load have on coating thickness, density, strength, and anisotropy; variation in coating thickness from particle to particle; and particle shape. Such studies are needed for both low- and high-density carbon coatings as well as for SiC coatings.

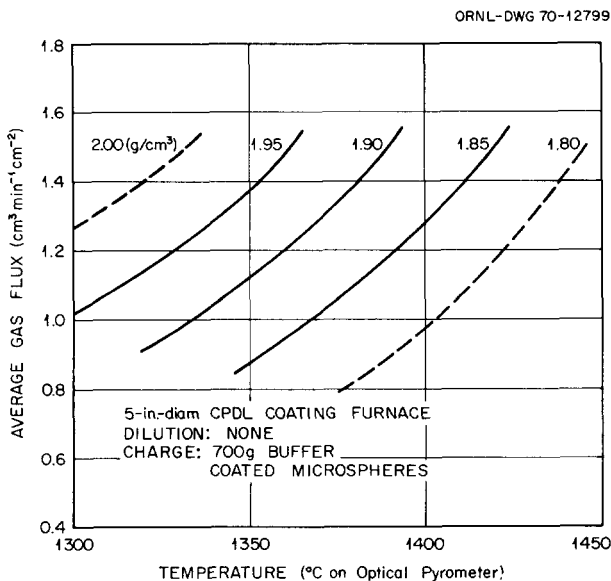


Fig. 3.5. Effect of gas flux and deposition temperature on density of propylene-derived coatings.

### 3.1.2 Particle Inspection

The most important single measurement in particle inspection is the diameter of the bare kernel and the

coated particle after application of the various coatings. Our current concept for the TURF demonstration involves two different methods of performing these measurements — use of an automatic particle size analyzer and measurement of particles from micro-radiographs.

The particle size analyzer, described previously,<sup>3</sup> is an electronic instrument for counting and measuring the diameter of particles at the rate of several hundred particles per minute. The analyzer will be used primarily as a process control means, in that a sample from every coating run will be counted and measured. Modifications to the electronics of the instrument have been completed and initial trials run. The results on tests for reproducibility on various particle sizes are listed in Table 3.2. The reproducibility is adequate, but important items that remain to be investigated are whether particle color (i.e., bare vs coated) or dusting of the coating will have any effect on the calibration of the machine.

Table 3.2. Reproducibility of results from the particle size analyzer

Approximate particle size (μm)	Mean pulse height (V)	Number of runs	Range	
			Volts	Micrometers
153	0.1137	2	0.0028	1.6
156	0.1156	3	0.0064	3.5
177	0.1558	2	0.0031	1.6
310	0.5535	3	0.0065	3.8
323	0.5610	3	0.0037	0.8

The measurement of particle diameter from contact microradiographs will be used only as a quality assurance measure in that radiographs of blends from several coating batches will be made and measured to ensure that such blends meet specifications for the mean and standard deviations of particle diameter, coating thickness, etc. The measurement of microradiographs has been improved by adding a digital output to the Vickers split-image eyepiece. A PDP8/E digital computer has been procured and will be mated directly to the eyepiece output to eliminate all intermediate data handling. This arrangement is expected to reduce the time required to analyze a radiograph by 75 to 80%.

3. F. J. Furman and R. A. Bowman, *Status and Progress Report for Thorium Fuel Cycle Development for January 1, 1969 through March 31, 1970*, ORNL-4629, p. 80.

We are investigating the precision of the various analyses on coated particles. The determination of carbon weight by burnoff was found to have a standard deviation of 0.15% for buffer-coated material, while the determination of particle density was found to have a standard deviation of 0.20 g/cm<sup>3</sup> for the same type material.

### 3.1.3 Particle Handling

Particle handling involves the development of devices to remotely store, classify, blend, and sample kilogram amounts of <sup>233</sup>U-bearing particles. Most commercial materials handling equipment is not suitable, since either it is designed to handle ton quantities or it is laboratory equipment and thus not readily adaptable to remote or automatic operation. We have developed equipment to perform these tasks.<sup>4</sup>

Before the design of the remote equipment can be completed, information is required regarding (1) the stability and accuracy of the material inventory monitors, (2) the long-term performance of the individual components, (3) the amounts and cause of particle damage, and (4) operating parameters for pneumatic transfer.

In addition, we must design and test remote connectors (electric and pneumatic) and design and test a system for separating the solids (dust and particles) from the gas. To generate the above data a particle handling test stand, shown in Fig. 3.6, has been fabricated. Several of the components are shown in Fig. 3.7. The stand includes gravity and pneumatic transfer lines, transfer line valves and connecting storage hoppers, material inventory monitors, and feed devices. The same basic hopper design is used throughout the system, but several different valve designs are being used because of the different functions to be performed. For material inventory monitors the test stand contains a capacitor liquid level probe and a strain-gage bridge circuit.

Classification of microspheres includes the separation of both nonspherical particles and over- and undersized particles. A shape separator to remove nonspherical particles is a flat-plate vibratory feeder with the plate tilted slightly downward in respect to the direction of feeding action and tilted also 90° to this direction. This

4. F. J. Furman, J. T. Meador, and J. D. Sease, *Microsphere Handling Techniques*, ORNL-TM-2782 (March 1970).

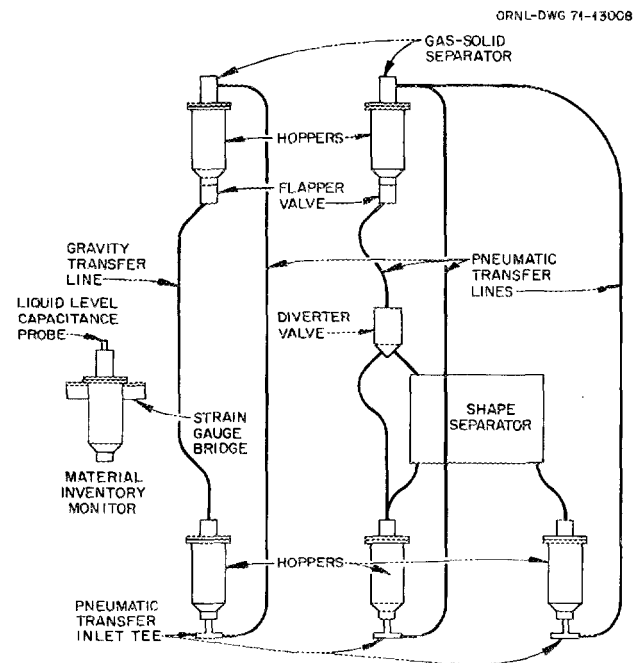


Fig. 3.6. Particle handling test stand.

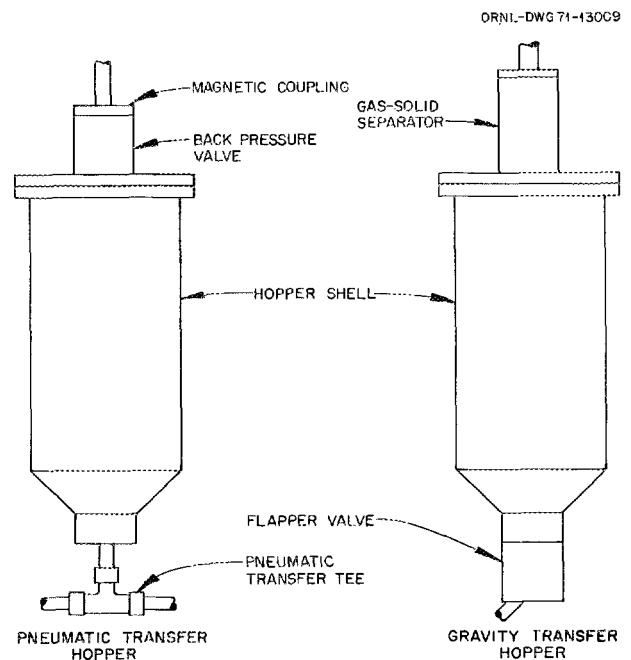


Fig. 3.7. Typical hoppers and accessories.

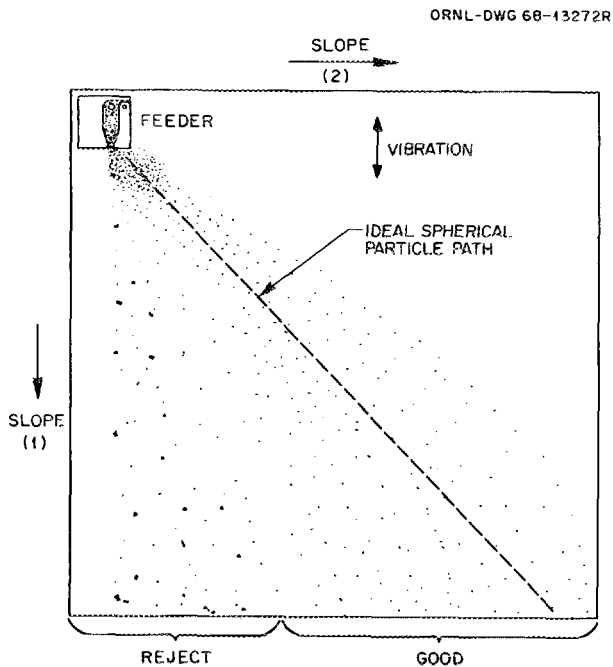


Fig. 3.8. Shape separator.

equipment is shown in Fig. 3.8. For the size classification we used a modified 18-in.-diam SWECO gyratory separator, described previously.<sup>5</sup>

### 3.2 Fuel Stick Fabrication

R. A. Bradley C. F. Sanders D. D. Cannon

The purpose of this work is to develop processes and design equipment suitable for fabricating about 9000 HTGR fuel sticks per day at TURF. The fuel sticks are about  $\frac{1}{2}$  in. in diameter by 2 in. long and contain mixtures of fissile and fertile coated particles bonded by a matrix of coal-tar pitch and graphite filler.

The principal activities in fuel stick fabrication are blending and loading particles into molds, injecting the matrix into a bed of particles to form a stick, and carbonizing and annealing the stick. A series of inspections are then performed on the stick prior to loading it into the fuel element.

#### 3.2.1 Particle Blending and Loading

The fissile and fertile particles must be blended and loaded into the mold in such a manner that the fissile

5. F. J. Furman, *Status and Progress Report for Thorium Fuel Cycle Development for January 1, 1969 through March 31, 1970*, ORNL-4629, pp. 65-69.

and fertile particles are distributed uniformly throughout the fuel stick. If the fissile and fertile particles are of different sizes or if their densities are appreciably different, blended particles will segregate in feed hoppers. Therefore it appears that blending by simultaneously feeding the different particles from controlled feeders is necessary to achieve a uniform distribution in each fuel stick.

Preliminary experiments with a controlled-orifice feeder-blender did not yield satisfactory results. We are presently evaluating a roll feeder similar to that shown in Fig. 3.9. This feeder consists of a silicone roller rotating in close proximity to a vertical surface. As the roll turns, particles are fed from the feed hopper into the mold. The standard deviation of the weight of 50 samples batched with a prototype roll feeder was found to be about 1%. If additional experience shows this

ORNL-DWG 71-4200

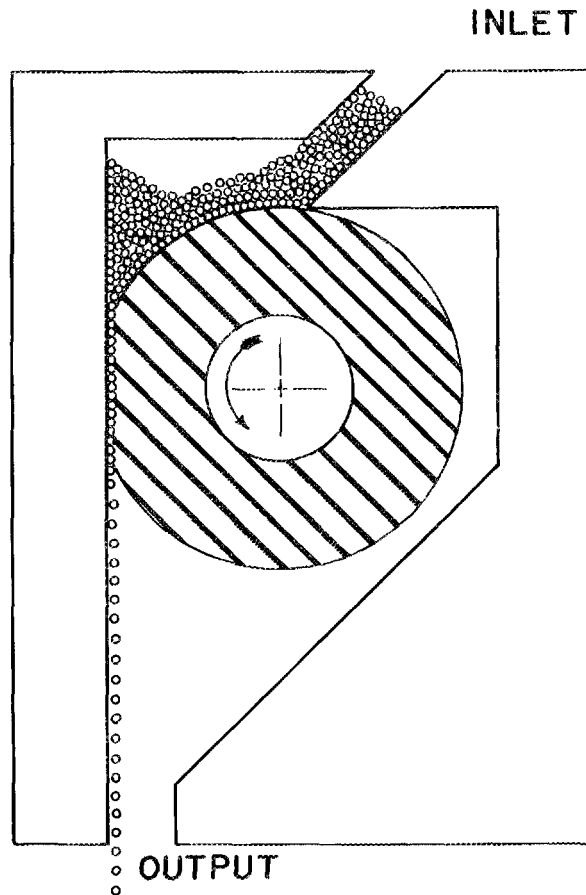


Fig. 3.9. Schematic of roll feeder.

type of feeder to be sufficiently accurate and reliable, two or more roll feeders will be used to simultaneously feed the different-type particles.

### 3.2.2 Preparation and Characterization of Matrix

The chemical, microstructural, and rheological properties of the matrix must be known to develop the fuel stick fabrication process and to design equipment for remote operation. Although we have concentrated our effort on the Fort St. Vrain reference matrix, 27 to 30 wt % Asbury 6353 natural flake graphite in Allied Chemical Company 15V coal-tar pitch, we have also investigated mixtures of 40 to 60 wt % Thermax in 15V pitch.

We found that holdup of material in mixing containers could cause variations of  $\pm 5$  wt % from the nominal filler content of small batches of matrix. To determine our ability to reproducibly prepare batches of matrix containing the desired amount of filler, we prepared two batches at each of the following nominal flour contents: 20, 24, 27, and 28.5 wt %. These 300-g batches were blended in a Helicone<sup>6</sup> mixer at 135°C for 40 min. Two samples from each of the eight batches were analyzed for filler content by dissolution in pyridine and correcting for the undissolved solids in the pitch. The results of these analyses showed that we can prepare matrix containing within about 0.5 wt % of the desired amount. An analysis of variance showed the standard deviation due to sampling and analytical error to be 0.38 wt %.

We developed another technique for determining the filler content of matrix material which uses the relationship between graphite filler content,  $f$ , and the density,  $\rho_m$ , of warm-pressed compacts of matrix. This relationship is expressed by

$$\frac{1}{\rho_m} = \frac{1}{\rho_p} - \left( \frac{\rho_c - \rho_p}{\rho_p \rho_c} \right) f \quad (1)$$

where  $\rho_p$  is pitch density and  $\rho_c$  is graphite density. Using values of 1.28 and 2.25 g/cm<sup>3</sup> for the densities of pitch and graphite, respectively, the filler content of eight batches of matrix determined from the above equation agreed very closely with the results obtained by dissolution in pyridine. Measurements of the density of five warm-pressed compacts showed that this tech-

nique has about the same precision as dissolution of two samples in pyridine.

### 3.2.3 Fuel Stick Molding

A fuel stick is formed by injecting hot (150 to 190°C) matrix under pressure into a mold containing coated particles. After cooling, the fuel stick is ejected from the mold. During injection of the matrix both the temperature and pressure must be closely controlled. Temperature affects not only the viscosity of the matrix but also the decomposition and volatilization of the hydrocarbons in the pitch binder. Pressure must be sufficiently high to force the matrix into the interstices of the particle bed but not so high that it cracks the coatings on the particles.

The processes that have been used previously for making 2-in.-long fuel sticks need to be more automated and simplified for use in TURF. The hot injection system used by GGA<sup>7</sup> and in the past by ORNL<sup>8</sup> does not appear to be suitable for use in TURF. One major disadvantage is lack of control of injection pressure. Another is the tendency of the graphite powder to settle if the matrix is held at elevated temperatures for any length of time without agitation. The process we are investigating for molding fuel sticks eliminates these two problems. This process, called slug injection, is illustrated in Fig. 3.10. A preformed slug of matrix is inserted into the mold containing particles, the mold is heated to melt the matrix slug, and then the matrix is injected into the bed of particles by applying pressure to the top punch. Entrapped air and excess matrix are forced through small orifices at the bottom of the die.

We have made several hundred 2-in.-long fuel sticks by the slug-injection technique using Fort St. Vrain reference matrix, 27 to 30 wt % natural flake graphite in coal-tar pitch, and matrix containing 40 to 60 wt % Thermax in pitch. The following conclusions may be drawn from this work:

1. A 2-in.-long bed of 500- to 700- $\mu$ m particles can be injected with any of the above matrix compositions to form a good fuel stick with an acceptable end cap.

7. W. V. Goeddel, W. D. Winkler, and C. S. Luby, "HTGR Fuel Irradiation Performance and Implications of Fuel Design," *Proceedings of Gas-Cooled Reactor Information Meeting at ORNL*, CONF-700401.

8. J. D. Sease et al., "Fueled-Graphite Fabrication Development," *GCR-TU Programs Semiannu. Progr. Rep. Sept. 30, 1970*, ORNL-4637, pp. 104-9.

6. Helicone mixer, model 2CV, product of Atlantic Research Corp., Alexandria, Va.

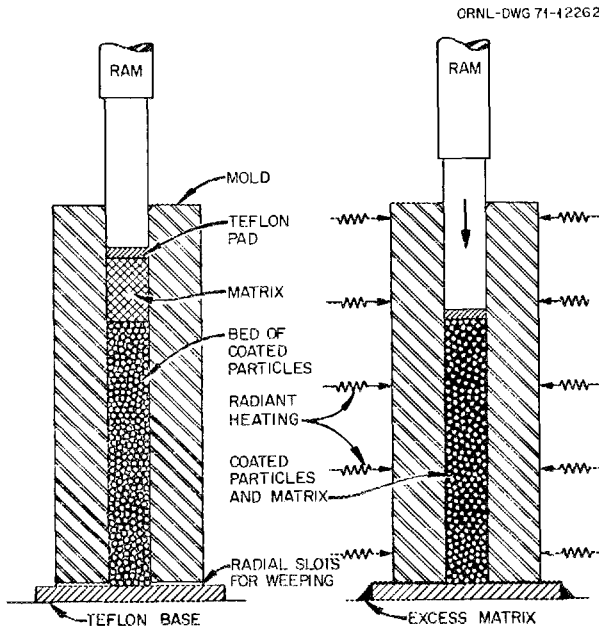


Fig. 3.10. Slug-injection technique for fabricating HTGR fuel sticks.

2. The ability to inject the reference matrix is strongly dependent on filler content. As the filler content approaches 30 wt %, the time required for injection increases appreciably and the rejection rate due to excessive end cap also increases.

3. The ability to inject the matrix is very pressure sensitive. In most cases we have limited the injection pressure to 1000 psi to minimize the potential for breaking particles. However, we have found that increasing the injection pressure to 1500 psi not only reduces the injection time but also makes it possible to inject some matrix compositions that cannot be injected at 1000 psi.

4. The injection time varies inversely with injection temperature; however, the maximum injection temperature is limited by the tendency to trap gas evolved from the pitch as the temperature approaches 200°C. At practical injection temperatures and 1000 psi the injection time for the reference matrix is about 1½ to 2 min.

5. The injection time for matrix containing Thermax filler is about 10 to 20% of that for reference matrix.

6. A binary blend of 300- and 600- $\mu$ m particles could not be injected with the reference matrix. Sticks with this type of particle loading may require a variation of the slug-injection process in which the matrix is loaded in granular form simultaneously with the particles or the use of a different filler material such as Thermax.

### 3.2.4 Carbonization and Annealing

After molding, the sticks must be heated to about 700 to 1000°C to carbonize the pitch binder and then annealed at 1800°C to remove residual volatiles, partially graphitize the pitch coke, and stabilize the dimensions. Sticks made both with reference matrix and with matrix containing 40 to 60 wt % Thermax have been carbonized using both fast (500°C/hr) and slow (40°C/hr) cycles. We have selected a cycle that employs a rapid heating rate (~600°C/hr) through the temperature range where the pitch is soft but not yet decomposing appreciably (100 to 200°C) and a slower heating rate (~180°C/hr) through the temperature range where most of the pitch decomposition occurs (200 to 450°C). Various packing media, for example, natural flake graphite, Al<sub>2</sub>O<sub>3</sub>, SiO<sub>2</sub>, and SiC, have been used to support the sticks during carbonization. Natural flake graphite and Al<sub>2</sub>O<sub>3</sub> appear to be comparable.

In general, the results of carbonization experiments have shown that sticks containing more than 27 wt % natural flake graphite filler can be carbonized in a packed bed of graphite and maintain reasonable dimensional stability. However, even with this matrix there is considerable stick-to-stick variation, and only about 80% of the sticks have diameters within  $\pm 0.003$  in. of the nominal diameter. Sticks made with Thermax filler have even greater dimensional variation. The variation in diameter ( $D_{\max} - D_{\min}$ ) of carbonized sticks made with Thermax is 0.005 to 0.010 in.

Because of the serious problems in dimensional control during carbonization, it appears desirable to consider in-block carbonization for the operations in TURF.

We have annealed a number of fuel sticks at 1800°C and have encountered no problems.

### 3.2.5 Stick Inspection

In this operation a series of inspections are made on the green sticks to characterize the matrix, the fuel loading, and the dimensions, and another series of inspections are made on the fired sticks to characterize the uranium and thorium contamination (surface contamination and broken coatings) and dimensions. The filler distribution for the green sticks will be determined by dissolution, and the particle distribution will be determined by screening the residue after dissolution. Another inspection which will be used along with the dissolution for determining fissile distribution is gamma scanning. On the fired sticks, we will determine the heavy-metal contamination by the fission-gas release test and the hydrolysis test or acid leach.

In the fission-gas release test a fuel stick is irradiated in the ORR poolside facility, and then the ratio of the  $^{85m}\text{Kr}$  released at  $1100^\circ\text{C}$  to the amount of  $^{85m}\text{Kr}$  produced during irradiation is determined. This test is a measurement of the uranium contamination. A number of samples have been irradiated to date, but the correlation between our results and those of GGA is not very good. We are performing additional experiments.

The hydrolysis test for determining the amount of thorium contamination consists in converting the oxide to carbide, hydrolyzing the thorium carbide, collecting the gaseous products, and determining the amount of methane or ethane in the gases. Since the amount of methane and ethane is directly related to the amount of heavy-metal contamination, this system can be calibrated using known amounts of  $\text{ThO}_2$ . We have been investigating the above inspections for the last few months but are not sure of the correlation between the results and the properties that are being measured.

### 3.2.6 Fuel Stick Molding Machine

The conceptual design of a prototype fuel stick molding machine capable of producing 500 fuel sticks per day is illustrated in Fig. 3.11. This concept employs a 24-station index table which indexes 24 fuel stick molds through the molding sequence. The molds are spring loaded downward against a stationary skid ring which acts as the end closure of the mold. A filled Teflon pad is situated on top of the skid ring to reduce the friction between the mold and the skid ring. Heating and cooling are accomplished in zones using up to eight stations each and allowing a maximum of approximately 6 min for each. The number of stations included in the heating and cooling zones will be adjusted when more detailed heat transfer analysis is completed. Preliminary heat transfer calculations have resulted in modifying the original concept in an attempt to obtain a more uniform temperature distribution in the particle bed and pitch slug. These calculations also

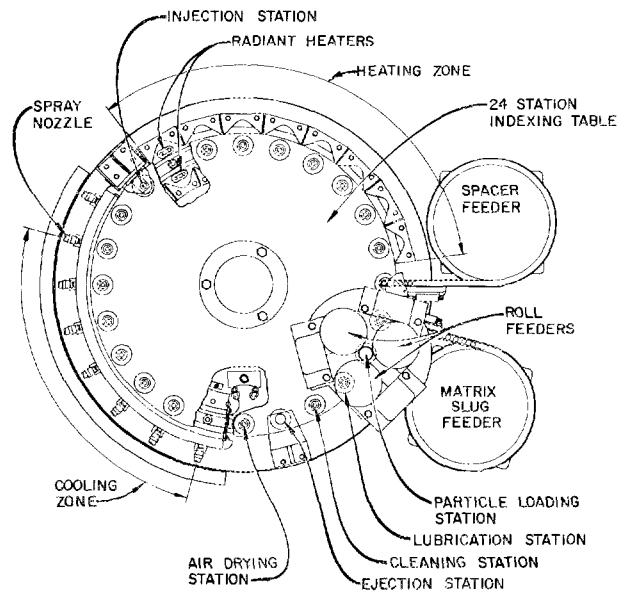


Fig. 3.11. Prototype fuel stick machine.

indicated the need for liquid spray cooling rather than air cooling, which is more desirable for the in-cell model.

Some samples of an all-polymeric fluorocarbon material (Rulon) have been tested for use as skid ring surface and spacer material. First attempts to use this material were unsuccessful because of creep and adherence of the fuel stick to the spacer. However, more recent tests using a well-cleaned spacer and a matrix containing a large weight percent Thermax filler gave good results. Samples of glass and graphite-filled Teflon have been obtained for testing as spacer materials. A prototype mold incorporating both the spacer and skid ring and an aluminum mold has been fabricated and will be evaluated in the near future.

## 4. HTGR Fuel Recycle Pilot Plants

A. L. Lotts

The HTGR fuel recycle development program will culminate in the demonstration of recycle technology in pilot-scale operations. Ideally, such operations would be carried out in an integrated pilot plant, but because of the number of alternatives that are available to the program, the work has been divided among three plants: the Head-End Pilot Plant, the Acid-Thorex Pilot Plant, and the Refabrication Pilot Plant. This chapter reports the activities involved in the design, construction, and operation of these pilot plants with regard to both facilities and equipment. During the past year, ORNL has been conceptually designing the three pilot plants, and we have also continued to maintain the Thorium-Uranium Recycle Facility in a state of readiness for processing and refabricating HTGR fuel.

### 4.1 HEAD-END PILOT PLANT DEMONSTRATION

J. W. Anderson	T. J. Golson
J. P. Jarvis	J. W. Snider
R. E. Hill	J. M. Chandler

A conceptual design of a pilot plant was prepared, based on the assumption that the hot head-end demonstration task of the program will be performed in facilities at ORNL.<sup>1</sup> This plant would be installed in TURF, Building 7930, and use portions of the MSRE

facility, Building 7503, as an interim fuel handling and storage facility. Figure 4.1 is a schematic of the plant, showing the major functional elements of the plant and its interfaces with other plants or activities.

The plant would have a fuel reprocessing rate of about ten FSVR fuel elements per day, which is about 10% of the throughput required for a 1-ton (heavy metal) per day reprocessing plant for fuel from HTGRs. Thirty 1000-MW(e) reactors would have a reprocessing requirement of about 1 ton/day.

Operation of the pilot plant with spent FSVR fuel was assumed to begin immediately following the first discharge from the reactor and its 100-day cooling time. It was assumed that an average of six-sevenths of an element per day will arrive at the pilot plant, that two shipping casks are available, that each spent fuel container transported with the shipping cask will contain six elements, and that each cask requires 13 to 14 days to make the round trip between FSVR and the pilot plant. Initially the spent fuel would be received, unloaded, and stored in Building 7503. After the facilities are completed at Building 7930, shipments would be received, handled, and stored there. The fuel would then be shuttled as required from the Building 7503 facilities to the 7930 facilities for reprocessing.

#### 4.1.1 Design of Processing Equipment

The processing equipment portion of the plant was divided into seven major systems: (1) burner-feed preparation, (2) burning, (3) burner ash handling, (4) classified ash treatment, (5) scrap recycle, (6) off-gas handling and decontamination, and (7) process services.

---

1. Present plans are to perform the hot head-end pilot plant demonstration at the Idaho Chemical Processing Plant. However, the work described here is still useful in planning that task.

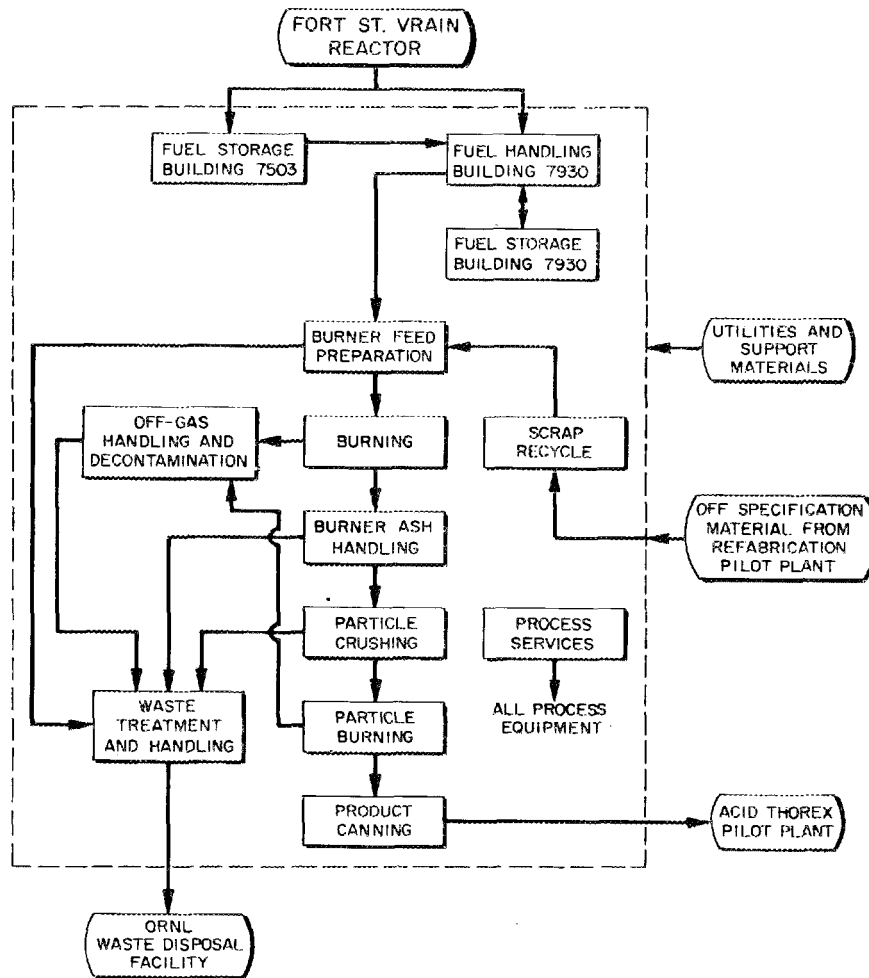


Fig. 4.1. Head-end pilot plant -- schematic.

These systems were then arranged into subsystems and components of related equipment items. Conceptual design of processing equipment was concentrated on equipment items where the greatest unknowns were judged to exist in either the processes or the equipment.

The conceptual design work was also based on the assumption that a fluidized-bed burner would be used as a primary fuel burner and that this burner would consume all the graphite in a fuel element and produce the greatest amount of gaseous waste that would have to be handled in the off-gas handling and decontamination system. It was further assumed that the off-gas system would use the hot-carbonate absorption method of removing the  $\text{CO}_2$  from the off-gas stream.

The basic steps of processing are shown in Fig. 4.2. Concept designs were prepared for a saw, a crusher, and

a screen tumbler in the burner feed preparation system; a fluidized-bed burner in the burning system; and the  $\text{CO}_2$  absorption columns of the off-gas handling and decontamination system.

#### 4.1.2 Design of Waste Treatment and Disposal Equipment

A major system of the pilot plant provides for waste treatment and disposal. This system was further divided into subsystems of equipment for handling solid, liquid, and gaseous waste streams. Since the handling of solid waste is the most difficult problem, the conceptual design effort was concentrated in this area. Concept designs were prepared for equipment to collect, package, and transfer solid waste from the processing cell to

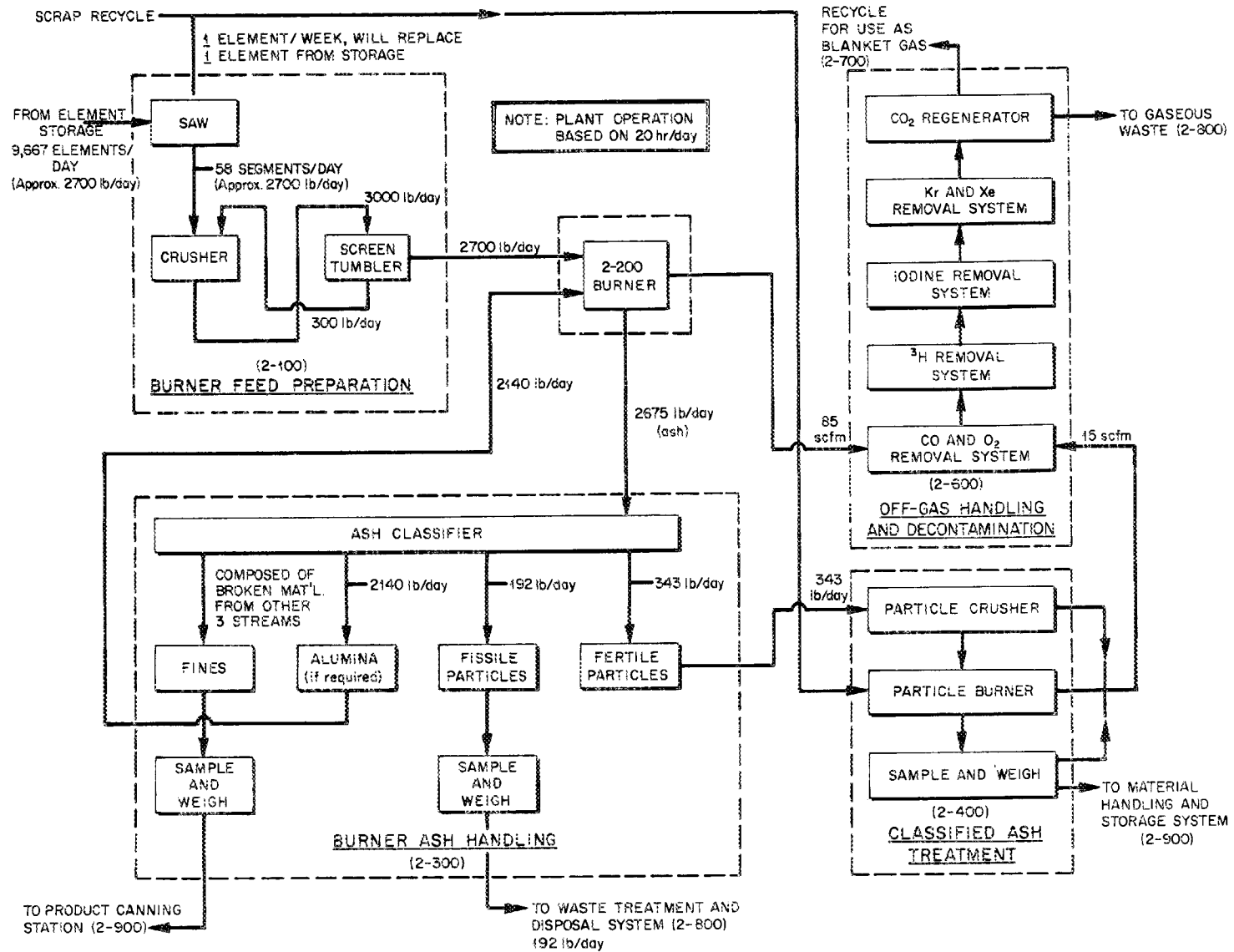


Fig. 4.2. Head-end pilot plant – process flow diagram.

central ORNL facilities for disposal either by on-site methods or by transfer to a national repository.

#### 4.1.3 Design of Materials Handling Equipment and Facilities

Equipment and facilities for handling feed, product, and process support materials, organized as a system of the pilot plant, received a great deal of attention during the conceptual design effort. Since most of the requirements of this system are independent of the development work carried on in other parts of the program, reasonably definitive concept designs could be prepared.

Designs were prepared for converting three cells of the Molten-Salt Reactor Experiment facility (Building 7503) into an interim storage facility. This facility would be capable of receiving the FSVR shipping assembly, removing the cask from the trailer, and transferring (under containment) the spent fuel container full of spent fuel elements into a storage rack in one of the cells. Equipment would be provided for extracting the container from its storage location and placing it in a transfer shield for movement to Building 7930 for processing operations. Included in the designs were the modifications required to Building 7503 as well as special handling equipment and fixtures for handling the FSVR shipping cask and the transfer shield for handling the spent fuel containers during storage and transfer operations.

At Building 7930 a modification to the facility would be required, adding approximately 4800 ft<sup>2</sup> of floor space, including hot cells. One cell structure would provide a fuel handling space wherein spent fuel containers could be inserted and the elements could be removed and reloaded into a single element shield for transfer into the processing cell. The other cell structure would provide space for storing fuel containers loaded with spent fuel elements until they were ready for reprocessing. The design of these facilities included the addition to the building, the hot-cell structures, and the special handling equipment and transfer shields necessary to perform the material transfer operations. Designs were also prepared for a product collection and packaging station where the reclaimed fuel values from the processing operations could be packaged, transferred out of the processing cell, and delivered to the Acid-Thorex Pilot Plant for subsequent reprocessing operations.

#### 4.2 ACID-THOREX PILOT PLANT DEMONSTRATION

J. W. Anderson    T. J. Golson  
J. P. Jarvis        J. W. Snider  
R. E. Hill          J. M. Chandler

A conceptual design of the pilot plant was prepared based on the assumption that the hot demonstration task of the program will be performed in facilities at ORNL. This plant would utilize existing equipment and facilities in Building 3019, with additions and modifications required to perform the necessary operations. Figure 4.3 is a schematic of the plant, showing the major functional elements of the plant and its interfaces with other plants or activities.

The existing equipment in Building 3019 for Thorex processing has a throughput capacity of approximately 6 kg of heavy metal per day. Additions and modifications to this equipment would be made to maintain this processing rate capacity. It is expected that feed for this

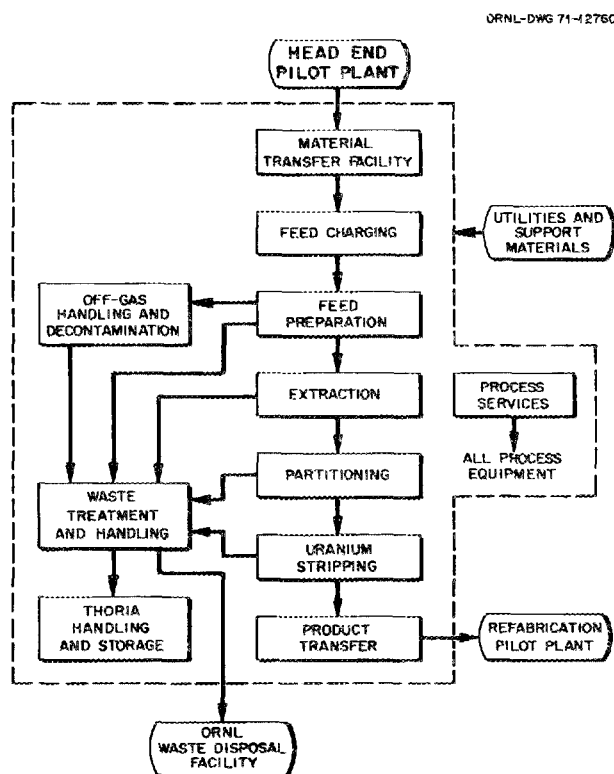


Fig. 4.3. Acid-Thorex pilot plant – schematic.

pilot plant would be the product from the Head-End Pilot Plant reported in Sect. 4.1. Since the throughput capacity would exceed the product flow rate from the Head-End Pilot Plant, it is expected that this plant would not be required to operate on a continuous basis.

The plant would be capable of receiving recovered fuel values from head-end processing operations, preparing them for solvent extraction processing, purifying them, separating the thorium from the uranium, and preparing the product for shipment to the Refabrication Pilot Plant for fuel fabrication operations.

#### 4.2.1 Design of Processing Equipment

The processing equipment portion of the plant was divided into six major systems: (1) feed preparation, (2) extraction, (3) partitioning, (4) uranium stripping, (5) off-gas handling and decontamination, and (6) process services. These systems were then arranged into subsystems and components of related equipment items. Conceptual design of processing equipment was concentrated on equipment items in the feed preparation and the off-gas handling and decontamination systems, where the greatest unknowns were judged to exist in either the processes or the equipment. The basic steps of processing are shown in Fig. 4.4. Concept designs were prepared for a leacher, a washer, a centrifuge, and a dryer in the feed preparation system and for a caustic scrubber and krypton adsorption and desorption columns of the off-gas handling and decontamination system.

#### 4.2.2 Design of Waste Treatment and Disposal Equipment

This major system of the pilot plant provides waste treatment and disposal capabilities. This system was further divided into subsystems of equipment for handling solid, liquid, and gaseous waste streams. Since the handling of solid waste is the most difficult problem, the conceptual design effort was concentrated in this area. Concept designs were prepared for equipment to collect, package, and transfer solid waste from the processing equipment in the feed preparation system to central ORNL facilities for disposal either by on-site methods or by transfer to a national repository.

#### 4.2.3 Design of Materials Handling Equipment and Facilities

Equipment and facilities for handling feed, product, and process support materials received a great deal of

attention during the conceptual design effort. Included in the design was a new transfer cubicle to be constructed over the roof of cell 3 of Building 3019, in which not only materials handling equipment but also the solid waste handling equipment would be installed. Concept designs were also prepared for the special handling and transfer equipment necessary to receive canned fertile particles as product from the Head-End Pilot Plant, unload these cans, and charge the contents to the feed preparation system. Equipment was also provided for handling packaged solid waste within the cubicle and transferring this waste out of the cubicle and into shielded carriers, where it could be moved safely from the building. A concept design was also prepared for a transfer glove box facility capable of being attached to an existing liquid transfer carrier. This facility would be used for transferring the product solution from the uranium stripping system into the carriers for transfer to the Refabrication Pilot Plant.

### 4.3 REFABRICATION PILOT PLANT DEMONSTRATION

J. W. Anderson      J. D. Sease  
J. P. Jarvis          F. C. Davis  
J. M. Chandler

On the assumption that the hot demonstration task of the program will be performed in facilities at ORNL, a conceptual design of a pilot plant for this task was begun. This plant would be installed in TURF, Building 7930. The plant would have a fuel refabrication rate of about two recycle fuel elements per day and would be fed with uranyl nitrate solutions coming from the Acid-Thorex Pilot Plant as product material. The plant would have facilities for receiving fuel shipments, unloading the fuel carrier, and transferring the uranyl nitrate to the equipment in the processing cell and for refabrication of recycle fuel elements and placing these elements in containers capable of being shipped to a reactor for subsequent fueling or test purposes.

#### 4.3.1 Design of Processing Equipment

The processing equipment portion of the plant was divided into seven major systems: (1) sol preparation, (2) microsphere preparation, (3) microsphere coating, (4) fuel stick fabrication, (5) fuel element assembly, (6) scrap recycle, and (7) process services. Each of these systems was then arranged into subsystems and components of related equipment items. The first draft of a

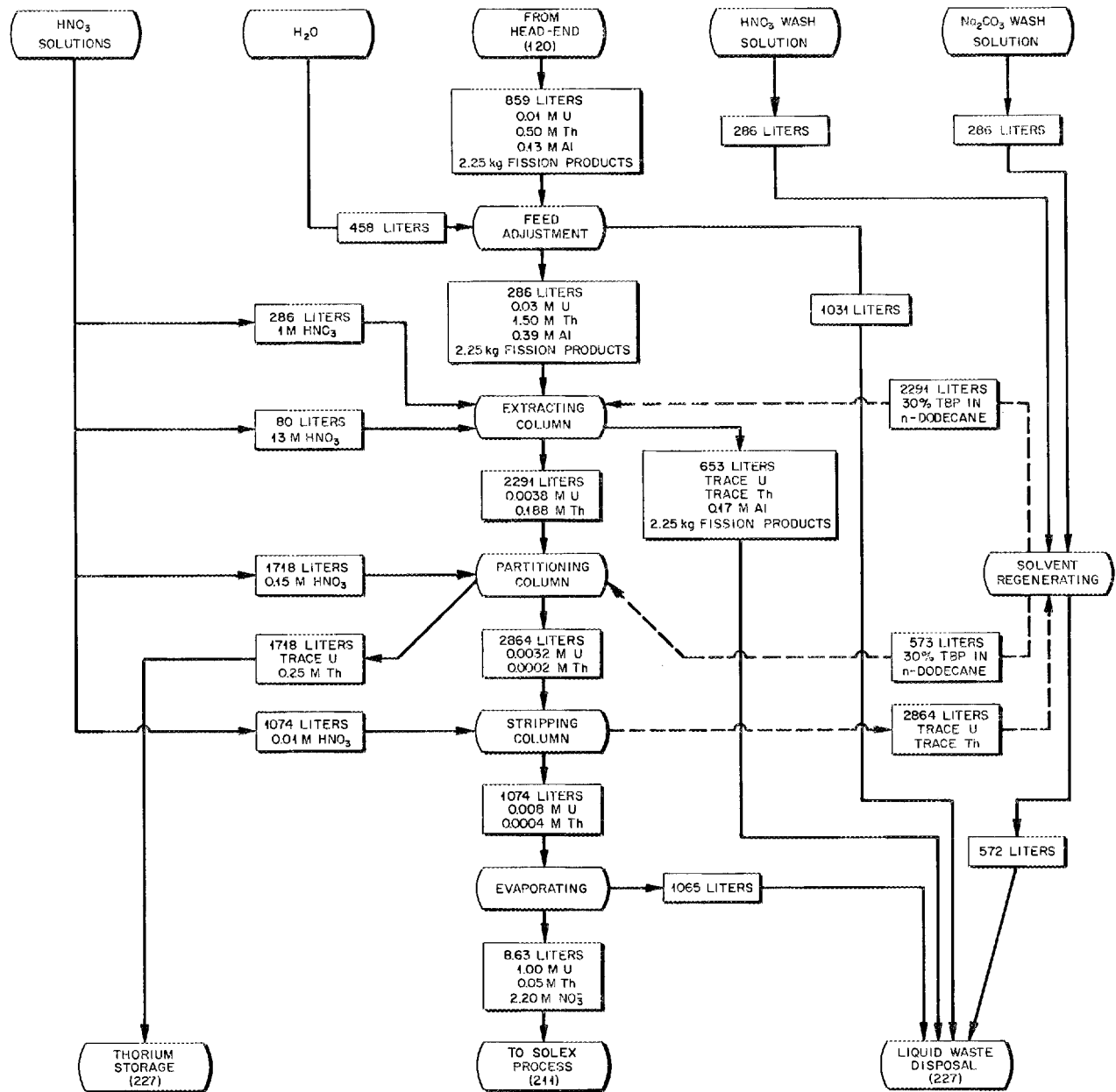


Fig. 4.4. Acid-Thorex pilot plant – process flowsheet.

diagram showing these related pieces of equipment was prepared, along with process flowsheets for the micro-sphere coating, fuel stick fabrication, and fuel element assembly processing systems.

To assist in preparing conceptual designs of processing equipment components, basic performance, design, and development requirements were defined and

documented for the following equipment items: storage hoppers, diverter valves, bulk weighers, batch weighers, classifier feeders, classifiers, shape separators, sampler, batch blender, fuel particle feeder, pitch slug feeder, fuel stick loading machine, coating furnace, coating furnace exhaust equipment, and fuel stick carbonizing and annealing furnace.

### 4.3.2 Design of Waste Treatment and Disposal Equipment

A major system of the pilot plant provides for waste treatment and disposal. This system was further divided into subsystems and equipment for handling solid, liquid, and gaseous waste streams. Design work thus far has been concentrated on identifying the waste products that would be generated in fabrication operations and scoping the requirements that must be met by equipment and systems sufficient to handle, treat, and dispose of those products.

### 4.3.3 Design of Materials Handling Equipment and Facilities

Equipment and facilities for handling feed, product, and process support materials were organized into a system of the pilot plant. Design work in this area concentrated on identifying the basic requirements for packaging of refabricated fuel elements and the methods for transferring these elements from the processing cell to facilities where they may be loaded in the shipping carriers for transfer to a reactor.

## 4.4 THORIUM-URANIUM RECYCLE FACILITY

J. M. Chandler

The Thorium-Uranium Recycle Facility was constructed to provide safe and suitable work space to develop, on a pilot plant scale, technology for processing and refabricating irradiated thorium fuels.

Biological shielding and containment are provided in 2120 ft<sup>2</sup> of the floor area of the four shielded processing cells that are equipped for remote maintenance and operation of the in-cell equipment. Three additional auxiliary cells plus an air-lock cell and the receiving area provide access, work, and storage areas in support of equipment and activities inside the process cells.

Work was conducted to maintain the TURF equipment in operational readiness in support of the heavily shielded process cells and the auxiliary cells and their fixtures. This work involved repairing or replacing some electric motors, replacing dirty or damaged off-gas filters, and replacing broken or leaking water lines. Also, repairs were made as needed to in-cell hoisting and manipulator equipment to make it operable.

Final acceptance tests were completed, and official acceptance for select risk coverage was received, via ORO-AEC, from Factory Mutual Insurance Company, for the TURF in-cell CO<sub>2</sub> fire protection system. This is

a culmination of more than three years of work in TURF in which numerous tests, revisions, and retests of this unique in-cell fire protection method were conducted. The system is ready for use.

The 2-in.-diam cast-iron rubber-gasket-jointed pipe intermediate level waste line (ILW) connecting the Melton Valley waste (MVW) tanks located adjacent to and west of the MSRE, with connections to the TURF and TRU waste tanks, developed leaks at several joints and was removed from service. A new 2-in. sched-40 304L stainless steel line of high-quality all-welded construction was installed to replace the abandoned leaking line serving to collect TURF and TRU waste. Late in 1971 the ILW line connecting MVW tanks with the ORNL tank farm developed leaks and was replaced with an all-welded high-quality stainless steel line.

Emergency electric power was supplied to the large-capacity (300-cfm) TURF air compressor. This was necessary because the small air compressor, initially provided with emergency power, does not provide adequate compressed air. Now, the diesel-engine-powered generator providing TURF emergency electrical power is loaded to its capacity of 220 kVA.

Work was completed for rearrangement and relocation of the pillow block bearings of the two facility hot off-gas fans. We moved one bearing from its original position inside the duct to a location outside the duct and beside the other bearing. Both fans were treated alike. This made an "overhung" fan arrangement and permits maintenance of the bearings without entry inside the contaminated off-gas duct. High-speed impellers were specified and purchased but not provided in the original fan installation. This error was corrected gratis by the fan manufacturer, and impellers of the proper speed were installed.

We are preparing operating instructions to be used in conjunction with operating procedures prepared previously for work involving the in-cell crane and manipulator systems. These instructions are being written with the aid of operating personnel, who supply wording that is more familiar to trainee operators learning to use the equipment.

One of the two vessel hot-off-gas filter assemblies failed to meet the 99.95% dioctyl phthalate efficiency test. The surfaces of the assemblies were found to be severely corroded inside and outside the metal housing into which the fiber-glass filters are packaged. Moisture and some other corrosive atmosphere had entered the filter housing and attacked the iron surfaces, causing the Amercoat surface coating to peel off in large pieces. Some of these large pieces of plastic plugged the filter

housing outlet. Since a replacement housing cost was estimated to be \$10,000 the unit was decontaminated, repacked with fresh absolute filters, and returned to standby service. Fortunately, the contamination was only  $6.6 \times 10^5$  dis/min of alpha activity from uranium and not alpha activity from the  $^{252}\text{Cf}$  being handled by the on-stream filter. This made cleanup work possible. It was found that a steam trap that formerly discharged into the drainage system serving the HOG filters had caused the corrosive atmosphere in the filter pit.

A second failure occurred of tubes in the recirculating water heat exchanger (RWHX-1) (a replacement unit supplied when the original RWHX-1 failed). We now believe that failure of the second unit was caused by water hammer in the HFIR tower water circulation system supplying cooling water to the RWHX-1 system at TURF. Efforts are being made to isolate the cause of the damage to the RWHX-1 units so that corrective measures may be taken.

A study was made of the materials handling requirements at TURF for conducting the work prescribed in the National HTGR Program Plan.<sup>2</sup> Basically this plan would involve the reprocessing and refabrication processes to produce 150 recycle fuel elements from  $^{233}\text{U}$  and thorium at a rate of about 2 FSVR elements per day.

A 25,000-Ci  $^{60}\text{Co}$  source was used in cell B in experiments conducted to determine the gamma radiation sensitivity of neutron detectors. This work was conducted by the Instrumentation and Controls Division. This  $^{60}\text{Co}$  produced a radiation level in cell B 3 ft from the source of about  $4 \times 10^5$  rads/hr. Since this is the highest gamma radiation level handled in TURF to date, we decided to x-ray cell B and determine the location of radiation leakage, if any, from cell B penetrations into the occupied area around the cell. Gamma shines ranged from 5 millirems/hr through electrical service sleeves to 3800 millirems/hr around shield plugs in unused master-slave manipulator ports. With the source against the 15-in.-thick shield door No. 1, 140 millirems/hr was measured penetrating the door. As expected, only 0.2 millirem/hr was measured at the out-of-cell surface of a 50-in.-thick oil-filled laminated glass construction shield window when the  $^{60}\text{Co}$  source was against the in-cell surface of the window. Unexpectedly, a high reading of 800 millirems/hr was shining out the end of shield door No. 1 containment envelope

when the  $^{60}\text{Co}$  source was placed 5 ft above the cell floor level and against the cell side of the door. Apparently a pinhole exists through the shielding at that location. Knowledge of these hot spots allows us to protect personnel from the hazard.

Twelve 4-in. by 5-in. by 20-mil-thick tantalum foils irradiated in the Stanford linear accelerator were received at TURF and placed in cell B. The lead shielding container was opened, and the foils were separated and packaged in individual plastic bags and loaded individually or in selected groupings into a portable shielded container for transport to the EGCR facility for use in physics experiments by members of the Chemistry Division. All handling and packaging at TURF were performed remotely in cell B. TURF facilities were used for this job because alpha-activity-free hot-cell space was available.

Operations such as those discussed above which can be conducted without contaminating the work space are being performed in TURF even though they are not related to the Thorium Utilization Program because they help support, financially, the skeleton operating and maintenance force necessary to keep TURF in operational readiness.

We designed and placed into service a portable dry box—decontamination box for use in removing master-slave manipulator parts and electromechanical manipulators from cell G for repair. The box was necessary because no such equipment was provided at the time TURF was constructed. We have used the box repeatedly to decontaminate the slave ends of model A manipulators removed from cell G for repair.

Two model A master-slave manipulators were removed from cell G service and were replaced by a pair of model E extended-reach manipulators. These units are much preferred and are more serviceable.

During the past year, 75 pneumatic transfers involving 195 mg of  $^{252}\text{Cf}$  were made through the 700-ft-long transfer line between the TURF and TRU buildings. The largest source transferred contained 35 mg of  $^{252}\text{Cf}$ .

Ten 304L stainless steel disk activation specimens were placed inside cell G at locations that receive the highest neutron bombardment from the  $^{252}\text{Cf}$  and other neutron emitters being treated there. From the amount of activation received by these specimens, we expect to get some values for the amount of activation of the 304L stainless steel cell liners. These data will be necessary and useful in planning cleanout of cell G. One of the ten type 304L stainless steel disks was removed from cell G after 20 days of exposure to about 90 mg of  $^{252}\text{Cf}$ , and the disk counted 82,000 dis/min of

2. Oak Ridge National Laboratory and Gulf General Atomic, *National HTGR Recycle Development Program Plan*, ORNL-4702 (August 1971).

beta-gamma activity immediately upon removal from the cell and after the transferable contamination was removed from its surfaces. One day later the disk counted 4600 dis/min, and after four days its induced radioactivity was 3400 dis/min. Two and one-half months later there remained a count of 1500 dis/min of beta-gamma activity with a half-life for radioactive decay of 2½ months. Radioactive contamination measured on manipulator parts removed from cell G has been greater than 300,000 dis/min.

A 30-gal container was filled with plastic bottles 1 liter and smaller in size, and the bottles were placed piecemeal into a heated 1-gal syrup bucket. As softening occurred and the plastic compacted, additional plastic bottles were added until all had been used. A total of 1.4 gal of solid plastic was recovered from the 30-gal volume of bottles for a 21.4-fold volume reduction. A temperature of 400°F was required to soften the plastic to the fluidity needed for reasonable flow. The temperature outside the can was 600°F. A

4000-W, 220-V Calrod heater 10 ft long was coiled around a 6-in.-OD pipe to provide the heating nest in which the syrup bucket was inserted for heating. The flammability of the heated plastic was measured at 400 and at 500°F. At the higher temperature of 500°F the plastic could be ignited by a match flame held 30 sec in contact with the surface. This plastic volume reduction demonstration shows promise in reducing the volume requirement for disposal of plastic containers resulting from hot-cell work. Furthermore, the smaller volume of waste would simplify the task of waste removal from the hot cell and would simplify waste handling to and at the disposal place.

The TURF facility continues to be of great interest to visitors to ORNL. We honor requests for numerous tours of the facility each month. Recently people from Asia have joined the Europeans in showing interest in the HTGR fuel recycle program and the place of its demonstration work at TURF.

## 5. Recycle Fuels Irradiation and Evaluation

T. N. Washburn    J. H. Coobs  
R. B. Fitts        A. R. Olsen

The irradiations of the HTGR fuel recycle program have two main objectives: (1) to provide irradiated fuel for head-end processing studies and (2) to proof test recycle fuels produced in prototype equipment. The test conditions of interest include fuel temperatures between 600 and 1300°C, burnup to 20% fissions per initial actinide metal atom (FIMA) in the (Th,U)O<sub>2</sub> particles, and fast-neutron fluences up to  $8 \times 10^{21}$  neutrons/cm<sup>2</sup> ( $E > 0.18$  MeV).

The program involves capsule irradiations in research reactors, pilot-scale irradiations in the Peach Bottom Reactor, and a series of tests in the Fort St. Vrain Reactor (eventually including remotely fabricated recycle test elements). The first two stages of this program are currently being implemented: (1) irradiation of recycle test elements (RTEs) in the Peach Bottom reactor and (2) accelerated-burnup-rate capsule irradiations.

### 5.1 Recycle Test Elements

R. B. Fitts

The irradiation of the first six recycle test elements<sup>1</sup> (RTEs) began in the Peach Bottom Reactor in July of 1970, and the tests have progressed without incident since that time. In April 1971 the first of these test elements to be removed from the reactor (RTE-7) was

discharged, and an additional element (FTE-11, previously designated RTE-1) was inserted. Two of the six elements presently in the reactor are scheduled for discharge in June 1972, and the remainder will remain in the reactor until June 1973 or longer.

The discharged element, RTE-7, contains combinations of fuel particles identical to those in the other RTEs with the exception of a UO<sub>2</sub> Triso plus ThO<sub>2</sub> Biso combination which was only incorporated in the last element (FTE-11). The combinations of particles used in the RTEs have been reported.<sup>1</sup> The location of these combinations in RTE-7 is shown along with the operating temperature ranges in Table 5.1. In RTE-7 the particles are loaded into the holes as bonded fuel

Table 5.1. RTE-7 fuel loading

Body	Combination <sup>a</sup>				Operating temperature range (°C) <sup>b</sup>
	W	X	Y	Z	
6	a	c	f	g	900–1050
5	a	c	f	g	980–1150
4	b	g	h	d	950–1230
3	b	d	g	i	925–1230
2	b	d	g	i	900–1130
1	b	d	g	i	590–880

<sup>a</sup>Particle combinations as given by R. B. Fitts, *GCR-TU Programs Semiannu. Progr. Rep. Sept. 30, 1970*, ORNL-4637, Table 12.2. The capital letters represent quarter sections of the fuel bodies.

<sup>b</sup>From Fig. 5.2.

1. R. B. Fitts, "Recycle Test Elements," *GCR-TU Programs Semiannu. Progr. Rep. Sept. 30, 1970*, ORNL-4637, pp. 111–113.

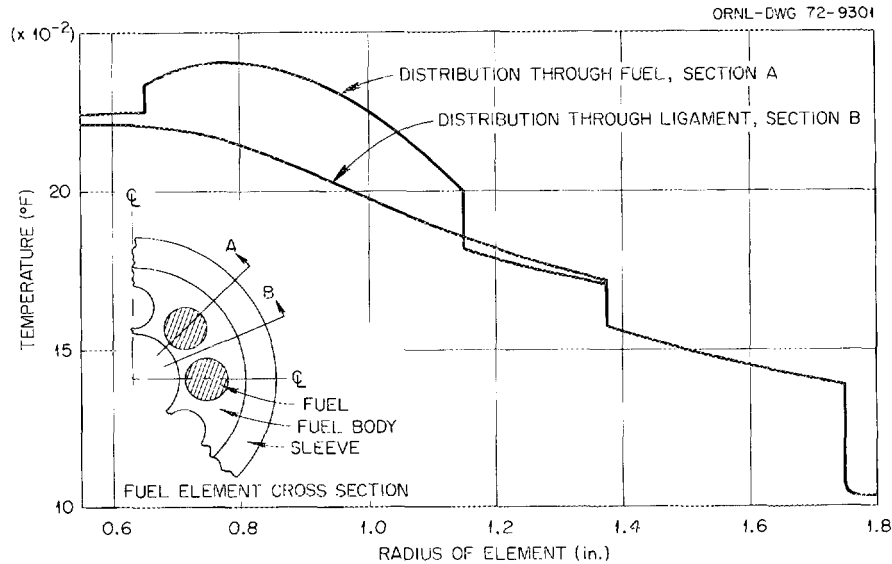


Fig. 5.1. Radial temperature profile at point of peak axial temperature for a body with bonded rods.

sticks held together with a bonding mixture of 30 to 40 wt % Poco graphite in 15V pitch.<sup>2</sup>

Irradiation of capsule RTE-7 began in the Peach Bottom Reactor on July 14, 1970, and continued there until April 22, 1971, at which time 252 effective full-power days of exposure had been accumulated. The average element burnup was predicted by Gulf General Atomic (GGA) to be 2.38% FIMA at this time. A peak fast-neutron fluence of about  $1 \times 10^{21}$  neutrons/cm<sup>2</sup> was accumulated.

The operating temperatures were calculated by GGA on the physical model depicted in Fig. 5.1, and the details of fuel stick maximum temperature distribution in RTE-7 are shown in Fig. 5.2. The fuel columns are actually about 12.5 to 12.8 in. long, with a rapid temperature decrease at the ends of the columns. The inside of the graphite body in which the fuel sticks operate is 50 to 100°F cooler than the fuel center line, and the outsides of the bodies are 300 to 600°F cooler than the fuel, with most of the temperature decrease occurring within the fuel sticks themselves.

This recycle test element will be returned to ORNL in November 1971. The present plan for examination of the element calls for the separation of all six fuel bodies

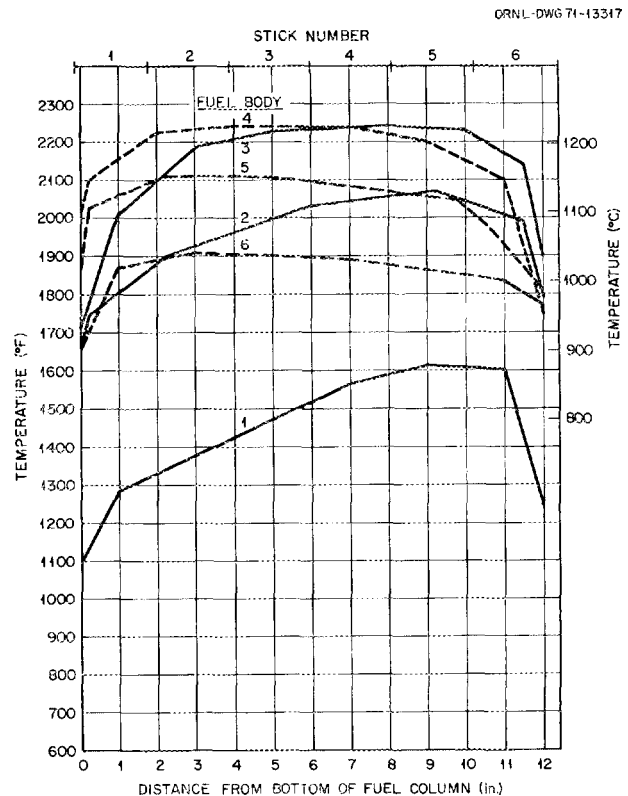


Fig. 5.2. Fuel stick temperature over the central 12 in. of fuel in each RTE-7 fuel body.

2. J. M. Robbins and J. H. Coobs, "Development of Bonded Beds of Coated Particles for HTGR Fuel Elements," *GCR-TU Semiann. Progr. Rep. Sept. 30, 1970*, ORNL-4637, pp. 9-11.

from the Peach Bottom fuel element sleeve and end fittings. The sleeve and end fittings will be available for separate examinations as desired. Bodies 1, 2, 4, and 6 will be stored intact unless visual examination reveals unusual characteristics that require detailed examination at that time. Fuel bodies 3 and 5 will be disassembled to recover five quarters for head-end reprocessing studies and nine samples of fuel sticks for metallographic examination. These samples will provide material for head-end studies on Triso-coated  $UC_2$  and  $ThC_2$  samples, the accelerated-burnup recycle fuel (combinations c and d), and the oxide fuel system (combination g) at the maximum temperature ranges available in this test. The metallographic samples include each type of fuel particle tested at the peak temperature ( $\sim 1200^\circ C$ ) and the intermediate temperature ( $\sim 1000^\circ C$ ) ranges. Additional samples will be available from bodies 1, 2, 4, and 6, as required.

## 5.2 CAPSULE TESTS

A. R. Olsen R. B. Fitts

The initial phases of design and fabrication of these accelerated-burnup-rate capsule tests have been described.<sup>3</sup> The capsules (H-1 and H-2) were inserted in the ETR in May 1971 and will be discharged early in 1972.

A schematic of the H capsule design is shown in Fig. 5.3. These capsules are each 1.068 in. in diameter and 36 in. long. The exterior of each capsule, which is made up of a type 304 stainless steel tube 0.988 in. in diameter with a 0.060-in. wall thickness, is surrounded by a cylindrical thermal-neutron shroud of hafnium or zirconium-hafnium alloy which has a nominal wall thickness of 0.040 in. Each capsule contains two graphite sleeves, each with a 0.500-in. inner diameter and a variable outer diameter to provide a tapered gas gap to control the irradiation temperature. The fuel test regions contain pyrocarbon-coated fissile and fertile particles as bonded fuel sticks or blended packed beds (see Table 5.3). The fissile material is  $^{235}U$ , and the fertile material is thorium. Both materials, whether individually or combined, are in the form of oxide or dicarbide ceramic microspheres forming the core of the pyrocarbon-coated particles. The fuel regions are divided by graphite plugs into 13 test beds in each capsule. Ten of these in each capsule are approximately

$2\frac{1}{8}$  in. long, and the three short beds are approximately  $\frac{1}{2}$  in. long.

The fuel particle combinations in these capsules are given in Table 5.2. The a, c, f, and g combinations are the main ones used in the RTEs described previously. The R combination is made with a Biso-coated uranium-loaded strong-acid resin particle and a coated  $ThO_2$  Biso particle. The distribution of these samples in the two capsules and the planned irradiation temperatures are given in Table 5.3.

The H capsules are being irradiated in the ETR. The test exposure began in May 1971 and is scheduled to end in early 1972. The peak fast ( $E > 0.10$  MeV) flux at the sample is about  $8 \times 10^{14}$  neutrons  $cm^{-2} sec^{-1}$ ,

Table 5.2 Fuel particle combinations in HTGR recycle irradiation capsules

Combination	Kernel and coating type	
	Fissile particle	Fertile particle
a	4/1 (Th/U) $O_2$ Biso	$ThO_2$ Biso
c	2/1 (Th/U) $O_2$ Biso	$ThO_2$ Biso
f	$UC_2$ Triso	$ThC_2$ Biso
g	$UO_2$ Biso	$ThO_2$ Biso
R	Resin UOS Biso	$ThO_2$ Biso

Table 5.3. Fuel loading in HTGR recycle irradiation capsules

Sample	Fuel combination	Nominal fuel bed center temperature ( $^\circ C$ )	
		Capsule H-1	Capsule H-2
13	$g^a$	1300	750
12	g	1300	750
11	c	1300	750
10	a	1300	750
9	f	1300	750
8 <sup>b</sup>	R	1300	750
7 <sup>b</sup>	R	1050	950
6 <sup>b</sup>	$a^a$	1050	950
5	f	1050	950
4	a	1050	950
3	c	1050	950
2	g	1050	950
1	f	1050	950

<sup>a</sup>Loose beds of particles; all others are pitch-bonded fuel sticks with Poco graphite filler.

<sup>b</sup>Short samples,  $\sim 0.5$  in. long; all others are  $\sim 2\frac{1}{8}$  in. long. Sample diameter is 0.5 in.

3. A. R. Olsen, "Capsule Tests," *GCR-TU Programs Semi-annu. Progr. Rep. Sept. 30, 1970*, ORNL-4637, pp. 110-11.

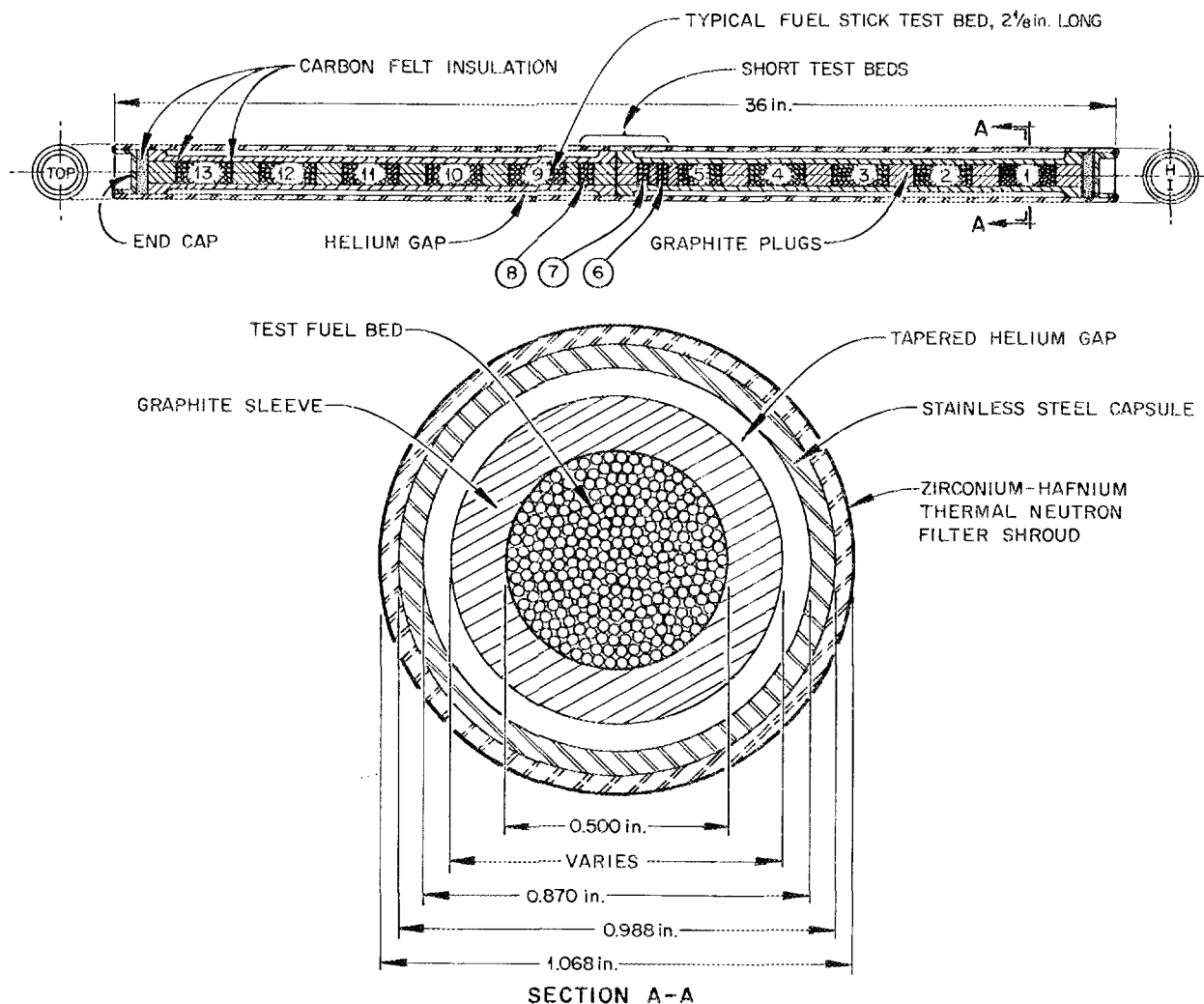


Fig. 5.3. Schematic of HTGR recycle irradiation capsule.

and peak total fast fluence will be about  $8 \times 10^{21}$  neutrons/cm<sup>2</sup>. The fuel burnup in the 4/1 (Th/U)O<sub>2</sub> fuels will be about 13% FIMA and in the UO<sub>2</sub> fuels about 50% FIMA. The fluxes were verified by analysis of fission monitor data from the ETR critical assembly mockup capsules and will be reevaluated on the basis of

postirradiation analysis of the fuel burnup and flux monitors incorporated in the fuel capsules themselves.

The H capsule fuel samples are scheduled for detailed fuel performance evaluation and head-end reprocessing studies. All the samples will be visually examined, and all the fuel sticks will be dimensionally inspected.

## 6. Commercial Recycle Plant Studies

A. L. Lotts

---

The objective of the commercial recycle plant studies is to obtain an understanding of commercial plant requirements so as to properly factor these requirements into the fuel recycle development program. The work performed within these studies includes collecting and coordinating data from the research and development effort on HTGR fuel recycle technology. At present, emphasis is on the analysis of the HTGR fuel cycle under various conditions and on analysis of alternative means of processing and fabricating HTGR fuels.

### 6.1 REACTOR PHYSICS STUDIES

L. L. Bennett    W. E. Thomas

The analysis of HTGR fuel cycle costs is influenced by a number of design parameters, among which are fuel particle size, fuel stick size, fuel composition, plutonium recycle, and  $^{236}\text{U}$  penalty. A number of revisions to existing computer codes and additional development have been required in order to accurately represent the physics effects due to these parameters. These developments are described below.

Accurate treatment of spectrum effects caused by parameter changes requires use of many neutron energy groups and accurate cross-section data. To meet this need, the XLACS code under development at ORNL was selected. This code is designed to accept basic cross-section data from ENDF/B files or other sources and prepare multigroup libraries for spectrum and cell-averaging codes (such as XSDRN). Additional development work has been required to bring XLACS to operational status. This work is now largely completed,

and check-out runs are in progress. As soon as the check-out is completed, the code will be used to prepare XSDRN libraries for the parametric studies.

The XSDRN code is used to calculate broad-group cross sections which have been weighted over flux distributions in energy and space. These broad-group data are then used in depletion codes such as CITATION. In these parametric studies, XSDRN is used to treat the physics effects due to changes in fuel configuration, fuel density, isotopic composition, etc. Again, code modifications have been needed to properly account for all these effects. The most important modification was related to the doubly heterogeneous geometry (dense fuel grains embedded in a fuel stick surrounded by bulk moderator) of the HTGR core. The XSDRN code has been modified to allow the user to perform a "double cell" calculation. In this manner, the cross sections are first weighted over the spatial flux distribution for a typical "grain cell" consisting of the fuel kernel surrounded by interstitial matrix carbon. The resulting "stick average" cross sections are then used in a "rod cell" calculation. This cell consists of a typical homogenized fuel stick surrounded by bulk graphite moderator. Thus the double cell calculation includes flux depression in the fuel stick and the further depression of the flux in the grain kernel.

These modifications to XSDRN have been made, and exploratory calculations have been undertaken. Upon completion of check-out, this method of cross-section averaging will be used in studies of particle size and rod size effects.

This task also includes studies of the fuel cycle cost penalty caused by accidental cross mixing of some

fraction of the fissile and fertile particles during the chemical reprocessing operation. This cross mixing might occur as a result of accidental breakage of silicon carbide-coated fissile particles or incomplete separation of fertile particle ashes from the intact fissile particles. Cross mixing would result in some fraction of the fissile particles (containing a high fraction of  $^{236}\text{U}$ ) being recycled to the reactor and/or some fraction of the  $^{233}\text{U}$  (from the fertile particle) being retired with the burned fissile particles. Either mode of cross mixing (from fissile to fertile or from fertile to fissile) is undesirable, since either will increase fuel cycle costs. Thus there is some economic incentive to effect a complete separation of the two types of particle. The purpose of this study is to determine the magnitude of that incentive. Studies of fuel reprocessing costs vs degree of separation then will be needed to determine if there is an overall optimum separation efficiency.

The first requirement was to obtain fuel cycle mass balances with different fractions of cross mixing. Gulf General Atomic agreed to perform the necessary calculations, and mass balances have been provided for the eight cases listed below. These data include mass flows for all cycles from startup to equilibrium.

- Case 1. Reference case for comparisons. Selective recycle with no accidental cross mixing of particle streams.
- Case 2. Reference cycle but with *no* recycle.
- Case 3. Recycle commencing at reload 2 with 2% of bred uranium being retired with the residual makeup uranium.
- Case 4. Recycle at reload 2 with 10% of bred uranium being retired with the residual makeup uranium.
- Case 5. Recycle at reload 2 with 30% of bred uranium being retired with the residual makeup uranium.
- Case 6. Recycle at reload 2 with 10% of residual makeup uranium recycled with bred uranium.
- Case 7. Recycle at reload 2 with 20% of residual makeup uranium recycled with bred uranium.
- Case 8. Recycle at reload 2 with 100% of residual makeup uranium recycled with bred uranium.

These mass balances are currently being processed through a fuel cycle cost code. Since the work is incomplete at this time, results will be reported in the next progress report.

## 6.2 FUEL VALUE OF $^{233}\text{U}$ IN HTGRs

L. L. Bennett

The fuel value studies described in this section were conducted by ORNL several years ago but were never reported in the open literature. Since the initial work was performed in 1965, the study was based on plant design and cost information available at that time. No attempt has been made to update the ground rules to current conditions. However, the final  $^{233}\text{U}$  value results were related to  $^{235}\text{U}$  value and can be modified to be consistent with current  $^{235}\text{U}$  prices. A complete report on the studies has been prepared and will be published.<sup>1</sup> A summary of the results is presented here.

The reactor fuel value of bred  $^{233}\text{U}$  contained in recycled uranium was determined by comparing its performance to that of  $^{235}\text{U}$  in the form of 93.5%-enriched uranium mixed with thorium. The fuel value of fissile material contained in the recycled fuel was calculated by an "indifference value" approach similar to that used in other fuel value studies.<sup>2,3</sup> In this approach the value of discharged bred fuel is defined to be the market price for the fuel at which the operator would obtain the same fuel cycle cost whether he recycled the fuel or sold it.

### 6.2.1 Characteristics of HTGR Design

The HTGR concept studied was described in a previous ORNL evaluation of advanced converters.<sup>4</sup> However, an all-graphite fuel element was substituted in the HTGR for the BeO-graphite element analyzed in the advanced converter study.

The HTGR design was based on the TARGET concept<sup>4</sup> of the General Atomic Division, General Dynamics Corporation (now Gulf General Atomic). Each fuel element was a machined graphite cylinder 4.65 in. in diameter with a 1-in.-diam central coolant channel. The fuel, which was in the form of loose pyrolytic-carbon-coated particles of  $\text{ThC}_2$  and  $\text{UC}_2$ ,

1. L. L. Bennett, *A Study of the Fuel Value of  $^{233}\text{U}$* , ORNL-TM-3822, to be published.

2. S. Jaye, L. L. Bennett, and M. P. Lietzke, *A Study of the Fuel Value of Plutonium*, ORNL-CF-60-2-34 (Feb. 11, 1960).

3. S. Jaye, L. L. Bennett, and M. P. Lietzke, *A Study of the Fuel Value of  $^{233}\text{U}$* , ORNL-CF-60-4-79 (Apr. 11, 1960).

4. M. W. Rosenthal et al., *A Comparative Evaluation of Advanced Converters*, ORNL-3686 (January 1965).

was contained in fourteen 0.5-in.-diam cylindrical channels with centers equally spaced on a circle  $\sim 0.5$  in. from the periphery of the cylinder. The graphite shape was made up of four consecutive vertical parts which were machined, fueled, capped, inspected, and then screwed together. The fuel consisted of an intimate mixture of 1000- $\mu$ -diam  $\text{ThC}_2$  particles coated with 100  $\mu$  of pyrolytic carbon and of 200- $\mu$ -diam  $\text{UC}_2$  particles coated with 100  $\mu$  of pyrolytic carbon.

The main characteristics of the reactor and fuel elements are given in Table 6.1.

Table 6.1. Characteristics of the HTGR for  $^{233}\text{U}$ -value study

Thermal power, MW	2270
Net electrical power, MW	1008
Core diameter, ft	31
Active core length, ft	15
Average core power density, kW/liter	7.0
Average C/Th atom ratio	200
Total core loading of thorium, kg	45,600
Typical fissile U/Th weight ratio	0.06
Typical core loading of fissile uranium, kg	2736

In this conceptual design, the HTGR core was divided into 12 batches of fuel, 1 of which was replaced at each shutdown. The fuel cycle calculations were based on six-month refueling intervals (at 80% plant factor), so the fuel residence time was six years.

Since the uranium and thorium can be kept separate in the HTGR, a number of recycle modes were available, of which four were considered in this study. These are shown schematically in Fig. 6.1 and described below.

1. Nonrecycle: Feed  $^{235}\text{U}$  to reactor and sell the discharged uranium. Makeup  $^{235}\text{U}$  is kept separate from thorium and bred uranium.

2. Full recycle: All the recovered uranium is recycled with  $^{235}\text{U}$  makeup. Uranium and thorium are mixed together in one particle.

3. Type I segregation: Only bred uranium from the thorium particle is recycled, and it is recycled one time only. The recycle uranium and makeup  $^{235}\text{U}$  are combined in a particle separate from the thorium particle. Material recovered from this uranium particle following irradiation is not recycled but, instead, is sold or discarded.

4. Type II segregation: Makeup  $^{235}\text{U}$  is kept separate from thorium and recycle uranium, and its residue is not recycled. Bred uranium is recycled back into the thorium particle, and no bred material is sold.

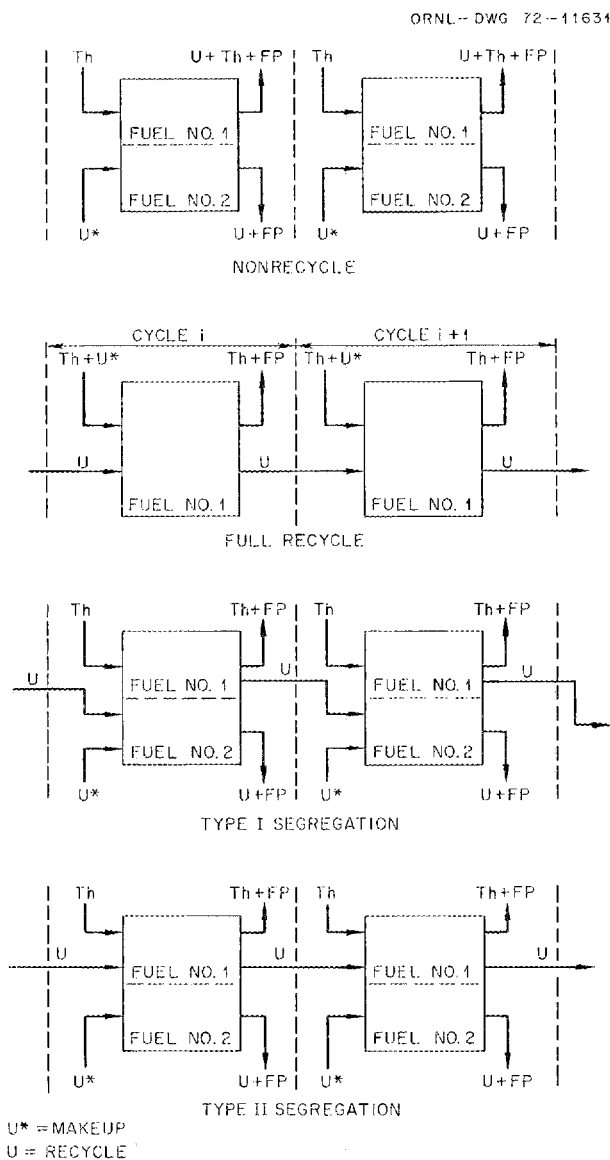


Fig. 6.1. Schematic description of recycle modes considered for the HTGR.

## 6.2.2 Ground Rules and Assumptions

*Processing and fabrication costs.* The costs for processing and fabrication of HTGR fuels in the thorium-uranium cycle were estimated for a range of assumed conditions.<sup>5</sup> Estimated costs are presented in Fig. 6.2 as a function of plant capacity.

5. M. W. Rosenthal et al., "A Study of Costs and Other Factors Associated with Processing, Fabrication and Shipment of Recycled Thorium-Uranium Fuels," unpublished ORNL report.

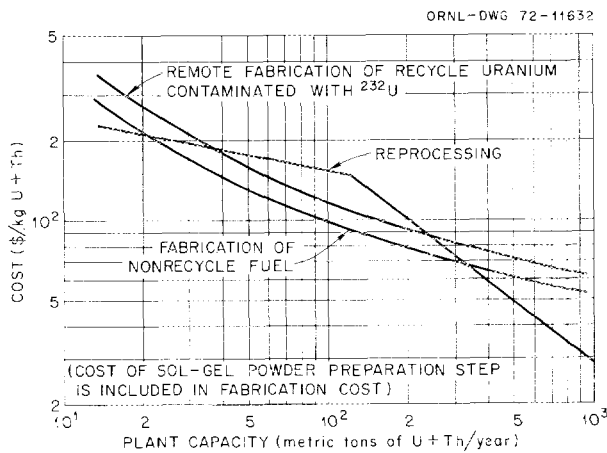


Fig. 6.2. Fabrication and processing costs estimated for HTGR.

To establish the plant capacity, an industry supporting five 1000-MW(e) reactors was assumed. With this assumption, the annual throughput of fuel is dependent on the fuel residence time and the reactor core loading. All these cases have about six-month refueling intervals, and the batch sizes are all very nearly the same. The annual fuel requirement for a five-reactor industry is about 40 metric tons of uranium plus thorium per year.

**Shipping cost.** Shipping costs were also estimated in ref. 5 as a function of recycle conditions and annual tonnage of fuel shipped. Costs chosen for use in this study are presented in Table 6.2.

Table 6.2. Economic parameters used in  $^{233}\text{U}$ -value study

Fabrication (nonrecycle)	\$147 per kilogram of U + Th
Processing	\$185 per kilogram of U + Th
Shipping cost (total)	
Nonrecycle	\$23 per kilogram of U + Th
Recycle	\$28 per kilogram of U + Th
Cost of uranium ore	\$8 per pound of $\text{U}_3\text{O}_8$
$^{235}\text{U}$ value (in 93.5%-enriched U)	\$12.7/g
Thorium price	\$5 per pound of $\text{ThO}_2$
Accounting method	Present value discounting, compounding semiannually
Discount rate	6%/year
Interest on fuel and fabrication	10%/year
Interest on processing and shipping	6%/year
Preirradiation holdup time	6 months
Postirradiation holdup time	6 months

### 6.2.3 Procedure for Determining Value of Fuel Mixtures Containing $^{233}\text{U}$

The reactor was fueled initially with  $^{235}\text{U}$  and thorium. At the end of the first cycle, the reactor operator has the choice of selling the  $^{233}\text{U}$ - $^{235}\text{U}$  mixture (and starting again with a fresh  $^{235}\text{U}$  loading) or of recycling it, along with sufficient  $^{235}\text{U}$  makeup to maintain the desired reactivity. Similarly, at the end of each subsequent cycle, he must decide whether to recycle fissile material or to sell the discharged fuel. Clearly the choice of whether to recycle or not is dependent on the sale price of the product  $^{233}\text{U}$ - $^{235}\text{U}$  mixture at each stage. If the market price for product fissile material is high, the reactor may be used as a  $^{233}\text{U}$  producer with no recycle; on the other hand, if the market price for  $^{233}\text{U}$  is low, it may be advantageous to recycle the material one or more times rather than sell it. The "indifference value" is defined to be the market price for  $^{233}\text{U}$  at which the reactor has the same average fuel cycle cost independent of whether product fissile material is sold or recycled.

The value analysis for the HTGR is complicated by the partial-reload fuel management scheme and the number of recycle modes which are possible. With partial-reload fueling, there is not a complete change of fuel at the end of each cycle, which complicates the analysis. Further, the startup cycles have higher cost than equilibrium cycles, due to unequal discharge exposures. Therefore the only approach which appeared practical was to compare 30-year average costs for the different recycle modes. A complete 30-year recycle history was generated for each of the recycle modes shown in Fig. 6.1 with  $^{235}\text{U}$  as the feed material. The full recycle and nonrecycle modes were also calculated with pure  $^{233}\text{U}$  feed. In addition to the 30-year histories, equilibrium cycle calculations were performed for the same six cases.

The fabrication cost for recycle fuels was estimated to be about \$35/kg higher than for nonrecycle fuel at the 40 metric tons per year industry size. This fabrication cost penalty ( $\Delta\text{FAB}$ ) was treated as a parameter in the  $^{233}\text{U}$  value studies.

The resulting fuel values for recycle fuels in the HTGR considering various  $\Delta\text{FAB}$  values are summarized in Table 6.3, based on the present value of  $^{235}\text{U}$  (\$12.7 per gram of  $^{235}\text{U}$  in highly enriched uranium).

Table 6.3. Estimated value of  $^{233}\text{U}$  and  $^{236}\text{U}$  in HTGR fuel mixtures

	$^{233}\text{U}$ value (dollars/g)	$^{236}\text{U}$ value (dollars/g)
Reference charges with $\Delta\text{FAB} = 0$	19.5	--14.6
Reference charges except for a $\Delta\text{FAB}$ equal to:		
\$15 per kilogram of U + Th	18.8	--14.1
\$30 per kilogram of U + Th	18.3	--13.6
\$35 per kilogram of U + Th	18.0	--13.4
Reference charges except that fuel and fabrication interest is 6%/year instead of 10%	21.1	--15.4

Using typical isotopic values, an *effective value* of  $^{233}\text{U}$  in recycle fuels was also calculated, which included the penalty for  $^{236}\text{U}$ . Specifically, the weighted average value of  $^{233}\text{U}$ - $^{236}\text{U}$  mixtures was calculated per gram of contained  $^{233}\text{U}$ ; on this basis the  $^{233}\text{U}$  value after repetitive recycle for 20 to 30 years in the HTGR was about \$16.0 to \$16.7 per gram of  $^{233}\text{U}$ , corresponding to isotopic concentrations of 10 to 15 parts  $^{236}\text{U}$  per 100 parts  $^{233}\text{U}$ .

### 6.3 EVALUATION OF PLUTONIUM USE IN HTGRs

P. R. Kasten    L. L. Bennett    W. E. Thomas

High-temperature gas-cooled reactors (HTGRs) are generally proposed for operation on the thorium fuel cycle using highly enriched  $^{235}\text{U}$  as initial and makeup fissile fuel, with recycle of the bred  $^{233}\text{U}$ . However, development of a fuel recycle technology also inherently develops the ability to fabricate plutonium-fueled HTGR fuel elements. Thus, fast breeder reactors (FBRs) producing excess plutonium (or  $^{233}\text{U}$ ) and HTGRs can work together.

At the present time, HTGRs are being offered commercially to utilities on the basis of  $^{235}\text{U}$ -Th fueling and the assurance of the USAEC of reasonable costs for recovering the bred  $^{233}\text{U}$ . Further, the AEC is supporting HTGR fuel recycle development, whose purpose is to develop the technology required for economically recycling bred fuel from HTGRs. This technology would also permit economic fabrication of plutonium-fueled HTGR fuel elements.

Light-water reactors (LWRs) presently built and under construction will in a few years provide large quantities of plutonium for use either in LWRs, HTGRs, or FBRs. While it is generally agreed that plutonium is best used in FBRs, the time of introduction of these reactors on a

commercial basis is far enough away that recycle of plutonium in LWRs or in HTGRs is highly probable. We conducted a study, which has been reported more fully,<sup>6</sup> to help clarify the role that HTGRs might play in utilizing plutonium from LWRs in the near future and from FBRs at times when plutonium production exceeds breeder reactor requirements. Thus we investigated the competitiveness of the HTGR in meeting the long-term industry expansion needs, considering competition from other nuclear and fossil plant types; in particular, the influence of using plutonium as makeup fuel on that competitiveness was studied. Effects of rising ore prices, separative work prices, values of bred fissile materials, changing capital costs, etc., were included in the calculations. Classes of power plants in competition with the HTGR were assumed to be: fossil (represented by coal-fired plants), light-water converters (represented by PWRs), and fast breeders (represented by LMFBs). Each of these classes has other plant types, such as oil-fired, BWR, and GCFBR; however, the use of the selected representative types should permit a realistic evaluation of the relative economic competition faced by the HTGR.

The basic tool used in these studies was a linear programming optimization model (ORSAC)<sup>7</sup> of the United States utility industry, which determines the optimum long-term expansion plan of the industry.

The computer model contains subroutines which project costs of fuel cycle services (fuel preparation, fabrication, processing, shipping, etc.) as a function of throughput of fuel from each reactor type. Using cost data prepared by the fuel cost subroutines and reactor mass balance data, the long-term optimization of plant selections was carried out.

#### 6.3.1 Ground Rules and Study Basis

Table 6.4 shows some of the ground rules chosen for this study. The period covered in the calculations was January 1, 1970, through December 31, 2039. However, all reported costs and other results cover only the 45-year period through December 31, 2015. The additional 24 years was used to reduce the probability of end-effects error in the period of interest.

A distribution of coal prices was used in the study, and the average price of coal from this distribution was about \$7.50/ton (about \$0.32/MMBtu).

6. P. R. Kasten, L. L. Bennett, and W. E. Thomas, *An Evaluation of Plutonium Use in High-Temperature Gas-Cooled Reactors*, ORNL-TM-3525 (October 1971).

7. F. G. Welfare et al., *The Oak Ridge Systems Analysis Code (ORSAC) Users' Manual*, ORNL-TM-3223 (June 1971).

Uranium reserves were entered as a table of quantities available at a given price, as shown in Table 6.5. The effect of cumulative ore usage on uranium prices was automatically included in the optimization process.

Table 6.4. Ground rules for ORSAC calculations

Separative work price	Through 2-21-71, \$26/kg Through 12-31-71, \$28.70/kg Thereafter, \$32/kg
Electrical energy demand	From FPC 1970 National Power Survey
Discount rate	7%/year
HTGR availability date	1978
LMFBR availability date	1986

Table 6.5. Uranium ore available at given prices<sup>a</sup>

Thousands of tons of U <sub>3</sub> O <sub>8</sub>	Average price (dollars per pound of U <sub>3</sub> O <sub>8</sub> )
0-300	7.25
300-700	9.00
700-1100	11.25
1100-1500	13.75
1500-1800	17.50
1800-2100	22.50
2100-2300	27.50
2300-2500	32.50
2500-2800	37.50
2800-4000	42.50
4000-10,000	50.00

<sup>a</sup>Based on current uranium reserves and estimates of additional available resources in recognized favorable geological environments.

Capital costs were estimated as a function of plant size for each plant type included in the study. We then superimposed a projection of plant size as a function of time, plus a curve of cost reductions due to "learning." The final result was a curve of capital cost vs time for each of the plant types. These costs are shown in Fig. 6.3. The costs shown in the figure are in constant 1970 dollars and do not include any escalation during construction. The reduction with time is due to the combined effects of increase in plant size plus learning. A complete discussion of the capital cost estimates is available.<sup>8</sup>

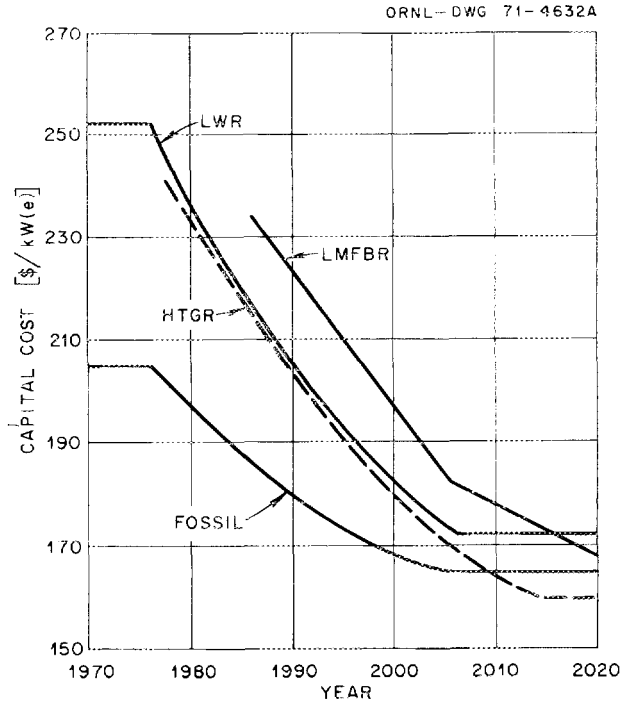


Fig. 6.3. Power plant capital costs used in ORSAC calculations. All costs are in constant 1970 dollars.

The fuel cycle calculations for the HTGR assumed that plutonium would replace highly enriched uranium (93.5% <sup>235</sup>U) as the purchased makeup material. However, <sup>235</sup>U was used for the initial loading and as part of the makeup material until <sup>233</sup>U had built up in the reactor (to simplify startup). The makeup plutonium composition was held constant with isotopic fractions typical of LWR discharge plutonium (60% <sup>239</sup>Pu, 24% <sup>240</sup>Pu, 12% <sup>241</sup>Pu, 4% <sup>242</sup>Pu). Since the HTGR was initially fueled with <sup>235</sup>U, this reactor type was not completely divorced from the diffusion plant. However, both ore and separative work requirements are greatly reduced, relative to use of the standard <sup>235</sup>U-make-up cycle. Table 6.6 presents 30-year fuel consumption data for the <sup>235</sup>U and plutonium makeup cycles. The net consumptions imply conversion ratios of about 0.8 for the <sup>235</sup>U-make-up case and about 0.6 to 0.65 for the plutonium.

8. H. I. Bowers and M. L. Myers, *Estimated Capital Costs of Nuclear and Fossil Power Plants*, ORNL-TM-3243 (March 1971).

Table 6.6. Summary of 30-year fuel requirements for a 1000-MW(e) HTGR with either  $^{235}\text{U}$  makeup or Pu makeup

	Reference $^{235}\text{U}$ -makeup cycle	Plutonium- makeup cycle
<b>Total makeup feed, kg</b>		
$^{235}\text{U}$	8055	1990
Fissile Pu		8685
<b>Total fuel remaining<sup>a</sup> at end of 30 years, kg</b>		
Fissile Pu		245
Bred $^{233}\text{U}$	1350	810
Bred $^{235}\text{U}$	175	90
Makeup $^{235}\text{U}$ <sup>b</sup>	1250	~275
<b>Net 30-year consumption, kg</b>		
Fissile Pu		8440
Bred uranium	-1525	-900
Makeup $^{235}\text{U}$	6805	1715
Total	5280	9255
<b>30-year supply requirements<sup>c</sup></b>		
Separative work, metric ton units	1908.5	471.5
$\text{U}_3\text{O}_8$ , short tons	1470.7	472.4

<sup>a</sup>Includes final reactor loading plus fuel discharged from recycle but which was still in the pipeline.

<sup>b</sup>Partially burned makeup  $^{235}\text{U}$  is stored but is not recycled due to high  $^{236}\text{U}$  content (no credit is taken for this material).

<sup>c</sup>With 0.2%  $^{235}\text{U}$  in diffusion plant tails.

### 6.3.2 Results of the Study

The items discussed in the preceding sections constituted the input to the linear programming model of the United States electric utility industry. All the plant types competed for the plant addition requirements to meet expansion needs of the industry. Figure 6.4 presents graphically the optimum plant addition as obtained from the ORSAC calculations. These results indicate that the HTGR is preferred to the LWR for using plutonium.

A comparable ORSAC case was also run without the plutonium-makeup HTGRs included, and the results are shown in Fig. 6.5. As expected, fewer HTGRs were built in the 1970--2015 period. The LMFBR captured the major part of the new capacity requirements, while the plutonium-fueled LWR was built to utilize the excess plutonium. Under the ground rules of the study, the  $^{235}\text{U}$ -makeup HTGR was built only during the period before the LMFBR was introduced, plus a few built to utilize the  $^{233}\text{U}$  made available by retirement of older HTGRs.

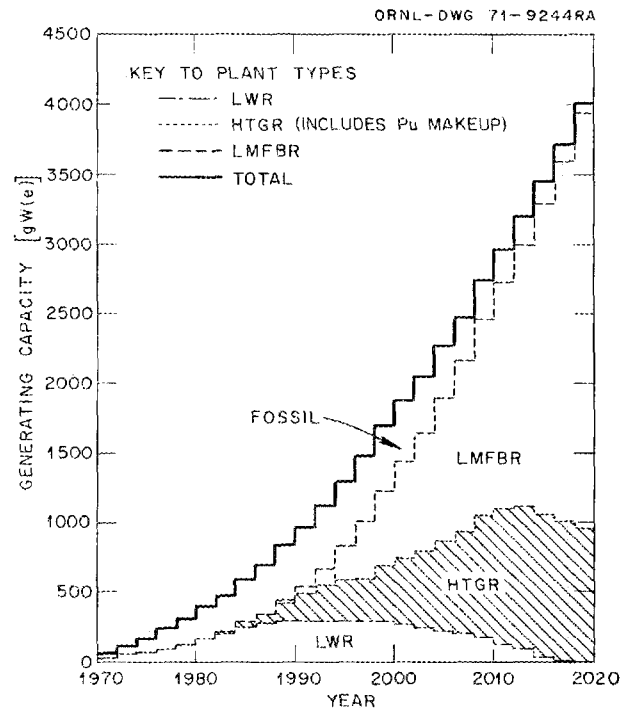


Fig. 6.4. Total generating capacity as a function of reactor type and time, including use of the plutonium-makeup HTGR (including additions and retirements during period).

The above results also indicate that high-performance fast breeders will be built in about the same numbers independent of the use of plutonium-fueled HTGRs and that they provide a major portion of the central station power plant needs. As FBRs are built in large numbers, large quantities of excess plutonium will be produced, and a system to use this plutonium will be needed. The favorable capital and fuel cycle costs for the HTGR make it a logical choice to fill this role, if the plutonium-makeup cycle is made available. (This result is in agreement with fuel cycle calculations performed previously at Gulf General Atomic and at Oak Ridge National Laboratory, which indicated that the value of fissile plutonium is higher in HTGRs than in LWRs.) If the plutonium-makeup cycle is not considered for the HTGR, then that reactor has a much smaller role in the optimum system expansion, and the plutonium-fueled LWR becomes the dominant system to supplement the FBR.

Additional significant information obtained in this study concerns the trends in power costs for the various reactor systems with time and the shadow price of

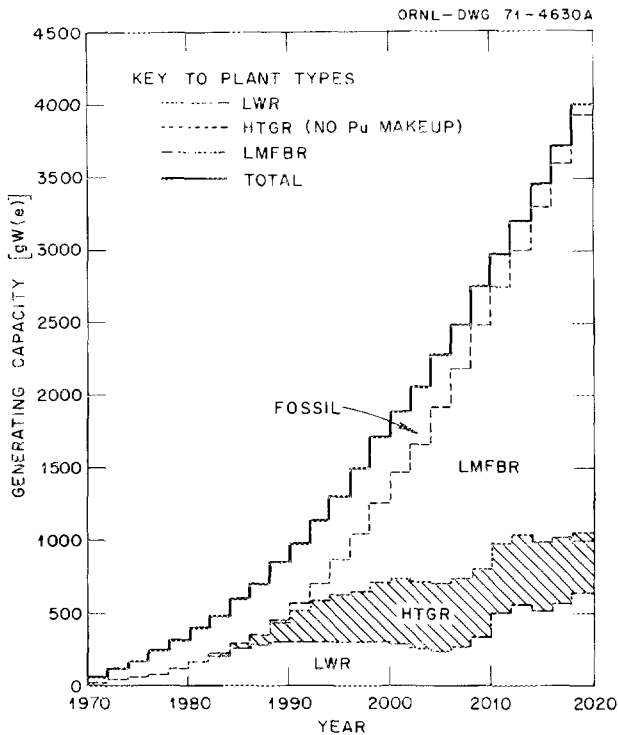


Fig. 6.5. Total generating capacity as a function of reactor type and time, excluding use of the plutonium-make-up HTGR (including additions and retirements during period).

fissile fuels. Figure 6.6 gives the power costs as a function of time for the different reactor types, considering various fuel cycles. For the cases calculated, the fast breeder reactor controls the power cost of the system, leading to FBR dominance in future years. Also, as the shadow price of plutonium falls, the power cost of the LWR fueled with plutonium and depleted uranium falls significantly, becoming lower than power costs from the plutonium-make-up HTGR about 2015. This is due to the increasing cost of uranium ore, causing the initial fueling cost of the HTGR to rise. At the same time, the initial fueling cost of the LWR is not influenced by the cost of uranium ore, since the value of tails material would not change significantly. If the HTGR were fueled with plutonium-thorium, however, the penalty associated with rising uranium ore prices would not occur. These results indicate that if plutonium-fueled HTGRs are to maintain dominance over plutonium-fueled LWRs in future years, use of plutonium as the initial as well as the makeup fissile fuel will be required. While this should be possible, specific studies of HTGRs fueled initially with plutonium need to be performed, considering the plutonium to be that produced by FBRs.

Figure 6.7 gives the shadow price of bred fissile materials as a function of time, and also the  $U_3O_8$  price, for the case which considered the plutonium-make-up HTGR. The increasing value of the fissile plutonium initially is due to its relatively high value in FBRs and the economic incentive to install FBR plants, while the decreasing value in future years is due to the production of excess plutonium by the large FBR capacity in existence at that time. The  $^{233}U$  value vs time has in general the same type behavior as does

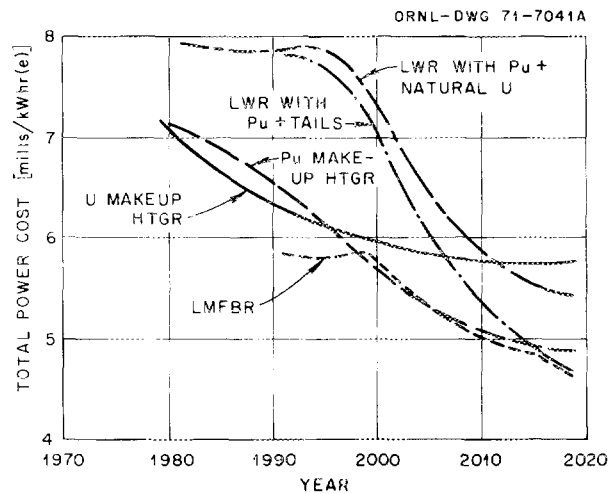


Fig. 6.6. Total power costs vs time.

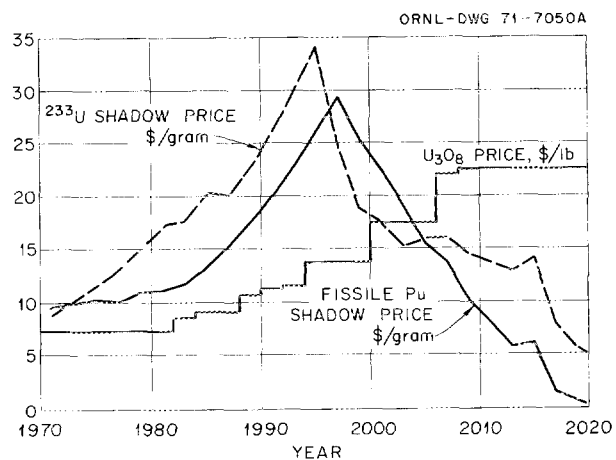


Fig. 6.7.  $U_3O_8$  price and shadow prices of bred fissile materials.

plutonium; however, somewhat surprising is the relatively high value obtained for  $^{233}\text{U}$ . This is due to the economic attractiveness of HTGRs and the high value of  $^{233}\text{U}$  relative to plutonium in HTGR plants. Also, it is significant that the value of  $^{233}\text{U}$  remains relatively high in future years, which indicates that when FBRs start producing excess fissile fuel, that material should be  $^{233}\text{U}$ . Figure 6.7 also indicates that even prior to the year 2000 there may be overall economic benefits if FBRs were to produce some  $^{233}\text{U}$  for use in HTGRs.

### 6.3.3 Conclusions

In summary, the results of this study show that (1) use of the plutonium-makeup fuel cycle permits HTGRs to have a much deeper penetration of the power market than use of the  $^{235}\text{U}$ -makeup fuel cycle alone; (2) plutonium makeup HTGRs are economically preferred over plutonium-fueled LWRs over the period of this study; (3) assuming that plutonium is the product from FBRs, as the price of uranium ore rises and the price of plutonium decreases, it will eventually be necessary for HTGRs to operate with plutonium as the initial fissile fuel if they are to compete with LWRs fueled with uranium tails and plutonium; (4) use of plutonium-makeup HTGRs has no significant influence on the introduction and use of FBRs; and (5) if FBRs produce excess fissile fuel it appears economically desirable that such fuel be  $^{233}\text{U}$  for use in HTGRs.

## 6.4 HTGR FABRICATION ECONOMICS

W. H. Pechin

We are conducting an economic study of the cost of fabricating HTGR fuel. This study is expected to be of major importance in any comparison of the thorium-uranium HTGR fuel cycle with other fuel cycles and will provide a basis for assessing the various alternative fabrication processes proposed for HTGR fuels. The study will include an investigation of the effects of plant size and fuel design on fabrication costs.

The major portions of the computer code to be used in the economic study are listed below along with their purpose and degree of completion.

INPUT --- subroutine which reads data such as particle design, equipment costs, materials costs, flowsheets under consideration, plant design basis, and economic ground rules, 50% complete.

OUTPT 1 --- subroutine for printing out the designs of the particles to be produced, 100% complete.

FLOSHT --- subroutine which calculates the amount of production to be done in various plant types and which accounts for losses and rejection at each process step and converts size of each process step from kilograms of heavy metal per day to those units appropriate to equipment cost and operating cost data, 100% complete.

OUTPT 2 --- subroutine which prints out the flowsheet under consideration and the size of each process step as adjusted in FLOSHT, 100% complete.

MATRLS --- subroutine which calculates the cost of nonfissile materials used in the plant, 100% complete.

FACTOR --- subroutine which calculates the factors relating cost for a given type plant to that for a contact plant, not begun.

CAPCST --- subroutine which calculates the capital cost for a plant with flowsheet under consideration, not begun.

OPCST --- subroutine which calculates the operating cost for a plant with the flowsheet under consideration, not begun.

OUTPT 3 --- subroutine which prints out fuel cost as a function of plant size for the flowsheet under consideration, not begun.

INTERP --- subroutine which performs the interpolation between data points for the equipment, operating, and materials costs, 100% complete.

SHEF, SHBF, SHOF --- function subprograms which adjust the cost of shielded plants for other than standard shield thickness, 100% complete.

A major portion of the study consists in the assembly of a catalog of capital and operating cost data as a function of throughput for the various process steps. This effort has just started.



## Part II. HTGR Development Program

---

### 7. Prestressed Concrete Pressure Vessel Development

G. D. Whitman

Most of the original objectives outlined in the program plan<sup>1</sup> developed in support of the technology of prestressed concrete pressure vessels (PCRVs) have been achieved. A majority of the activities sponsored by this program have been performed under subcontract to ORNL; however, work was stopped on the three remaining subcontracts during the reporting period. Included in this group were the structural model studies and the two projects on concrete materials investigations that were concerned with moisture migration and multiaxial creep. Most of the experimental portion of these projects was completed as defined in the scope of the subcontract documents, however, some of the reporting has not been completed because of inadequate funding. Hopefully this work can be properly documented at a future date. The small thermal cylinder experiment which is being performed at ORNL has been continued and is progressing as planned.

The small thermal cylinder test has been assembled and was cast in February 1971. Since that date the unit has been prestressed, heated, and pressurized to achieve the regimes of loading that were specified in the planning documentation, and a significant amount of data has been obtained. This experiment was designed to provide more complete verification of the adequacy

of the analytical techniques that were developed to predict time-dependent behavior and to evaluate structural adequacy under off-design thermal loads.

The major objective of the structural model tests is to study experimentally and analytically the strength of end slabs of PCRVs. Vessels with solid end slabs and vessels with penetrations were built and tested to failure or to overload pressure levels that induced sufficient structural action to deduce failure mode. Twenty-three models were tested under this program.

The concrete materials investigations for studying moisture movement in mass concrete and time-dependent deformation behavior were conducted over a period of approximately four years with considerable experimental success. Summary reports have been issued on one of two series of triaxial creep studies using a PCRV-grade concrete, and the remainder of the experimental work is completed. However, no reports have been prepared since the projects were stopped.

#### 7.1 PCRV THERMAL CYLINDER TEST

J. P. Callahan    J. M. Corum    M. Richardson

Prestressed concrete reactor vessels are unique with respect to concrete technology primarily because of the elevated operating temperatures employed. During the ORNL Prestressed Concrete Reactor Pressure Vessel Research and Development Program, analytical methods and basic test data for time-dependent deformation behavior of concrete have been developed. By

---

1. G. D. Whitman, *Prestressed Concrete Reactor Vessel Research and Development Program Summary*, ORNL-TM-2179 (Apr. 1, 1968).

incorporating these data into an appropriate analysis, predictions of time-dependent behavior of PCRVs can be made. Thus far, however, there have been limited means for assessing the accuracy of such analytical predictions. The thermal cylinder test is designed to provide the kind of information needed to make such an assessment.

The thermal cylinder is a model of the middle section of the cylindrical portion of a prestressed concrete reactor vessel which is subjected to simulated in-service operating conditions as shown in Fig. 7.1. The test structure, described in detail in refs. 2 and 3, is a thick-walled cylinder having a height of 48 in., a thickness of 18 in., and an outer diameter of 81 in.

All surfaces of the model are sealed to prevent any net moisture loss, and the ends are insulated thermally

to limit heat flow to the radial direction. The specimen is prestressed axially and circumferentially, and internal pressure is applied through a pressurization annulus at the inner surface. A thermal gradient is imposed by heating the inside surface of the cylinder to 150°F and cooling the outside surface to 75°F.

During the current reporting period the following major phases of the experiment were successfully completed:

1. calibration of instrumentation;
2. assembly of the test mold and installation of instrumentation ready for casting;
3. fabrication of temperature and pressure control systems;
4. casting of thermal cylinder and companion specimens;
5. execution of the planned testing program thus far consisting of posttensioning of reinforcement, heating of thermal cylinder inside surface and the 18- by 40-in. companion specimens to 150°F, and pressurization of annulus to 700 psi.

2. J. M. Corum and G. C. Robinson, Jr., "Thermal Cylinder Test to Simulate Behavior of Cylindrical Portion of a Prestressed Concrete Vessel," *GCR Program Semiannu. Progr. Rep. Mar. 31, 1969*, ORNL-4424, pp. 225-39.

3. J. M. Corum, J. P. Callahan, and M. Richardson, "PCRv Thermal Cylinder Test," *Semiannu. Progr. Rep. Sept. 30, 1970*, ORNL-4637, pp. 70-71.

ORNL - DWG 70-3135

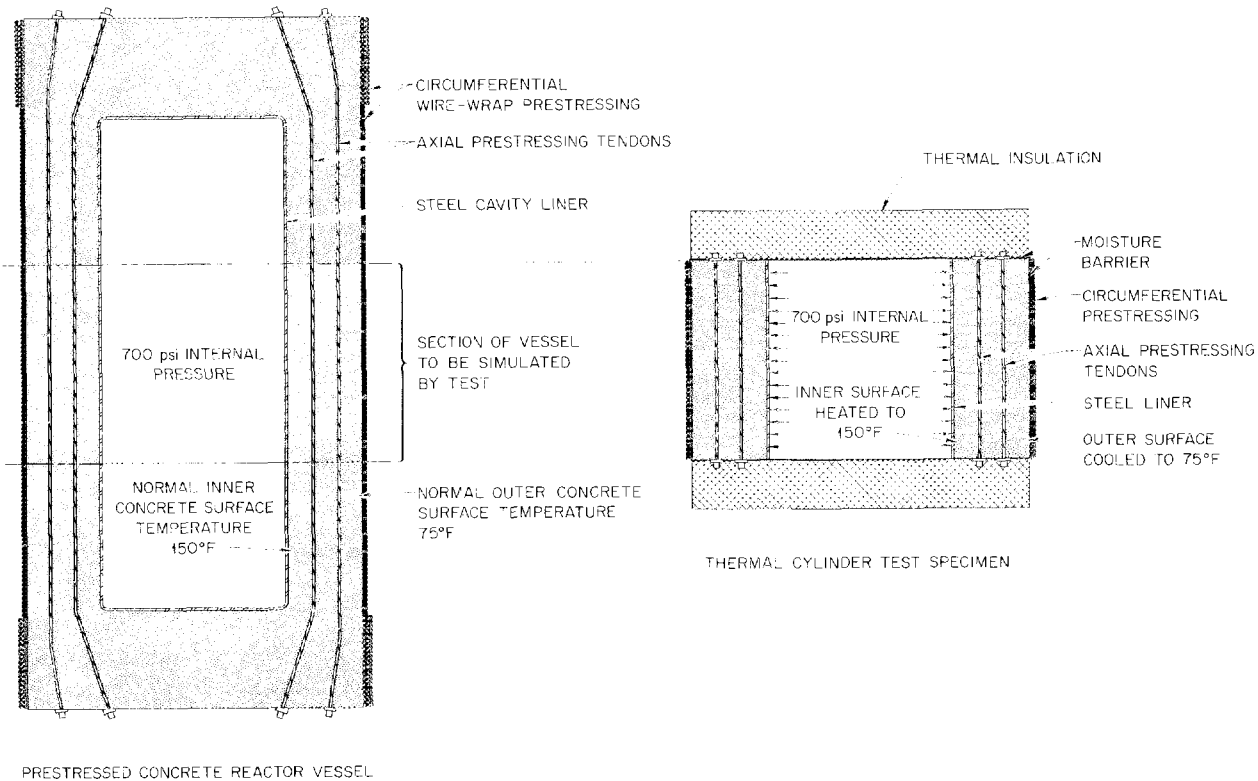


Fig. 7.1. Relation of thermal cylinder test specimen to prestressed concrete pressure vessel.

### 7.1.1 Calibration of Instrumentation

Prior to installation in the thermal cylinder mold assembly, 12 of the 52 axial prestressing tendons were instrumented with bonded electrical resistance strain gages and load-calibrated in a tensile testing machine. In addition, 12 load cells designed and fabricated for use with the instrumented axial tendons were load-calibrated in compression. This combination of instrumented tendons and load transducers is used to determine the relationship between the initial stress developed during posttensioning of the tendons and the final load transferred to the structure. In addition, it provides a means for monitoring possible creep and stress relaxation of the tendons. This information will also be used to evaluate strain readings obtained from strain gages bonded to 8 of the 16 circumferential tendons. In the case of the circumferential tendons, no practical way was found to include load cells.

Relaxation of the stress in concrete is an important consideration in the design of a PCRV. Two types of embedment devices having a potential for measuring stress relaxation have been developed at ORNL for this experiment. One device, consisting of two parallel concrete embedment strain gages, one of which has a pressure diaphragm attached, was described in ref. 3. The relatively thin cylindrical cell shown in Fig. 7.2 is another device designed for measuring stress in concrete. The cell consists of two machined titanium disks, shown disassembled in Fig. 7.3. The disks fit together in such a way as to continually deflect a cruciform-shaped spring steel beam instrumented with a four-arm bonded strain-gage bridge. The application of an axial compressive stress to the assembled cell will further deflect the cruciform beam as monitored by the strain gages.

In order to provide a means for measuring possible variations in strain readings unrelated to existing stress conditions, the titanium disk through which the strain gage leads pass (see Fig. 7.3) houses a miniaturized pneumatic ram. When activated, the ram deflects the cruciform beam to a fixed reference stop that is designed to remain independent of stress variations. Changes in successive readings of the beam gage in the fixed deflection position can be used to determine the amount of instrumentation drift. Upon release of the pressure, the beam returns to its former position.

The stress cell was fabricated from titanium in order to produce an embedment having a coefficient of thermal expansion compatible with that of the concrete. Thirteen titanium stress cells were load-calibrated under uniaxial compression. Nine of these were installed in the thermal cylinder, and four were installed

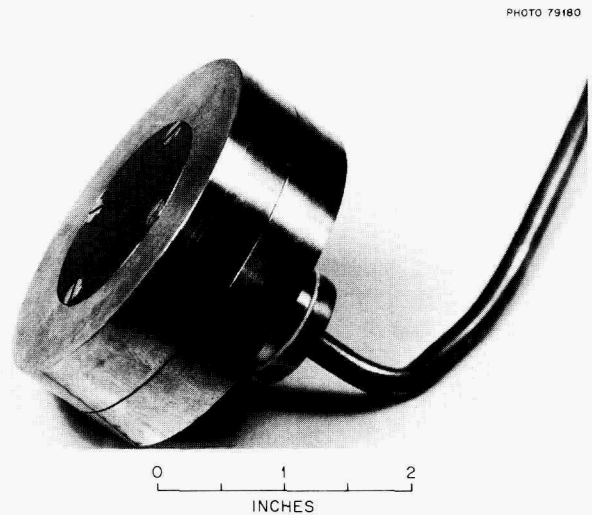


Fig. 7.2. Assembled titanium stress cell.



Fig. 7.3. Disassembled titanium stress cell.

in sets of two in the 18- by 40-in. companion specimen molds.

### 7.1.2 Assembly of the Test Mold

At the beginning of this reporting period, all components of the thermal cylinder formwork were available except for the top and bottom tori used to form the pressurization annulus between the two internal heat

exchangers. The tori were fabricated and made available when required in the assembly. The bottom support and insulating layers were assembled as shown in Fig. 7.4 to the sheet-metal moisture seal located directly above the asbestos cement board. The temporary support superstructure was then erected on the base support framework.

Upon completion of pressure testing of the panel-coil heat exchangers, an array of Nelson studs was attached to the surfaces of the two interior panel coils (heat exchangers *A* and *B*) which were to be in contact with concrete. The studs provide added assurance that a good bond is developed between heat exchangers and concrete. At this time, 20 Microdot weldable strain gages and 5 thermocouples were spot welded to heat

exchanger *B*, which forms the inside surface of the test section. The pressurization annulus was next fabricated by welding the top and bottom tori to heat exchangers *A* and *B*. All leads for instrumentation located inside the annulus pass through seals located in the upper torus. The resistance heater to be used for the hot-spot experiment was attached at this time to heat exchanger *B*. After leak testing, the assembled annulus was positioned inside the structural framework and welded to the bottom moisture seal. Assembly of the upper support framework was then completed, and the axial prestressing and moisture tubes were installed.

The Microdot concrete embedment strain gages were precast in concrete in the form of three-gage rosettes to protect these relatively delicate gages. It was also

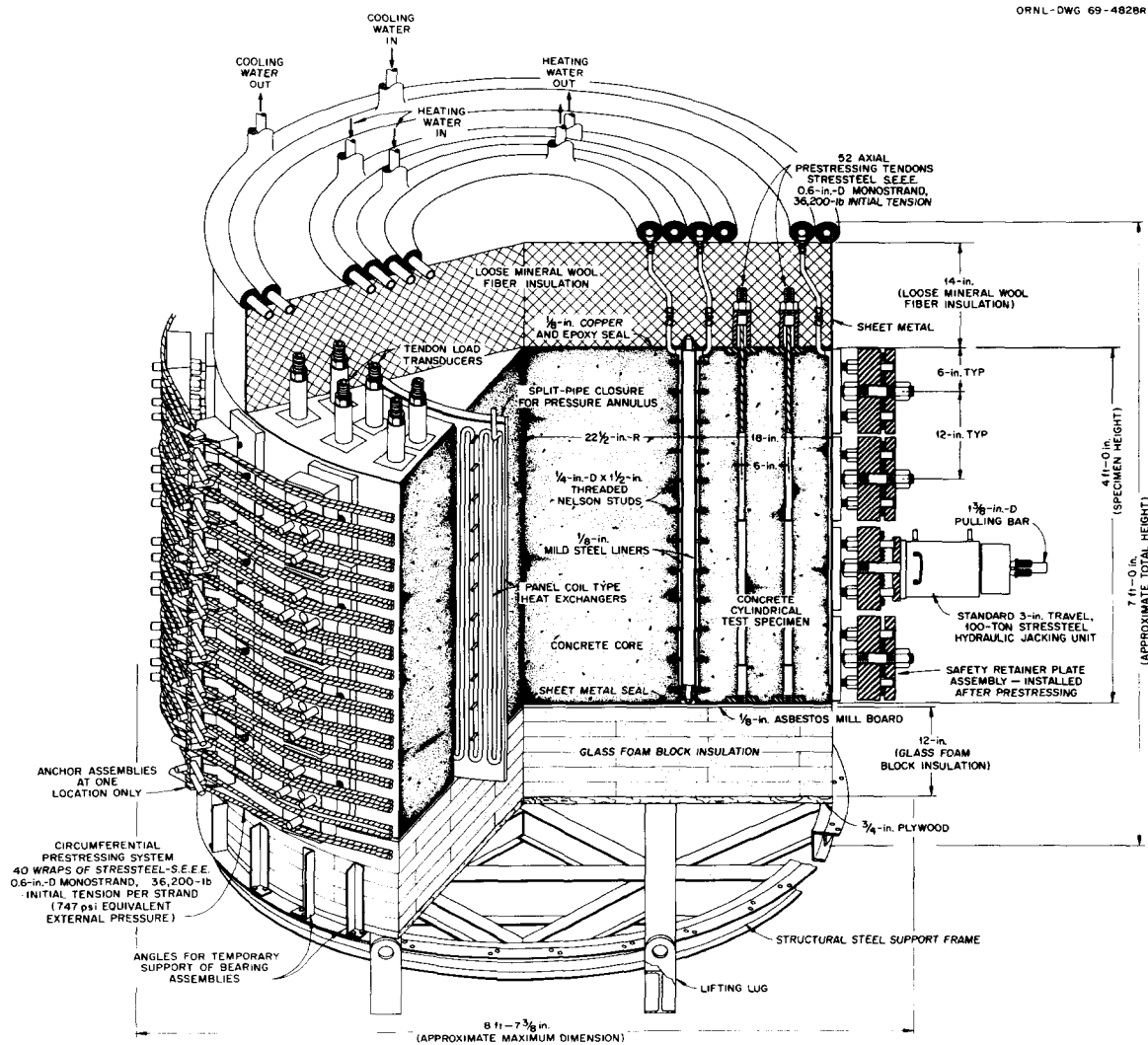


Fig. 7.4. Isometric of thermal-cylinder test structure.

necessary for the same reason to precast the ten pressure stress cell components consisting of individual Microdot strain gages attached to pressure diaphragms. The concrete embedment instrumentation was positioned along four gaged sections located 90° apart around the model. Three of the gaged sections can be seen in Fig. 7.5, which is a view of the mold assembly with the outer heat exchanger removed. Figure 7.6 shows a close-up of one gaged section. All gages were supported as shown by clamps attached to tubes housing the longitudinal prestressing. Shown in the section from bottom to top are axial titanium stress cells; Deakin vibrating-wire strain gages; precast Microdot strain-gage rosettes; circumferential titanium stress cells, to the right of which are Carlson-type strain gages; and, at the top, axially oriented Deakin gages.

After the embedment instrumentation was installed, the outer heat exchanger was positioned and welded to the bottom moisture seal.

#### 7.1.3 Fabrication of Temperature and Pressure Control Systems

The temperature and pressure control systems were assembled concurrently with the thermal cylinder mold. Basically, the temperature control system consists of two water circulation loops — one for heating and one for cooling. The two loops are essentially the same except for the inclusion of a water heater in the heating system. The hot water loop supplies both interior heat exchangers (*A* and *B* panel coils) from a common supply but at different flow rates. The cold water system supplies the outer heat exchanger (*C* panel coil). Each loop is equipped with an extra pump to supply necessary backup and allow for maintenance during periods of continuous operation of the system. The assembled system and control instrumentation are shown in Fig. 7.7.

The annulus pressurization system consists of four nitrogen bottles connected by a manifold to an oil expansion tank which is in turn connected to the annulus of the model. During pressurization the annulus and connecting line are filled with synthetic high-temperature hydraulic fluid to the oil expansion tank. The applied pressure is controlled by the gas manifold pressure regulators.

As a final step in the assembly of the thermal cylinder mold, the concentric circular inlet and outlet water circulation manifolds shown in Fig. 7.4 for each of the three heat exchangers were temporarily connected to the loops for an operational check-out of the completed system.

#### 7.1.4 Casting of Thermal Cylinder and Companion Specimens

In addition to the thermal cylinder mold, two 18- by 40-in. cylindrical molds were also fabricated and assembled. These specimens contain representative instrumentation of every type used in the thermal cylinder.

After the temperature control system was checked out, the water circulation manifolds and tubing connections were removed and the molds shipped by truck to the casting site. The specimens were cast at the Waterways Experiment Station (WES), Corps of Engineers, U.S. Army, Vicksburg, Mississippi. The Tennessee limestone concrete mixture used in the ORNL concrete program basic studies and used in casting these specimens was specified and qualified at this laboratory.

The molds were transported to the casting site on the flatbed trailer shown in Fig. 7.8. In this figure the upper part of the plastic and wooden covering has been removed for casting. The thermal cylinder, two 18- by 40-in. cylinders, forty 6- by 12-in. standard compression specimens, and three 6- by 16-in. creep specimens were cast using fourteen 13.5-ft<sup>3</sup> batches of concrete on February 3, 1971. The operation of placing concrete into the thermal cylinder mold is shown in Fig. 7.8. Upon completion of the finishing operation the exposed concrete was covered with wet burlap to prevent overnight drying. The following day all exposed concrete was sealed using a combination of epoxy and copper sheeting.

At the end of an initial 14-day curing period at WES, the trailer was returned to ORNL, where the specimens were prepared for testing. The water circulation manifolds and related piping were reinstalled, and the temperature control system was set at 75°F. With the exception of vibrating-wire and Carlson-type strain gages and control thermocouples, the instrumentation was connected to a 520-channel data acquisition system.

#### 7.1.5 Testing Program

Seven of the standard compression specimens and the three creep specimens were tested at WES. The remainder of the 6- by 12-in. standard cylinders were transported in wet sawdust along with the thermal cylinder to ORNL, where compression tests were conducted at concrete ages of 28, 90, and 180 days. The results of these tests, together with results of tests conducted at WES, are summarized in Table 7.1. The significant differences between 28-day compressive strengths of specimens tested at the two locations can

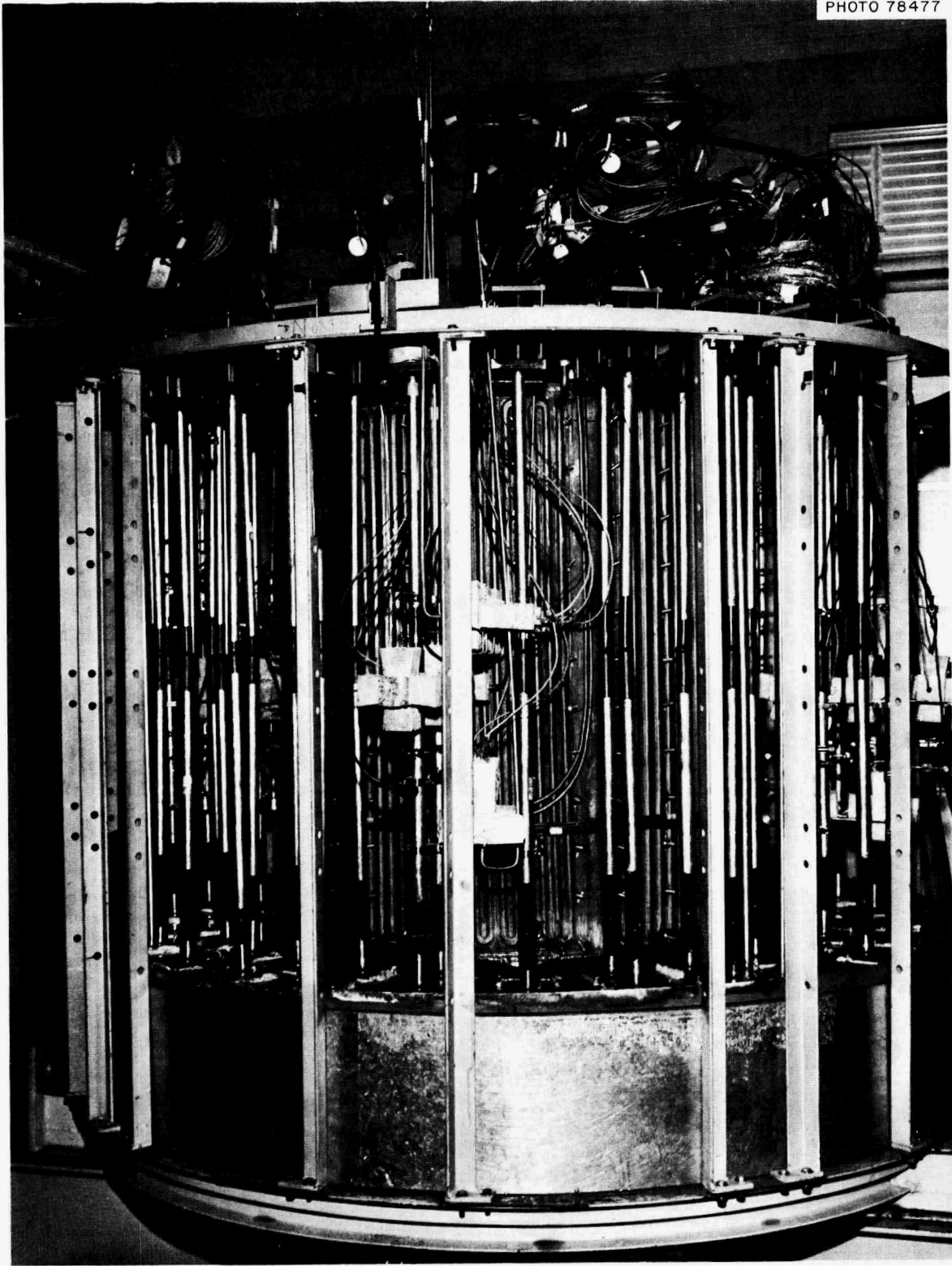


Fig. 7.5. Partially assembled mold with outer heat exchanger removed.

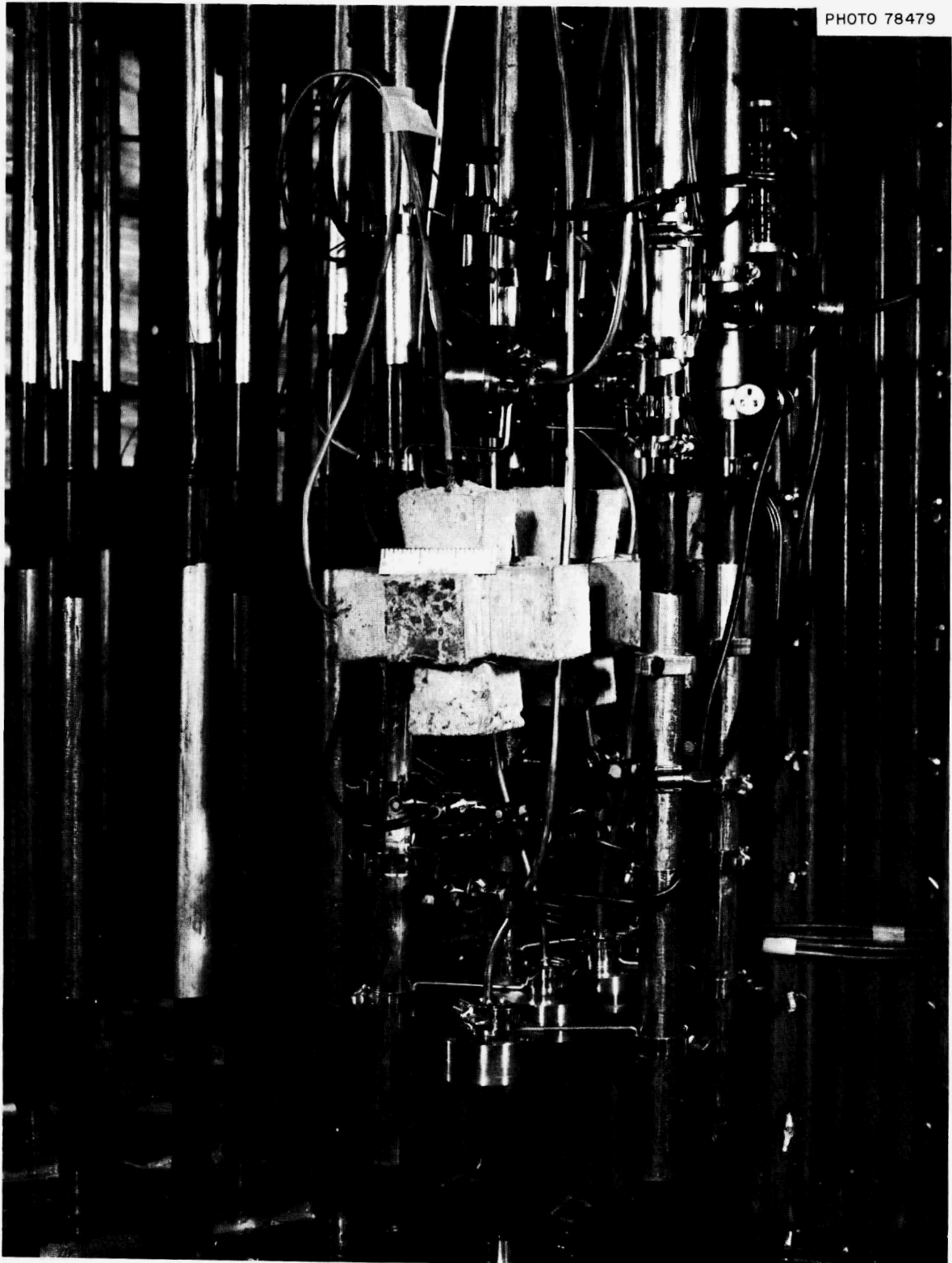


Fig. 7.6. Close-up of instrumentation at one of four gaged sections.

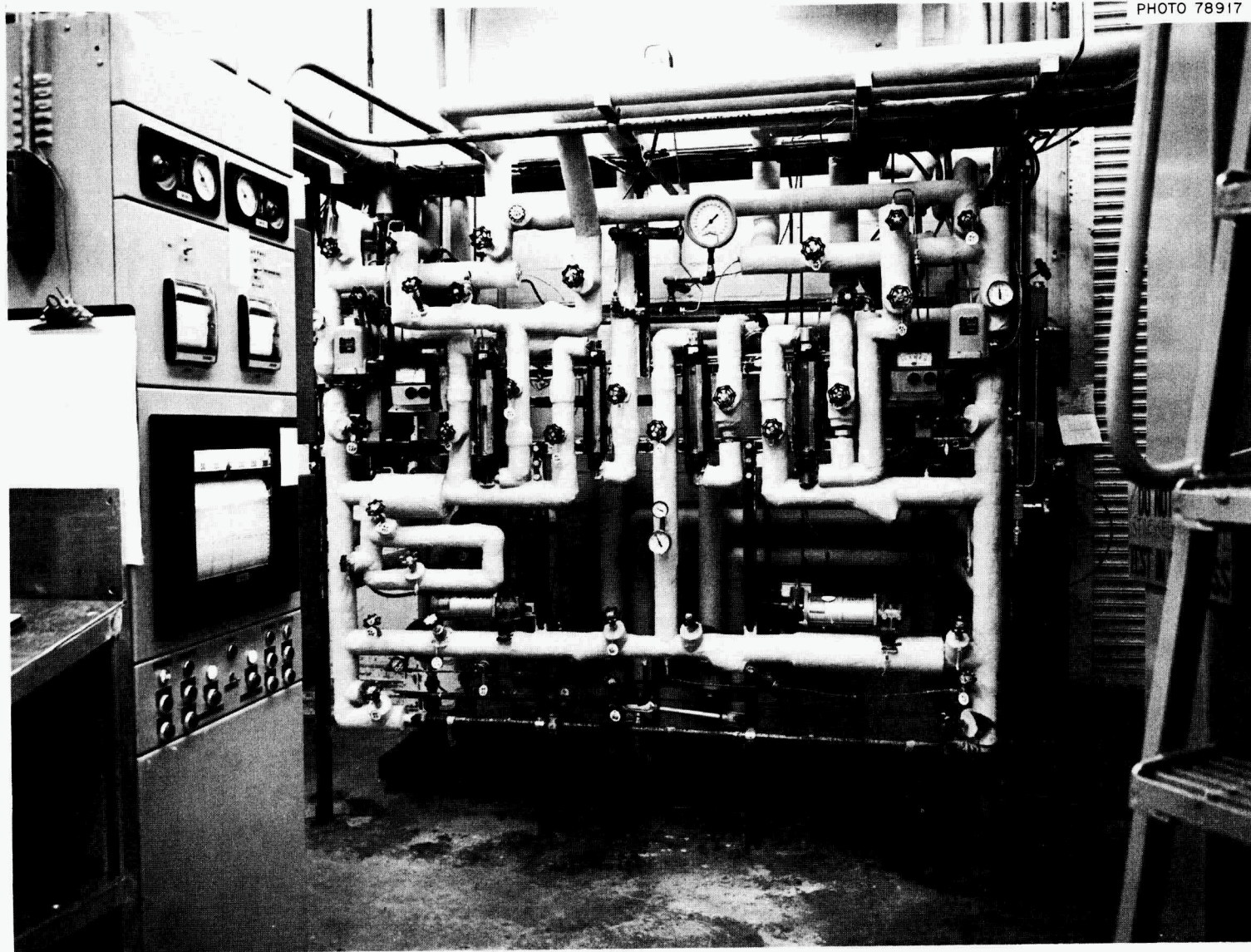


Fig. 7.7. Temperature control system.

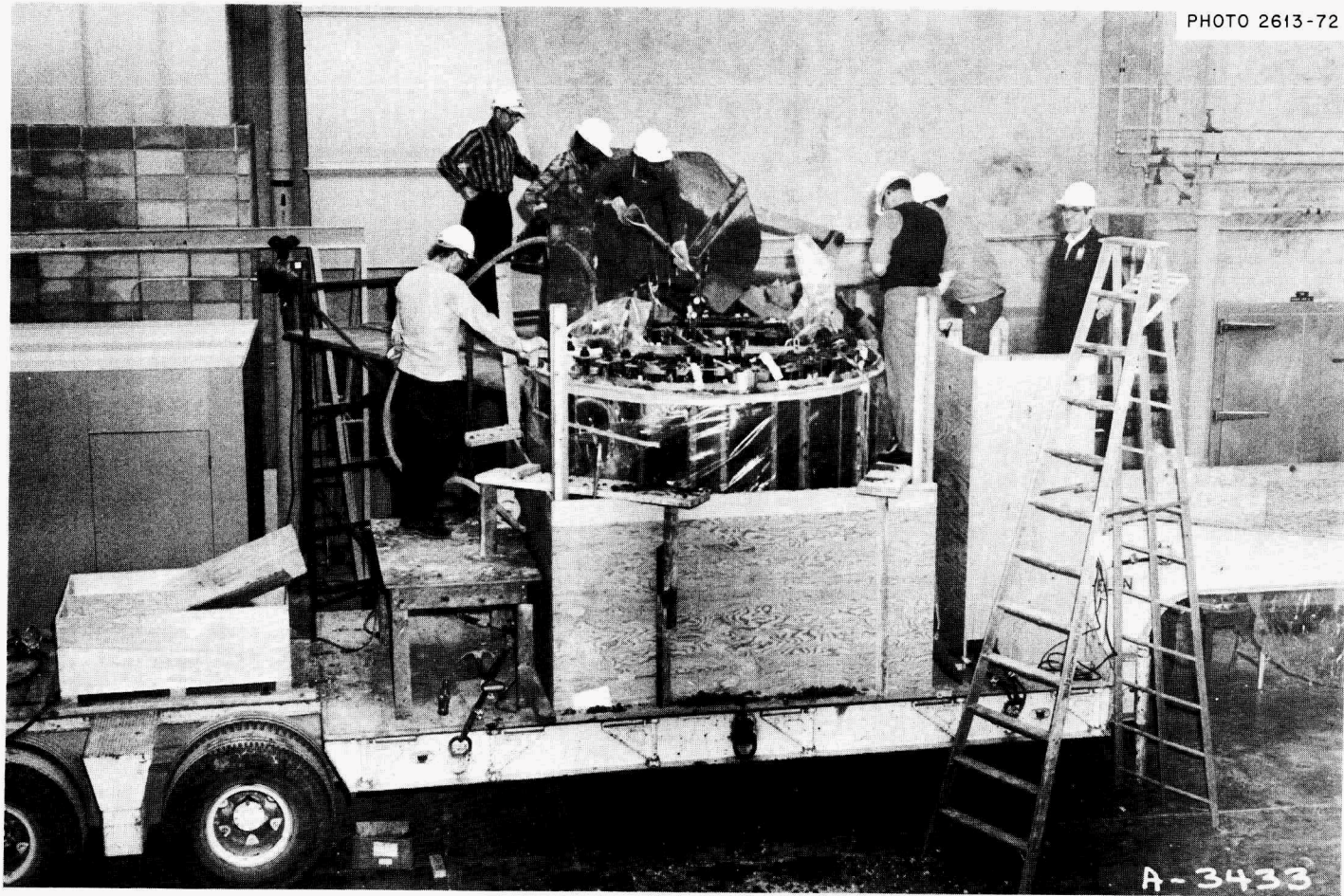


Fig. 7.8. Casting operation, showing placing of concrete into thermal cylinder mold.

Table 7.1. Summary of thermal cylinder unconfined compression test results

Days from casting	Number of specimens	Compressive strength (psi)	Modulus of elasticity (psi)	Poisson's ratio	Cure <sup>a</sup>	Test site
$\times 10^6$						
Trial batch mixture						
28	10	6790			Wet	WES
Thermal cylinder concrete						
7	3	4993			Wet	WES
28	4	7390	4.5	0.26	Wet	WES
28	3	6721	4.6		Wet	ORNL
90	6	8819	5.2	0.28	Dry	ORNL
90	6	8804	5.5	0.31	Wet	ORNL
180	4	9100	5.4	0.28	Wet	ORNL
180	3	9115	5.5	0.26	Dry	ORNL

<sup>a</sup>Wet, moist cured to time of testing; dry, moist cured for 28 days and air dried to time of testing.

be attributed to  $1\frac{1}{2}$  days of air drying required at WES for application of bonded strain gages. These differences are not seen when comparing ORNL 28-day strengths with WES trial batch results, where in both cases drying did not occur. A typical stress-strain curve and a plot of axial strain vs lateral strain are shown in Figs. 7.9 and 7.10 respectively.

Creep tests conducted at WES will provide data for comparison with results from earlier basic creep studies

conducted using the ORNL Tennessee limestone concrete. At the end of a 90-day curing period, two of the sealed specimens were loaded in uniaxial compression at  $75^\circ\text{F}$ ; the third cylinder will serve as an unstressed control specimen.

The thermal cylinder circumferential prestressing system was assembled after the specimen was installed at the ORNL test site. Posttensioning took place at a concrete age of 90 days. The circumferential tendons were stressed using seven 100-ton rams; six 30-ton rams were used to stress the axial tendons. The rams are shown positioned for posttensioning in Fig. 7.11. Each

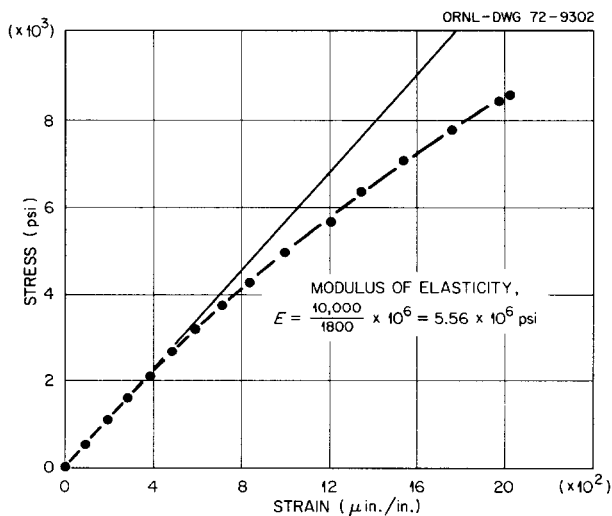


Fig. 7.9. Axial stress-strain curve for 180-day compression test of specimen 13 (28-day moist cure and 152-day air drying).

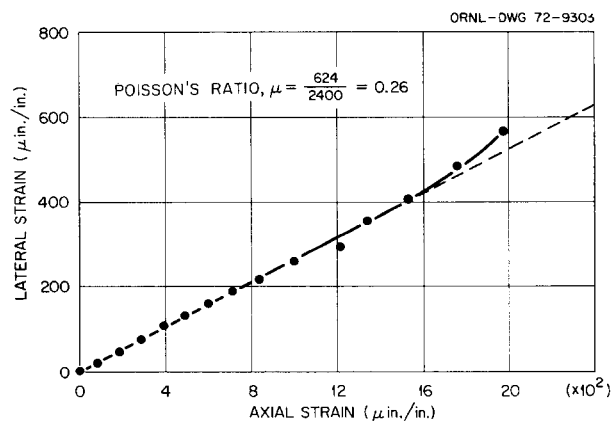


Fig. 7.10. Axial strain vs lateral strain curve for 180-day compression test of specimen 13 (28-day moist cure and 152-day air drying).

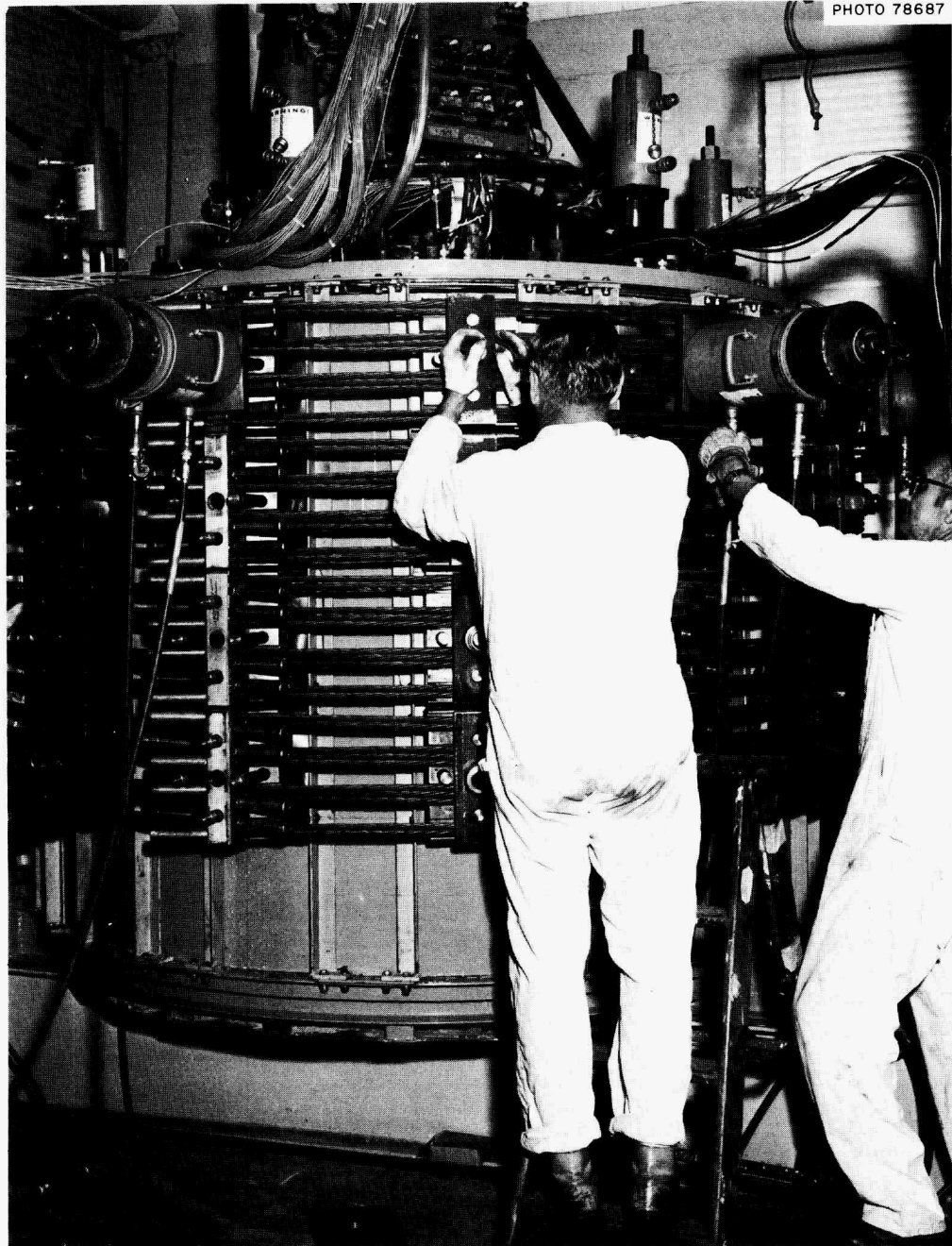


Fig. 7.11. Posttensioning operation, showing longitudinal and circumferential rams in position.

tendon was initially stressed to the half-load level using a predetermined loading schedule. The schedule was then repeated, with the stress in each tendon being increased to the design level. After correction of problems of localized crushing of the top moisture seal, good agreement was seen between the loading applied

to longitudinal tendons and final loadings as indicated by the tendon transducers. Good agreement was also seen between measured circumferential tendon strain and design values.

Upon completion of posttensioning, the remaining phases of assembly, consisting of installation of upper

insulation and moisture tube extensions and filling of the pressuring annulus with hydraulic fluid, were completed. The completed model is shown in Fig. 7.12.

The scheduled heating phase of the experiment was initiated at a concrete age of 130 days. While maintain-

ing the temperature of the outer heat exchanger at 75°F, the temperature of the interior (*A* and *B* panel coils) heat exchangers was increased at a rate of 5°F/day from the initial 75°F temperature to a final value of 150°F. The final through-the-wall thermal

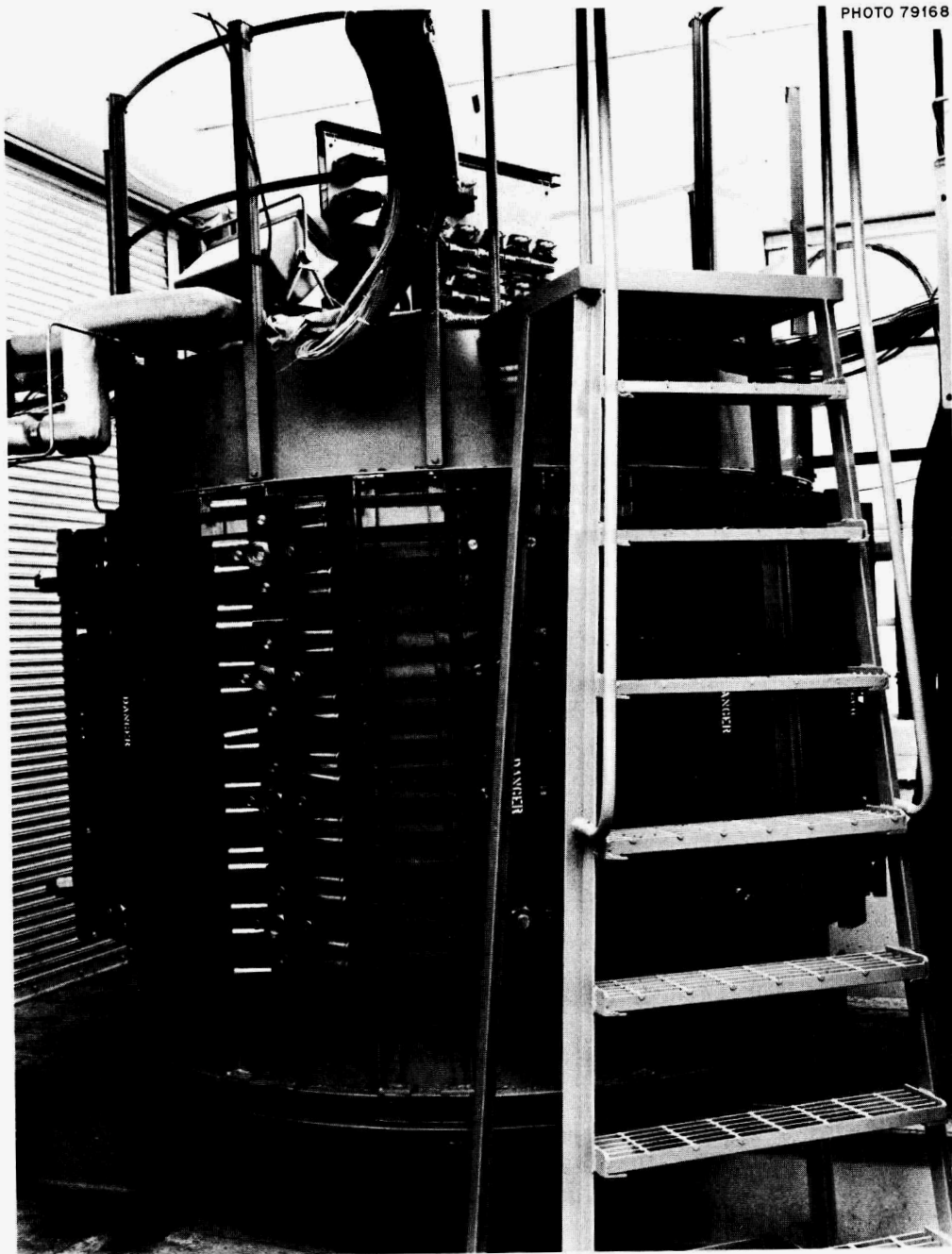


Fig. 7.12. Completed thermal cylinder model.

gradient shown in Fig. 7.13 will be maintained for the first year of the test.

In order to provide information with regard to the adequacy of the moisture seal and possible migration of moisture within the thermal cylinder, moisture readings are being made using a Troxler probe-type neutron and gamma-ray backscattering instrument. Readings have been taken periodically, beginning just prior to heatup, by lowering the moisture probe into sixteen 1-in.-OD thin-walled stainless tubes cast into the specimen along three radial lines. Initially, tube misalignment proved to be a problem; however, all tubes are now satisfactorily aligned and functioning properly. The probe is lowered to vertical positions 6, 18, and 30 in. from the bottom of the cylinder. Sets of three 1-min counts are made at each position, with standard counts being made at the beginning and end of a complete series of readings. Average readings for each radial tube position in the thermal cylinder are summarized in Table 7.2. The positions, as indicated from left to right in the table, extend from the center of the core (designated as center) out to the three positions located in the test sections (positions 3, 4, and 5). Position 3 is nearest to the 150°F surface, position 4 is located in the center of the section, and position 5 is nearest to the 75°F surface of the test section. Little variation can be seen in the readings at the radial positions in the cylinder, which indicates that so far little migration of moisture has resulted from heating. In addition, the moisture seal appears to be effective. The slightly higher moisture readings recorded in the core are probably the result of removal of the moisture seal from the top of the test section for the period of prestressing. The core remained sealed during this period. The absolute values of these moisture readings appear to be high when compared with the theoretical moisture content of the concrete, which is 17.7%. It is anticipated that this inconsistency will be resolved when results of a planned direct calibration of the Troxler moisture meter are available.

The thermal cylinder will remain exposed to the present combination of prestressing thermal and internal pressure conditions for a total duration of 180 days. This will be followed by 45 days with the internal pressure removed.

#### 7.1.6 Analysis of Thermal Cylinder

Modifications of the SAFE-CRACK computer program<sup>4</sup> to be used in analyzing the thermal cylinder model have been completed. Materials properties based on data obtained during the concrete materials investi-

gations portion of the ORNL Prestressed Concrete Pressure Vessel Research and Development Program have been incorporated into the analysis. Other modifications incorporated into the computer program include a new integration scheme and a new temperature treatment based on the shift principle. These improvements are most important in cases where the stress relaxation curve deviates appreciably from a straight line. The time-temperature shift treatment is applicable to creep behavior only. In addition, the new integration scheme will permit the use of larger time steps in the analysis, although this was not needed at this time for analyzing the thermal cylinder model.

The first of the planned analyses has been successfully completed. Results have been obtained for 55 time steps beginning with completion of prestressing and extending through the heat-up phase to the present combination of prestressing, 75 to 150°F thermal gradient, and internal pressure loading conditions. The analytical results are currently being prepared in the form of plots, and comparisons will be made with available experimental results.

## 7.2 SUBCONTRACT STUDIES

Three outside activities were brought to various stages of completion in accordance with the original planning, and none of these subcontracts were extended beyond July 1971. The following provides a summary of the status of these programs at that time and references the documentation that has been prepared to summarize the work.

### 7.2.1 Structural Behavior of Prestressed-Concrete Reactor Vessels University of Illinois, Subcontract No. 2906

The study of failure modes of PCRVs under increasing internal pressure loading is of particular importance to safety assessments of these structures. Primary emphasis in this series of tests has been placed on the failure of end slabs in shear, since this mechanism is not clearly defined and the prevention of such a failure is of the utmost importance to safe operation of a vessel.

A total of 23 model vessels have been tested, with principal features as shown in Fig. 7.14 and listed in Table 7.3. Further details of the vessels have been

---

4. Y. R. Rashid, *Nonlinear Quasi-Static Analyses of Two-Dimensional Concrete Structures*, GA-9994 (Mar. 23, 1970).

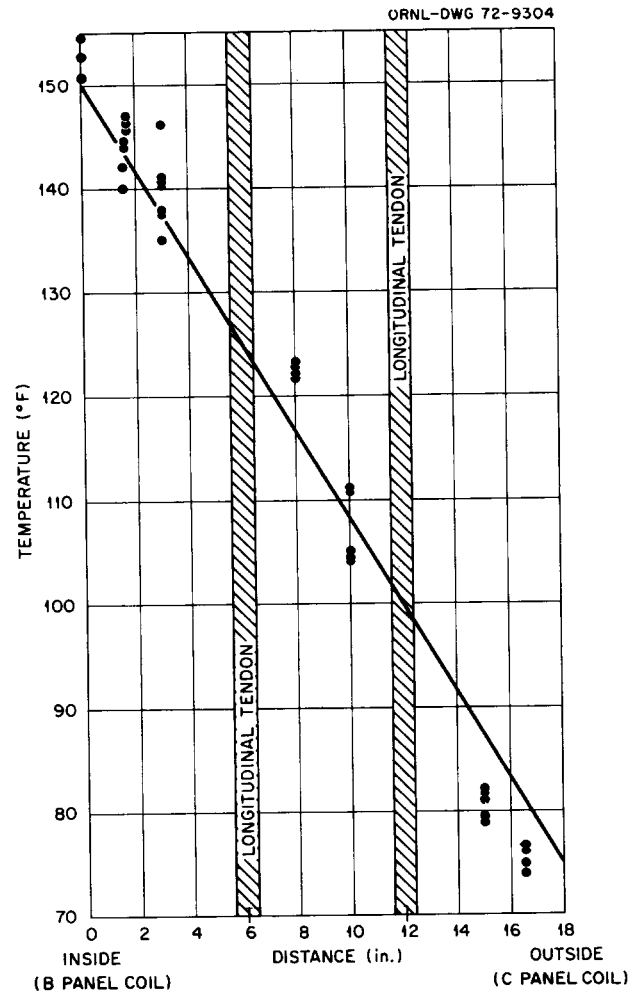


Fig. 7.13. Final thermal cylinder temperature gradient. Points indicate individual temperature readings of thermocouples and precision resistors.

Table 7.2. Moisture content at various moisture tube positions in thermal cylinder

Days from casting	Moisture (% by volume)						Status of experiment
	Core			Annulus			
	Center	Position 1	Position 2	Position 3 (hot)	Position 4 (middle)	Position 5 (cold)	
130		22.6	21.0	20.9	20.8	20.3	75°F-75°F
135	23.0	24.1	22.6	22.1	22.4	21.8	105°F-75°F
146	23.2	24.3	22.6	22.3	22.6	22.1	150°F-75°F
175	23.6	24.4	22.9	22.2	23.1	22.5	150°F-75°F
223	23.7	24.5	22.7	22.4	23.0	22.5	Before pressurization
236	23.7	23.7	22.3	21.9	22.5	22.2	After pressurization

Table 7.3. Dimensions and properties of test vessels

Geometry parameters			Circumferential prestress parameters					Longitudinal prestress parameters			Concrete			Maximum internal pressure (psi)	Mode of failure <sup>e</sup>	End slab penetration parameters				
Mark	Slab thickness (in.)	Wall thickness (in.)	2R/H ratio <sup>a</sup>	Wire diameter (in.)	Wire spacing (in.)	Force per wire (kips)	Circumferential prestress <sup>b</sup> (psi)	Tendon type <sup>c</sup>	Number	Total force (kips)	Compressive strength $f'_c$ (psi)	Tensile strength <sup>d</sup> (psi)	Young's modulus (psi)			Number and diameter of penetrations	Distance from center of slab (in.)	Percent of perimeter removed <sup>f</sup>	$\beta g$ (%)	Percent of slab removed <sup>h</sup>
													$\times 10^6$							
PV1	6	5	5	0.192	1.0	4.55	228	Rod	10	388	5680	432	4.2	295	F				100	
PV2	6	5	5	0.192	1.0	4.45	222	Strand	24	388	4955	398	3.5	240	L				100	
PV3	7.5	5	4	0.192	1.0	4.68	234	Strand	24	392	6250	450	4.2	370	F				100	
PV4	6	5	5	0.102	0.67	4.49	336	Strand	24	583	5680	380	4.2	390	F				100	
PV5	7.5	5	4	0.192	0.67	4.59	344	Strand	24	524	6250	439	4.1	465	F				100	
PV6	9	5	3.3	0.192	0.67	4.51	336	Strand	30	606	5805	398	4.1	570	L				100	
	6.1					4.48				639				585	L				100	
	6.2					4.47			22	469				555	F				100	
PV7	9	5	3.3	0.192	0.33	4.23	635	Strand	30	693	6720	506	4.6	870	F				100	
PV8	7.5	5	4	0.192	0.33	4.09	617	Strand	30	626	7230	443	4.8	625	L				100	
	8.1									700				640	F				100	
PV9	9	5	3.3	0.192	0.33	4.10	615	Strand	30	750	7140	446	4.3	887	F				100	
PV10	7.5	5	4	0.192	0.33	4.12	619	Strand	30	750	7005	394	4.0	740	F				100	
PV11	7.5	7.5	3.3	0.250	0.25	6.06	1143	Rod	30 <sup>i</sup>	694	6830	504	4.5	2040	S				100	
	11.1					5.72				1030									100	
PV12	10	7.5	2.5	0.250	0.25	5.73	1144	Rod	30	727	5860	456	4.4	2650	L.O.				100	
PV13	12.5	7.5	2	0.250	0.25	5.82	1145	Rod	60	1356	6750	490	4.2	3450	W-L.O.				100	
PV14	15	7.5	1.67	0.250	0.25	5.56	1111	Rod	60	1370	6880	465	4.3	3690	W-L.O.				100	
PV15	7.5	7.5	3.3	0.250	0.25	6.47	1292	Rod	60	1200	7340	531	4.2	2300	S				100	
PV16	10	7.5	2.5	0.250	0.25	6.03	1187	Rod	60	1995	7450	518	4.0	3200	S				100	
PV17	10	7.5	2.5	0.250	0.25	6.33	1265	Rod	60	2080	7180	534	3.8	3000	S	3, 4 in.	8	25	75	7.7
PV18	10	7.5	2.5	0.250	0.25	5.94	1188	Rod	60	1818	7590	447	4.0	3000	L	6, 4 in.	8	50	50	15.3
PV19	10	7.5	2.5	0.250	0.25	5.85	1170	Rod	60	2300	7470	406	3.9	3500	L	6, 2 in.	8	50	50	3.8
PV20	10	7.5	2.5	0.250	0.25	5.78	1155	Rod	60	2140	6890	469	3.8	3300	S	12, 2 in.	8	50	50	7.7
PV21	10	7.5	2.5	0.250	0.25	5.65	1130	Rod	60	2300	7400	496	3.7	3300	S	6, 2 in.	8	25	75	3.8
PV22	10	7.5	2.5	0.250	0.25	5.64	1128	Rod	60	2086	6060	500	3.9	2900	L				100	
PV23	10	7.5	2.5	0.250	0.25	5.22	1044	Rod	60	2580	6750	540	3.9	2750	L	6, 4 in.	8	50	50	15.3

<sup>a</sup>Ratio of the inside radius to the slab thickness.

<sup>b</sup>Circumferential prestress is the external radial pressure on the vessel caused by the circumferential reinforcement.

<sup>c</sup>0.75-in. round stress steel rods or 0.5-in. round seven-wire strand.

<sup>d</sup>From 6- by 6-in. split cylinder tests.

<sup>e</sup>Modes of failure: F, flexure; L, leak in the seal; L.O., lift off base; S, shear; W, wall.

<sup>f</sup>Length of perimeter removed divided by total perimeter along the circle that passes through the centers of the penetrations.

<sup>g</sup>Solid perimeter divided by total perimeter along circle that goes through the center of the penetrations.

<sup>h</sup>Horizontal area of penetrations divided by inside area of slab ( $\pi \times 12.5^2$ ).

<sup>i</sup>This vessel was prestressed longitudinally with 28 rods and 2 lengths of strand.

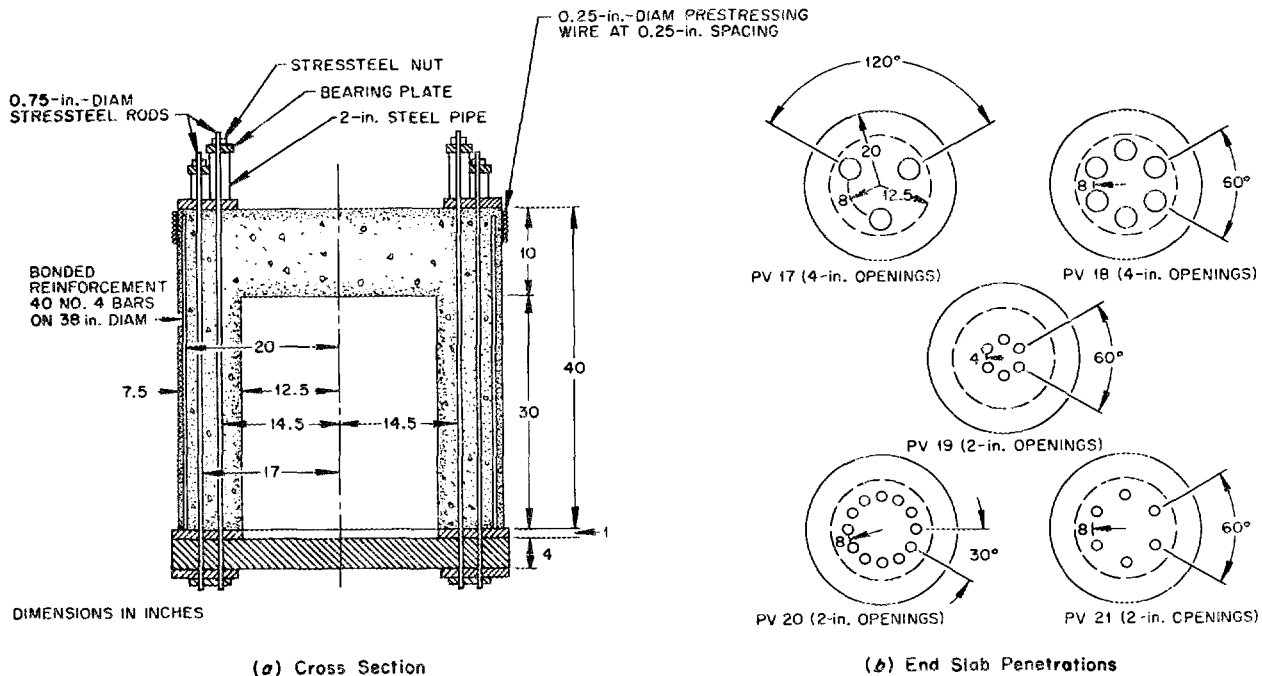


Fig. 7.14. Structural model test vessels configuration.

described in previous progress reports.<sup>5-8</sup> The results of tests of the first 16 vessels have been presented,<sup>9</sup> and a method to calculate flexural strength of the end slab was described. The response in the elastic range and part of the nonelastic range up to and including the initiation of a shear crack has been successfully predicted. However, the development of an elaborate

computer program to predict the shear strength of end slabs is presently not justified because of the lack of explicit criteria to define cracking and failure of the end slab.

A summary report<sup>10</sup> has been prepared evaluating the results of recent tests performed on five additional model vessels to investigate shear strength of the end slab and the effect of penetrations on shear strength. Observations have indicated that the end slab fails in shear as a result of the following mechanism: A critical crack forms in the end slab tending to transform the slab into a dome. Collapse occurs by the failure of the concrete in the remaining dome. A method was developed to estimate the shape of the dome and the failure load. The latter was based on finite-element analyses of the remaining dome and a failure criterion for concrete subjected to triaxial stresses.

Penetrations that are located in the section in which the inclined crack is initiated precipitate the formation of the crack; however, in the experiments performed, the penetrations did not affect the strength of the

5. M. A. Sozen, W. C. Schnobrich, and S. L. Paul, "Structural Behavior of Prestressed Concrete Reactor Vessels," *GCR Program Semiannu. Progr. Rep. Mar. 31, 1969*, ORNL-4424, pp. 204-225.

6. M. A. Sozen, W. C. Schnobrich, and S. L. Paul, "Structural Behavior of Prestressed Concrete Reactor Vessels," *GCR Program Semiannu. Progr. Rep. Sept. 30, 1969*, ORNL-4508, pp. 151-57.

7. M. A. Sozen, W. C. Schnobrich, and S. L. Paul, "Structural Behavior of Prestressed Concrete Reactor Vessels," *GCR Program Semiannu. Progr. Rep. Mar. 31, 1970*, ORNL-4589, pp. 140-53.

8. M. A. Sozen, W. C. Schnobrich, and S. L. Paul, "Structural Behavior of Prestressed Concrete Reactor Vessels," *GCR Program Semiannu. Progr. Rep. Sept. 30, 1970*, ORNL-4637, pp. 65-73.

9. S. L. Paul et al., *Strength and Behavior of Prestressed Concrete Vessels for Nuclear Reactors*, vol. I, University of Illinois, Civil Engineering Studies, Structural Research Series No. 346, Urbana, July 1969.

10. B. I. Karlsson and M. A. Sozen, *Shear Strength of End Slabs with and without Penetrations in Prestressed Concrete Reactor Vessels*, University of Illinois, Civil Engineering Studies, Structural Research Series No. 380, Urbana, July 1971.

vessels even though the penetrations in some tests removed up to half of the circumference on which they were located. It has not been possible to produce estimates of the number of penetrations that can be introduced without affecting the strength of the end slab.

Two additional vessels have been tested to make up a final phase of this project. These tests were similar to those performed on previous specimens except that the instrumentation was more extensive. The main addition was the installation of wire grids in the end slab with strain gages attached to the grids at various locations. Data were obtained on the strain that initiated the inclined crack within the end slab and on strain distributions in the dome following the formation of the fully developed inclined crack. A report summarizing these tests is in preparation.

### 7.2.2 Concrete Triaxial Creep Tests at the University of Texas Subcontract No. 2864

The reports<sup>11-13</sup> summarizing the results of the first phase of the triaxial creep studies on concrete have been issued.

---

11. T. W. Kennedy and E. S. Perry, *An Experimental Approach to the Study of the Creep Behavior of Plain Concrete Subjected to Triaxial Stresses and Elevated Temperatures*, The University of Texas at Austin, Department of Civil Engineering Research Report 2864-1, June 1970.

12. G. P. York, T. W. Kennedy, and E. S. Perry, *Experimental Investigation of Creep in Concrete Subjected to Multiaxial Compressive Stresses and Elevated Temperatures*, The University of Texas at Austin, Department of Civil Engineering Research Report 2864-2, June 1970.

13. J. W. Chuang, T. W. Kennedy, and E. S. Perry, *An Approach to Estimating Long-Term Multiaxial Creep Behavior from Short-Term Uniaxial Creep Results*, The University of Texas at Austin, Department of Civil Engineering Research Report 2864-3, June 1970.

The concrete specimens that were cast to evaluate the effect of age prior to loading remain under test, although no funding is available to evaluate the data. Included in this series are as-cast and air-dried specimens loaded after 183 and 365 days of curing. One specimen of each curing history and age is loaded under 600 and 2400 psi uniaxial stress conditions, so that eight samples remain under test.

### 7.2.3 Concrete Moisture Migration Study and Multiaxial Creep Tests Waterways Experiment Station, Interagency Agreement AT-(40-1)-3636

Information on the nature of moisture movement and the rate of moisture loss in a concrete pressure vessel wall is of interest in view of the influence these parameters have on the properties of concrete. An experimental study was initiated in October 1968 to study these factors in a specimen representing a section through a 9-ft-thick wall. After the initial temperature excursion resulting from the heat of hydration released during curing, the specimen was operated isothermally for 1½ years. In March 1970, an 80°F temperature gradient was applied, and the unit was operated under this condition until March of 1971, at which time it was terminated.

Data were obtained routinely on temperature, strain, and moisture level. Based on a preliminary assessment of the data, there was no appreciable change in the specimen's moisture content, and it may be tentatively assumed that the moisture movement was not significant for the period of the test.

The last of the multiaxial creep specimens was unloaded in February 1971. The data acquisition phase of this project was completed in May 1971, at which time the taking of creep recovery measurements from these specimens was discontinued.

Hopefully, completion reports can be prepared on the moisture movement and multiaxial creep experiments at a future date.

## 8. HTGR Fuel Element Development

J. H. Coobs    J. L. Scott  
W. P. Eatherly

The objectives of the fuel element development program are: (1) to demonstrate HTGR reference design coated particles and fuel sticks to the full fluence and burnup of the reactor, (2) to develop alternative fabrication processes with either better economics or performance than reference fuel fabrication methods, and (3) to develop advanced fuels with higher temperature capability than reference materials. To meet these objectives, we have a three-phase program. The first phase involves fabrication studies of new designs or methods. When new types of materials are successfully fabricated, they then enter the second phase of the work, irradiation testing and evaluation. The third phase involves those theoretical or analytical studies required to explain basic phenomena involved in phases 1 and 2.

During the past year, emphasis has been placed on fabrication of fuel kernels by use of ion exchange resins, development of simpler coatings than the reference four-layer coating (i.e., buffer, inner isotropic pyrolytic carbon, SiC, and outer isotropic pyrolytic carbon), and development of alternative filler and binder materials to make fuel sticks. We have also concentrated on methods of characterizing materials for better quality control and quality assurance.

### 8.1 RESIN PARTICLE DEVELOPMENT

C. B. Pollock

An alternative method of fabricating HTGR "fissile" fuel particles from ion exchange resins has been

developed at ORNL.<sup>1</sup> The fabrication process utilizes two properties of ion exchange resins: the chemical exchange capacity and the thermosetting characteristics of the resin. Spherical cation resin particles are contacted with uranyl or plutonyl nitrate solution until the exchange reaction is complete or until all the active sites in the resin have been occupied by heavy-metal groups. The loaded resins are then washed, dried, and carbonized to form porous carbon microspheres with the fuel uniformly dispersed. Figure 8.1 shows the resins in these various stages. After carbonization, the fuel particles are coated with pyrolytic carbon and silicon carbide to form fissile fuel particles.

#### 8.1.1 Kernel Fabrication

During the past year we have continued investigations of the kinetics of loading ion exchange resins with uranium and plutonium. The process schematic shown in Fig. 8.2 is very similar to our present experimental procedure for loading resins with uranium. The results we have achieved with strong-acid resins have been very consistent, with loadings ranging from 95 to 105% of theoretical. Figure 8.3 shows the structure of a weak-acid resin and the loading reactions that lead to a fuel particle. We have had less success in achieving theoretical loadings with some weak-acid resins. Those formed

1. J. L. Scott, J. M. Leitnaker, and C. B. Pollock, "Preparation of Coated Fuel Particles from Ion-Exchange Resins," *GCR Program Semiannu. Progr. Rep. Mar. 31, 1970*, ORNL-4589, pp. 3-7.

Y-108881A

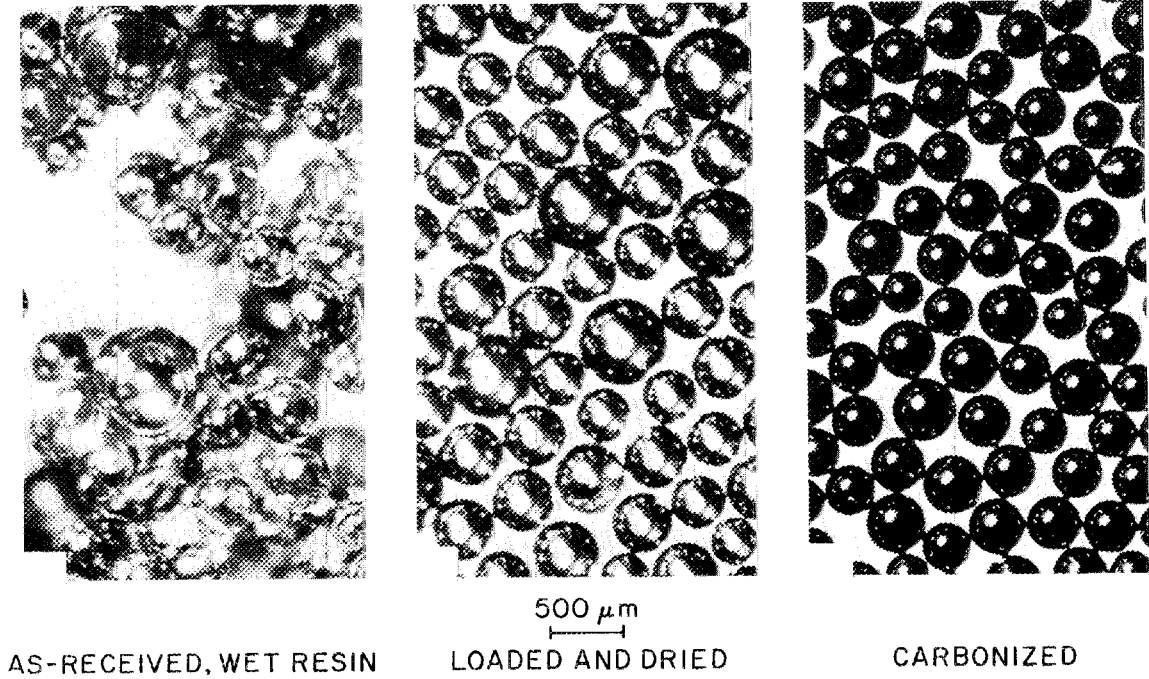


Fig. 8.1. Preparation of resin-derived microspheres.

ORNL-DWG 71-5339

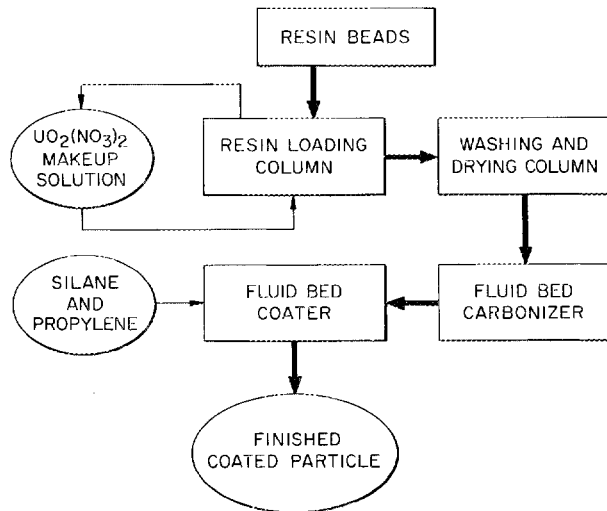


Fig. 8.2. Process schematic for resin-based fuel particles.

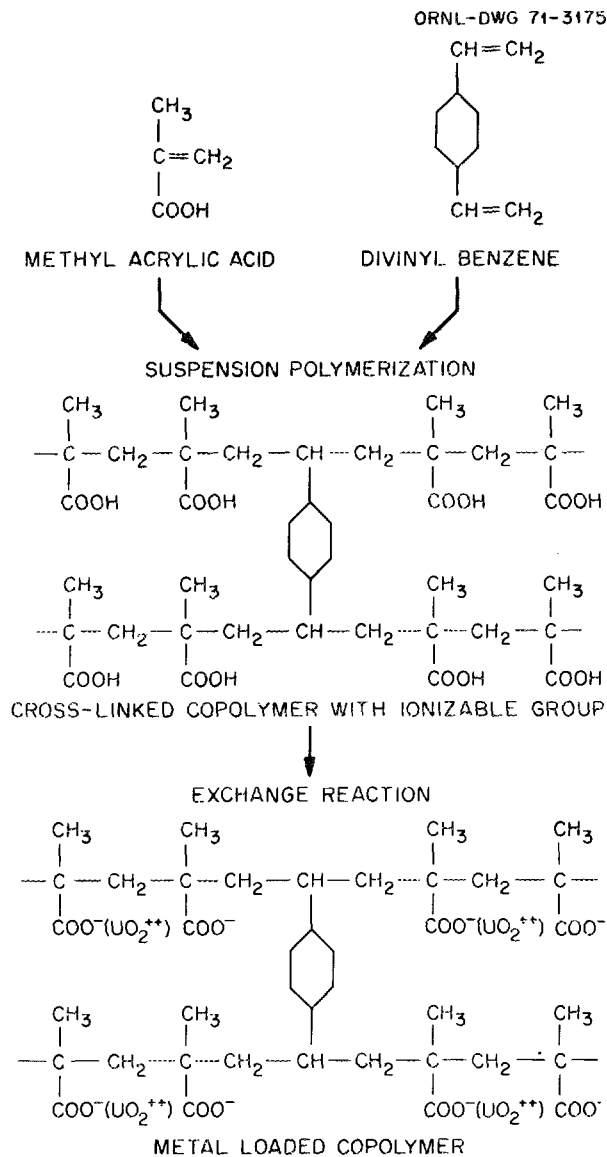


Fig. 8.3. Structure of polymerized and metal-loaded weak-acid ion exchange resin.

with methylacrylic acid which is cross-linked with appreciable quantities of divinylbenzene (DVB) load in a manner similar to the strong-acid resins. However, these resins are usually poorly formed spheres, and the yield tends to be quite low. Spherical weak-acid resins formed from acrylic acid and DVB are commercially available, but they are difficult to load. The acrylic acid resin is much less acidic than methylacrylic acid resin and is therefore much more sensitive to pH changes. We can load this resin to approximately 50% of theoretical, and the resulting fuel particle is similar in uranium density to that derived from our strong-acid resin. Table

Table 8.1. Typical compositions of fuel particles derived from ion exchange resins<sup>a</sup>

Resin	Composition (wt %)			
	Uranium	Carbon	Sulfur	Oxygen <sup>b</sup>
Dowex 50W-X8 <sup>c</sup>	48.7	35.5	10.3	5.5
	50.2	33.2	10.0	6.6
IRC 120 <sup>d</sup>	50.4	33.0	10.6	6.0
IRC 50 <sup>e</sup>	69.9	17.7		13.0
	65.6	22.1		12.3
	69.3	18.0		12.7
IRC 84 <sup>f</sup>	48.6	37.3		14.1
	42.3	45.3		12.4
	46.5	44.0		9.5

<sup>a</sup>All particles carbonized to 1000°C under argon.

<sup>b</sup>Oxygen by difference.

<sup>c</sup>Resins formed from styrene cross-linked with 8 wt % DVB; functional group SO<sub>3</sub>H; Dow Chemical Co.

<sup>d</sup>Similar to *c* except Rohm and Haas Co.

<sup>e</sup>Resin formed from methylacrylic acid cross-linked with approximately 5% DVB; functional group COOH; Rohm and Haas Co.

<sup>f</sup>Resin formed from acrylic acid cross-linked with approximately 5% DVB; functional group COOH; Rohm and Haas Co.

8.1 lists typical compositions obtained from the three resins.

We also performed an exploratory experiment to determine the feasibility of preparing plutonium fuel particles using this technique. We used a strong-acid resin and loading medium of aqueous plutonium nitrate. The first particles prepared were 35% plutonium by weight after being carbonized to 1000°C. Apparently the plutonium ion had an effective valence of 3 in solution and therefore required 50% more sites than UO<sub>2</sub><sup>2+</sup> in the same resin. In order to achieve higher loadings we need to complex the plutonium solution to obtain an effective valence of 2.

### 8.1.2 Carbonization and Thermal Stability

The quality of the carbonized fuel particles is very dependent on the drying and heating rates, and we have studied the carbonization cycle up to 1000°C with the aid of differential thermal analysis (DTA) and thermogravimetric analysis (TGA) apparatus.<sup>2</sup> We also systematically studied the dimensional changes that occur

2. C. B. Pollock and J. L. Scott, "Coated Fuel Particles Derived from Carbonized Ion-Exchange Resin," *GCR Program Semiannu. Progr. Rep. Sept. 30, 1970*, ORNL-4637, pp. 3-9.

during the drying and carbonizing so that we can choose a starting material of the right size and therefore minimize postcarbonization processing such as screening. It is difficult to follow diameter changes in batches of particles, but volume changes can easily be measured. Average diameter change can be deduced since diameter is proportional to volume. With strong-acid resins cross-linked with 8% DVB, there is a slight decrease in volume in loading, typically 4 to 5%. The dried loaded beads occupy 52% of the original volume, which implies that there has been an approximate 20% decrease in diameter. Finally, the carbonized fuel beads occupy 26% of the original volume, and the average diameter of

the carbonized beads is 34% less than that of the starting resin. The dimensional changes observed are very dependent on cross-linkage. We observed greater changes in a batch of material that was cross-linked with 4% DVB.

Gulf General Atomic (GGA) has subjected a number of resin-derived fuel particles to an "amoeba" test or a thermal gradient test. Particles have been tested in a temperature gradient of  $0.7^{\circ}\text{C}/\mu\text{m}$  with a center-line temperature of  $1800^{\circ}\text{C}$  for 31 hr. Resin-derived particles were unaffected by this treatment, while fully dense carbide particles experienced substantial fuel migration. Figure 8.4 shows a microradiograph of the

Y-106184A

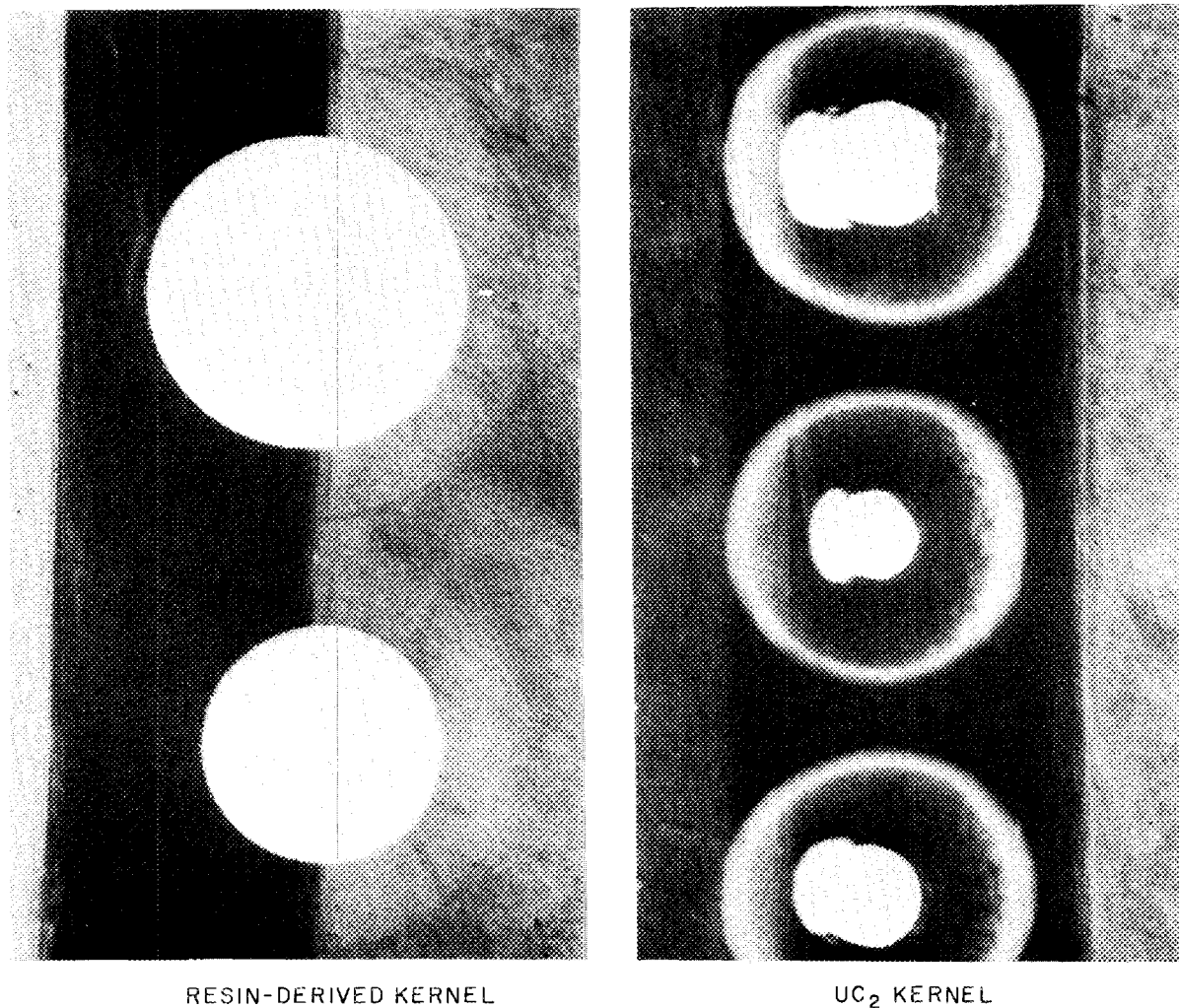
 $T = 1800^{\circ}\text{C}$      $\Delta T = 300^{\circ}\text{C}/\text{PARTICLE}$      $t = 11 \text{ h}$ 


Fig. 8.4. Fuel migration in a temperature gradient.

two kinds of particles after the thermal gradient test. The resin-derived particles on the left show no evidence of fuel migration, while the conventional carbide particles on the right show a distorted kernel and fuel in the carbon coatings. We are continuing experimentation in this area to further demonstrate the thermal stability of these particles.

### 8.1.3 Particle Design

The STRETCH code by Prados and Scott<sup>3</sup> and the Kaae code<sup>4</sup> were developed to predict the performance of coated fuel particles under HTGR conditions of fluence and temperature. These codes have been used to predict stresses on Biso and Triso coatings on fuel particles derived from ion exchange resins. Resin-derived fuel particles contain a substantial volume of closed porosity in the carbonized form, and our particle designs have been based on the premise that a low-density buffer coat would not be necessary. The Prados-Scott code and the Kaae code have verified the prediction for Biso and Triso coats respectively. Therefore, we have simplified particle coatings as shown in Table 8.2. We have fabricated and are testing all these designs in the HFIR. On fully loaded fuel particles derived from weak-acid resins subjected to full burnup, a thin low-density buffer layer might be required.

3. J. W. Prados and J. L. Scott, *Mathematical Model for Predicting Coated Particle Behavior*, ORNL-TM-1405.

4. J. L. Kaae, "A Mathematical Model for Calculating Stresses in a Pyrocarbon- and Silicon Carbide-Coated Fuel Particle," *J. Nucl. Mater.* 29, 249-66 (1969).

### 8.1.4 Irradiation Testing

Table 8.3 summarizes irradiation results from fuel particles derived from ion exchange resins. We have now subjected resin-derived fuel particles to HTGR conditions of fluence and temperature. Figure 8.5 shows a particle fueled with 10%-enriched uranium before and after an irradiation test. The kernel diameter has decreased, and porosity is quite visible in the kernel. The low-density buffer coat densified significantly, and the outer coating density increased from 1.95 to 2.1 g/cm<sup>3</sup>. The integrity and isotropy of the outer coating were unaffected by the test. Another batch of particles that was fueled with 74%-enriched uranium was irradiated in HRB-2 to a burnup greater than 70% of the fissionable atoms. All the particles survived this test.

Metallographic examination is now under way.

## 8.2 COATING DEVELOPMENT

C. B. Pollock

In our coating development we concentrated on three areas during the last year. First, we have demonstrated our ability to produce carbon- and SiC-coated PuO<sub>2</sub> particles. Second, we produced an array of conventional Triso II particles with widely varying coating densities in order to study the interactions between coatings. Third, we produced several new coating designs for use on resin-derived fuel particles.

### 8.2.1 PuO<sub>2</sub> Coating Development

The Carbon Technology Group has a small experimental coating furnace in a plutonium glove box. We

Table 8.2. Description of particle designs being considered for HTGR Application

Typical particle batch	Coating description			Irradiation
	Layer	Material	Density	
OR-1442	Monolayer	PyC	2.0 ± 0.1	HT-5, HT-8
OR-1295	Inner	PyC	1.75 ± 0.1	HT-5, HT-8, HRB-2 C1-28
	Outer	PyC	2.0 ± 0.1	
OR-1522	Inner	PyC	1.75 ± 0.1	HT-8, HRB-2, C1-28
	Middle	SiC	<3.18	
	Outer	PyC	2.0 ± 0.1	
SC-57	Monolayer	SiC	<3.18	HRB-2
OR-1417	Inner	SiC	<3.18	HRB-2
	Outer	PyC	2.0 ± 0.1	

Table 8.3. Summary of fuel particles tested to date

Particle No.	Resin	Coating design	Peak			Survival (%)
			Fluence (neutrons/cm <sup>2</sup> )	Temperature (°C)	Burnup (% FIMA)	
OR-1100	Dowex 50W-X8	Monolayer	$6 \times 10^{21}$	1050	8.5	<75
OR-1101	Dowex 50W-X8	Monolayer	$6 \times 10^{21}$	1050	8.5	<75
OR-1117	Dowex 50W-X8	Biso	$6 \times 10^{21}$	1050	8.5	<75
OR-1295	Dowex 50W-X8	Biso	$7.2 \times 10^{21}$	1030	18.5	100
OR-1316	Dowex 50W-X8	Biso	$7.2 \times 10^{21}$	1080	8.5	100
OR-1319	Dowex 50W-X8	Biso	$5.0 \times 10^{21}$	<1550	>60	100
OR-1522 <sup>a</sup>	Dowex 50W-X8	Triso	$1 \times 10^{22}$	1050	12	10
OR-1489	Dowex 50W-X8	Triso	$1 \times 10^{22}$	1050	12	100
OR-1487 <sup>a</sup>	Dowex 50W-X8	Biso	$1 \times 10^{22}$	1050	12	75
OR-1442	IRC-50	Monolayer	$1 \times 10^{22}$	1050	12	100
OR-1440 <sup>a</sup>	Dowex 50W-X8	Biso	$1 \times 10^{22}$	1050	12	100
OR-1401	IRC-50	Monolayer	$1 \times 10^{22}$	1050	12	100
SC-57	Dowex 50W-X8	SiC	$8 \times 10^{21}$	1150	14	90
OR-1417	Dowex 50W-X8	Biso	$8 \times 10^{21}$	1150	14	100
OR-1392	Dowex 50W-X8	Biso	$8 \times 10^{21}$	1150	14	100

<sup>a</sup>Failures in these particles appeared to associate with the low-density inner pyrocarbon layer (1.5 g/cm<sup>3</sup>); inner layer densities are now 1.7 g/cm<sup>3</sup>.

Y-105686

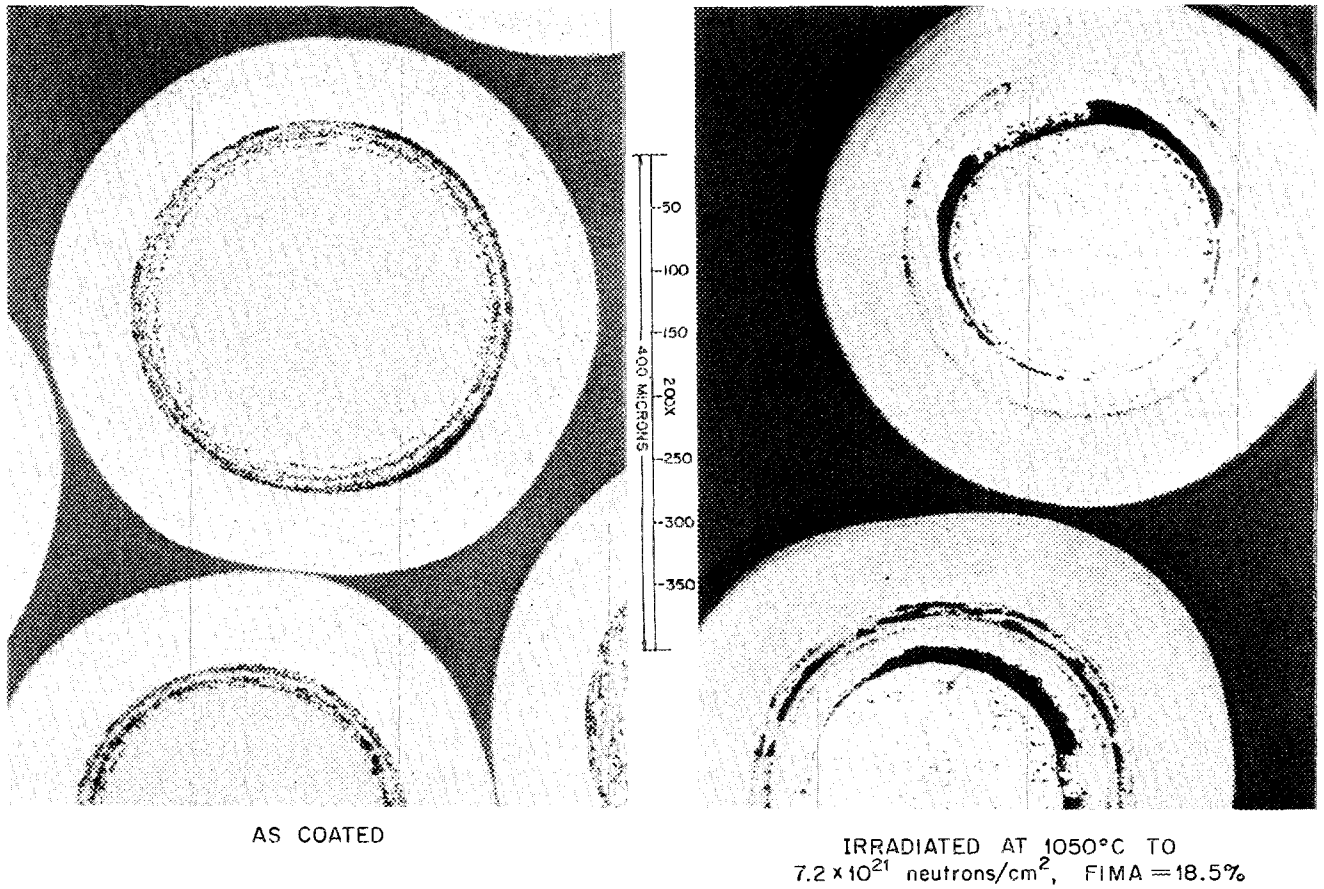


Fig. 8.5. Fissile particles made from ion exchange resins.

have used this coater in the past year for three different purposes. The first was to coat a small quantity of sol-gel PuO<sub>2</sub> with Biso (two-layer) carbon coating for irradiation testing. This was accomplished in a reasonable time period, and the coated particles had the desired properties. Second, we coated a large quantity (3500 g) of sol-gel PuO<sub>2</sub> microspheres with a massive monolayer of carbon for thermal and irradiation testing. The major requirement of this undertaking was that the coatings be dense (>1.8 g/cm<sup>3</sup>) and that they be free of activity. All the coatings were dense, and activities remained below 500 dis min<sup>-1</sup> g<sup>-1</sup> for all batches. Finally, we are in the process of coating microspheres of PuO<sub>2</sub> for use in prototype HTGR fuel elements by GGA. The particles are of different size and composition, but all are to be coated with Triso II coatings. This will be our first attempt to deposit SiC coatings in a glove box. We designed and built new off-gas scrubbers that will remove HCl from the furnace off-gas. In the past we have simply washed out the HCl with water, but this process requires the handling of large quantities of contaminated water. Therefore, at the suggestion of K. Notz of ORNL Chemical Technology Division, we have built a dry scrubber utilizing Ascarite (NaOH + asbestos) and Drierite (CaSO<sub>4</sub>). The system has performed quite well in cold runs and is now being used in the hot laboratory.

### 8.2.2 Coating Properties

An important consideration in fuel particle design is the interaction between coatings under HTGR conditions of fluence and temperature. Therefore, we prepared a series of coated particles utilizing the Triso II design that could be irradiated for this purpose. The major variable was pyrolytic carbon density, as shown in Table 8.12; however, we also varied the thickness of the silicon carbide layer and added an additional buffer layer to one particle design. These kernels were made from carbon, and the particle design is like the largest fertile particle used by Fort St. Vrain. They were irradiated to fluences of 5, 10, and 15 × 10<sup>21</sup> neutrons/cm<sup>2</sup> ( $E > 0.18$  MeV) in order to study the effects of fluence on the particle coatings. (See Sect. 8.6.5 for irradiation results.)

### 8.2.3 Particle Design

Theoretical modeling of resin-derived fuel particles has predicted that such particles can survive HTGR conditions of fluence, temperature, and burnup without the need for a low-density buffer layer, and early

irradiation tests have supported this prediction. The low-density buffer coat is the least controllable and the most difficult of all to apply; therefore coating processes would be greatly simplified if we can eliminate this coating. We have prepared and irradiated a number of coated particles utilizing different designs (see Sect. 8.1).

An irradiation experiment was planned and designed to compare the new coating designs on resin particles with conventional coating designs on dense oxide and carbide particles. Table 8.3 describes the properties of these particles. After irradiation the particles will be subjected to thermal tests that compare their ability to retain fission products and that measure the diffusion rates of different fission products through the coatings.

### 8.2.4 Optical Anisotropy Factor (OPTAF) Studies

D. M. Hewette II     R. J. Gray

We have obtained optical equipment that is designed for measuring reflectance intensities of pyrolytic carbon coatings on fuel microspheres. Reflectance characteristics of areas 5 to 10 μm in diameter are measured using a plane-polarized light source and a microphotometer. OPTAF<sup>5</sup> values near 1.0 indicate a low optical anisotropy, a desirable characteristic to maintain coating integrity during fast-neutron exposure. A Leitz microscope photometer (Fig. 8.6) has been applied to the examination of nonradioactive materials, and a Reichert microphotometer has been adapted to a Bausch & Lomb Research I metallograph (Fig. 8.7) for use with our glove box metallograph for the evaluation of coatings on alpha-radioactive fuels.

As reference samples, two single crystals of graphite were prepared, one with its basal planes parallel to the plane of polish and the other with its basal planes perpendicular to the plane of polish. Characteristic curves taken of these samples using the Reichert microphotometer–Bausch & Lomb metallograph combination are shown in Fig. 8.8. These curves are representations of the reflectivity variation from a 63-μm spot as the stage is rotated through 360°. Curves *A* and *B* are representative of how the single crystal would behave when evaluated using plane-polarized incident light and no analyzer. Curve *A* was taken of a cleaved basal plane surface since we could not successfully polish a crystal with its basal planes parallel to

5. OPTAF =  $I_{\max}/I_{\min}$ , where  $I_{\max}$  and  $I_{\min}$  are the maximum and minimum reflectivities of the same microscopic field after 360° rotation.

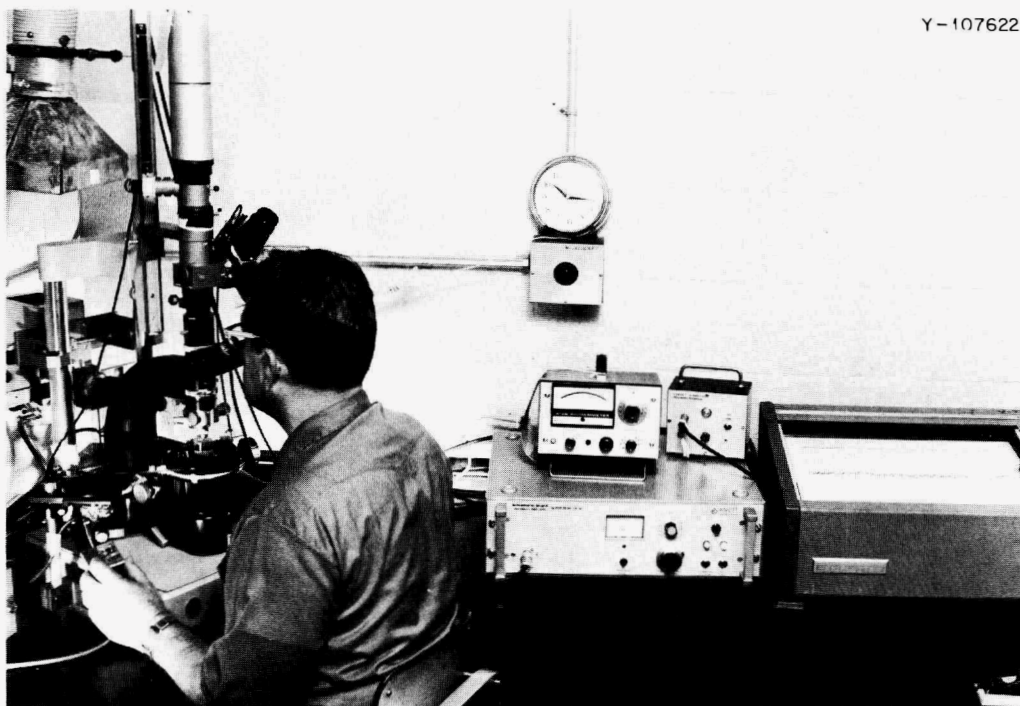


Fig. 8.6. Leitz microscope adapted for examination of nonradioactive materials in OPTAF studies.

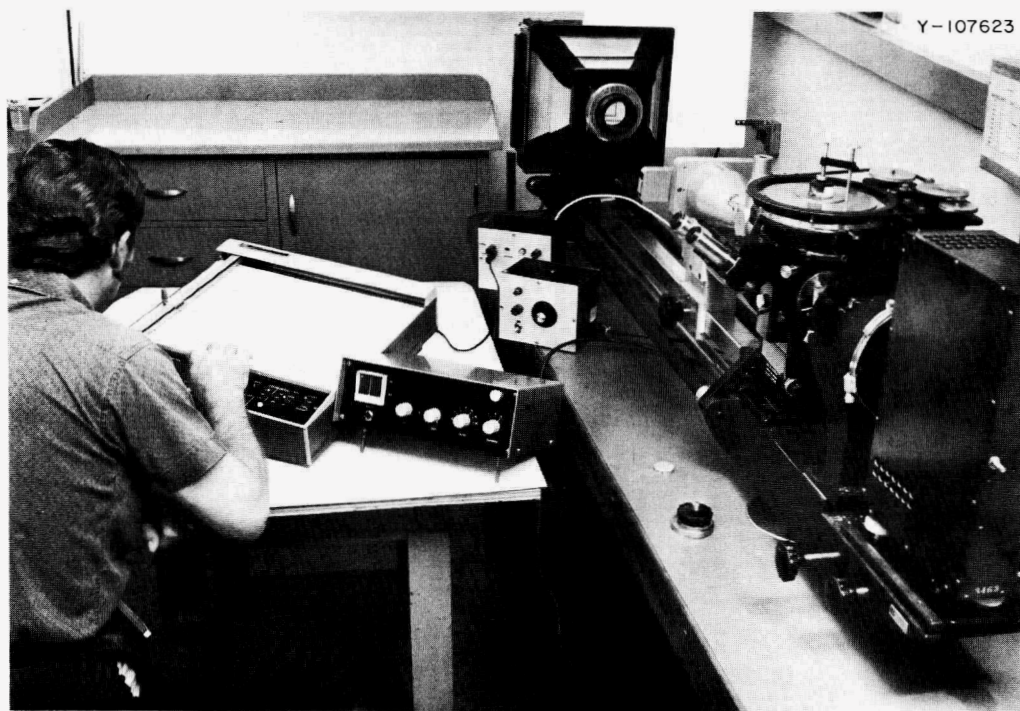


Fig. 8.7. Reichert microphotometer and Bausch & Lomb Research I metallograph adapted for glove-box evaluation of coatings on alpha-radioactive fuels.

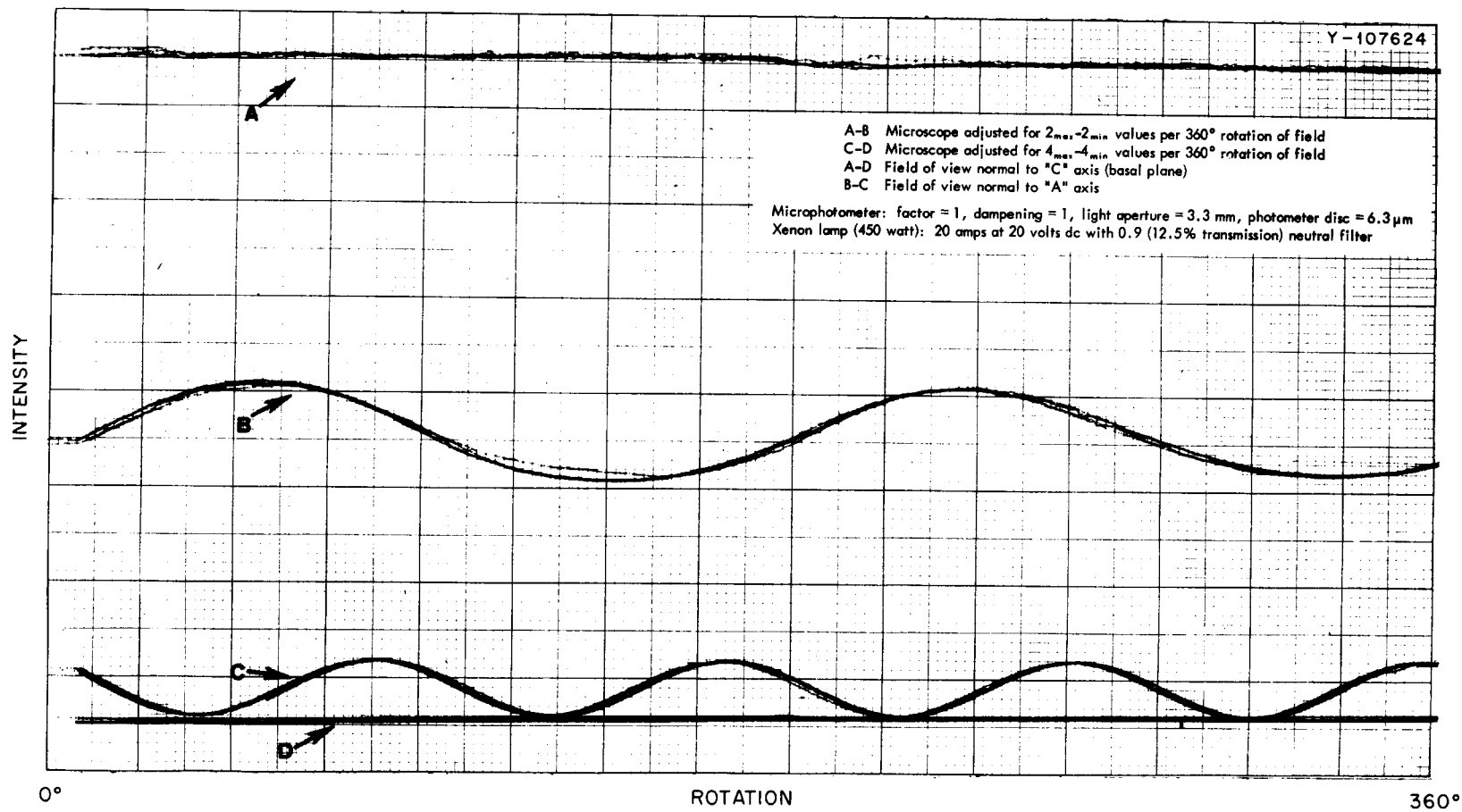


Fig. 8.8. Optical anisotropy factor (OPTAF) values on single-crystal graphite.

the plane of polish. Curve *B* was taken of a polished sample, the one with its basal planes perpendicular to the plane of polish. Curve *B* exhibits two symmetrical peaks. The maxima represent the reflectivity  $r_a$  in the *a* direction of the crystal, and the minima represent the reflectivity  $r_c$  in the *c* direction.

Curve *A* represents the reflectivity in the *a* direction and gives no variation in reflectivity since the measurement is taken looking along the axis of symmetry. In principle, curve *A* should be tangent to the maxima of curve *B*, but it lies considerably above. This effect is

due to lower reflectivity of the polished sample. Curves *C* and *D* are representative of results obtained with the basal planes of the graphite crystal perpendicular to the plane of polish. The reaction of pyrolytic carbons with polarized light under these conditions has been described by Gray and Cathcart.<sup>6</sup> This explanation can best be made with reference to Figs. 8.9 and 8.10. In Fig. 8.9, the eight photomicrographs of pyrolytic

6. R. J. Gray and J. V. Cathcart, *J. Nucl. Mater.* 19, 81–89 (1966).

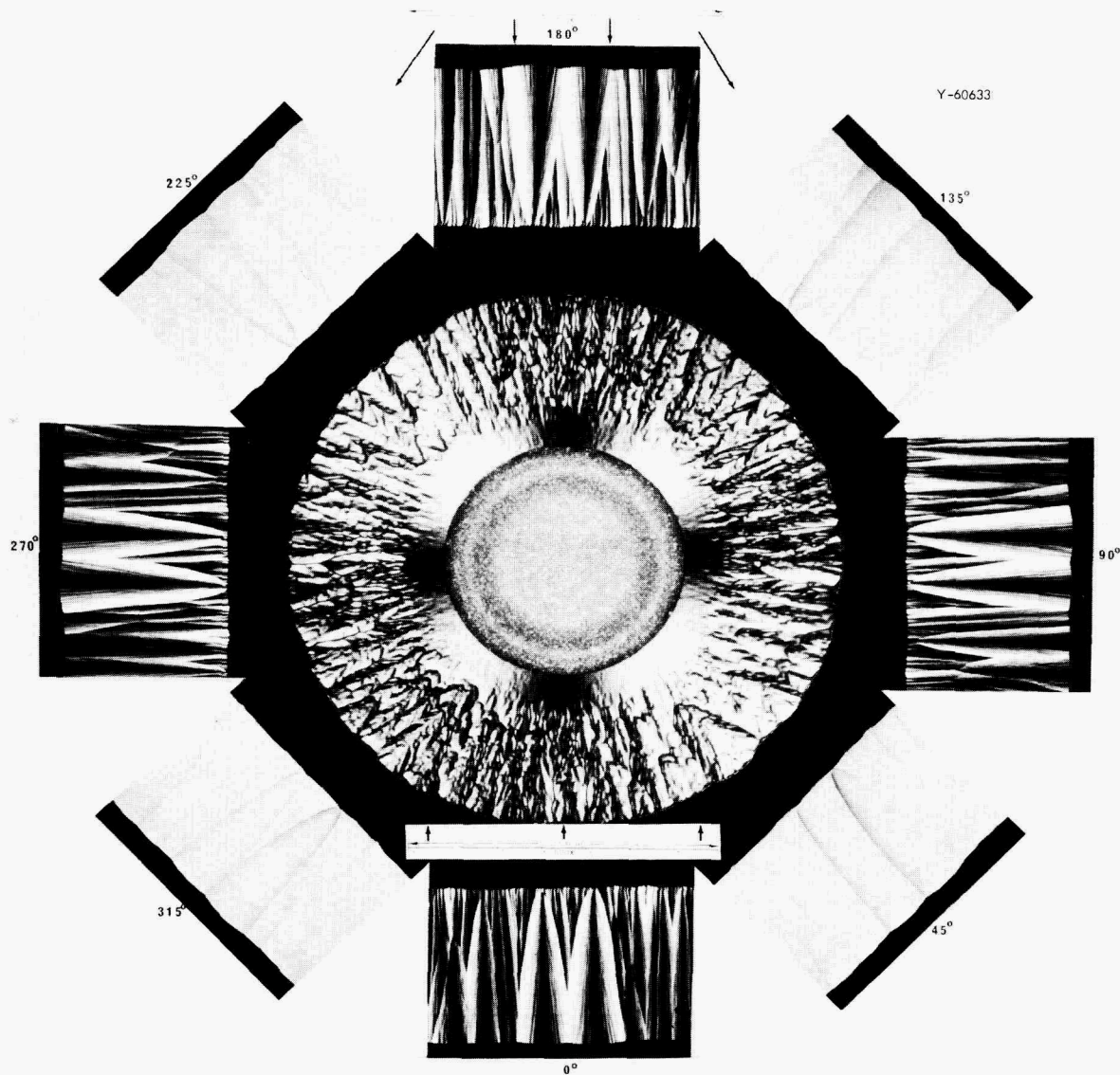


Fig. 8.9. Comparative microstructures of pyrolytic carbon deposited on spherical and flat substrates.

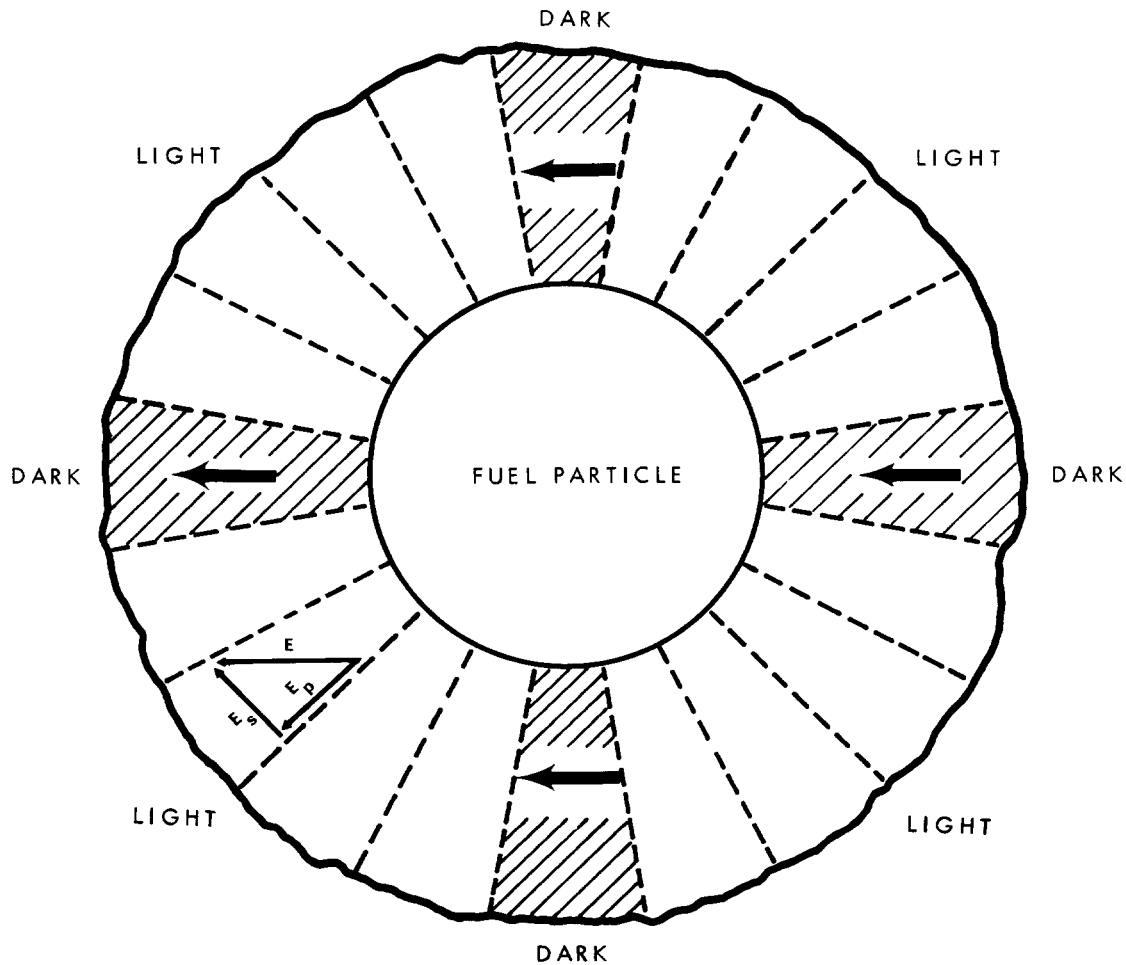


Fig. 8.10. Schematic representation of the median plane of a pyrolytic-carbon-coated fuel particle viewed in polarized light.

carbon deposited on a flat substrate show the microstructures at eight positions of stage rotation with polarized light. Because of its fiber texture the pyrolytic-carbon-coated sphere has essentially all the orientations (relative to the plane of vibration of the polarized light) shown by the flat pyrolytic carbon in a complete 0 to 360° rotation of the stage. In Fig. 8.10, the  $c$  axes of the PyC fibers are indicated by the dotted lines; in the drawing the principal planes of the fibers contain these lines and are perpendicular to the plane of the paper. Resolution of the incident electric vector  $E$  into its components parallel and perpendicular to the principal plane of a fiber is shown schematically in the lower left quadrant of the drawing. The dark areas represent areas of the PyC where the incident  $E$  vector

is either parallel or perpendicular to the principal planes (i.e., either  $E_s$  or  $E_p$  is zero).

Reflectivity measurements taken on particles should yield a series of four peaks similar to those shown in curve  $C$  of Fig. 8.8. Of course for fast-neutron stability, nearly or completely isotropic coating is desired, and such a particle would appear uniformly black with no evidence of a Maltese cross as shown by the particle coating of Fig. 8.10. Consequently, the peaks would be less distinct, but, if present at all, they should show fourfold symmetry with four equal minima. A completely isotropic coating, however, would yield a straight line.

A reflectivity trace obtained from a typical particle coating is shown in Fig. 8.11. As shown here there are

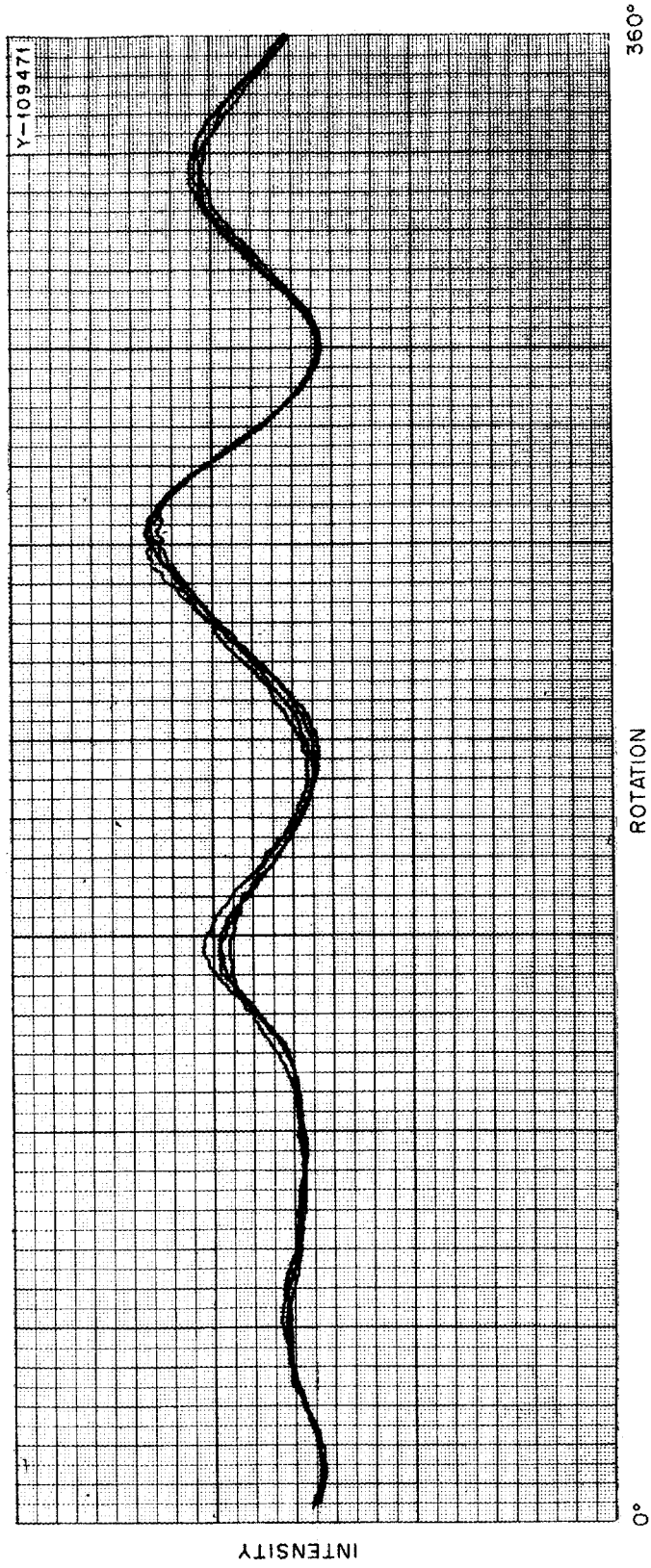


Fig. 8.11. Optical anisotropy factor (OPTAF) trace on a typical particle coating. Reichert microphotometer adapted to Bausch & Lomb Research I metallograph.

four peaks, but the maxima and minima do not compare with each other favorably.

### 8.3. BONDED FUEL DEVELOPMENT

R. L. Hamner    J. M. Robbins  
D. L. McElroy

#### 8.3.1 Fabrication by Intrusion Bonding

The length that fuel rods can be fabricated by the conventional "grease-gun" intrusion technique, using high-filler-content bonding materials, seems to be limited to about 2 in. This practical limitation is imposed primarily by the filtering action of the particle bed on the filler during intrusion when the bonding material is forced along the full length of the fuel bed. The use of the conventional technique also results in "end capping" during carbonization. An "end cap" forms at the intrusion end of the specimen and consists of a matrix-rich region that shrinks more during carbonization and, therefore, tends to separate from the adjacent particle-rich region. To eliminate these undesirable features, a mold was designed for radial intrusion so that the bonding mixture had to travel only about 0.25 in. through the fuel bed. The mold design, shown in Fig. 8.12, consists of two concentric tubes with a small annulus between them. The inner tube, which contains the fuel bed, has small holes provided for intrusion of the bonding matrix. The "grease gun" is attached at the side of the mold, the bonding mixture is forced into the annulus and then into the fuel bed, and the excess flows out through slotted end caps. The feasibility of such a technique was demonstrated by preparing 6-in.-long specimens using a bonding matrix of 27 wt % NF 6353 graphite filler in 15V pitch.

By use of the conventional axial intrusion technique for preparing bonded beds, preliminary experiments were conducted to compare the behavior of calcined coke (1300°C) with that of graphitized coke. In these experiments Robinson and No. 2 coke (an anode grade) in 15V pitch were used with and without Thermax additions. The results of these experiments showed that much more calcined filler than graphitized filler could be added to the bonding matrix (47 vs 35 wt %). Filler contents greater than these increased the viscosity of the mixtures to the extent that they could not be intruded into the fuel bed. A similar relationship was observed when 12 wt % Thermax was added to the bonding mixture.

Previous studies have shown that intrusion-bonded specimens carbonized in close-fitting ATJ graphite tubes usually resulted in broken coatings, whereas

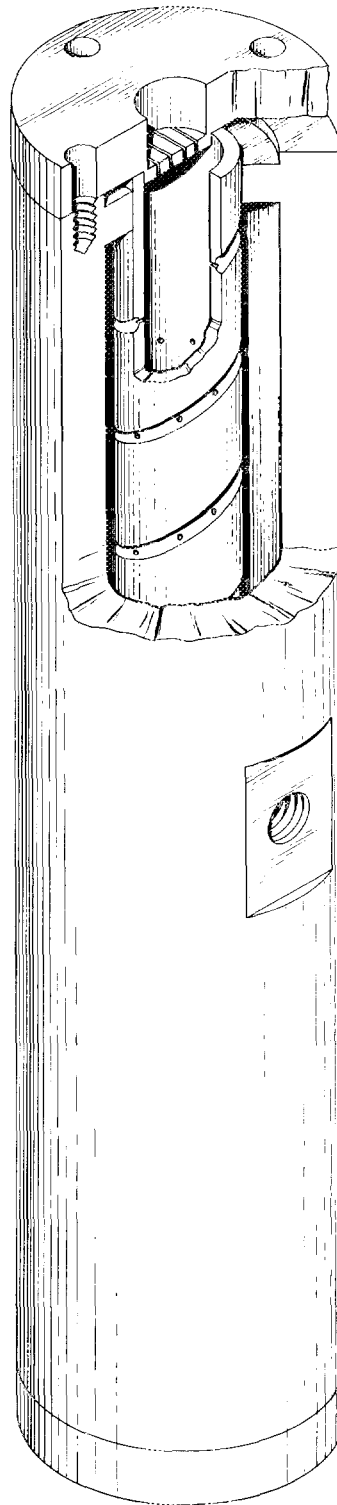


Fig. 8.12. Radial intrusion mold for fuel rod fabrication.

broken coatings were seldom observed in specimens carbonized in a packed bed of graphite or alumina powder.<sup>7</sup> In anticipation of specimen preparation for experiment HT-8, in which particles having different coating characteristics were to be used, additional carbonizing experiments were conducted with specimens in which particles representative of the types to be used were bonded. Carbonization was carried out in both modes. In confirmation of previous results it was shown that carbonizing in closely fitting tubes resulted in broken particles, whereas carbonizing in a packed bed did not. There seemed to be no correlation between broken coatings and crushing strength, density, or thickness of the coatings.

### 8.3.2 Fabrication by Slurry Blending and Warm Molding

It has been calculated that by increasing kernel sizes of fissile and fertile particles to 600  $\mu\text{m}$ , volume loadings could be reduced to as low as 26% and still meet heavy-metal requirements for fuel elements. This would provide for an essentially continuous and a relatively dense matrix for improved strength and thermal conductivity. It could also make feasible the technique for extrusion to obtain long fuel rods. We initiated studies to fabricate such elements by the slurry-blending-warm-molding technique. At the present state of the art, all compounds (pitch, filler, and coated particles) are blended as a slurry in a benzene-acetone mixture. The blend is then dried, granulated, and formed in a steel die at about 150°C and 1000 psi. After cooling and ejection the specimens are carbonized and heat treated in the same manner as those prepared by intrusion bonding.

Filler materials were generally restricted to Poco AXZ, graphitized No. 2 coke, graphitized Robinson Coke, and GLC 1074 (Great Lakes Carbon Corporation) coke. We favor the latter because it is isotropic and readily available at a relatively low cost (~\$2.00/lb) in the ground and purified state. The binders were restricted, for the most part, to thermoplastic types, all of which are readily graphitizable: grade 15V pitch (Allied Chemical Corporation) and grades 170 and 240 pitch (Ashland Oil and Refining Company). Ashland grade 240 was selected as the most suitable on the bases of workability and carbon yield (51 vs 36% for grade

170 and grade 15V). A cursory survey was made of graphitizable thermosetting binders from Quaker Oats Company; these are mixtures of furans and coal tar or petroleum pitches. The major interest in this type of binder is that it can be polymerized during a curing cycle so that the specimen does not deform during subsequent carbonization; this would eliminate the objectionable practice of embedding specimens in graphite or alumina powders, particularly for remote operations which involve handling large volumes of bulk powders (about ten times the specimen volume) that must be brushed from the specimens and discarded after each carbonization. This feature of the binders was demonstrated by warm molding specimens at temperatures ranging from 50 to 150°C and at 1000 psi, subjecting them to a 30-min cure at 80°C, and carbonizing on a graphite block without excessive deformation. Although the matrix densities were moderately high (1.3 g/cm<sup>3</sup>), the specimens had many surface defects such as cracks, large voids, and exposed fuel particles. Obviously, conditions for the use of such binders have not been optimized, and their study was postponed in favor of the thermoplastic binders with which we have had more experience.

Most of the development work in fabricating slurry-blended, warm-molded bonded beds was directed toward the preparation of specimens for planned irradiation tests and for thermal conductivity measurements. The major variables involved were volume loading and matrix composition, in which Ashland grade 240 pitch, GLC 1074 filler, and Thermax were used. The results are summarized below.

For the same volume loading a bonding matrix with 25% pitch resulted in higher densities than one with 30 wt % pitch (1.50 vs 1.46), although surface appearances were not consistently as good. Pitch contents of 35 and 40 wt % resulted in gross distortion of specimens during carbonization. For the same volume loading but with variation of Thermax-content levels (15, 25, and 35%), matrix densities decreased with increasing Thermax content.

The effect of volume loading on matrix densities and diametral linear shrinkage is shown in Table 8.4. The values in the table represent average values for many specimens made with the same bonding matrix and heat treated at 1800°C. The results indicate that volume loadings between about 20 and 40% do not affect matrix density but do result in an increase in shrinkage with decreasing volume loading. However, matrix density starts to decrease when volume loadings significantly exceed 40%, and the specimens become poorer in surface appearance. Our results also indicate that

7. J. M. Robbins and J. H. Coobs, "Development of Bonded Beds of Coated Particles for HTGR Fuel Elements," *GCR-TU Programs Semiannu. Progr. Rep. Sept. 30, 1970*, ORNL-4637, pp. 9-11.

Table 8.4. Effect of volume loading on matrix density and linear shrinkage

Volume loading (%)	Matrix density (g/cm <sup>3</sup> )	Diametral linear shrinkage (%)
21.1	1.46	1.74
30.4	1.45	1.2
41.3	1.46	0.88

within the range of volume loadings noted we can produce sound specimens having matrix densities  $\geq 1.4$  g/cm<sup>3</sup> by using a matrix composition of 30 wt % Ashland 240 pitch, 55 wt % GLC 1074 filler, and 15 wt % Thermax. A comparison of microstructures of specimens formed by intrusion bonding and specimens formed by the slurry-blending–warm-molding technique is shown in Fig. 8.13.

One factor that must be considered in preparing bonded bed specimens by either the intrusion bonding

or the slurry-blending–warm-molding process is the possibility that particle coatings will fail under pressure during fabrication. Specimens with nominal 40 wt % loadings of coated ThO<sub>2</sub> particles were prepared at pressures of 1000 to 4000 psi and submitted for acid leach tests. Calculation of broken particles from the analysis data indicated that from 2 to  $5 \times 10^{-6}$  of the particles had broken coatings when specimens were formed at 1000 and 2000 psi; this value rose by a factor of 20 for specimens formed at 3000 and 4000 psi. These values must be considered relative only, since the validity of these results has been estimated. Further investigation of the acid leach test is continuing. In the meantime, a specimen containing highly enriched uranium was prepared for light irradiation and heating, which is the best technique for indicating broken particles.

Specimens nominally 3 in. long and 0.5 in. in diameter were prepared for electrical resistivity and thermal conductivity measurements as a function of volume loading. Three specimens were of the warm-

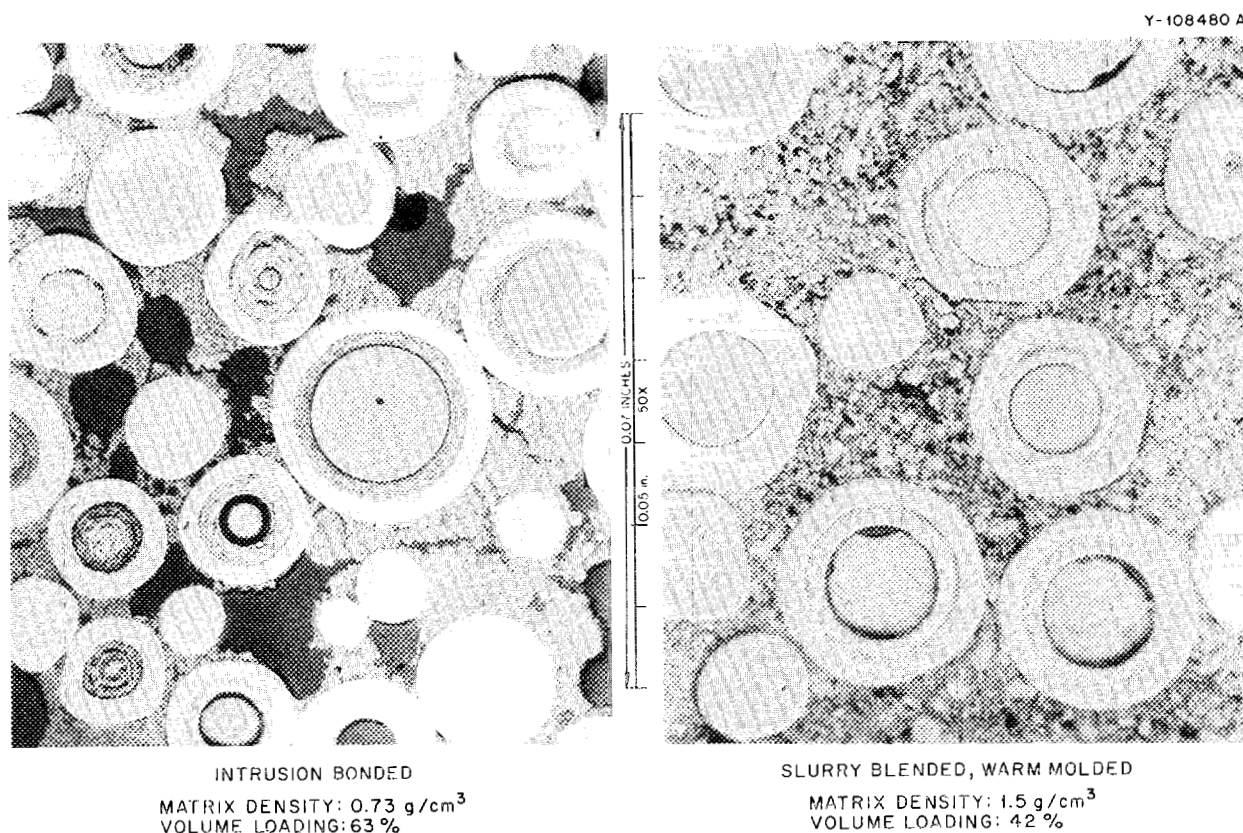


Fig. 8.13. Bonded fuel stick microstructures.

molded type and had volume loadings of 30, 37½, and 44% with matrix densities of 1.45, 1.43, and 1.4 g/cm<sup>3</sup> respectively. One intrusion-bonded specimen was included that had a volume loading of 73% and a matrix density of 0.85 g/cm<sup>3</sup>.

### 8.3.3 Thermal Conductivity and Electrical Resistivity

R. S. Graves    W. M. Ewing  
D. L. McElroy

Thermal conductivity  $\lambda$  and electrical resistivity  $\rho$  measurements were completed in the range 80 to 400°K on two sets of bonded fuel samples (0.5- by 3-in.-long rods): set 1, eight samples, containing 65 wt % inert carbon particles and 35 wt % matrix (Poco graphite and pitch) treated in argon at 1500°C to a bulk density of ~1.29 g/cm<sup>3</sup>; and set 2, three samples, containing 30.4, 37.5, and 43.9 vol % inert carbon particles in a 1.44-g/cm<sup>3</sup> matrix. The  $\lambda$  and  $\rho$  values were determined as a function of temperature in a guarded longitudinal heat flow apparatus<sup>8</sup> that has a most probable accuracy of ±3% for the  $\lambda$  of these samples.

**Set 1 results.** These eight samples showed a 4% variation in  $\rho$  (300°K) about an average value of 7900  $\mu\Omega$ -cm, with individual samples varying by 1%. Table 8.5 lists  $\lambda$  and  $\rho$  values for two specimens and shows  $\lambda$  to increase with temperature. These results suggest that any means to decrease  $\rho$  would lead to an increase in  $\lambda$ .<sup>9</sup>

**Set 2 results.** The  $\lambda$  (300°K) of these three specimens was about 60% of the set 1 values. Measurements on the 37.5 vol % sample were discarded since this sample appeared to contain a major flaw. Table 8.6 lists the  $\lambda$  and  $\rho$  values obtained. These  $\lambda$  values are about 50% greater than recent results,<sup>10</sup> which suggest the  $\lambda$  of HTGR fuels to be independent of temperature from 400 to 1500°K.

8. M. J. Laubitz and D. L. McElroy, *Metrologia* 7, 1-15 (1970).

9. D. L. McElroy et al., *Room Temperature Measurements of Electrical Resistivity and Thermal Conductivity of Various Graphites*, ORNL-TM-3470 (July 1971).

10. R. P. Type and K. Koyama, "The Thermal Conductivity of Some Unirradiated HTGR Fuel Elements Materials," *XI International Thermal Conductivity Conference*, Albuquerque, N.M., Sept. 28-Oct. 1, 1971.

Table 8.5. Thermal conductivity and electrical resistivity of bonded fuel specimens, set 1

Temperature (°K)	Specimen JG 25-1		Specimen JG 25-8	
	Electrical resistivity ( $\mu\Omega$ -cm)	Thermal conductivity (W cm <sup>-1</sup> deg <sup>-1</sup> )	Electrical resistivity ( $\mu\Omega$ -cm)	Thermal conductivity (W cm <sup>-1</sup> deg <sup>-1</sup> )
100	9132	0.0135	8478	0.0141
200	8622	0.0306	7999	0.0334
300	8159	0.0428	7593	0.0465
400	7815	0.0477	7247	0.0544

Table 8.6. Thermal conductivity and electrical resistivity of bonded fuel specimens, set 2

Temperature (°K)	Specimen JH 105-1, 30.4 vol %		Specimen JH 112-1, 43.9 vol %	
	Electrical resistivity ( $\mu\Omega$ -cm)	Thermal conductivity (W cm <sup>-1</sup> deg <sup>-1</sup> )	Electrical resistivity ( $\mu\Omega$ -cm)	Thermal conductivity (W cm <sup>-1</sup> deg <sup>-1</sup> )
100	5537	0.0599	6919	0.0467
200	4953	0.1253	6303	0.0985
300	4779	0.1504	5838	0.1230
400		0.1598	5475	0.1274

## 8.4 FUEL MIGRATION STUDIES

T. B. Lindemer

The irradiation behavior of urania-bearing particles is observed to include the eventual release of fission gas from the particle when a temperature gradient exists across the particle.<sup>11</sup> An empirical correlation for this release is available from the results from the Dragon project. This failure of the coating of the particle is associated with the transport of carbon from the hot to the cold side of the particle and with the movement of the kernel up the temperature gradient.<sup>12</sup> Mechanisms that may produce the transport of carbon have been proposed in the literature,<sup>13</sup> but heretofore no mathematical model has been available to predict the behavior observed in the studies from the Dragon project.

Recently we have developed a model that is based on the transport of carbon by the interdiffusion of CO and CO<sub>2</sub> across the temperature gradient. This model assumes a uniform total pressure of all gases in the particle and local equilibrium in the C-CO-CO<sub>2</sub> system; the latter condition establishes a gradient in the partial pressure of CO and CO<sub>2</sub> and the conditions necessary for transport of carbon. The critical point in the development of the model was the realization that the residual gas from the coating operation and the fission gas affected the gradient in mole fraction of CO or CO<sub>2</sub>, namely,

$$\text{flux} \propto \frac{(P_{\text{CO}_H} - P_{\text{CO}_C})}{P_{\text{CO}} + P_{\text{CO}_2} + P_1 + P_2}, \quad (1)$$

where

$P_{\text{CO}_H}$  = partial pressure of CO at the hot side of the particle,

$P_{\text{CO}_C}$  = partial pressure of CO at the cold side of the particle,

$P_{\text{CO}}$  = average partial pressure of CO,

$P_{\text{CO}_2}$  = average partial pressure of CO<sub>2</sub>,

$P_1$  = partial pressure of the coating gas entrained in the buffer layer,

$P_2$  = partial pressure of the fission product gases.

11. L. W. Graham, "The Development and Performance of HTR Core Materials," pp. 494-517 in *Proceedings of Gas-Cooled Reactor Information Meeting, Oak Ridge National Laboratory, April 27-30, 1970*, CONF-700401.

12. J. A. Conlin et al., *GCR Program Semiannual Progr. Rep. Sept. 30, 1968*, ORNL-4353, p. 28.

13. R. H. Flowers and G. W. Horsley, *The Influence of Oxide Kernels on the Manufacture and Performance of Coated Particle Fuel*, AERE-R5949 (1968).

The expression for the removal of carbon from the hot side of the particle from zero burnup to the final burnup can be shown to be

$$m = \frac{Grt \Delta T (P_{\text{CO}} + P_{\text{CO}_2})'}{F_f - F_i} \times \int_{F_i}^{F_f} \frac{P_{\text{CO}} + P_{\text{CO}_2}}{P_{\text{CO}} + P_{\text{CO}_2} + P_1 + (nRT/a\theta)F} dF, \quad (2)$$

where

$P$  = pressure, atm,

$a$  = ratio, void space in the buffer layer/kernel volume,

$F$  = fissions per initial heavy metal atom (FIMA), %,  $f$  = final,

$G$  = geometrical factor,  $\leq 1.0$ ,

$i$  = initial,

$m$  = thickness of carbon removed,  $\mu\text{m}$ ,

$n$  = moles of fission gas per mole of fuel per % FIMA,

$R$  = 82.06 atm-cm<sup>3</sup> mole<sup>-1</sup> (°C)<sup>-1</sup>,

$r$  = rate of carbon transport via interdiffusion in the CO-CO<sub>2</sub> system,  $\mu\text{m hr}^{-1}$  (°C)<sup>-1</sup> atm<sup>-1</sup>,

$T$  = average temperature, °K,

$t$  = time at temperature,

$\Delta T$  = temperature gradient, °C,

$\theta$  = molar volume of the fuel, cm<sup>3</sup>/mole.

The integral in Eq. (2) results from using the mean value theorem to calculate the average effect of the increasing pressure of fission gas on the interdiffusion of CO and CO<sub>2</sub> during burnup. On integration from  $F_i = 0$  to  $F_f$ , one obtains

$$m = \frac{Grt \Delta T (P_{\text{CO}} + P_{\text{CO}_2})^2}{F_f (nRT/a\theta)} \times \ln \left[ 1 + \frac{(nRT/a\theta)F}{P_{\text{CO}} + P_{\text{CO}_2} + P_1} \right]. \quad (3)$$

The value of  $r$  is shown in Fig. 8.14. These results were calculated with a computer program using data obtained from Mason and Marrero<sup>14</sup> for interdiffusion in

14. E. A. Mason and T. R. Marrero, "The Diffusion of Atoms and Molecules," *Advances in Atomic and Molecular Physics*, vol. 6, pp. 156-232, Academic, New York, 1970.

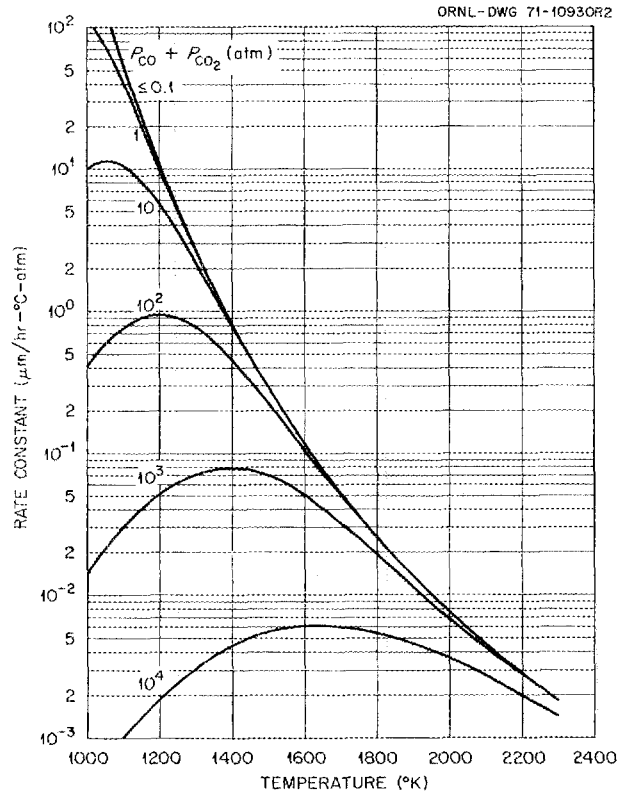


Fig. 8.14. Rate of carbon transport by the interdiffusion of CO and CO<sub>2</sub> in a temperature gradient and at specified total pressures of CO and CO<sub>2</sub>.

a system composed solely of CO and CO<sub>2</sub> and for a diffusion distance of 1000 μm at temperature gradients ranging from 1 to 215°C and at various total pressures of CO plus CO<sub>2</sub>. It should be noted that the results in Fig. 8.14 do not consider the effect of krypton and xenon on the interdiffusion of CO and CO<sub>2</sub>; therefore these values may be about 25% too high. The geometri-

cal factor  $G$  takes into consideration the lowering of the interdiffusion by the presence of a porous medium (e.g., the low-density buffer layer).

The mathematical model of Eq. (3) can be used along with the Dragon project data to show that the calculated thermodynamic behavior is consistent with the probable behavior of the system. The following conditions are assumed for the system:  $P_1 = 1$  atm,  $m = 100$  μm (failure of the coating),  $\Delta T = 100^\circ\text{C}$ ,  $a = 0.25$ , and  $n = 0.004\%$  FIMA. In addition, 0.5 W per particle was assumed for the rating of a particle and 0.001% FIMA/hr was assumed for the burnup rate; all these assumptions are about average for the Dragon project correlation. With these assumptions the results in columns 3 to 5 of Table 8.7 were calculated. These results and a reorganization of Eq. (3) resulted in an expression involving the sum of the pressures of CO and CO<sub>2</sub> as the only unknown; this was solved graphically to give the total pressures shown in Table 8.7. The sum of the pressures of CO and CO<sub>2</sub> for the SiC-SiO<sub>2</sub>-C equilibrium was also calculated and appears in Table 8.7; it can be seen that the pressures of CO and CO<sub>2</sub> in the Dragon particles appear to lie in the range of those for the SiC-SiO<sub>2</sub>-C system. This indicates that the SiC coating chemically buffers the urania kernel during irradiation; any oxygen released from the kernel via fission at a given temperature reacts with the SiC to form SiO<sub>2</sub>, thus fixing the pressure of CO.

## 8.5 DESIGN AND PREPARATION OF IRRADIATION EXPERIMENTS

W. P. Eatherly    R. L. Hamner  
J. H. Coobs        J. M. Robbins  
D. M. Hewette II

The HTGR program at ORNL includes irradiation testing in two types of capsules in the HFIR where the

Table 8.7. Performance and chemical characteristics of the Dragon project oxide kernels

Temperature (°K)	Exposure level <sup>d</sup> (days-W°C)	Days to failure	Percent FIMA	$nRT/a\theta$	$P_{\text{CO}} + P_{\text{CO}_2}$ (atm)			
					$G = 1$	$G = 0.1$	$G = 0.01$	SiO <sub>2</sub> -SiC-C equilibrium
1575	10 <sup>5</sup>	2000	48.	84.1	0.27	0.96	3.0	0.10
1765	10 <sup>4</sup>	200	4.8	94.1	0.72	2.4	8.5	1.29
2015	10 <sup>3</sup>	20	0.48	107.	2.4	9.3	45.0	16.0

<sup>d</sup>From L. W. Graham, "The Development and Performance of HTR Core Materials," pp. 494-517 in *Proceedings of Gas-Cooled Reactor Information Meeting, Oak Ridge National Laboratory, April 27-30, 1970, CONF-700401*.

combined effects of burnup and fast-neutron exposure can be evaluated. The instrumented and swept capsules that are exposed in the removable beryllium (HRB) facility have proved very useful, and a third capsule of this type is being fabricated. The small uninstrumented target (HT) capsules enable us to irradiate small samples of fuel element materials to high fast-neutron exposures representative of large HTGRs in about  $2\frac{1}{2}$  months. A series of experiments in the target capsules is in progress. In addition to the HFIR experiments, specimens for a sweep experiment in the ORR C1 facility and for a joint experiment with GGA in their P13-N capsule were designed and prepared. The preparation and properties of the specimens and the design and objectives of the various experiments are described below.

### 8.5.1 HRB-2 Experiment

The second capsule experiment in the HRB facility contained a column of bonded fuel stick specimens supported in an instrumented graphite sleeve. This sleeve consists of one piece of Poco graphite, whereas the sleeve for the HRB-1 capsule was made of three pieces of H-327 graphite. A set of ten fuel stick specimens made at ORNL all contained three types of coated particles and were bonded with various filler materials in 15V pitch, as tested in experiment HT6. The three types of particles have kernels that are (1) 10.16%-enriched  $UO_2$  in a carbonized resin, (2) sol-gel-derived  $ThO_2$  particles, and (3) inert, carbonized resin particles. These particles are described in Table 8.8.

In addition to the ten fuel stick specimens, six fuel rods prepared at GGA and three magazines containing samples of loose coated particles were included. The six GGA fuel rods include two 2-in.-long rods that contain preproduction Fort St. Vrain fissile and fertile particles and were bonded with the reference matrix material, 27 wt % NF 6353 graphite in 15V pitch. The column of 19 specimens and magazines is described in more detail in Table 8.9.

### 8.5.2 HRB-3 Experiment

A third experiment is being planned for the RB5 reflector position in HFIR. The experiment has four major objectives and one minor, as follows:

1. To test continuous matrix fuel rods made at ORNL at two volume loadings of particles, 33 and 43%. The objective is primarily to correlate dimensional behavior with composition and as a function of fluence.

Table 8.8. Characteristics of Biso-coated particles used in ORNL bonded beds for experiment HRB-2

Particle batch No.	OR-1295	OR-1290	OR-1331
Kernel material	UOS	$ThO_2$	Carbon
Uranium content, wt %	9.81		
$^{235}U$ enrichment, at. %	10.16		
Thorium content, wt %		34.1	
Average particle dimensions, $\mu m$			
Total diameter	462	435	674
Kernel diameter	252	201	437
Outer coating thickness	74	61	76
Total coating thickness	105	117	119
Density of coated particle, <sup>a</sup> $g/cm^3$	1.89	2.48	1.50
Density of outer coating, <sup>b</sup> $g/cm^3$	1.925	1.910	1.87

<sup>a</sup>Measured by mercury pycnometer.

<sup>b</sup>Measured by density gradient column.

Table 8.9. Characteristics of bonded fuel sticks for experiment HRB-2

Specimen designation <sup>a</sup>	Filler material <sup>b</sup>		Length (in.)	Weight (g)	Matrix density ( $g/cm^3$ )
	Type	Amount (wt %)			
JF-275-20	Asbury	35	0.705	2.211	0.76
GA-58-3	NF 6353	27	0.767	2.839	c
GA-52-3	NF 6353	27	0.771	2.958	c
GA-54-1	NF 6353	27	1.947	7.608	c
JF-275-10	Robinson	40	0.715	2.167	0.65
I <sup>d</sup>			0.450	1.457	
GA-57-4	NF 6353	27	0.769	2.829	c
GA-50-3	NF 6353	27	0.770	2.956	c
GA-53-3	NF 6353	27	1.950	7.588	c
III <sup>d</sup>			0.450	1.541	
JF-275-4	Thermax	50	0.710	2.308	0.90
JF-275-12	Robinson	40	0.710	2.113	0.67
JF-275-16	JOZ	40	0.711	2.262	0.83
JF-275-8	Santa Maria	40	0.711	2.208	0.73
JF-275-23	Poco AXZ	35	0.709	2.171	0.67
JF-275-14	JOZ	40	0.711	2.239	0.80
I <sup>d</sup>			0.450	1.537	
JF-275-2	Thermax	50	0.703	2.295	0.92
JF-275-7	Santa Maria	40	0.706	2.198	0.73

<sup>a</sup>In loading order beginning at top of graphite sleeve.

<sup>b</sup>Mixed with 15V pitch as binder material.

<sup>c</sup>Not determined.

<sup>d</sup>Loose particle magazines I, II, and III occupied these positions.

2. To test slug-injected fuel rods to full fluence. These are to be fabricated by ORNL using the technique currently anticipated for use in TURF.
3. To test fuel rods fabricated by GGA as prototype rods for a reference 1100-MW reactor design. These rods will contain oxide fuel kernels.

4. To measure the thermal conductivity of a continuous-matrix fuel rod.
5. To calibrate tungsten/rhenium thermocouples for use at elevated temperatures and determine the effects of radiation damage on their thermoelectric power.

In all, 15 samples will be irradiated, including ten  $\frac{3}{4}$ -in.-long rods of the continuous-matrix type, two 1-in. rods for GGA, and three 2-in. rods of the slug-injected type. All samples will contain Triso-coated fissile and Biso-coated  $\text{ThO}_2$  fertile particles. The capsule is to be irradiated for an anticipated 13 cycles (300 days). This will produce a maximum fluence of  $9 \times 10^{21}$  neutrons/cm<sup>2</sup> ( $E > 0.18$  MeV).

The experiment design is somewhat more complex than previous designs in that it involves obtaining isothermal conditions both along the length of the capsule and with time. The former is achieved by varying the axial fuel loading and gas gap. The latter is obtained by adjusting the  $^{235}\text{U}$ ,  $^{238}\text{U}$ , and thorium ratios to provide constant heat generation rates with burnup. The central fuel rod temperatures are thus designed to operate at a nominal 1200°C. Figure 8.15 shows a schematic configuration of the fuel column, graphite sleeve, and capsule containment.

The required sol-gel oxide fuel particles were manufactured at ORNL and shipped to GGA for coating and preparation of bonded specimens. The resin fissile particles and  $\text{ThO}_2$  particles for the ORNL rods were coated and characterized, and preparation of bonded specimens is in progress.

### 8.5.3 P13-N Experiment

In cooperation with GGA a set of ORNL-fabricated fuel sticks and particles will be irradiated in GGA's P13-N capsule at the Engineering Test Reactor. The purpose of the test is to obtain data on resin-derived fuels and continuous-matrix fuel sticks. The experiment is, therefore, complementary to our HRB-3 capsule for HFIR irradiation. A description of the experiment follows:

Fluence	$4 \times 10^{21}$ neutrons/cm <sup>2</sup> ( $E > 0.18$ MeV)
Stick center-line temperature	1500°C
Stick dimensions	0.735 in. long, 0.490 ± 0.003 in. diam
Fuel particle	Highly enriched U as resin-derived UCS, 400- $\mu\text{m}$ kernel diam, modified Triso coating
Fertile particle	Sol-gel $\text{ThO}_2$ , 400- $\mu\text{m}$ kernel diam, Biso coating
Fuel loading	
Total U, 90.83% enriched	
Position 1D	0.0665 g
Position 3A	0.0522 g
Total Th	
Position 1D	1.3132 g
Position 3A	1.4043 g
Volume loading	
Position 1D	43%
Position 3A	43%

The Triso-coated fueled resin fissile particles and Biso-coated  $\text{ThO}_2$  fertile particles were prepared and characterized. Two slurry-blended, warm-molded fuel stick specimens were fabricated and delivered to GGA

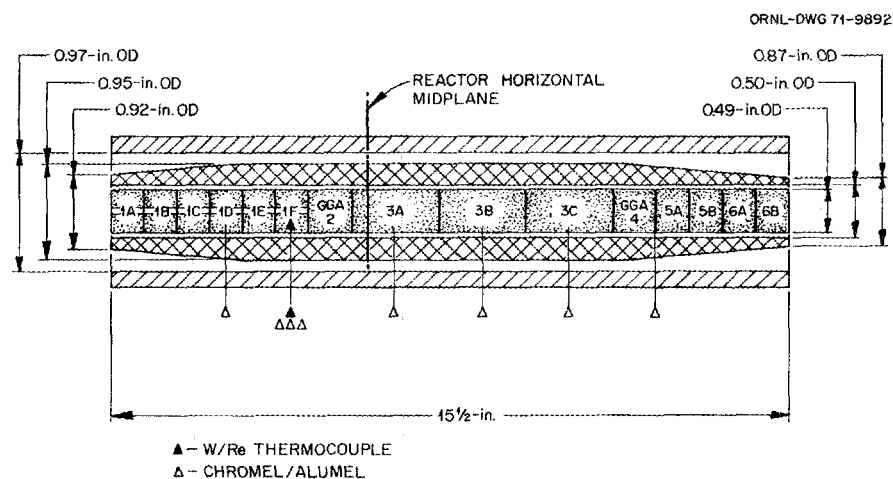


Fig. 8.15. HRB-3 configuration.

along with several spare samples for each experiment position. The specimens were molded at 165°C using 1000 psi pressure and had matrix densities of 1.43 g/cm<sup>3</sup> and particle volume loadings of 42.5% after carbonizing and heat treating to 1800°C.

#### 8.5.4 Sweep Capsule Irradiation in ORR

An experiment designated as C1-28 was designed and built for irradiation in the ORR facility. The objectives of the experiment are (1) to test resin-based fissile particles in intrusion-bonded particle beds under large temperature gradients and at high temperatures and (2) to irradiate at low temperature a selection of coated particles of conventional design [UO<sub>2</sub>, (Th,U)O<sub>2</sub>, and UC<sub>2</sub> kernels] and advanced design (fueled resin kernels) for use in annealing studies on metallic fission product release. The two bonded specimens contain carbonized sulfonic acid resin particles that were loaded with highly enriched fuel and have Biso coatings. One specimen contains kernels that were deoxidized before coating, while the other has particles coated in the as-carbonized condition. The characteristics of the coated particles are given in Table 8.10. Both specimens were bonded with 27 wt % Asbury NF 6353 graphite in 15V pitch, carbonized at 1000°C, and heat treated at

**Table 8.10. Characteristics of coated particles used in bonded beds for experiment ORR C1-28**

Batch No.	OR-1476	OR-1468	OR-1365
Fuel material	UCS	UOS	ThO <sub>2</sub>
Uranium content, wt %	18.4	24.6	
<sup>235</sup> U enrichment, at. %	91.5	91.5	
Thorium content, wt %			60.8
Average particle dimensions, μm			
Core particle	367	481	440
Total particle	551	663	680
Coating characteristics			
Type of coating	Biso	Biso	Biso
Inner coating			
Thickness, μm	25	22	50
Density, <sup>a</sup> g/cm <sup>3</sup>	1.5	1.5	1.2
Outer coating			
Thickness, μm	67	69	120 <sup>b</sup>
Density, <sup>c</sup> g/cm <sup>3</sup>	1.92	1.92	1.85
Density of coated particle, <sup>d</sup> g/cm <sup>3</sup>	1.98	2.09	3.94

<sup>a</sup>Calculated value.

<sup>b</sup>Thickness of total coating.

<sup>c</sup>By density gradient column.

<sup>d</sup>By mercury porosimetry at 15 psi.

**Table 8.11. Characteristics of bonded bed specimens for irradiation experiment ORR C1-28**

Specimen No.	JG-129-1 <sup>a</sup>	JG-129-5 <sup>b</sup>
Fissile kernel	UCS	UOS
Uranium content	0.0830	0.0830
<sup>235</sup> U content, g	0.0759	0.0759
Thorium content, g	1.9898	2.4506
Volume loading, %	60.4	64.0
Matrix density, g/cm <sup>3</sup>	0.69	0.72

<sup>a</sup>Specimen containing three thermocouple holes.

<sup>b</sup>Solid specimen.

1500°C for 30 min. Properties of the two specimens are given in Table 8.11.

A special technique was required to provide the holes in the specimens designed for insertion of thermocouples. A mold was designed that provided for positioning round wooden pegs around which the particles were poured and the bonding mixture intruded. The wooden pegs were left in place to maintain dimensional control during carbonization. Afterward, the carbon residue from the pegs was easily removed. Figure 8.16 shows the two types of carbonized and heat-treated specimens together with the graphite capsule. The specimens were stacked in the large central cavity of the capsule, with the solid specimen placed on the bottom. The smaller, outer holes in the capsule are provided to contain loose coated particles in the small graphite holders shown.

The 22 samples of loose coated particles being irradiated include coated oxide, carbide, and fueled-resin particles. Coatings of these samples consist of low-temperature isotropic (LTI), high-temperature isotropic (HTI), and heat-treated LTI outer coating layers, with and without an intermediate SiC barrier (Triso) coating layer.

#### 8.5.5 Target Capsule Experiments in HFIR

A series of capsules has been designed to study the fast-neutron-induced rheology of LTI pyrolytic carbons deposited over an unyielding substrate. The irradiation effects studied are the coating integrity, densification, and preferred orientation changes for Triso II particle coatings as a function of fluence for irradiation temperatures of 750 to 1100°C. In order to assess the effects of exposure, particles are being irradiated to fluences ranging from 5 to 15 × 10<sup>21</sup> neutrons/cm<sup>2</sup> ( $E > 0.18$  MeV) at 1050°C and to a lower range of fluences at

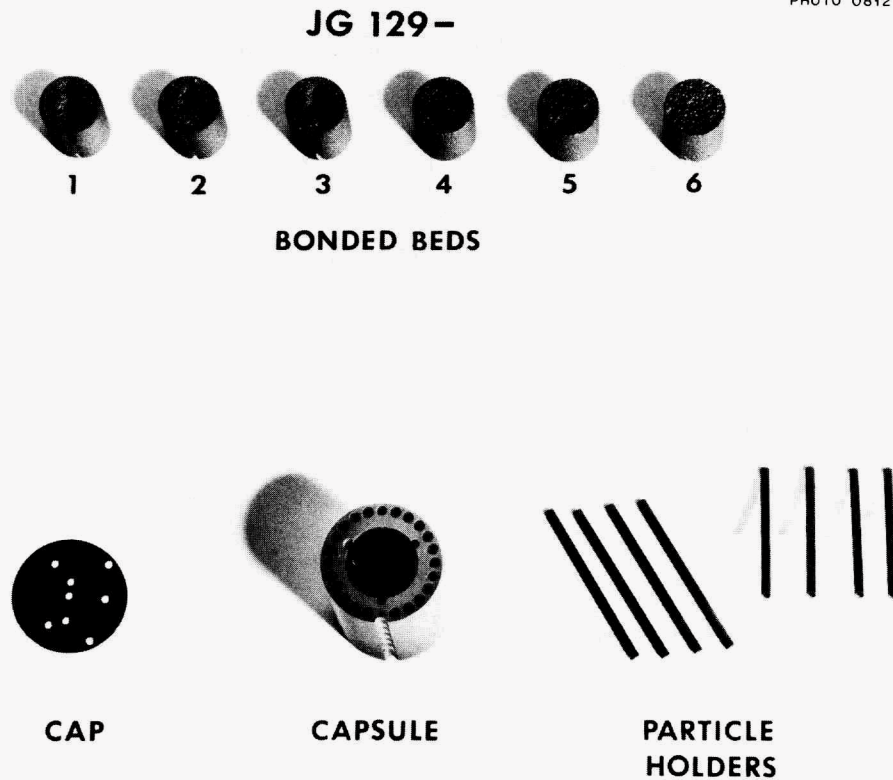


Fig. 8.16. Bonded beds and graphite parts for ORR-C1-28 experiment.

750°C. The information from these tests is needed to provide necessary input to coated-particle mathematical models.

A description of the particles being tested in the above-described series of irradiations is given in Table 8.12. The particles are mockups of Triso II particles. They consist of unfueled carbonized ion exchange resin kernels of 530  $\mu\text{m}$  diameter coated with a 50- $\mu\text{m}$ -thick buffer layer, a 20- $\mu\text{m}$ -thick precoat, either 10- or 20- $\mu\text{m}$ -thick SiC, and a 50- $\mu\text{m}$ -thick outer coating. The densities of the propylene-derived precoat and outer LTI coatings were varied from 1.7 to 2.0  $\text{g}/\text{cm}^3$ , and samples are being tested in the as-deposited and annealed conditions. The principal variables, therefore, are the density of the outer LTI coating and the effects of heat treatment on coating behavior; coating design (types B and C of Table 8.12) is a secondary variable.

The densities of the SiC layers were between 2.7 and 2.94  $\text{g}/\text{cm}^3$ , which is considerably lower than the intended 3.18  $\text{g}/\text{cm}^3$ . We feel that since the kernels are unfueled, this lower SiC density, which usually reflects a lower strength, will not be of consequence to this test since the SiC is always in compression. The optical

anisotropy factors (OPTAFs) given in Table 8.12 were determined by GGA. The OPTAFs for the as-deposited coatings are all quite low, but heat treatment increased all the values somewhat, indicating that some crystallite rearrangement accompanied the densification that occurred during heating at 1800°C.

The first set of these types of particles were irradiated at two temperatures in capsule HT-7. The loose particle samples are contained in small graphite bottles that are supported within graphite magazines. The graphite holders are centered in the bore of the capsule, which is filled with argon gas at 1 atm. Irradiation temperatures are set by the dimensions of the gas gap between graphite magazine and capsule wall. The HT-7 capsule was irradiated for four HFIR cycles to a maximum fluence of  $9.6 \times 10^{21}$  neutrons/ $\text{cm}^2$  ( $E > 0.18$  MeV). It was followed by an identical loading in capsule HT-9, which was irradiated for two cycles. At the present time, portions of each of the samples from HT-9 are being irradiated in capsule HT-10 for an additional four cycles to obtain a total exposure of  $\sim 15 \times 10^{21}$  neutrons/ $\text{cm}^2$ . During this time a set of intrusion-bonded specimens containing these same particles was

Table 8.12. Description of particles tested in capsule HT-7

Kernel: material, carbonized ion exchange resin; diameter, 530  $\mu\text{m}$ ; density, 1.3  $\text{g}/\text{cm}^3$

Buffer layer: thickness, 48  $\mu\text{m}$ ; density, 0.95  $\text{g}/\text{cm}^3$ ; deposited from acetylene gas

Seal coat: thickness, 3  $\mu\text{m}$ ; deposited from propylene gas

Type	Precoat <sup>a</sup>		Silicon carbide <sup>b</sup>		Outer coat <sup>a</sup>		OPTAF <sup>c</sup> outer layer
	Thickness ( $\mu\text{m}$ )	Density ( $\text{g}/\text{cm}^3$ )	Thickness ( $\mu\text{m}$ )	Density ( $\text{g}/\text{cm}^3$ )	Thickness ( $\mu\text{m}$ )	Density ( $\text{g}/\text{cm}^3$ )	
A	28	1.76	21	2.95	64	1.68	1.06
A' <sup>d</sup>						1.70	1.11
B	19	1.65	13	<i>e</i>	64	1.73	1.10
B'						1.74	1.13
C <sup>f</sup>	24	1.85	23	2.97	57	1.87	1.09
C' <sup>f</sup>						1.90	1.16
D	21	1.85	21	2.79	51	1.78	1.13
D'						1.80	1.21
E	24	1.99	22	2.93	47	1.97	1.11
E'						2.04	1.22
F	23	1.95	10	2.74	42	1.96	1.05
F'						1.99	1.17

<sup>a</sup>Deposited from propylene gas.

<sup>b</sup>Deposited from methyltrichlorosilane.

<sup>c</sup>Determined at GGA.

<sup>d</sup>The primed types are particles of unprimed designation that were heat treated at 1800°C.

<sup>e</sup>Not determined.

<sup>f</sup>For the C and C' types a buffer layer 10  $\mu\text{m}$  thick was deposited over the SiC layer.

prepared and irradiated in capsule HT-8. This test was designed to study the irradiation-induced interactions of these particle coatings with the reference matrix consisting of 27 wt % ND 6353 graphite filler in 15V pitch. Additional descriptive material on HT-8 and the results from examinations of HT-7 and HT-9 are given in Sect. 8.6.

## 8.6 EXAMINATION AND EVALUATION OF IRRADIATION EXPERIMENTS

J. L. Scott      J. M. Robbins  
J. H. Coobs      R. B. Fitts  
R. L. Hammer    D. M. Hewette II

We completed the examination and evaluation of two HFIR capsule experiments and are presently examining specimens from four other experiments. The results

from testing fuel stick matrix materials and fabrication techniques that culminated in the HT-6 target experiment are summarized, as are the final results from metallographic examination of the first HFIR sweep capsule, HRB-1. Examinations of the second sweep capsule in HFIR, HRB-2, and of three target capsules, HT-7, -8, and -9, are in progress.

### 8.6.1 Development of Bonding Materials for HTGR Fuel Elements<sup>1 5</sup>

The coated-particle fuels used for advanced high-temperature gas-cooled reactors (HTGRs) are bonded into fuel sticks or fuel rods before being inserted into

<sup>1 5</sup> Summary published in *Trans. Amer. Nucl. Soc.* **14**, 566 (1971).

the hexagonal graphite fuel blocks. The bonded sticks can be inspected for integrity and fuel distribution, and the matrix enhances bed conductivity and would inhibit spilling of fuel in the event of damage to a fuel block.

At ORNL we have carried out an extensive program to develop methods of bonding particles that would satisfy these objectives. The program involved fabrication studies, irradiation tests, and extensive postirradiation examinations. The fabrication method selected consists in vibrating loose particles into a die or mold, injecting a carbonaceous grease through the bed of particles, and finally curing and carbonizing the bonded fuel stick. When two early tests of fuel sticks bonded with a phenolic resin containing 15 to 25 wt % of flake graphite filler revealed poor stability and coating fracture under irradiation, we concentrated on improving the matrix density and filler content of injection-bonded beds. By adding large amounts of stable filler material (<40- $\mu\text{m}$ -diam Poco graphite flour or Thermax carbon black) to pitch or furfuryl alcohol, we made bonded specimens that had matrix densities as high as 1.25 g/cm<sup>3</sup>. A test in HFIR of coated inert particles bonded with these materials was the first demonstration that such bonded beds could survive full HTGR fast-neutron fluences.<sup>16,17</sup>

16. J. L. Scott et al., "Development of Bonded Beds of Coated Particles for HTGR Fuel Elements," *Trans. Amer. Nucl. Soc.* 13, 134 (1970).

17. J. L. Scott et al., "Development of Bonded Beds of Coated Particles for HTGR Fuel Elements," pp. 456-73 in *Proceedings of Gas-Cooled Reactor Information Meeting, Oak Ridge National Laboratory, April 27-30, 1970, CONF-700401*.

Since the isotropic filler material (Poco graphite powder) used in the successfully irradiated specimens is a rather expensive specialty material, fabrication experiments were conducted on bonding of fuel sticks with matrices consisting of Poco grades and a variety of more readily available and inexpensive filler materials in 15V pitch. These are described in Table 8.13. Workable mixtures containing these filler materials in amounts ranging from 27 to 50 wt % in pitch produced matrix densities from 0.64 to 0.90 g/cm<sup>3</sup>. Bonded specimens prepared with these experimental matrices showed some large pores but generally strong dense matrices. Coated fissile and inert particles bonded with this series of experimental matrices were exposed to fast-neutron fluences up to  $7.2 \times 10^{21}$  neutrons/cm<sup>2</sup> at 1070 and 800°C. All bonded specimens were intact and shrank as much as 6% in linear dimensions. The shrinkage was greater at the higher exposures and temperature and was generally controlled by the densification of the carbon coatings on the two kinds of particles. This behavior was expected because of the particle-to-particle contact in the bed and the higher shrinkage rate of the bonding matrix in a neutron flux.

Metallographic examination of these bonded fuel sticks indicated that all particle coatings were intact and that the matrix structure was not seriously affected. These results indicate that successful performance of bonded fuel sticks to full HTGR fast-neutron fluences ( $>7 \times 10^{21}$  neutrons/cm<sup>2</sup>) can be achieved by injection bonding with pitch containing a wide variety of carbonaceous filler materials.

Table 8.13. Experimental filler materials for bonded beds

Filler	Description	Filler content <sup>a</sup> (wt %)	Maximum particle size ( $\mu\text{m}$ )	Matrix density (g/cm <sup>3</sup> )
Thermax	Soft, spherical carbon black	50	<1	0.90
Poco AXZ	Isotropic graphite	35	40	0.65
Poco FXA	Experimental Poco graphite powder	40	40	0.70
JOZ	Needle coke graphite	35	40	0.67
H378	Reimpregnated JOZ graphite	35	27	0.70
Asbury 6353	Natural flake graphite <sup>b</sup>	27	40	0.64
Santa Maria	Graphitized isotropic coke	40	40	0.73
Robinson	Graphitized airblown coke	40	27	0.72

<sup>a</sup>15V pitch binder.

<sup>b</sup>Reference filler for core A of the Fort St. Vrain reactor.

### 8.6.2 HRB-1 Experiment

During metallographic examination of HRB-1 specimens we observed some unilateral migration (amoeba effect) of Triso-coated  $\text{UO}_2$  particles in one specimen. This specimen, which occupied position 4B in the experiment,<sup>18</sup> contained 7%-enriched  $\text{UO}_2$  and  $\text{ThO}_2$  particles, both with Triso coatings, and Biso-coated inert particles. The specimen was bonded with a matrix of 15 wt % flake graphite in phenolic resin.<sup>19</sup> A companion specimen, 5A, which contained coated  $(\text{Th,U})\text{O}_2$  and  $\text{ThO}_2$  fuel, did not exhibit fuel migration, but it was bonded with a more dense matrix consisting of 40 wt % Poco graphite flour in Varcum. Furthermore, specimen 5A was intact, while specimen

4B had debonded badly, indicating that temperatures may have been quite high due to poor conductivity of the debonded structure. Therefore, another companion specimen, 4A, was selected for examination because it contained the same fuel particles as specimen 5A but was bonded with the same matrix composition as 4B and suffered the same sort of debonding during irradiation. Calculations based on the thermal conductivity of a loose bed of particles [ $\sim 1.5 \text{ Btu hr}^{-1} \text{ ft}^{-1} (\text{°F})^{-1}$ ] indicated that central temperatures in these two specimens, 4A and 4B, may have been as high as  $1400^\circ\text{C}$ .

Examination of the polished section of specimen 4A did not reveal any evidence of fuel movement in the coated  $(\text{Th,U})\text{O}_2$  particles ( $\text{Th/U}$  ratio = 3.6). Void formation and swelling of the fuel kernels was normal for the 14% burnup experienced. This swelling caused some compression of the inner buffer coating, but all fuel kernels were well centered within their coatings, as illustrated by the particle shown in Fig. 8.17. Fracture

18. "Metallographic Examination of HRB-1," *GCR Program Semiannu. Progr. Rep. Sept. 30, 1970*, ORNL-4637, pp. 17-21.

19. "HRB-1 Capsule Irradiation," *GCR Program Semiannu. Progr. Rep. Mar. 31, 1970*, ORNL-4589, pp. 27-36.

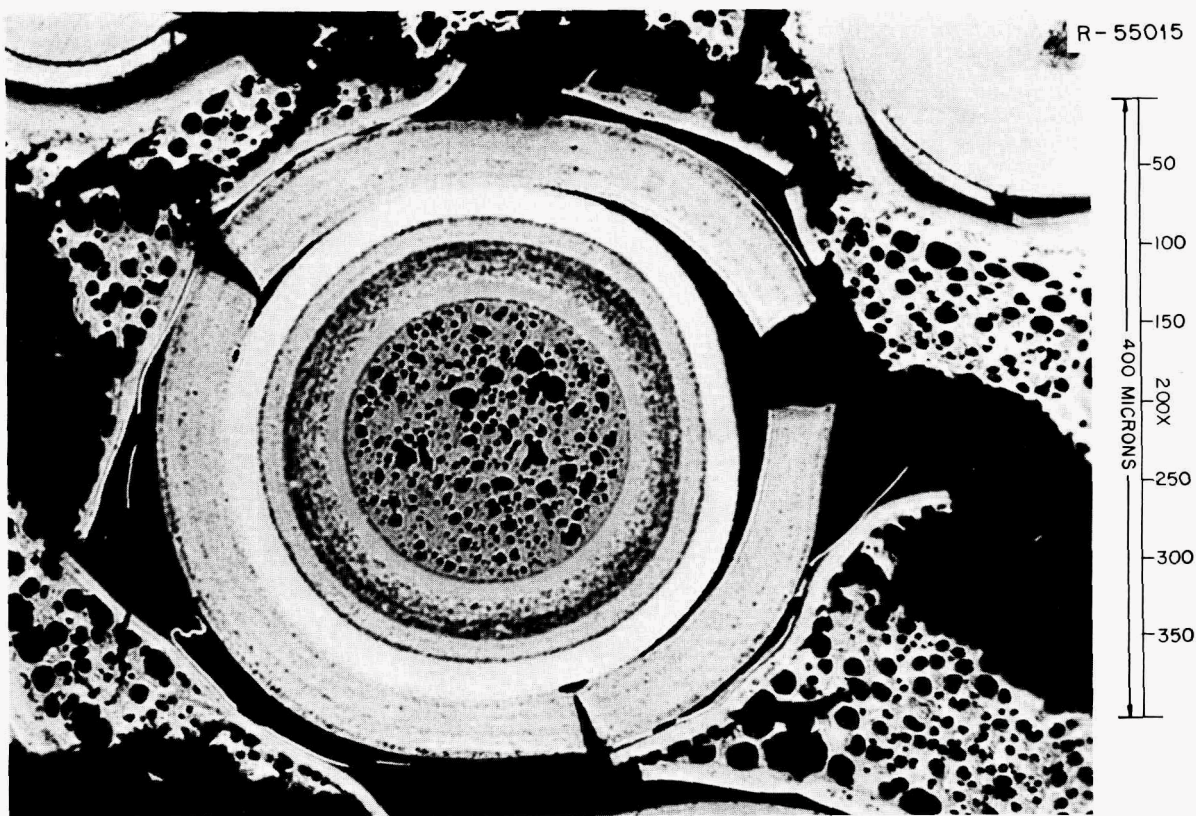


Fig. 8.17. Polished section of a Triso-coated  $(\text{Th,U})\text{O}_2$  particle irradiated to 14 at. % burnup and a fast fluence of  $5.3 \times 10^{21}$  neutrons/cm<sup>2</sup> ( $E > 0.18 \text{ MeV}$ ). Note the lack of any fuel movement. As polished. 200 $\times$ .

and deformation of the outer coating layer was observed in other specimens and was anticipated in these particles. The lack of fuel migration can be interpreted as evidence that mixed oxides and  $\text{ThO}_2$  are more stable at high heat ratings than  $\text{UO}_2$  or carbide particulate fuels.

### 8.6.3 HRB-2 Examination

The graphite sleeve holding the column of fuel stick specimens was removed intact from the assembly by cutting off the ends of the capsule and slitting the inner and outer containment. Two of the bonded fuel sticks (JF 275-20 and GA 58-3) dropped out of the top of the sleeve during disassembly. These were recovered, identified, and observed to be in good condition. All other specimens were forced out through the bottom of the graphite sleeve by tapping the sleeve against a metal pan and by bouncing the sleeve on blotter paper on the cell floor. A considerable period of tapping and bouncing was required in order to move the two 2-in.-long specimens. These specimens came out in three segments plus a small amount of loose material, while all other specimens were intact and in good condition. Some of the shorter specimens exhibited varying degrees of debonding at the edges; this was especially true of one ORNL specimen and three GGA specimens. In Fig. 8.18 the appearance of two ORNL fuel sticks bonded with pitch containing 50 wt % Thermax is shown before and after irradiation. Note that specimen 4, which received higher exposure, looks completely unaffected; this is perhaps due to its excellent condition before irradiation. Specimen 2, on the other hand, shows some evidence of debonding at the edges before irradiation.

The surface condition of the GGA fuel rod specimens after irradiation was good, even though the long specimens broke into three pieces and the shorter specimens exhibited some debonding. The surface appearance is illustrated in Fig. 8.19, which shows the middle segment of one long fuel rod (50-3) and a short fuel stick (53-3). The weight losses of the short (0.7-in.-long) specimens ranged from negligible (0.1%) in the case of fuel stick 275-4 up to 48 mg (1.75%) for GGA specimens 50-3 and 57-4. The weight losses could be correlated somewhat with preirradiation condition, in that specimens with well-bonded edges and square ends were relatively unaffected.

Dimensional changes were recorded on all specimens before further examination. The diametral shrinkages of the various specimens are given in Fig. 8.20 as a function of calculated exposure. The ten specimens that contained Biso-coated particles shrank as much as 4.5%,

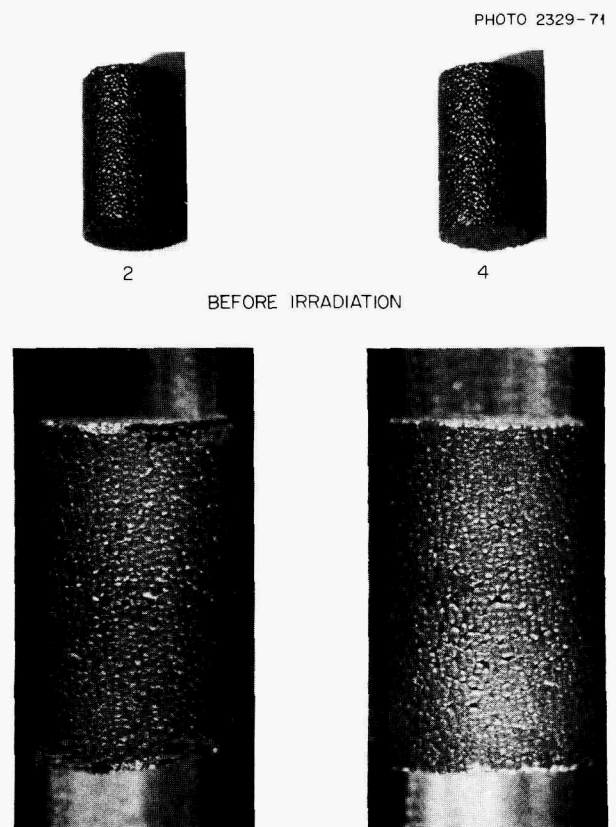


Fig. 8.18. Fuel sticks bonded with 50 wt % Thermax in pitch.

while the GGA specimens that contained only Triso-coated particles shrank only 1.0 to 1.6%. These dimensional changes are consistent with prior experiments on Triso-coated specimens and with the predicted shrinkage by densification of Biso coatings.

Visual examination of the bonded specimens and debonded material did not reveal any evidence of broken particles. Unloading of loose particle specimens from the three magazines and metallographic examination of selected specimens are proceeding.

### 8.6.4 Postirradiation Examination of Capsule HT-8

The HT-8 capsule was irradiated in the HFIR target facility for four cycles ending August 18, 1971, and is now undergoing postirradiation examination. The capsule contained samples of loose coated particles and bonded fuel sticks produced at GGA and ORNL. Duplicate samples were irradiated at 750 and 1050°C. The peak fast ( $E > 0.18$  MeV) fluence exposure was  $9.6 \times 10^{21}$  neutrons/cm<sup>2</sup>. The fuel burnup was about 9.2%

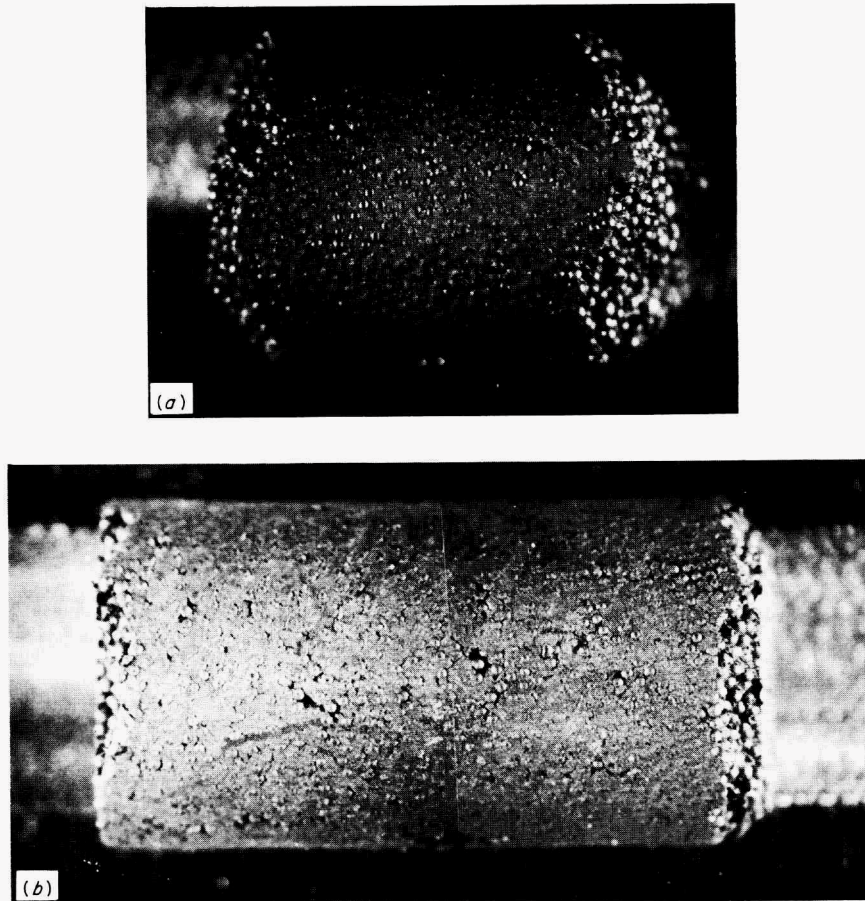


Fig. 8.19. View of two fuel stick specimens containing Triso-coated particles. (a) Middle segment of GGA specimen 53-3; (b) GGA specimen 50-3. Note good appearance of outer surface and good condition of particles exposed at debonded edges. 6X.

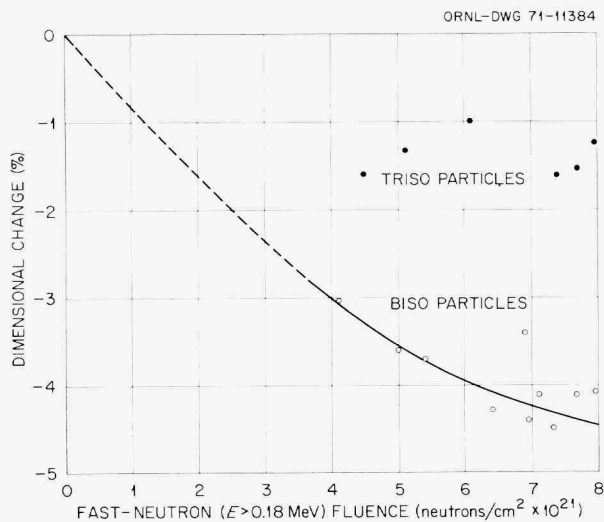


Fig. 8.20. Shrinkage of fuel sticks in HRB-2 experiment.

FIMA in the thorium-bearing samples from GGA and 19.6% FIMA in the uranium-bearing loose particle samples from ORNL. The bonded fuel sticks contained inert, coated carbon particles and therefore underwent no fuel burnup.

The GGA loose particle samples were Biso- and Triso-coated  $\text{ThC}_2$  and  $\text{ThO}_2$  fuels. These were tested for fuel performance evaluation and are being returned to GGA for detailed examination.

The ORNL loose particle samples were Biso-, Triso-, and monolayer-coated uranium-loaded strong- and weak-acid resin fuels. These samples are listed in Table 8.14. The Triso-coated strong-acid resin particles will be examined to determine their stability under irradiation and the effect of a small zirconium addition on the release of cesium during postirradiation annealing experiments. The Biso-coated strong-acid resin particles will be examined for the effect of oxygen level on fuel

Table 8.14. ORNL loose particle samples in capsule HT-8

Particle batch	Test sample	Calculated test temperature (°C)	Kernel				Coating						
			Type	Size (μm)	Uranium (wt %)	Oxygen (wt %)	Inner PyC		SiC		Outer PyC		
							Type	Thickness (μm)	Density (g/cm <sup>3</sup> )	Thickness (μm)	Density (g/cm <sup>3</sup> )	Thickness (μm)	Density (g/cm <sup>3</sup> )
1522	M-1-5 M-2-5	750 1050	Strong <sup>a</sup>	400	45	4	Triso	20	1.5	20	3.18	10 52	1.5 <sup>b</sup> 1.95
1489	CP-29-1 CP-31-1	750 1050	Strong <sup>a</sup>	360	48	4	Triso	20	1.5	24	3.18	48	1.95
1487	CP-29-2 CP-31-2	750 1050	Strong <sup>a</sup>	500	50	7-8	Biso	26.5	1.5			70	1.95
1440	CP-30-1 CP-32-1	1050 750	Strong <sup>a</sup>	400	50	0.5	Biso	22	1.0			64	1.90
1401	CP-30-2 CP-32-2	1050 750	Weak <sup>c</sup>	300	70	0.5	Monolayer					74	1.94
1442	M-1-6 M-2-6	750 1050	Weak <sup>c</sup>	350	70	7-8	Monolayer					60	1.95

<sup>a</sup>Strong-acid ion exchange resin Dowex 50W-X8 loaded with uranium. Batch 1522 also contains 0.5 wt % Zr.

<sup>b</sup>Duplex outer coating with lower-density inner portion.

<sup>c</sup>Weak-acid ion exchange resin IRL-50 loaded with uranium.

Table 8.15. Coated-particle description for HT-8 bonded stick samples<sup>a</sup>

Stick type	Inner isotropic PyC coat <sup>b</sup>		Silicon carbide coat <sup>c</sup>		Outer buffer PyC coat <sup>d</sup>		Outer isotropic PyC coat <sup>b</sup>			Particle	
	Thickness (μm)	Density (g/cm <sup>3</sup> )	Thickness (μm)	Density (g/cm <sup>3</sup> )	Thickness (μm)	Density (g/cm <sup>3</sup> )	Thickness (μm)	Density (g/cm <sup>3</sup> )	OPTAF	Type	Batch No.
1	28	1.76	21	2.95			64	1.68	1.06	A	OR-1410
2	<i>e</i>	<i>e</i>	<i>e</i>	<i>e</i>			<i>e</i>	1.70	1.11	A <sup>f</sup>	OR-1410 HT
3	24	1.85	23	2.97	10	0.95	57	1.87	1.09	C	OR-1412
4,8	21	1.85	21	2.79			51	1.78	1.13	D	OR-1414
5	<i>e</i>	<i>e</i>	<i>e</i>	<i>e</i>			<i>e</i>	1.80	1.21	D <sup>f</sup>	OR-1414 HT
6	24	1.99	22	2.93			47	1.97	1.11	E	OR-1409
7	<i>e</i>	<i>e</i>	<i>e</i>	<i>e</i>			<i>e</i>	2.04	1.22	E <sup>f</sup>	OR-1409 HT

<sup>a</sup>All made from natural flake graphite in 15V pitch as binder. All particles based on 530-μm, 1.3-g/cm<sup>3</sup> carbonized ion exchange resin overlaid with 48 μm of 0.95-g/cm<sup>3</sup> buffer coat and a 3-μ sealer coat deposited from acetylene and propylene gas respectively.

<sup>b</sup>Deposited from propylene gas.

<sup>c</sup>Deposited from methyltrichlorosilane gas.

<sup>d</sup>Deposited from acetylene gas.

<sup>e</sup>Not measured but essentially identical to companion un-heat-treated batch.

<sup>f</sup>Particles heat treated at 1800°C (see Table 8.12).

particle performance. The monolayer-coated weak-acid resin particles will be compared with the strong-acid type for irradiation stability and oxygen effects.

Eight different types of ORNL bonded fuel sticks were tested in this capsule; one sample of each was exposed at 750°C and one at 1050°C. The fast fluence exposures ranged from 4.1 to 8.25 × 10<sup>21</sup> neutrons/cm<sup>2</sup> at 750°C and from 7.7 to 9.6 × 10<sup>21</sup> neutrons/cm<sup>2</sup> at 1050°C. The principal material variables were the particle coating types. The binder matrix in each was composed of 27 wt % natural flake graphite, grade NF 6353, in 15V pitch. Seven of the stick types were formed by the standard intrusion process and one by slug injection. In the set of seven intrusion-bonded sticks, each type contained Triso-coated carbon kernels with varying coating layers. In Table 8.15 the eight fuel stick types are listed along with the description of their related particles. The fuel sticks will be examined physically for overall integrity and dimensional stability and metallographically for particle coating integrity and matrix microstructure.

In addition to the ORNL fuel sticks, four bonded rods prepared by GGA were tested in the experiment. These are also being returned to GGA for detailed evaluation.

### 8.6.5 Target Capsules HT-7 and HT-9

The magazines containing the graphite bottles were recovered after disassembly, and all samples (loose particles) from capsules HT-7 and HT-9 were unloaded, visually inspected, and radiographed. In the HT-9 test there were no particle failures of any of the sample types at either irradiation temperature. A complete description of the irradiation conditions is given in Table 8.16. As mentioned before, the peak fluence in the HT-9 test at the higher nominal design temperature of 1050°C is about 5 × 10<sup>21</sup> neutrons/cm<sup>2</sup> ( $E > 0.18$  MeV), while the fluence at the lower nominal design temperature would be less than 4 × 10<sup>21</sup> neutrons/cm<sup>2</sup>. About 50 particles from each of the HT-9 samples were taken for density and metallographic evaluations, and roughly 200 particles of each sample were reloaded into the HT-10 test.

In the HT-7 test, no particle failures were observed in the samples irradiated at the nominal design temperature of 750°C and fluences of about 5 × 10<sup>21</sup>. For the samples irradiated at 1050°C to a fluence of about 10<sup>22</sup> neutrons/cm<sup>2</sup>, a few failed particles were found. For the sample type A, which had an outer pyrolytic carbon coating of lowest density, about 1.7 g/cm<sup>3</sup>,

Table 8.16. Irradiation conditions for tests HT-7 and HT-9

Position	Sample type	Design irradiation temperature <sup>a</sup> (°C)	Fluence, $F$ (>0.18 MeV ( $10^{21}$ neutrons/cm <sup>2</sup> ))	
			HT-9	HT-7
1A	A	750	3.65	7.3
1B	B	750	3.75	7.5
2A	C	750	3.85	7.7
2B	D	750	3.9	7.8
3A	E	750	4.1	8.2
3B	F	750	4.2	8.4
4A	A	1050	4.6	9.2
4B	B	1050	4.65	9.3
5A	C	1050	4.7	9.4
5B	D	1050	4.75	9.5
6A	E	1050	4.77	9.54
6B	F	1050	4.8	9.6
7A	F'	1050	4.8	9.6
7B	E'	1050	4.77	9.54
8A	D'	1050	4.75	9.5
8B	C'	1050	4.7	9.4
9A	B'	1050	4.65	9.3
9B	A'	1050	4.6	9.2
10A	F'	750	4.2	8.4
10B	E'	750	4.1	8.2
11A	D'	750	3.9	7.8
11B	C'	750	3.85	7.7
12A	B'	750	3.75	7.5
12B	A'	750	3.6	7.3

<sup>a</sup>Initial condition; the maximum temperatures are about 100° higher.

about 96% of the particles survived with intact coatings. In examining sample type B, which had the same coating density but a 10- $\mu$ m-thick SiC layer, ten failed particles were found, which means that about 96% of these particles also survived. Examination of the heat-treated counterparts of the above samples, types A' and B', showed that essentially all the particles survived. This indicates that although heat treatment did not significantly increase their densities, it did enhance the irradiation stability of these coatings in spite of increases in the preferred orientation (OPTAF values).

The densification of sample types C and C' was determined after irradiation in HT-9. These samples had a 10- $\mu$ m-thick buffer layer that was deposited over the SiC coating before depositing the outer coating. This outer buffer layer facilitated removal of the outer layer. Removal of the outer layers from other samples by a simple cracking process has proved difficult. Trouble was encountered even with sample type C, irradiated in the high-temperature position, in spite of its outer buffer over the SiC. The densification results are presented in Table 8.17. Although the heat treatment increased the as-deposited densities slightly, from 1.86 to 1.90 g/cm<sup>3</sup>, the final densities for both types were essentially about 1.95 g/cm<sup>3</sup> at the low irradiation temperature and about 2.03 g/cm<sup>3</sup> at the high temperature. Therefore annealing the coatings does provide marginal benefit, since the fractional densification was slightly less for the annealed types.

Table 8.17. Densification of pyrolytic carbon outer layers from sample types C and C'

Sample type	$\rho_0$ (g/cm <sup>3</sup> )	$\rho_f$ (g/cm <sup>3</sup> )	
		750°C, $3.9 \times 10^{21}$ neutrons/cm <sup>2</sup>	1050°C, $4.7 \times 10^{21}$ neutrons/cm <sup>2</sup>
C,	1.87	1.94	2.03
C'	1.90	1.95	2.02

## 9. Irradiation Experiments

J. A. Conlin

---

The HTGR irradiation program at ORNL includes irradiation of capsules in the HFIR and in the ORR. The HFIR irradiations include two types of capsule in which the combined effects of burnup and high fast-neutron exposure representative of typical end-of-core-life conditions in an HTGR can be attained. One type of capsule, the target or HT capsule, is a small uninstrumented device designed to fit into one of the target positions in the HFIR. These capsules contain small specimens of HTGR fuels and fuel element materials in the form of loose particles, bonded fuel sticks containing coated particles, blended coated-particle beds, pyrolytic-carbon disk specimens, and graphite specimens. The specimens can be irradiated at temperatures up to 1100°C and to representative HTGR end-of-fuel-life fast-flux exposure in about 2½ months. The HT capsules have the advantage of low cost and short irradiation time to attain representative exposure, but they have certain limitations. Only small specimens with very small amounts of fissionable material can be accommodated. Since the capsules are uninstrumented, temperatures are not monitored during irradiation and can only be deduced by postirradiation analysis of silicon carbide monitors. The capsules are sealed, and no gas sweep is possible. Therefore the composition of the atmosphere is somewhat uncertain, and fission-gas release cannot be measured during irradiation.

The second type of HFIR capsule is irradiated in the removable beryllium (HRB) facility. These devices are large (1.3-in.-OD) instrumented gas-swept capsules with provision for specimen temperature control and fission-

gas release measurement. The capsules accommodate fuel specimens in a graphite support sleeve that is geometrically representative of a single fuel channel of a Fort St. Vrain type HTGR fuel element. Fuel loading, temperature, power density, and burnup rate are limited only by the capability of the fuel.

The ORR capsules are small instrumented devices which fit in an air-cooled facility tube in the C-1 core lattice position of the ORR. These capsules provide the capability for testing at temperatures of 1500°C or higher and to heavy-metal burnup, depending on the fuel composition, of more than 50%. The maximum thermal flux, which is about  $10^{14}$  neutrons  $\text{cm}^{-2}$   $\text{sec}^{-1}$ , and the fact that the capsules can be positioned vertically to control the flux permit the use of highly enriched fuel and the achievement of high burnup without the loss of temperature and/or power with time and burnup. Also, the capsule is swept with high-purity gas with a means for sampling the effluent for fission-gas release measurements.

### 9.1 HFIR IRRADIATIONS

B. H. Montgomery

#### 9.1.1 Removable Beryllium Facility Irradiation Tests

**Capsule HRB-2.** The second instrumented irradiation test of bonded HTGR coated-particle fuels in the HFIR removable beryllium facility was completed on September 14, 1971, after 256 days at 100 MW reactor power. The design of this capsule, designated HRB-2, was the

same as that of the first capsule, HRB-1 (refs. 1 and 2), with exception of the test fuel and the graphite fuel support sleeve.

The capsule, shown in Fig. 9.1, was a double-walled water-cooled stainless steel vessel 1.292 in. in outside diameter and 0.967 in. in inside diameter. The test fuel specimens consisted of a series of 0.412-in.-diam bonded fuel sticks having a total stack length of 14 in. The specimens were supported in a one-piece sleeve made of Poco graphite,<sup>3</sup> grade AXF-5Q. Design test conditions (1180°C peak fuel temperature and 940°C in the graphite wall at 3.3 kW/ft fission heat rate) were intended to match conditions typical of an HTGR.

Fuel temperatures were monitored by nine sheathed 0.062-in.-diam Chromel/Alumel thermocouples. The stainless steel thermocouple sheaths were coated with a 0.005-in.-thick protective barrier of chemically vapor-deposited tungsten. The thermocouples were located in axial holes in the graphite sleeve adjacent to fuel specimens as shown in Figs. 9.1 and 9.2. Three titanium flux monitor wires, each enclosed in a platinum tube, were located in the graphite sleeve in similar axial holes. The graphite sleeve and the fuel specimens were continuously swept with a 3600-cm<sup>3</sup>/hr high-purity helium-neon gas mixture at 1 to 2 atm, and gas samples of the sweep effluent were taken periodically for fission-gas release determination.

The fueled specimens are described in Table 9.1, which includes a drawing showing the relative sizes and positions of the bonded fuel sticks. The coated particles and bonded stick fabrication are described further in Sect. 8.5.

The fuel mixtures were designed to give a uniform axial <sup>235</sup>U loading (0.0037 g/cm<sup>3</sup>), which provided an initial fission power generation of 3.3 kW/ft at the reactor midplane. The heat rate is reduced at either end of the fuel stack in direct proportion to the local neutron flux. Because of the high thermal flux in the HFIR-RB facility, the <sup>235</sup>U is consumed rapidly (50% in about 16 days at the reactor midplane). To provide for continuing fission power, the fuel specimens were also loaded with <sup>232</sup>Th and <sup>238</sup>U so that the fission

power from the <sup>233</sup>U and <sup>239</sup>Pu produced would match that of the initial <sup>235</sup>U loading. This is not quite possible in practice, however. There is an initial drop in power as the <sup>235</sup>U is consumed, followed by a gradual buildup which varies with time, axial position, and fertile material (<sup>232</sup>Th or <sup>238</sup>U) to a power approximating that produced by the initial fissile loading. This is shown graphically in Fig. 9.3, which presents the calculated fission power generated by two specimens (JF 275-4 and GGA sample 53-3) at the reactor horizontal midplane.

The linear fission heat rate for the GGA sample drops significantly more than that for the ORNL bed during the first cycle. This is a consequence of the rapid burnout of the initial loading of <sup>235</sup>U and the fact that additional fission power in the GGA sample depended primarily on the <sup>232</sup>Th → <sup>233</sup>U chain, with its longer characteristic conversion time than the <sup>238</sup>U → <sup>239</sup>Pu chain of the ORNL bed.

The capsule was designed to obtain reasonably uniform axial temperatures by tapering the graphite sleeve so as to increase the gas gap at either end, thus varying the thermal resistance of the gas gap between the graphite sleeve and water-cooled capsule inversely with the calculated initial axial power. To compensate for overall power variations with time, the composition of the helium-neon sweep gas mixture which occupies the gap was varied to maintain the peak fuel temperature at the design level.

Capsule HRB-2 was inserted in the removable beryllium facility on December 17, 1970, and was irradiated for 11 HFIR fuel cycles (256.5 days at 100 MW reactor power). The irradiation was completed and the capsule removed as scheduled on September 14, 1971. Capsule operation was stable throughout the irradiation, and all test parameters were within design limits.

The calculated fuel burnup and fluence for each sample are shown in Table 9.2. The maximum heavy-metal fissile particle burnup in the ORNL specimens (at the reactor midplane) was 31% and in the GGA sample, 23.6%. The maximum heavy-metal burnup in the fertile particles for both the ORNL and GGA specimens was 12%.

The helium-neon sweep gas effluent was sampled periodically to measure fission-gas release. The ratios of release rate to birth rate (R/B) of selected isotopes vs accumulated irradiation time are shown in Fig. 9.4. The birth rates used in this calculation take into account the depletion of <sup>235</sup>U and the fissions of bred-in <sup>233</sup>U and <sup>239</sup>Pu. We first calculated the daily change in isotopic composition of the fuel for each specimen and then the fission product yield from each fissionable isotope. As

1. J. L. Scott et al., *An Irradiation Test of Bonded HTGR Coated Particle Fuels in an Instrumented Capsule in HFIR*, ORNL-TM-3640.

2. J. A. Conlin et al., "Irradiation Tests on HTGR Fuel Elements," *Gas-Cooled Reactor and Thorium Utilization Programs Semiannual. Progr. Rep. Sept. 30, 1970*, ORNL-4637, pp. 11-23.

3. Poco graphite, a product of Poco Graphite, Inc., a subsidiary of Union Oil Company of California.

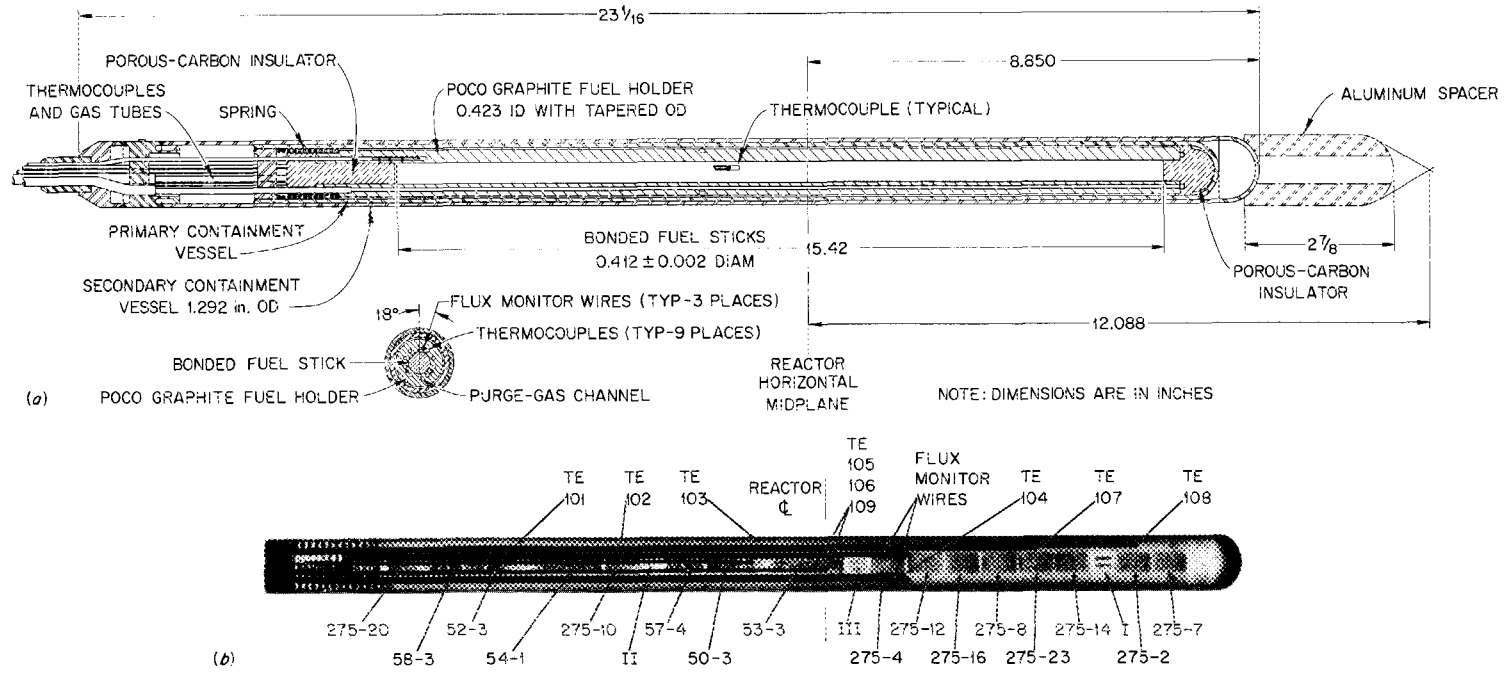


Fig. 9.1. HTGR instrumented capsule HRB-2 for irradiation in HFIR removable beryllium facility. (a) Schematic drawing of capsule; (b) radiograph of capsule after assembly.

Table 9.1. HTGR HRB-2 capsule fuel specimen description

Sample No.	Sponsor	Length (in.)	Weight (g)	Volume (cm <sup>3</sup> )	Bonded bed loading			Fertile particle: <sup>232</sup> Th (g/cm <sup>3</sup> )	Inert material (g)	Reactor horizontal midplane to sample center line (in.)	Average <sup>a</sup> thermal flux (E < 0.414 eV) (neutrons cm <sup>-2</sup> sec <sup>-1</sup> )	Fast flux (E > 0.183 MeV) <sup>a</sup> (neutrons cm <sup>-2</sup> sec <sup>-1</sup> )	Average gamma plus neutron heat <sup>b</sup> (W/g)	
					<sup>235</sup> U (g/cm <sup>3</sup> )	<sup>238</sup> U (g/cm <sup>3</sup> )	<sup>232</sup> Th (g/cm <sup>3</sup> )							
TE-101	JF275-20	ORNL	0.705	2.2106	1.5402	0.00370	0.03292	0.10992	1.9792	8.05	0.385	1.850	9.00	
	58-3	GGA	0.77	2.434	1.6822	0.00380	0.00029	0.01755	0.13029	2.1720	7.35	0.465	2.050	9.75
	52-3	GGA	0.77	2.521	1.6822	0.00368	0.00029	0.01680	0.13116	2.2592	6.60	0.560	2.250	10.70
	54-1	GGA	1.95	6.618	4.2601	0.00378	0.00028	0.01737	0.12976	5.9578	5.25	0.720	2.710	12.10
TE-102	JF275-10	ORNL	0.7145	2.1669	1.5599	0.00365	0.03250	0.10853	1.9355	3.95	0.866	3.100	13.30	
	II <sup>c</sup>	ORNL	0.450	~0.8640	0.00023	0.00741	0.00810			3.25	0.946	3.240	13.85	
	57-4	GGA	0.77	2.434	1.6822	0.00380	0.00029	0.01755	0.13029	2.1720	2.70	1.000	3.333	14.20
TE-103	50-3	GGA	0.77	2.521	1.6822	0.00368	0.00029	0.01680	0.13116	2.2592	2.00	1.063	3.440	14.50
	53-3	GGA	1.95	6.618	4.2601	0.00378	0.00028	0.01737	0.12976	5.9578	0.50	1.155	3.575	14.70
TE-105	Reactor midplane													
TE-106														
TE-109														
TE-104	III <sup>c</sup>	ORNL-GGA	0.450	~0.8640		0.00440		0.05393		-0.70	1.185	3.575	14.55	
	JF275-4	ORNL	0.710	2.3079	1.5561	0.00366	0.03258	0.10880	2.0765	-1.25	1.185	3.530	14.35	
	JF275-12	ORNL	0.7101	2.1130	1.5443	0.00369	0.03283	0.10963	1.8816	-2.00	1.170	3.440	14.00	
	JF275-16	ORNL	0.7107	2.2624	1.5501	0.00368	0.03271	0.10922	2.0310	-2.70	1.145	3.333	13.65	
	JF275-8	ORNL	0.7105	2.2075	1.5549	0.00366	0.03261	0.10888	1.9761	-3.40	1.105	3.210	13.20	
TE-107	JF275-23	ORNL	0.7090	2.1709	1.5539	0.00367	0.03263	0.10895	1.9395	-4.10	1.055	3.050	12.80	
	JF275-14	ORNL	0.7109	2.2392	1.5468	0.00368	0.03278	0.10945	2.0078	-4.75	0.998	2.875	12.30	
TE-108	I <sup>c</sup>	ORNL-GGA	0.450	~0.8640	0.00011	0.00023	0.07222			-5.40	0.930	2.650	11.75	
	JF275-2	ORNL	0.7025	2.2954	1.5307	0.00372	0.03312	0.11060	2.0640	-5.95	0.872	2.470	11.30	
	JF275-7	ORNL	0.7058	2.1978	1.5394	0.00370	0.03293	0.10998	1.9664	-6.75	0.780	2.225	10.50	

<sup>a</sup>Average flux over reactor cycle based on latest evaluation of flux monitors from previous experiments.

<sup>b</sup>Gamma heat as measured in graphite.

<sup>c</sup>Graphite holder with fissile and fertile loose particles.

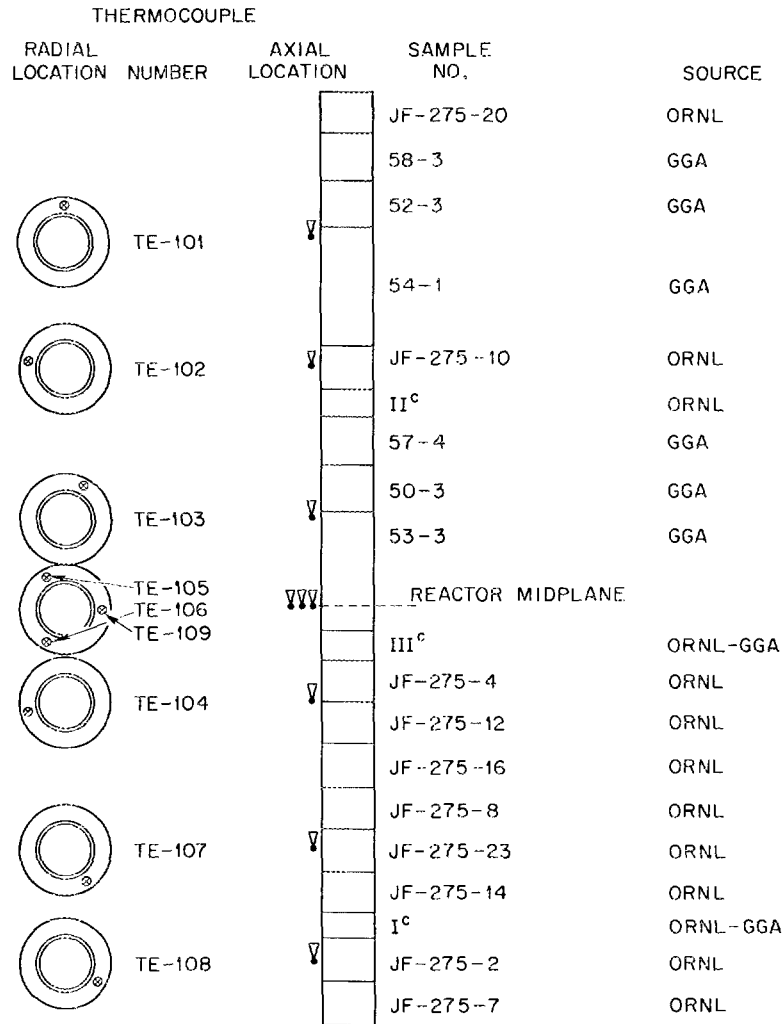


Fig. 9.2. HRB-2 fuel specimen and thermocouple locations.

may be seen in Fig. 9.4, the R/B ratio remained moderate throughout the irradiation.

Typical plots of the time-temperature history of five of the nine thermocouples for one cycle of operation are given in Figs. 9.5 and 9.6. Operating temperature was controlled by maintaining TE-109 at 940°C through March 13, 1971. At that time the control temperature was reduced to 915°C for the remainder of the experiment in order to avoid temperatures higher than the design conditions. The data of Figs. 9.5 and 9.6 show an additional reduction in the control setting on May 3 as the temperature of TE-107 rose somewhat above that of the control thermocouple. The maximum graphite temperature attained during irradiation was 966°C on TE-107, adjacent to fuel specimen JF-275-23.

Figures 9.5 and 9.6 show that the temperatures near the midplane of the capsule (TE-105, -106, -109, and -107) remain reasonably constant, whereas the temperatures at either end show large changes (low temperatures at the start of a cycle which increase at the end) as illustrated by TE-101. This is a consequence of several factors. The greatest part of the change is caused by the large increase in neutron flux at either end of the reactor core toward the end of each cycle. The capsule is located immediately outside the cylindrical control plates which surround the core. As the core burns out, the plates are pulled out, one set upward and the other downward, thus increasing the flux at either end of the core. Since the midplane temperatures are in general the highest, we adjust our sweep gas mixture to control

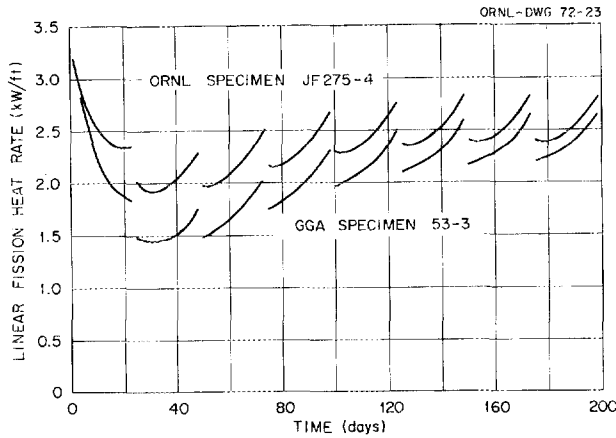


Fig. 9.3. Typical linear fission heat rate vs time (HFIR-HRB-2 capsule). Based on (1) peak measured flux at reactor horizontal midplane and (2) HFIR cycles of 23 days operating and 2 days down.

Table 9.2. Capsule HRB-2 fuel burnup and fluence for each bonded bed

Bed identification <sup>a</sup>	Fuel burnup (% FIMA)		Exposure (10 <sup>21</sup> neutrons/cm <sup>2</sup> )	
	Fissile	Fertile	Thermal (E < 0.414 eV)	Fast (E > 0.18 MeV)
JF-275-20	18.6	3.9	8.5	4.1
58-3	13.2	5.0	10.3	4.5
52-3	15.2	6.0	12.4	5.0
54-1	18.2	7.9	16.0	6.0
JF-275-10	28.0	9.3	19.2	6.9
57-4	22.0	10.4	22.2	7.4
50-3	22.7	11.0	23.6	7.6
53-3	23.6	12.0	25.6	7.9
JF-275-4	31.0	12.0	26.3	7.8
JF-275-12	30.5	11.9	25.9	7.6
JF-275-16	29.9	11.6	25.4	7.4
JF-275-8	29.2	11.2	24.5	7.1
JF-275-23	28.1	10.6	23.4	6.8
JF-275-14	27.0	9.9	22.1	6.4
JF-275-2	24.6	8.5	19.3	5.5
JF-275-7	23.0	7.4	17.3	4.9

<sup>a</sup>Numbers prefixed by JF are ORNL capsules; all others are GGA.

midplane temperatures and accept the resulting temperature variation at the ends. Other factors also contribute to the changes, in particular, the continuing variation with time and reactor cycle life of the local fissile atom content of a given fuel specimen. This fissile content is at a peak at the start of a core cycle due to the buildup of <sup>238</sup>Pu or <sup>233</sup>U which occurs during reactor shutdowns. This buildup is greatest at the midplane.

There is a short low-temperature period for all thermocouples at the beginning of each cycle. This was caused by capsule operation with 100% helium sweep, which reduces the thermal resistance of the gap

between the graphite sleeve and the capsule wall and results in the lower temperatures. The capsule was operated with 100% helium periodically to provide a relative measure of the power generation as a function of temperature without the complication of an uncertain gas conductivity.

A comparison of the calculated temperatures for the HRB-2 midplane specimens (GGA 53-3 and JF-275-4) is given in Table 9.3 for the initial and final test conditions. Condition 1 is for the initial startup using the initial fuel loadings, reactor fluxes, and as-built dimensions. Condition 2 corresponds to the conditions at the end of the irradiation. In the latter calculation we

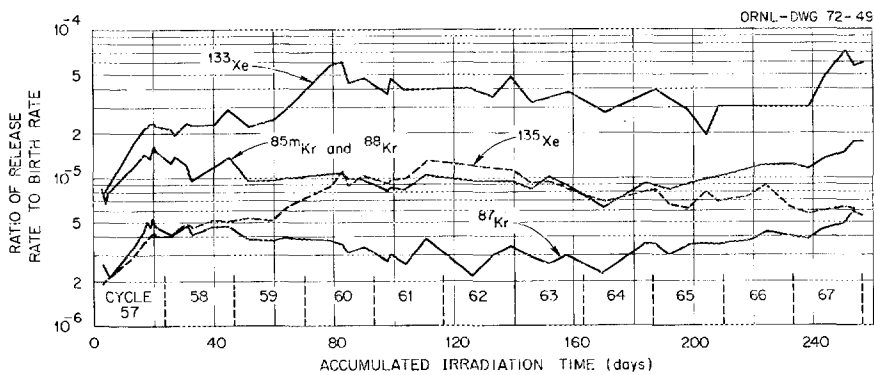


Fig. 9.4. Fission-gas release rate to birth rate ratio vs accumulated irradiation time (capsule HRB-2).

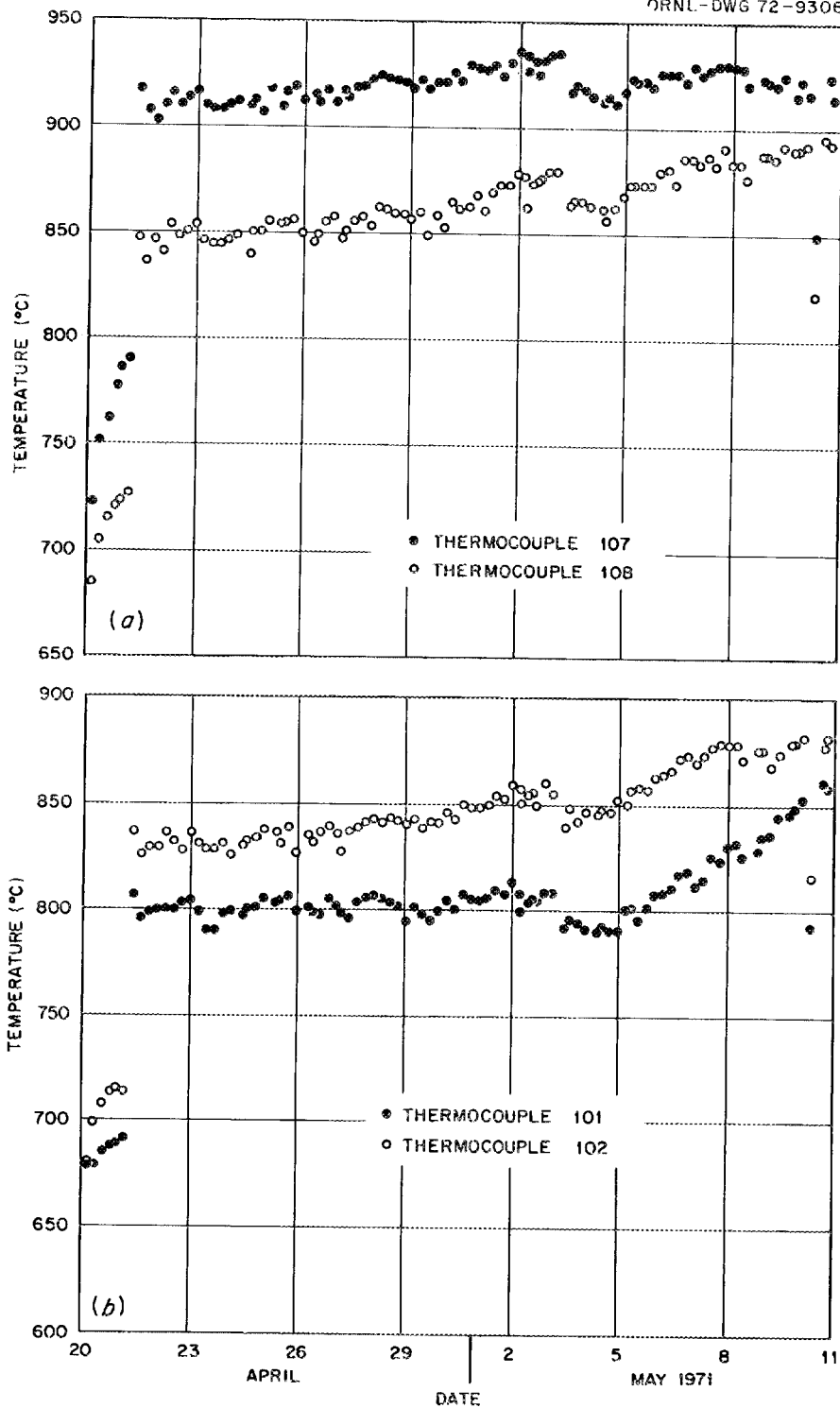


Fig. 9.5. Temperatures measured in HTGR-HFIR capsule HRB-2 during cycle 62.

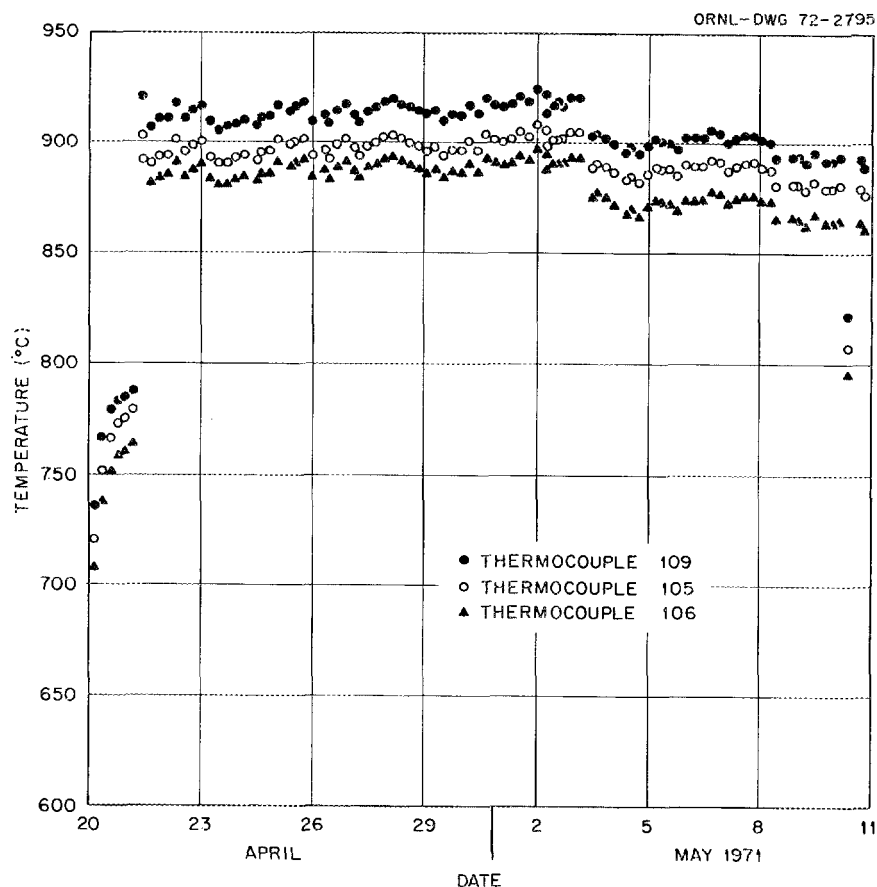


Fig. 9.6. Temperatures measured in HTGR-HFIR capsule HRB-2 during cycle 62.

Table 9.3. HFIR-HTGR HRB-2 capsule calculated midplane fuel temperature for startup and end of irradiation

	Condition 1 <sup>a</sup>		Condition 2 <sup>b</sup>	
	GGA 53-3	ORNL 275-4	GGA 53-3	ORNL 275-4
Linear fission heat rate, kW/ft	3.33	3.33	2.65	2.8
Bonded bed density, g/cm <sup>3</sup>	1.78	1.485	~1.8	~1.5
Bonded bed conductivity, Btu hr <sup>-1</sup> ft <sup>-1</sup> (°F) <sup>-1</sup>	3.47	3.47	3.47	3.47
Bonded bed diameter, in.	0.4115	0.4125	0.406	0.396
Graphite sleeve ID, in.	0.423	0.423	0.4273	0.4273
Graphite sleeve OD, in.	0.904	0.904	0.9115	0.9115
Temperature, °C				
Bonded bed center	1228	1213	1294	1356
Bonded bed surface	1052	1041	1147	1209
Mean graphite sleeve	905	905	905	905

<sup>a</sup>Initial startup using initial fuel loadings, fluxes, and as-built dimensions.

<sup>b</sup>End of irradiation using calculated isotopic compositions, fluxes, and postirradiation measurements of the beds and graphite sleeve.

used the calculated isotopic compositions, the end-of-core-life reactor fluxes, and the postirradiation measured dimensions of the bonded fuel sticks and graphite sleeve.

**Capsule HRB-3.** The third test in this series of irradiations, capsule HRB-3, has been designed, and assembly is approximately 20% completed. The capsule proper is identical to capsule HRB-2, but the test element differs. The temperature-instrumented graphite sleeve has been designed for larger, 0.49-in.-diam, bonded fuel stick specimens. A central thermocouple has been added to monitor the central temperature of one specimen. The design peak fuel temperature is 1250°C.

In addition to ORNL specimens, two fuel rod specimens are being prepared by GGA for testing in this experiment. Additional descriptive material on the capsule design and specimens is given in Sect. 8.5. The irradiation is scheduled to begin in January 1972.

### 9.1.2 Target Irradiation Tests

The five HT (target) capsules along with their operating conditions are described briefly below. More complete descriptions of the test specimens and results from the examination and evaluation of the experiments are given in Sect. 8.5 and 8.6.

**Capsule HT-6.** The sixth in a series of irradiation experiments, designated HT-6, was irradiated in the HFIR target region. The exterior capsule design and containment are identical to previous capsules HT-1 through HT-5 (refs. 4–7).

The capsule, shown in Fig. 9.7, was formed by a 0.654-in.-OD by 0.062-in.-wall aluminum tube. Four Poco graphite magazines (CP-20, -21, -22, and -23) and two special Poco graphite holders (M-2 and M-4) were contained within the tube. The magazines were supported on 0.125-in.-diam graphite pins, which were in turn supported by a spider consisting of a graphite disk and four small nickel centering pins which serve the dual function of a centering device and flux monitor.

The lower end of the stack of magazines was supported on a graphite spacer pedestal with pyrolytic-

carbon foils to insulate the magazine from the pedestal. The carbon foils were also used on both sides of every graphite spacer in the stack to minimize end losses. An Inconel X spring was installed at the top of the stack to prevent the specimens from shifting upward during handling into the space at the top provided for axial expansion. The capsule was sealed with 99.9% pure argon at 5 psig.

The graphite magazines supported bonded fuel sticks containing coated ThO<sub>2</sub> and coated inert particles. Small longitudinal slots were machined in the ends of each magazine for loose Fort St. Vrain Reactor pre-production fertile particles containing ThC<sub>2</sub>. The two graphite holders, M-2 and M-4, also contained <sup>232</sup>Th-fueled loose particles in longitudinal slots. Table 9.4 lists the design temperature and fast fluence for each specimen. The graphite magazines were tapered to provide a varying insulating gas gap to compensate for the axial variation in heat generation in the specimens. The maximum temperatures were expected to occur at the start of the third cycle, at which time the buildup of <sup>233</sup>U in the fuel would reach a peak. Four silicon carbide temperature sensors were included for postirradiation evaluation of the irradiation temperature.

Table 9.4. Capsule HT-6 design temperature and fast flux exposure

Graphite magazine	Design temperature (°C)		Fast fluence ( $E > 0.18$ MeV) ( $10^{21}$ neutrons/cm <sup>2</sup> )
	Initial	Maximum	
M-1	800	~870	4.1
M-2	1130	~1250	7.1
M-3	1070	~1200	6.5
M-4	1000	~1100	5.0
CP-20	800	~870	2.5–5.7 <sup>a</sup>
CP-21	1070	~1200	5.9–7.1 <sup>a</sup>
CP-22	1070	~1200	5.8–7.2 <sup>a</sup>
CP-23	800	~870	2.3–4.3 <sup>a</sup>

<sup>a</sup>Variation over specimen length.

4. J. H. Coobs et al., "Irradiation Experiments in HFIR," *Gas-Cooled Reactor Program Semiannu. Progr. Rep. Mar. 31, 1969*, ORNL-4424, pp. 20–25.

5. J. H. Coobs et al., "Irradiation of Loose and Bonded Coated Particles in HFIR Target," *Gas-Cooled Reactor Program Semiannu. Progr. Rep. Sept. 30, 1968*, ORNL-4353, pp. 47–54.

6. *Ibid.*, pp. 29–30.

7. H. C. McCurdy et al., "Instrumented Capsules for Fuel Tests in HFIR," *Gas-Cooled Reactor Program Semiannu. Progr. Rep. Sept. 30, 1969*, ORNL-4508, pp. 27–37.

The HT-6 capsule was inserted in the A-3 position of the HFIR target region on August 27, 1970, and irradiated for three fuel cycles (71 days at 100 MW reactor power).

**Capsule HT-7.** Capsule HT-7 was identical to HT-6 with the exception of the specimens. As in previous capsules, graphite magazines were used as the specimen containers. This was the first of a series of recycling

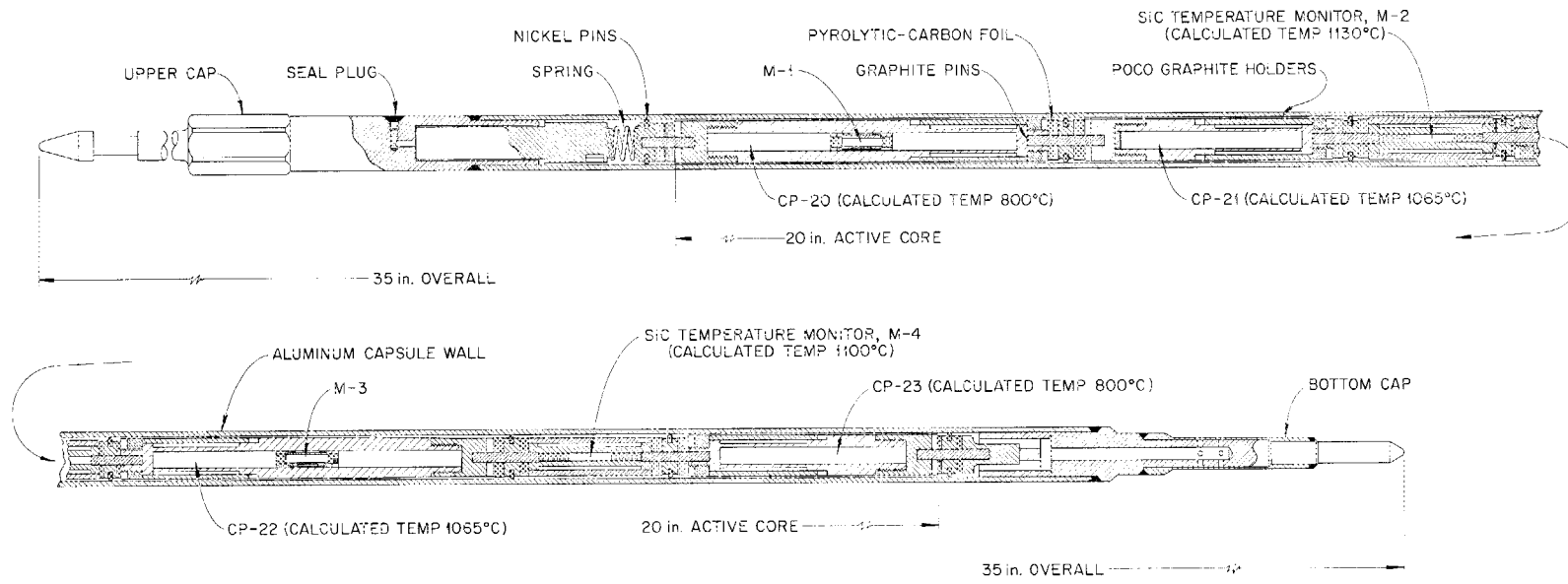


Fig. 9.7. Target capsule HT-6.

tests whereby some of the specimens, after postirradiation inspection, would be reirradiated in a succeeding capsule. Small loose particle holders, loaded inside the graphite magazines, housed different varieties of coated inert particles. The design temperatures for the loose particles were 750 and 1050°C. In addition to the loose particles, three different types of graphite were irradiated at 750°C. These graphite pieces were also contained within the graphite magazines.

This capsule was inserted in the A-3 position of the HFIR target region on December 17, 1970, and was removed March 25, 1971, after 93.7 days at 100 MW reactor power. The peak fast fluence on these specimens was  $9.6 \times 10^{21}$  neutrons/cm<sup>2</sup> ( $E > 0.18$  MeV).

**Capsule HT-9.** The design of capsule HT-9 was the same as that of capsule HT-6, the only modification being a change in the type of graphite material used in making the magazines. The capsule was inserted in the A-3 position of the HFIR target region on March 26, 1971, and was removed on May 13, 1971, after 45.9 days at 100 MW reactor power. The peak fast fluence on these specimens was  $4.8 \times 10^{21}$  neutrons/cm<sup>2</sup> ( $E > 0.18$  MeV).

**Capsule HT-8.** Capsule HT-8 was similar to capsule HT-6, having the same graphite magazine design with the longitudinal particle slots and the special graphite holders. Similar fuel loadings were also used. The capsule was inserted in the A-3 position of the target region on May 14, 1971, and was removed on August 18, 1971, after 93.1 days at 100 MW reactor power. The peak fast fluence was  $9.6 \times 10^{21}$  neutrons/cm<sup>2</sup> ( $E > 0.18$  MeV).

**Capsule HT-10.** Capsule HT-10, similar to HT-6, contained some of the specimens irradiated in HT-7 and HT-9. The capsule was inserted in the A-3 position of the target region on August 20, 1971, for four HFIR fuel cycles. It is scheduled for removal in December 1971.

## 9.2 ORR IRRADIATIONS

J. A. Conlin

A new irradiation test series was begun this year in the ORR-C1 capsule facility.<sup>8</sup> The capsule, designated ORR C1-28, was intended to irradiate coated particles made from uranium-loaded carbonized ion exchange resins in a steep temperature gradient to determine if

these particles are subject to the amoeba effect. In addition, the capsule provides for the irradiation of several batches of loose coated particles with conventional (UO<sub>2</sub> and UC<sub>2</sub>) kernels and with resin-derived kernels for postirradiation fission product release studies.

The test element consists of a graphite cylinder 0.91 in. OD, 0.54 in. ID, and 1.56 in. long. The center of the cylinder contains two small bonded specimens of coated resin-derived particles which were designed to evaluate the amoeba effect. The fabrication and characterization data on these specimens were presented in Sect. 8.5. The upper of the two specimens is instrumented with three tungsten-rhenium thermocouples located at three different radial positions. In addition, there are three tungsten-rhenium thermocouples located in grooves cut into the ID of the graphite cylinder. Provision is made for a continuous helium sweep over the fuel and for sampling of the sweep effluent for fission-gas release measurements.

The graphite cylinder has 21 axial holes drilled in the wall. Inserted in these holes are small (0.078-in.-OD, 0.032-in.-ID) graphite tubes containing the several types of loose coated particles. These particles are included for postirradiation fission product release studies.

The planned irradiation test conditions called for a center-line temperature of 1500°C and a heavy-metal burnup of about 50%. The irradiation began June 23, 1971, and the capsule was held in the fully retracted position in the facility from June 23, 1971, to August 26, 1971. Under these conditions the fuel central temperature was 120°C, and the fission heat generation is estimated to have been <10% of the fully inserted power (0.75 kW).

When the capsule was lowered on August 26 to within 6.5 in. of fully inserted, there was a very sharp rise in sweep gas gamma activity, so that automatic control action retracted the capsule. Maximum fuel temperature reached at that time was 930°C. Subsequently the capsule was reinserted to 7 in. from the fully inserted position. Fuel center-line temperature was 1005°C, and the sweep gas effluent gross gamma monitor read 80 mR/hr. Approved operating procedures with the facility require an automatic retract setting of 150 mR/hr gross gamma activity. The activity has thus been too high to permit operation at design conditions. Fission-gas release measurements indicated R/B ratios of  $4 \times 10^{-4}$  for <sup>85m</sup>Kr,  $1.6 \times 10^{-4}$  for <sup>87</sup>Kr,  $5.8 \times 10^{-4}$  for <sup>88</sup>Kr, and  $5.1 \times 10^{-5}$  for <sup>135</sup>Xe. These release rates are based on an estimated power generation of 0.38 kW (about one-half of design). The power estimate is based on

8. R. M. Carroll et al., "Fission Density, Burnup, and Temperature Effects on Fission-Gas Release from UO<sub>2</sub>," *Nucl. Sci. Eng.* 38, 143-55 (1969).

previous flux measurements. Normally a flux measurement would be made for this capsule by adding a small fraction of argon to the sweep gas and measuring the argon activation. However, the gross sweep gas activity is too high to permit the measurement of the argon activity.

We maintained the maximum conditions feasible without exceeding the automatic retract set point of 150 mR/hr gamma activity from the sweep effluent line. The capsule position has been maintained at between 9 and 12 in. from fully inserted with a fuel center-line temperature of 675 to 825°C during most of the irradiation. There has been a moderate increase in the activity release with time at a given fuel temperature, but it is not possible to give meaningful values. The flux is not well known, and the flux varies considerably with reactor core life at the operating position of the capsule, which is near the top of the fueled region of the core. Plans are to remove the capsule in mid-November. This will give a heavy-metal burnup in the loose particles of at least 5%, which will make fission product release studies on these particles feasible.

We have no explanation for the high fission-gas release rate from this capsule. Determination of the cause must await postirradiation examination.

### 9.3 ANALYSIS OF IRRADIATION CONDITIONS

J. D. Jenkins    H. T. Kerr

#### 9.3.1 Dosimeter Data from HT and HRB Capsules

Fast- and thermal-flux dosimeters have routinely been included in both the target and removable beryllium irradiation capsules since the beginning of the program. Many of the initial difficulties in interpreting the data have been resolved, and some dosimeter results from the long-term irradiation capsules are now available which are consistent with the results of other dosimetry experiments<sup>9,10</sup> and with the HFIR design calculations.<sup>11</sup> However, the situation is still not satisfactory in that considerable scatter exists even in the better sets of data and reliable results are not routinely obtained from any single capsule's dosimeters.

9. W. A. Hartman, *Spatial and Energy Distributions of the Fast Neutron Flux: A Comparison of Calculations with Measurements in the HFIR*, ORNL-CF-67-1-55 (January 1967).

10. F. B. K. Kam and J. H. Swanks, *Neutron Flux Spectrum in the HFIR Target Region*, ORNL-TM-3322 (March 1971).

11. F. T. Binford and E. N. Cramer, *The High Flux Isotope Reactor, a Functional Description*, vol. 1, ORNL-3572 (May 1964).

The difficulties in interpreting HFIR capsule dosimeter results arise from the following sources: (1) The high thermal-flux levels in HFIR and the long exposures of the samples lead to severe depletion of the active product nuclides which are counted in the analysis process. For example, over 90% of the active  $^{58}\text{Co}$  produced in the  $^{58}\text{Ni}(n,p)^{58}\text{Co}$  reaction is transmuted to  $^{59}\text{Co}$  by thermal-neutron capture in the course of a typical HT capsule irradiation. The cross sections for the active daughter products are not in general well known, leading to errors in the calculated corrections. In addition, the thermal-neutron flux is very sensitive to local perturbations, and, since it enters strongly into the calculation of the fast-flux dosimeter results, these results become sensitive to changes in the core configuration despite the fact that the fast flux is relatively unaffected. (2) The high radioactivity of the capsule and dosimeters requires hot-cell disassembly with resulting contamination of the dosimeters. (3) The high operating temperatures of the capsules lead to chemical reactions of the dosimeters with other capsule constituents, resulting in loss of dosimeters and a possible preferential leaching of active products from the dosimeter material.

Several steps have been taken to overcome these problems. First, the capsule dosimeter data have been used in an attempt to derive more accurate corrections for thermal-neutron depletion of the active daughter products.<sup>12</sup> Second, the dosimeters for the HRB capsules are now encapsulated in platinum tubes, and nonreactive metallic plating (e.g., gold) is contemplated for the HT capsule dosimeters. Third, attempts are made to keep the dosimeters free from extraneous hot-cell contaminants.

#### 9.3.2 HFIR Dosimetry Experiment

In order to avoid the difficulties described above, a special dosimetry experiment was designed to determine the damage flux and spectrum in the central hydraulic tube (CHT), the outer peripheral target (OPT), and the removable beryllium reflector (RBR) irradiation positions in the HFIR. The effort was supported jointly by this program, the Molten-Salt Reactor Program, and the Cladding and Materials Program of the Metals and Ceramics Division, all of which use these HFIR positions for irradiations.

12. J. D. Jenkins, "The Thermal Neutron Cross Section for  $^{54}\text{Mn}$ ," *Trans. Amer. Nucl. Soc.* **14**(1), 353 (June 1971).

The basic objective of this experiment was to determine the time and spatial dependence of the neutron damage flux and spectrum in the HFIR. For this purpose 15 experimental capsules were needed for short-term (minutes) irradiations in the central hydraulic tube to provide differential measurements of the flux and spectra at specified times during the fuel cycle. One capsule for the OPT position and one for the RBR position were needed for full-cycle irradiations to provide integral measurements of the flux and spectra. The experimental capsules contain activation dosimeters and utilize gadolinium as a thermal-neutron filter to increase the relative high-energy neutron activations in the target and to reduce the thermal-neutron captures in the product. The design, fabrication, irradiation, and disassembly of six CHT capsules and both full-cycle capsules have been completed, and the data are being analyzed. The remaining nine CHT capsules, which need slight design modifications, will be irradiated in a later fuel cycle.

The experimental data analysis is based on a spectrum-unfolding technique described in ref. 13. Given the measured activation data, a library of energy-dependent neutron reaction cross sections, and an initial guess at the neutron energy spectrum, an iterative adjustment procedure is applied to the input spectrum to make the spectrum-weighted cross sections consistent with the input measured activities. The validity of the converged energy spectrum will depend on the uncertainties in the measured activities and reaction cross sections and on the adequacy of the energy range coverage provided by the dosimeter set.

---

13. W. N. McElroy et al., *SAND-II, Neutron Flux Spectra Determination by Multiple Foil Activation -- Iterative Method*, AFWL-TR 67-41, vol. 1--4 (September 1967).

As the experimental data for each dosimeter set become available, the unfolded "experimental" spectrum for that position will be determined. These experimental spectra will serve as normalization points for the purely analytic spectra described below.

To complement the experimental program, an analytic effort is in progress to determine the time and spatial dependence of the damage flux and spectra in the HFIR. First a nine-group CITATION<sup>14</sup> diffusion theory calculation is made of the HFIR fuel cycle with stepwise control rod withdrawal. This calculation provides isotopic concentrations and power distributions at specified times during the fuel cycle. Next, a many-group DOT<sup>15</sup> transport theory calculation is made at each of the selected times during the fuel cycle using the isotopic concentrations and the power distribution from the corresponding time in the CITATION calculation. Each DOT calculation provides detailed energy spectra at all positions of interest at that time during the fuel cycle. For a given spatial point, a comparison of results from the DOT calculations will show any time dependence in the neutron damage spectrum.

The CITATION calculation has been completed, and preparations are being made to do the DOT calculations. As previously mentioned, the experimentally "measured" spectra will be used to normalize the analytic spectra. The normalized analytic spectra will provide a complete time and spatial map of the damage spectra in the HFIR which is consistent with the current experimental results.

---

14. T. B. Fowler and D. R. Vondy, *Nuclear Reactor Core Analysis Code: CITATION*, ORNL-TM-2496, Rev. 2 (July 1971).

15. F. R. Mynatt, *A Users Manual for DOT*, K-1694 (1968).

## 10. Irradiation Experiment Analysis and Fission Product Transport

O. Sisman    M. D. Silverman

---

In HTGRs the release of fission products is controlled by the use of coated fuel particles. Both Biso (porous carbon plus isotropic pyrolytic carbon) and Triso (porous carbon, SiC, and pyrolytic carbon layers) coatings are used in present HTGR designs. The Triso-coated particles will hold all fission products better than the Biso-coated particles but are more expensive to produce and reprocess; for some reactors pyrolytic carbon coatings will retain a sufficient portion of the fission products. Therefore the diffusion and stability characteristics are being studied for both types of coated particles. Also, both types are being evaluated because the SiC layer in the Triso coating may fail, whereupon the coating behaves like a Biso coating.

High-density isotropic pyrocarbon coatings are manufactured by deposition from methane at about 2000°C or by deposition from propylene at about 1250°C. Part of this study was designed to determine the difference in cesium and strontium diffusion in the two types of coatings. Other phases of the study deal with the distribution of fission products in bonded beds of coated fuel particles and the effects of burnup and fast fluence on cesium diffusion in pyrocarbon.

Fission products released from coated particles are not released directly into the coolant stream of HTGRs. The fuel matrix carbon tends to retain fission products; further, the graphite moderator serves as a barrier to fission product transport into the coolant. To study the latter effect, a high-temperature, pressurized helium loop was operated, in which the transport of cesium

through graphite was studied. In addition, the deposition characteristics of cesium throughout the loop were investigated.

### 10.1 FISSION PRODUCT RELEASE FROM BONDED BEDS

M. T. Morgan    R. L. Towns  
L. L. Fairchild

Irradiated bonded beds of Biso-coated fuel particles were annealed at 1250°C to study the cesium and strontium release; to determine the distribution of these fission products in the coated particles, the matrix, and the graphite can as a result of the annealing; and to show the effect of burnup on fission product release. Irradiated bonded beds of Triso-coated UO<sub>2</sub> particles were annealed at 1700 and 2000°C to study the stability of the coatings, but data for this study are not complete.

The Biso-coated UO<sub>2</sub> particles used in the bonded beds had a 230- $\mu$ -diam kernel, a 41- $\mu$ -thick porous pyrolytic carbon buffer layer, a 64- $\mu$ -thick high-density isotropic pyrolytic carbon outer layer derived from propylene, and an 18- $\mu$ -thick sacrificial coating. Biso-coated ThO<sub>2</sub> particles were used as diluent particles in the bonded beds. The Triso-coated UO<sub>2</sub> particles had 240- $\mu$ -diam kernels, a 40- $\mu$ -thick outer layer of high-density isotropic pyrolytic carbon, and a 14- $\mu$ -thick sacrificial coating.

The beds were bonded with phenolic resin containing 24 wt % graphite flour. The rate of polymerization was accelerated by the addition of 10 wt % maleic anhydride. The beds were 0.29 in. in diameter and 0.22 in. long after baking at 1000°C for 24 hr. They were placed in graphite cans having a wall thickness of 0.050 in.

Two capsules, each containing 15 samples in graphite cans, were irradiated to 10 and 20% fissions per initial metal atom (FIMA), respectively, at an irradiation temperature of less than 800°C in the B9 facility of the ORR. The fast fluence was approximately 10% of the thermal fluence. The 15 samples included eight bonded beds of Triso-coated particles, six bonded beds of Biso-coated particles, and one sample each of loose Triso- and Biso-coated particles.

The bonded beds containing Biso-coated particles were annealed one at a time in graphite cans in a resistance furnace. A purified helium atmosphere flowing at a rate of approximately 50 cm<sup>3</sup>/min was maintained in the furnace tube. The helium was passed through a liquid-nitrogen-cooled molecular sieve trap after it left the furnace in order to collect any fission gas released. The furnace was cut off and the components were analyzed for cesium every 200 and 240 hr of annealing time. No fission gas (<sup>85</sup>Kr) was detected in the trap on any annealing run. The sensitivity for <sup>85</sup>Kr was approximately 100 dis/min.

The cesium release data from the anneals of bonded bed B51, irradiated to 20% FIMA and annealed for 2500 hr at 1250°C, were reported previously.<sup>1</sup> The B51 bonded bed was disintegrated in nitric acid by an electrolytic method, and some of the coated particles were cracked and analyzed. The distribution of strontium and cesium in the various components is given in Table 10.1.

Cesium is highly volatile at 1250°C, and little was absorbed in the porous matrix of the bonded bed;

however, 34% of the total cesium was found in the dense isotropic pyrolytic carbon coating, which appears to be controlling the release of the cesium. It has been shown in our previous experiments that strontium and barium pass rapidly through dense pyrolytic carbon coatings, and the large fraction of strontium (68%) found in the core, compared with 0.5% in the coating, indicates that the release of strontium was controlled by the release from the core. While only 2.7% of the strontium was absorbed in the matrix, it would be expected that in a gas-cooled reactor a large fraction of the strontium would be held up in the massive graphite components. The distribution of cerium in the core and coating is about the same as that of an unannealed sample; the fraction of the cerium in the coating is mostly from recoils into the coating during irradiation.

Since the holdup of cesium in the matrix of the bonded beds and the graphite cans was negligible, we assumed that the dense outer coating of the coated particles was the only controlling factor; therefore we calculated diffusion coefficients for cesium in the pyrolytic carbon coating from the data obtained from the anneals of the bonded beds. These diffusion coefficients, along with those obtained from postirradiation anneals of loose coated particles, are presented in Sect. 10.2.

## 10.2 FISSION PRODUCT TRANSPORT THROUGH PARTICLE COATINGS

M. T. Morgan R. L. Towns  
L. L. Fairchild

Postirradiation anneals of loose coated particles were made using a high-temperature induction furnace.<sup>2</sup> The graphite crucible was drilled to accommodate eight tungsten tubes, as shown in Fig. 10.1. Each tungsten tube was fitted with a graphite thimble in the bottom to prevent the coated particle from contacting the tungsten. The temperature difference between the eight positions is less than the precision of measurements made with the optical pyrometer; therefore, we compare different samples at very precisely the same temperature.

Table 10.1. Distribution of fission products in B51 experiment after a 2500-hr anneal at 1250°C

Component	Percent of total fission products		
	Cs	Sr	Ce
Core	41	68	97
Coating	34	0.3	3
Matrix	0.075	2.7	ND <sup>a</sup>
Released from bonded bed	25	28	ND

<sup>a</sup>Not detected.

1. C. D. Baumann, M. T. Morgan, and R. L. Towns, "Fission Product Release from High-Burnup Coated Fuel Particles by Postirradiation Anneals," *GCR-TU Programs Semiannu. Progr. Rep. Sept. 30, 1970*, ORNL-4637, pp. 24--29.

2. M. T. Morgan and R. L. Towns, *Techniques and Apparatus for Inspection, Handling, and Annealing Highly Radioactive Fuel Microspheres*, ORNL-TM-2493 (March 1969).

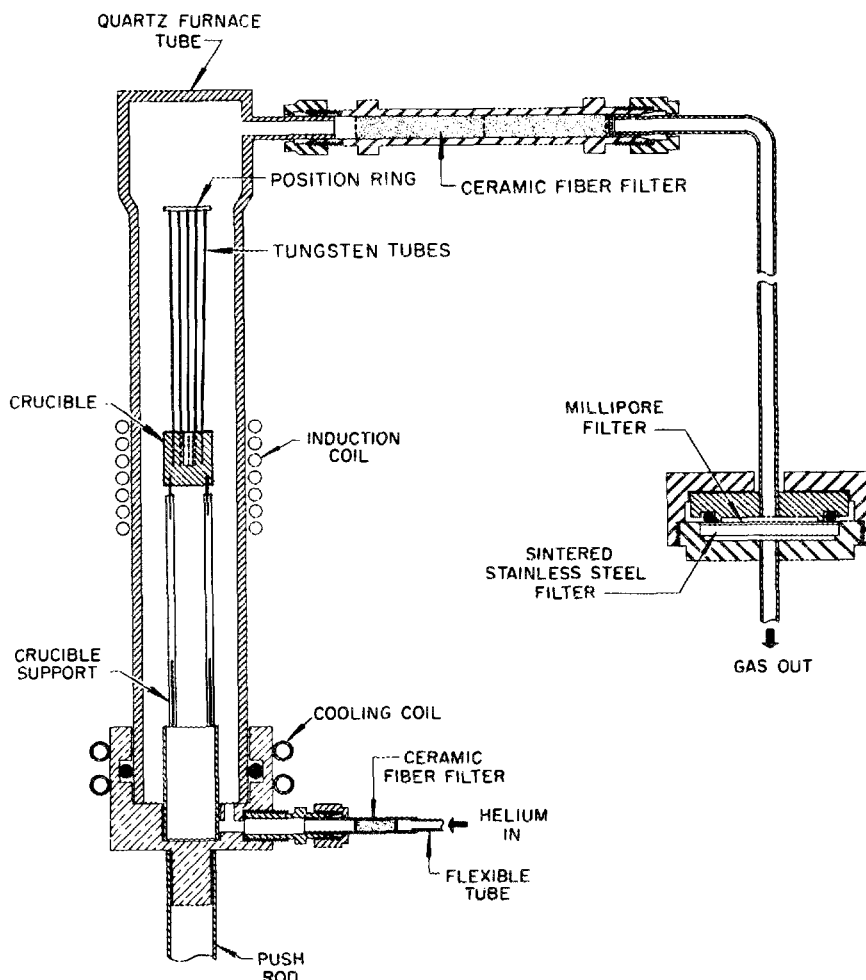


Fig. 10.1. Furnace tube assembly.

Anneals were made to determine diffusion coefficients for cesium in pyrolytic carbon, to compare diffusion in low-temperature isotropic pyrocarbon derived from propylene (LTI-PyC) with that in high-temperature isotropic pyrocarbon derived from methane (HTI-PyC), and to compare diffusion in LTI-PyC coatings on particles with 10% FIMA burnup with that in LTI-PyC coatings on particles with 20% FIMA burnup. The LTI-PyC-coated particles were from the ORR-B9 irradiations described in Sect. 10.1, except for one sample irradiated in the HFIR to a fast fluence of  $4 \times 10^{21}$  neutrons/cm<sup>2</sup> ( $E > 0.18$  MeV). The HTI-PyC-coated particle sample was also irradiated in the HFIR in the same capsule.

The irradiation temperature of all samples was less than 800°C; therefore we assumed that no cesium or

strontium had diffused into the outer coating of the coated particles. We assumed that the porous buffer layer offered no resistance to the passage of fission products, that the fission product concentration at the fuel-to-carbon interface was constant during the anneals, and that the fission product concentration at the carbon-to-helium interface was zero. Diffusion coefficients were calculated from the relation<sup>3</sup>

$$\bar{D} = L^2/6t,$$

where  $D$  is diffusion coefficient, cm<sup>2</sup>/sec,  $L$  is coating

3. J. Crank, *Mathematics of Diffusion*, pp. 47-48, Clarendon Press, Oxford, 1956.

thickness, cm, and  $t$  is time required for fission product to penetrate coating, sec.

The diffusion coefficients obtained for cesium are listed in Table 10.2 and are plotted vs reciprocal temperature in Fig. 10.2. These values include data from four bonded beds discussed in Sect. 10.1. An activation energy for cesium diffusion in LTI-PyC of 106 kcal/mole was calculated from these data. This is more than twice the 42 kcal/mole for the cesium diffusion in HTI-PyC obtained by Gethard and Zumwalt,<sup>4</sup> their data are plotted in Fig. 10.2 for comparison. Data point 7, for cesium diffusion at 1400°C in HTI-PyC with high fast fluence, falls close to this line.

Annealing runs in the multiple-type crucible, made at the same time and temperature, permit direct comparisons between data points 4 and 5 for effects of burnup and between data points 6 and 7 for LTI vs HTI pyrocarbon. The differences between the diffusion coefficients obtained on materials irradiated to 10 and 20% FIMA are within the experimental variations and show no significant effect of burnup in these samples. The difference between the diffusion coefficients obtained from LTI and HTI coated particles in data points

6 and 7 is more than a factor of 10. This experiment is still in progress, since the cesium has not yet penetrated the 90- $\mu$ -thick HTI-PyC coating after 2000 hr at 1400°C.

The difference between the diffusion coefficient for cesium in the LTI-PyC with high fast fluence (data point 6) and that obtained from anneals of LTI-PyC-coated particles with low fast fluence is slight (data points 3, 4, and 5). This indication that fast-neutron damage has little effect should be verified by a direct comparison on coated particles from the same batch irradiated to different levels of fast-neutron dose.

Crude measurements of diffusion coefficients for strontium in LTI and HTI pyrocarbon were made during the anneals of the HFIR samples (see data points 6 and 7 in Table 10.2). At periodic intervals during the early part of the anneal, the coated particles were removed from the tungsten tubes, and bremsstrahlung counts were made on the tubes in a fixed geometry. Since the cesium had not yet penetrated the coatings and other gamma and beta emitters had decayed, <sup>90</sup>Sr was the only major radioisotope on the tungsten tubes, and the amount should be proportional to the bremsstrahlung measurement. A graph of bremsstrahlung activity vs annealing time is shown in Fig. 10.3. The diffusion coefficients for strontium at 1400°C were  $4 \times 10^{-9}$  cm<sup>2</sup>/sec in the LTI-PyC and  $9 \times 10^{-10}$  cm<sup>2</sup>/sec in the HTI-PyC.

4. P. E. Gethard and L. R. Zumwalt, "Diffusion of Metallic Fission Products in Pyrolytic Carbon," *Nucl. Appl.* 3, 679 (1967).

Table 10.2. Diffusion coefficients for cesium in pyrolytic carbon obtained from postirradiation anneals of Biso-coated particles

Data point <sup>a</sup>	Temperature (°C)	Average $D$ (cm <sup>2</sup> /sec)	Number of determinations	Range of $D$ (cm <sup>2</sup> /sec)	Burnup (% FIMA)	Coating <sup>b</sup>
1	1250	$2.9 \times 10^{-12}$	2 each, bonded beds	1.6 to $4.2 \times 10^{-12}$	10	LTI-PyC
2	1250	$6.0 \times 10^{-12}$	2 each, bonded beds	5.1 to $6.8 \times 10^{-12}$	20	LTI-PyC
3	1400	$8.8 \times 10^{-11}$	7 each, coated particles	2.6 to $13 \times 10^{-11}$	10	LTI-PyC
4	1400	$8.3 \times 10^{-11}$	4 each, coated particles	5.5 to $9.7 \times 10^{-11}$	20	LTI-PyC
5	1400	$5.7 \times 10^{-11}$	4 each, coated particles	5.3 to $6.3 \times 10^{-11}$	10	LTI-PyC
6	1400	$3.6 \times 10^{-11}$	4 each, coated particles	3.3 to $4.2 \times 10^{-11}$	<i>c</i>	LTI-PyC
7	1400	$< 2 \times 10^{-12}$	4 each, coated particles	Exp. still in progress	<i>c</i>	HTI-PyC
8	1500	$6.1 \times 10^{-10}$	8 each, coated particles	4.5 to $8.3 \times 10^{-10}$	10	LTI-PyC
9	1600	$2.0 \times 10^{-9}$	8 each, coated particles	1.3 to $2.6 \times 10^{-9}$	10	LTI-PyC

<sup>a</sup>The as-coated outer coating densities for coated particles in data points 6 and 7 were 1.99 and 1.82 g/cm<sup>3</sup> respectively; all others had densities of about 1.83.

<sup>b</sup>LTI-PyC is an abbreviation for low-temperature isotropic pyrocarbon deposited at low temperatures from propylene; HTI-PyC is a high-temperature isotropic pyrocarbon deposited from methane.

<sup>c</sup>Irradiated to  $4 \times 10^{21}$  neutrons/cm<sup>2</sup> fast fluence ( $E > 0.18$  MeV). These experiments used Biso-coated ThO<sub>2</sub> particles irradiated in the HFIR. All other materials were Biso-coated UO<sub>2</sub> particles irradiated in the ORR.

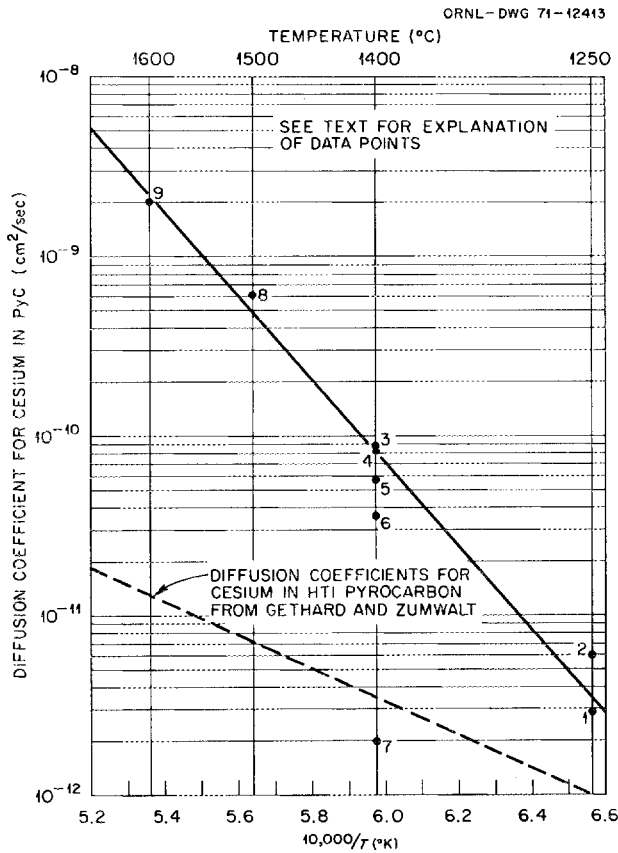


Fig. 10.2. Arrhenius plot for cesium diffusion in pyrolytic carbon from postirradiation anneals of coated particles.

### 10.3 RESULTS AND ANALYSIS OF FISSION PRODUCT LOOP TESTS

M. D. Silverman G. E. Mills  
M. N. Ozisik<sup>5</sup>

Cesium transport and deposition studies in the fission product deposition loop (FPD) were discontinued at the end of June 1971 because of insufficient funding for fiscal year 1972. Since the last reporting period, three additional experiments were completed, and a fourth was aborted because of fabrication difficulties.

Previous reports<sup>6-11</sup> have presented detailed descriptions of the loop and its components. To summarize, cesium is released from a quartz capsule and allowed to diffuse through static helium down a molybdenum tube, to which is brazed a graphite section acting as an evaporator. The metallic cesium vapor serves as an axial source, moves through the evaporator into turbulently flowing helium, and then deposits downstream on a test deposition tube monitored by a traveling

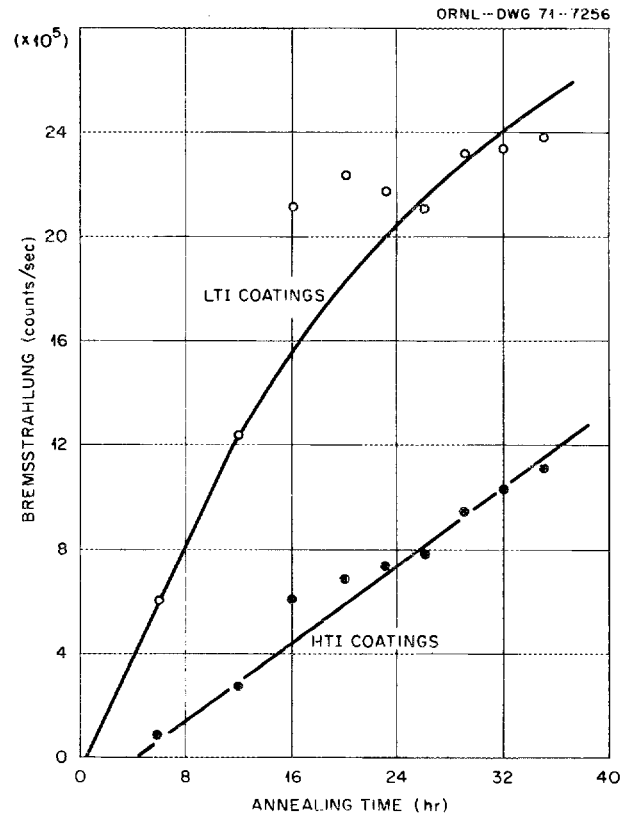


Fig. 10.3. Bremsstrahlung activity vs annealing time.

sodium iodide crystal counter and on other metallic surfaces in the loop. Chemical and radiochemical analyses at the end of each experiment are used to determine cesium concentrations for the appropriate

5. Consultant to the Reactor Division, ORNL, from North Carolina State University, Raleigh.

6. M. D. Silverman and F. H. Neill, "Fission-Product Deposition Loop," *GCR Program Semiannu. Progr. Rep. Sept. 30, 1968*, ORNL-4353, pp. 69-73.

7. D. L. Gray and F. H. Neill, *Design Report for Fission-Product Deposition Tests up to 1500°F*, ORNL-TM-2532 (June 1969).

8. M. D. Silverman and F. H. Neill, "Fission-Product Transport and Deposition," *GCR Program Semiannu. Progr. Rep. Mar. 31, 1969*, ORNL-4424, pp. 55-58.

9. M. D. Silverman, F. H. Neill, and G. E. Mills, "Fission Product Transport and Deposition," *GCR Program Semiannu. Progr. Rep. Sept. 30, 1969*, ORNL-4508, pp. 42-49.

10. M. D. Silverman and G. E. Mills, "Fission Product Transport and Deposition," *GCR Program Semiannu. Progr. Rep. Mar. 31, 1970*, ORNL-4589, pp. 50-56.

11. M. D. Silverman, M. N. Ozisik, and G. E. Mills, "Fission Product Transport and Deposition," *GCR-TU Programs Semiannu. Progr. Rep. Sept. 30, 1970*, ORNL-4637, pp. 29-33.

portions of the loop and its components. Hollow graphite evaporators were employed except for the final experiment, in which dummy fuel sticks mounted on the central molybdenum thermocouple tube within the evaporator section simulated the geometry of an HTGR fuel assembly. Operating conditions for the experiments completed this past year are summarized in Table 10.3.

Experiment C-6 was run for several reasons: (1) to check out the new heater bundle installed upstream of the cesium injector, (2) to test the efficacy of the modification discussed previously,<sup>11</sup> and (3) to verify the data obtained in experiment C-3, where inductive heating was used to raise the graphite evaporator from gas temperature (680°) to 800°C. By contrast, in C-6 additional heat supplied by the newly installed heater bundle enabled us to obtain a more uniform temperature spectrum in the evaporator because all the heat came from the turbulently flowing helium.

By employing in experiment C-7 a "tight" AXF graphite whose permeability was estimated to be about  $10^4$  less than that of H-327, we hoped to eliminate transverse flow (practically) through the evaporator and thus allow diffusion to become the sole mode of cesium transport. Unfortunately, only after the experiment was under way did we learn that its permeability was only about 160-fold less than that of H-327. As a result, transverse flow was not entirely eliminated, but it was reduced to the extent that in this experiment approximately one-third of the cesium transport took place via this mechanism while the major amount (two-thirds) resulted from diffusion. Considerable difficulty was encountered in making the molybdenum-graphite joints because the brazing alloy (Zr, Ti, Nb) used for all previous experiments apparently did not wet or pene-

trate the AXF graphite. The porosity of H-327, by contrast, had allowed easy penetration by the alloy in fabricating all the previous evaporators. This problem was solved by coating the ends of the graphite with chromium oxide and reducing it to the carbide, so that the gold or copper brazing alloy effectively wetted the graphite.

In our last experiment, C-9, we mounted dummy fuel sticks (prepared from matrix material and loaded with cesium by Gulf General Atomic and irradiated in the BSR) on the molybdenum thermocouple tube within the graphite evaporator to simulate the geometry of the Fort St. Vrain fuel assembly. However, instead of the cesium partial pressure of  $10^{-8}$  atm that we had hoped to obtain (estimated end-of-life condition for Cs in the FSV fuel element), we learned that  $\sim 10^{-4}$  atm of cesium was produced by the source material in the dummy fuel sticks. Furthermore, during the 1-hr check-out of the rf heating coil, cesium transport through the graphite evaporator was observed. Examination of the injector assembly revealed that leakage at the molybdenum-graphite joint (caused by incomplete brazing) had occurred, which terminated the experiment. Radial cuts of the evaporator gave the typical spectrum of cesium activity observed in previous experiments (e.g., Fig. 3.3 of ref. 9) where transverse flow predominated. It is interesting to note here that a uniform axial concentration of cesium must have been present inside the evaporator, as shown by a gamma scan of the evaporator after the experiment and later verified by detailed analysis. This was in contrast to that observed in all the other experiments (e.g., Fig. 3.4 of ref. 9), where cesium vapor supplied by the external source resulted in a nonuniform axial concentration.

Table 10.3. Operating conditions for FPD loop experiments

Experiment	Duration (hr)	Gas temperature <sup>a</sup> (°C)	Cesium vapor pressure <sup>b</sup> (atm)	Graphite evaporator <sup>c</sup>		Deposition tube	
				Type	Temp. (°C)	Material	Temp. <sup>d</sup> (°C)
			$\times 10^{-3}$				
C-6	116	760	0.66	H-327	740-750	316 SS	720-690
C-7A	102	663	3.6	AXF	760-805	Mild steel	600-570
C-9	1	665	~0.1	H-327	876-905	316 SS	600-570

<sup>a</sup>Gas pressure 200 psig; Re  $\sim 20,000$  in deposition section and about 7000 to 8000 in annulus.

<sup>b</sup>Based on source temperature for all experiments except C-9, which is based on Gulf General Atomic data.

<sup>c</sup>Length 15.2 cm, thickness 0.2 cm.

<sup>d</sup>These temperatures are estimated from thermocouple readings taken for He entering the Cs injector section and after leaving the deposition section respectively.

In our last report<sup>11</sup> we correlated the data obtained from previous experiments<sup>7-10</sup> in the FPD loop on the transport of cesium through the graphite evaporators with an analytical model<sup>12</sup> based on the transverse flow of helium through the graphite. This model has been widened to cover the proposed FSV fuel assembly configuration as well as that for the hollow evaporator, as indicated in Fig. 10.4 [the hollow evaporator is a limiting case where the gap width between the fueled region and the graphite sleeve becomes quite large ( $\geq 100$  mils, as compared with a fuel element specification of  $\sim 5$  mils)]. A summary of this broader analytical model will be given here, and a more detailed treatment is presented elsewhere.<sup>13</sup>

Previously<sup>11,12</sup> we showed that

$$W_f = m_f \frac{K a_m P_1}{4\mu t P_m} (P_1 - P_2), \quad (1)$$

where

$W_f$  = rate of transport of fission product through the graphite tube into the outer stream, g/sec,

$a_m$  = mean lateral surface area of graphite tube,  $\text{cm}^2$ ,

$t$  = thickness of the graphite, cm,

$P_1, P_2$  = inlet and outlet pressure, respectively, of the coolant gas in the outer channel, atm,

$P_m$  = mean gas pressure, atm,

$\mu$  = viscosity of gas, cP,

$m_f$  = mass fraction of fission product in the gas inside the graphite tube,  $\text{g}/\text{cm}^3$ ,

$K$  = permeability coefficient for graphite, darcys.

Also,  $P_1 \cong P_m$  for most practical cases.

Equation (1) is really a special case of the general solution<sup>13</sup>

$$W_f = \frac{m_f a_m K (P_1 - P_2)}{2\mu t} Z, \quad (1a)$$

where

$$Z \equiv \frac{1}{Y^2} \left( 1 - \frac{1}{\cosh Y} \right) \quad (1b)$$

and  $Y$  is a function of  $K$  and the dimension of the graphite evaporator.

When  $Y \ll 1$  we obtain the solution for the large gap (or hollow evaporator) given in Eq. (1); when  $Y \gg 1$ , we have, for the narrow gap,

$$W_f = \frac{m_f a_m K (P_1 - P_2)}{2\mu t} \frac{1}{Y^2}. \quad (2)$$

In this case, fission product removal by transverse flow is proportional to the third power of the diametral gap. However, reducing gap thickness does not significantly reduce the transverse flow until a very small diameter gap width ( $\sim 2$  mils) is attained, as demonstrated by the following calculated values, based on our experimental geometry.

12. M. N. Ozisik and M. D. Silverman, *Trans. Amer. Nucl. Soc.* 13(2), 586-87 (November 1970).

13. M. N. Ozisik and M. D. Silverman, *J. Nucl. Technol.* 14(3), 240-46 (June 1972).

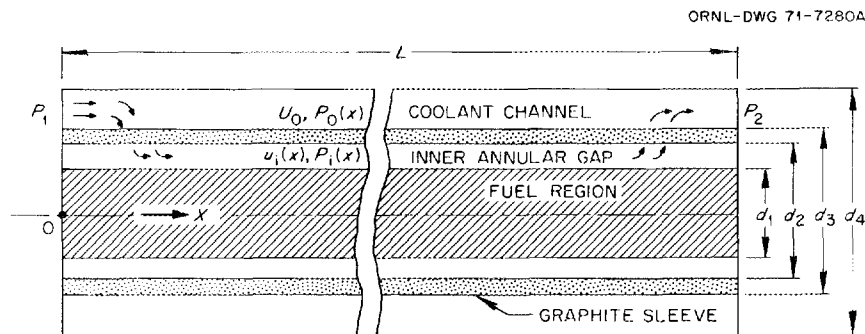


Fig. 10.4. Geometry and coordinate system for an HTGR-type fuel assembly.

Diametral difference (mils)	$\gamma^2$	$W_f$ (g/sec)
1	700	$\sim 3 \times 10^{-10}$
2	85	$2.5 \times 10^{-9}$
10	0.7	$1 \times 10^{-7}$
20	0.08	$1 \times 10^{-7}$
50	0.005	$1 \times 10^{-7}$

Table 10.4 lists values of  $W_f$  predicted from Eq. (1) and those determined experimentally, including those previously reported.<sup>11</sup> If a surface in-pore diffusion mechanism is assumed, the values of  $W_f$  would be of the order of  $10^{-6}$ , using a condensed-state cesium diffusion coefficient of about  $10^{-8}$  cm<sup>2</sup>/sec and adsorption data presented by GGA<sup>14</sup> for the test graphite. It is apparent from a comparison of fission product transport by both mechanisms that in-pore diffusion alone underestimates the cesium transport by about two orders of magnitude for the experimental conditions. However, the values obtained from consideration of the transverse flow mechanism are in reasonable agreement with the experimental data.

It should be noted that in the high-temperature gas-cooled Fort St. Vrain reactor<sup>15</sup> the pressurized (48 atm) helium coolant will flow past the fuel assembly at  $Re \sim 40,000$ ; furthermore, the length of the assembly

will be 31 in., as compared with our 6-in. evaporator. For such a case the pressure drop term ( $P_1 - P_2$ ) in Eqs. (1) and (2) will be increased over 5-fold due to the increased length, over 5-fold because of the increased Reynolds number of the gas, and over 1.6-fold because of the increased velocity of the coolant. The sum total of these effects is an increase of approximately 40-fold in ( $P_1 - P_2$ ) for the reactor case over that experienced in our experiments. Further, the pressure in the FSV reactor is 700 psi, vs about 200 psi in the FPD loop. At the same time, the cesium vapor pressure in an HTGR is estimated to be much less than the value employed in the above experiments, which has a major effect on the ratio of transverse to diffusive transport. Based on a cesium vapor pressure of  $10^{-8}$  atm (estimated end-of-life conditions for a Fort St. Vrain reactor fuel element assembly) and the FSVR flow conditions, we have calculated cesium transport into the helium coolant by transverse flow (for a graphite whose permeability is 50 millidarcys) and compared it with cesium transport for the case of diffusive flow under equilibrium conditions. On the above bases, the ratio of transverse to diffusive flow for cesium was about 1.

Experiments were also performed to study the deposition of cesium on surfaces downstream of the graphite evaporator; plate-out data were obtained on a number of materials used for the deposition surface, and these data are summarized in Table 10.5. An "isothermal" 1-in.-diam deposition tube was used in these experiments; it was contained within a section of 2-in. sched 80 type 316 stainless steel loop piping and located just beyond the evaporator region. Except for experiment C-1, in which a thick graphite guide spacer placed in the molybdenum tube limited the flow of cesium into the evaporator region, the cesium vapor pressure, or concentration, and consequently the driving force for flow through the evaporator into the turbulently flowing helium were controlled by the source temperature, which did not vary greatly from run to run. As a result, the cesium concentration present in the helium passing the evaporator did not vary more than sixfold (calculated from the total amount of cesium collected past the evaporator averaged over time). Consequently, the effect of this variable on deposition in these experiments was minor. This is verified by comparing runs C-4 and C7A, which utilized mild steel for the deposition

Table 10.4. Transport of cesium by transverse flow

Test No.	$W_f$ (g/sec)	
	Eq. (1)	Expt.
	$\times 10^{-8}$	$\times 10^{-8}$
CS-2	9.8	2.8
CS-3	11.6	4.0
CS-4 <sup>a</sup>	7.4	13
CS-5	13.2	2.0
CS-6	8	7.5
CS-7A <sup>b</sup>	1.0	2.0

<sup>a</sup>0.5-cm-thick graphite tube.

<sup>b</sup>In experiment CS-7A we employed a "tight" graphite whose permeability was approximately 160-fold less than that of the porous graphite used for all the other experiments. The values of CS-7A listed in the table are for the amount of cesium transported only by transverse flow, which we calculated assuming no dilution of the cesium concentration in the gas phase. Based on calculations, in this experiment approximately 65% of the cesium moved through the graphite by diffusion, as estimated from known diffusion coefficients for cesium in graphite and cesium concentrations found in the graphite evaporator, and this factor was used in obtaining the "experimental" value listed above.

14. C. E. Milstead, A. B. Reidinger, and L. R. Zumwalt, *Carbon* 4, 99 (1966).

15. A. L. Habush and R. F. Walker, *The Fort St. Vrain HTGR, GA-7817* (1967).

Table 10.5. Deposition data from FPD loop experiments

Experiment	Duration (hr)	Cesium concentration in He <sup>a</sup> (g/cm <sup>3</sup> )	"Isothermal" deposition tube				Deposition discharge elbow <sup>d</sup> (μg/cm <sup>2</sup> )	Adiabatic section <sup>e</sup> (μg/cm <sup>2</sup> )
			Material pretreatment <sup>b</sup>	Temperature <sup>c</sup> (°C)	Amount of cesium deposited (μg/cm <sup>2</sup> )	Number of monolayers		
		× 10 <sup>-13</sup>						
C-1	288	0.15	316 SS	570-560	0.36	4.1		
C-2	69	1.6	Nickel	570-560	0.65	7.4		
C-3	95	2.3	316 SS	610-580	1.0	11.4		
C-4	170	7.4	Mild steel	600-570	2.7	30.6		
C-5	264	1.2	Graphite	580-560	0.26	3.0	0.51	0.4
C-6	116	3.9	316 SS	720-690	0.21	2.4	0.53	0.85
C-7A	102	2.9	Mild steel	600-570	4.8	54.5	0.87	0.5
C-9	1	5.2	316 SS	600-570	0.08	0.9	0.017	~0.002

<sup>a</sup>Based on total cesium transported through graphite averaged over time.

<sup>b</sup>C-4 pretreated to give fairly thick layer of adherent Fe<sub>3</sub>O<sub>4</sub>, estimated as 5000 to 10,000 Å.

<sup>c</sup>Estimated from thermocouple readings taken for He entering the Cs injector section and after leaving the "isothermal" deposition section respectively.

<sup>d</sup>Geometry of section (after deposition tube) was changed between experiments C-5 and C-6. Surface area for this section obtained from straight portion plus  $L/D = 13$  for elbow effect, that is, equivalent length of straight pipe ( $\Delta P$ ).

<sup>e</sup>Ten-foot-long section of straight pipe cooled by natural convection, installed between experiments C-5 and C-6.

tube. In run C-4 the tube was treated to produce a fairly thick film (5000-10,000 Å of Fe<sub>3</sub>O<sub>4</sub>, by heating in air at 800°C) and was also exposed to a relatively high concentration of cesium in the helium stream; however, the tube in the C-4 run retained less cesium than that in C-7A. Again, in test C-6, less cesium was retained by the 316 stainless steel deposition tube than in C-3, which is what one would expect because of the higher temperature of the surface, even though the cesium concentration in the gas phase was about twice as high in run C-6 as in C-3.

Plate-out of cesium on stainless steel and nickel was lower than on mild steel in our experiments, in agreement with that observed by GGA.<sup>15</sup> However, our values (column 7) are an order of magnitude lower than those reported by Milstead and Zumwalt.<sup>16</sup> At the same time, our deposition tubes (except for C-4) were relatively "oxide free"; moreover, they were exposed to a reducing atmosphere, both during the preoperational period (at least 200 hr) and during the experimental testing time.

Studies were also performed to determine whether the conventional relations between heat and mass transfer applied to cesium deposition. For these studies

we placed a small bundle containing six staggered rods, two per row, within a straight section of the 2-in. loop piping during experiment C-7A. This unit was used to simulate heat exchanger tubes placed at right angles to the flow of the turbulent helium gas stream. For turbulent flow of a gas inside a circular tube<sup>17</sup> and also for cross-flow conditions across a cylinder,<sup>18</sup> the Nusselt number is directly proportional to the Reynolds number raised to either the 0.8 or the  $n$ th power and is proportional to the Prandtl number raised to about the 0.3 power. Similarly, the analogous equations for mass transfer state that the Sherwood number is directly proportional to the Reynolds number raised to the 0.8 power for turbulent flow inside a tube and the  $n$ th power for flow across tubes and directly proportional to the Schmidt number raised to about the 0.3 power. By dividing the equations for flow across the cylinder to that for flow inside a tube, we obtain

$$\frac{h_{cyl}}{h_{tube}} = \frac{C}{0.023} \left( Re_{tube} \right)^{n-0.8} \left( \frac{d_{tube}}{d_{cyl}} \right)^{1-n}, \quad (3)$$

17. H. P. Colburn, *Trans. Amer. Inst. Chem. Eng.* **29**, 174-210 (1933).

18. Frank Kreith, *Principles of Heat Transfer*, 2d ed., International Textbook Co., Scranton, Pa., 1965.

16. C. E. Milstead and L. R. Zumwalt, *Cesium Plateout on Stainless and Carbon Steels*, GAMD-7525 (October 1966).

where

$h_{\text{cyl}}$  = mass transfer coefficient for cross flow across tubes,

$h_{\text{tube}}$  = mass transfer coefficient inside tube,

$n, C$  = constants,

$\text{Re}_{\text{tube}}$  = Reynolds number based on tube diameter,

$d_{\text{tube}}$  = inside diameter of deposition tube,

$d_{\text{cyl}}$  = outside diameter of cylindrical tubes placed perpendicular to coolant flow.

Equation (3) expresses the ratio of the mass transfer of cesium to the rods (placed perpendicular to flow)

relative to transfer to the tube wall (parallel to helium flow). Kreith<sup>18</sup> lists the appropriate values of  $C$  and  $n$  for varying Reynolds number. For the flow conditions in this experiment,  $C = 0.615$  and  $n = 0.466$ , giving

$$h_{\text{cyl}}/h_{\text{tube}} = 3.6 \text{ (calc).}$$

The results obtained experimentally gave  $h_{\text{cyl}}/h_{\text{tube}} = 3.0$ . The good agreement between the calculated and experimental values indicates that deposition tube results can be utilized to estimate cesium deposition on cross-flow-type heat exchanger surfaces.

## Part III. Gas-Cooled Fast Breeder Reactor Program

---

### 11. GCFBR Irradiation Experiments

J. A. Conlin

A joint ORNL--Gulf General Atomic (GGA) irradiation testing program is being conducted in support of fuel development for the Gas-Cooled Fast Breeder Reactor (GCFBR). The testing program consists of both thermal- and fast-flux tests of oxide fuel in metallic cladding. The thermal-flux tests are performed in the Oak Ridge Research Reactor (ORR) poolside facility. The testing of 20 fuel pins of the sealed type (capsules, P-1 through P-8) has been completed in the ORR thermal flux. This type of pin is now the backup concept for the GCFBR. A test of a vented pin (capsule GB-9) is in progress in the ORR, and a follow-up experiment (capsule GB-10) has been designed. The fast-flux testing is being performed in the EBR-II. The irradiation of eight pins (the F-1 series) containing charcoal fission product traps and large plenum volumes to minimize fission gas pressure buildup and thus simulate vented pins is in progress in the EBR-II fast flux.

The current irradiation tests, both in thermal and fast fluxes, are designed to permit evaluation of the reference GCFBR fuel rod concept -- the vented-and-pressure-equalized rod. In this concept the coolant pressure (85 atm of He) and the rod internal pressure are equalized by venting the rod interior to a pressure-equalizing and fission-gas cleanup system. This type of pin eliminates any large pressure differential across the cladding and permits utilization of fuel and cladding technology developed in the LMFBR program.

In the preirradiation analysis of capsule GB-10, an improved technique for predicting fission heat generation rates and detailed radial power distributions within the fuel was implemented. Calculations of this type are required for the GCFBR thermal-flux capsules to determine the power asymmetry across the fuel pellets and the effect of this asymmetry on the readings of thermocouples used to monitor the fuel rod temperature and power during operation.

#### 11.1 IRRADIATION OF GCFBR-ORR CAPSULE GB-9

A. W. Longest	J. A. Conlin
C. W. Cunningham	K. R. Thoms
E. D. Clemmer	L. P. Pugh

The irradiation of GCFBR-ORR poolside capsule GB-9 (formerly designated O4-P9), which began in April 1970, is continuing. The test conditions include operation of the fuel rod at a heat generation rate of 16 kW/ft and a cladding outer surface temperature of  $685 \pm 15^\circ\text{C}$ . As of October 27, 1971, the accumulated irradiation time at full power was 450 days, and the estimated fuel burnup was 51,000 MWd per metric ton of heavy metal; planned exposure is 75,000 MWd/metric ton.

The capsule GB-9 test is a joint effort of ORNL and GGA. The capsule was designed to permit evaluation of the overall performance and adequacy of the GCFBR

vented-and-pressure-equalized fuel rod.<sup>1,2</sup> Test conditions are typical of a GCFBR fuel rod except for fast-neutron exposure. Measurements are made during the irradiation of the fission product release from the charcoal trap and blanket regions of the rod. The experimental results obtained are providing a basis for much of the GCFBR vented fuel rod and pressure equalization system design.<sup>3</sup> Many of the results will also be applicable to LMFBR fuel rods, since the materials and operating conditions are similar in many respects.

The capsule and fuel rod design, planned operating conditions, and experimental results obtained early in the irradiation have been reported previously.<sup>4-7</sup> However, for the sake of completeness, some of this information will be repeated here.

The GB-9 capsule (Fig. 11.1) contains a (U,Pu)O<sub>2</sub>-fueled, stainless-steel-clad rod with a charcoal trap (Fig. 11.2). The test rod, which simulates a GCFBR vented-and-pressure-equalized fuel rod, has a full-length charcoal trap but shortened blanket and fuel regions. The rod is connected to a 1000-psig helium sweep system (Fig. 11.3) which provides for nearly constant-pressure operation at sweep flow rates between 150 and 1300 cm<sup>3</sup> STP/min. An automatic pressure control valve maintains the sweep pressure  $25 \pm 0.1$  psi above the pressure in the normally static 975-psig gas system external to the fuel rod cladding. Fission product release from the rod can be monitored with the sweep flowing either across the top of the trap, which is the normal case, or upward through the trap (when the inlet flow is transferred to the supply line that goes to the bottom of the trap).

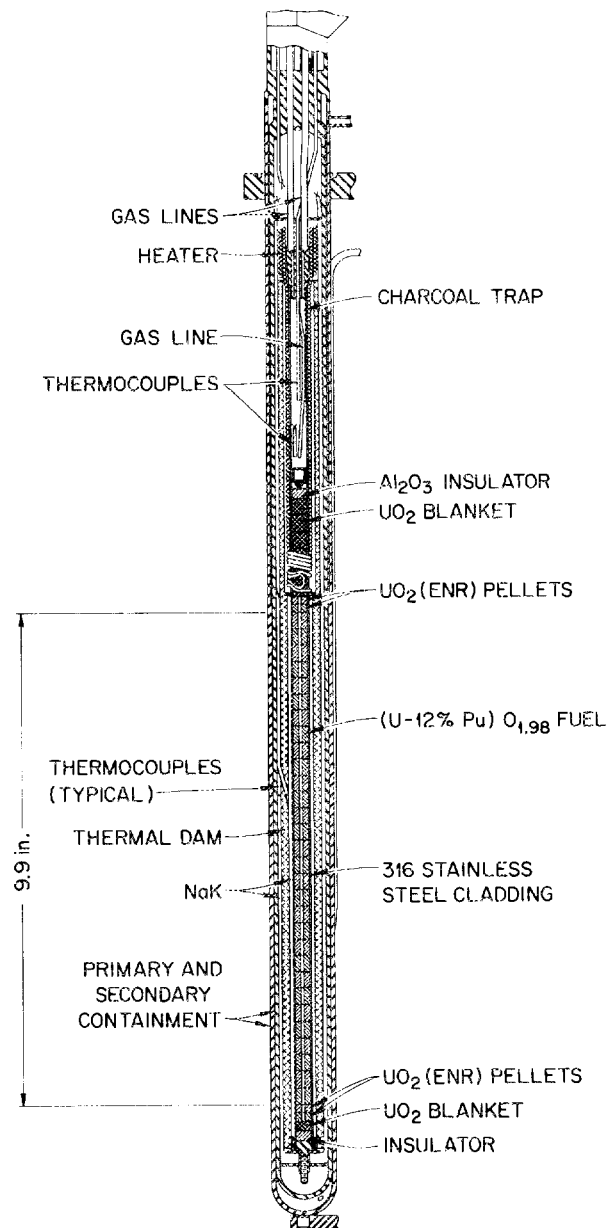


Fig. 11.1. GCFBR-ORR capsule GB-9.

The fuel rod and its charcoal trap are operated under the steady-state conditions listed in Table 11.1. Sweep-gas flow is maintained, normally across the top of the trap, at all times the fuel rod is at power. Sweep-gas samples are taken periodically and analyzed by gamma-ray spectrometry to determine isotopic fission-gas release rates. The sweep flow rate, normally 150 to 250 cm<sup>3</sup> STP/min during nonsampling periods to conserve

1. J. R. Lindgren et al., *Planned Thermal Irradiation of Manifolded-Vented (U,Pu)O<sub>2</sub>-Fueled Rod in ORR Capsule P-9*, GA-9896 (1970).

2. P. Fortescue and W. I. Thompson, *The GCFR Demonstration Plant Design*, GA-10036 (1970).

3. R. J. Campana, "Pressure Equalization System for Gas-Cooled Fast Breeder Reactor Fuel Elements," *Nucl. Technol.* 12, 185 (October 1971).

4. A. W. Longest et al., "Irradiation of GCFR-ORR Capsule O4-P9," *GCR-TU Programs Semiannu. Progr. Rep. Sept. 30, 1970*, ORNL-4637, pp. 40-47.

5. A. W. Longest et al., "Fission-Gas Release Measurements from Fast Breeder (U,Pu)O<sub>2</sub> Fuel," *Trans. Amer. Nucl. Soc.* 13, 604 (1970).

6. J. R. Lindgren et al., "Irradiation Testing of Fast Breeder Reactor (U,Pu)O<sub>2</sub> Fuels," *Trans. Amer. Nucl. Soc.* 14, suppl. 1, 33 (1971).

7. R. J. Campana et al., *Fuel Element Development for Gas-Cooled Fast Breeder Reactor (GCFR). Part 2. Vented Fuel-Rod Development*, GA-10657 (June 1971).

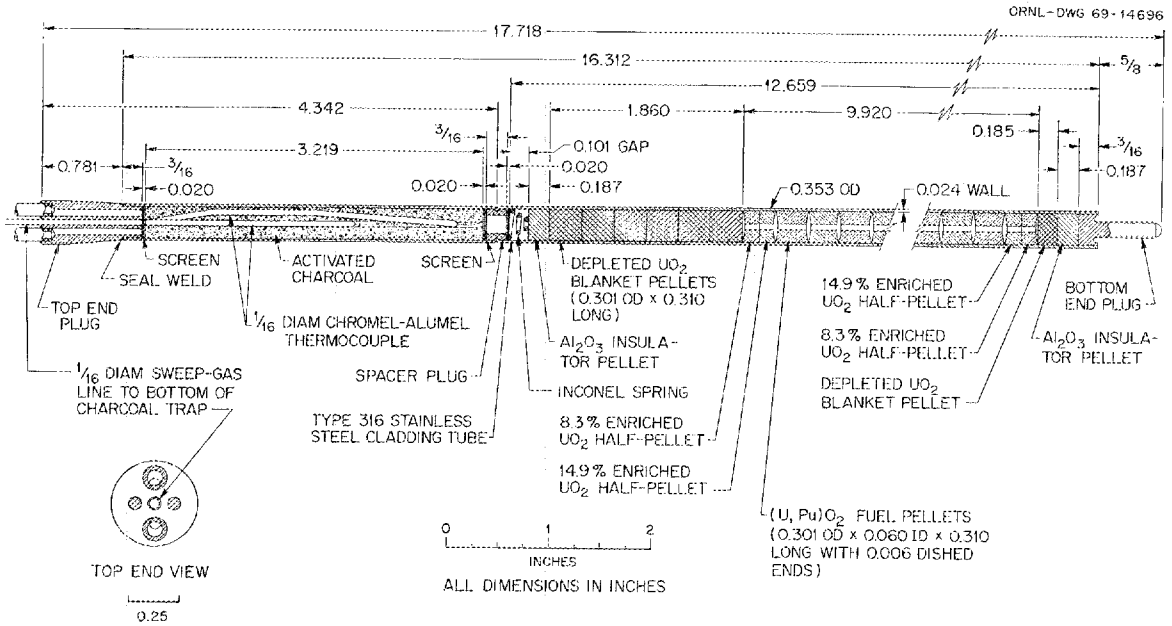


Fig. 11.2. Gas-cooled fast breeder reactor fuel-rod specimen in ORR capsule GB-9.

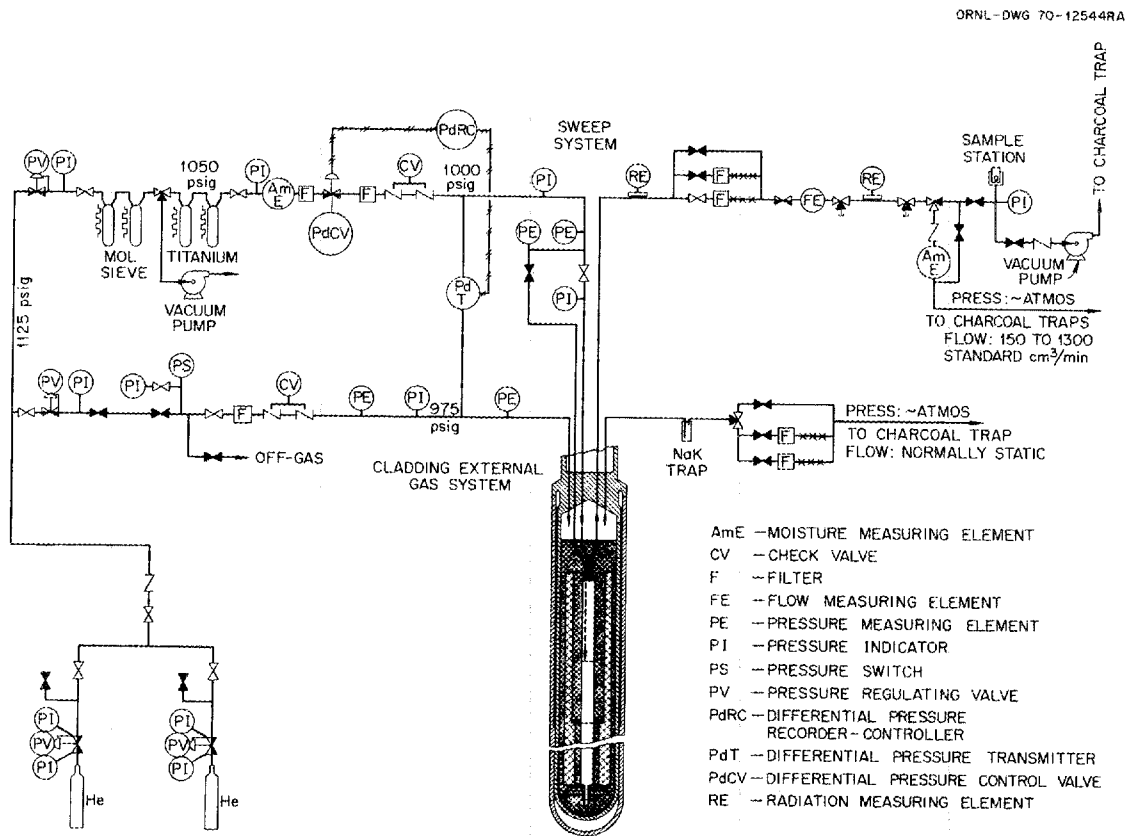


Fig. 11.3. Sweep and cladding external gas systems, GCFBR-ORR capsule GB-9.

Table 11.1. GCFBR-ORR capsule GB-9 operating conditions

Steady-state design conditions	
Cladding temperature, OD, °C	
Fuel region, peak	685 ± 15
Midregion of upper blanket region	~350
Charcoal trap	300
Fuel region heat generation rate, kW/ft	
Peak	16.1
Average	~15.0
Thermal-neutron flux (equivalent 2200 m/sec), neutrons cm <sup>-2</sup> sec <sup>-1</sup>	~1.4 × 10 <sup>13</sup>
Cladding pressure, psig	
External	975
Internal	1000
Planned exposure	
Irradiation duration at power, days	~660
Burnup of (U,Pu)O <sub>2</sub> , MWd/metric ton of heavy metal	~75,000
Fast-neutron exposure ( <i>E</i> > 0.18 MeV), neutrons/cm <sup>2</sup>	~7 × 10 <sup>19</sup>

helium, is increased to 1300 cm<sup>3</sup> STP/min (~19 cm<sup>3</sup>/min at 1000 psig) prior to sampling. At the sampling flow rate of 1300 cm<sup>3</sup> STP/min, the sweep-gas transient time from the fuel rod to the sampling point is only 47 sec, thereby making possible analysis for short-lived fission gases.

Although the capsule is operated under the steady-state design conditions most of the time, special tests have also been performed to determine fission-gas release dependence on charcoal trap temperature, fuel region temperature, and sweep pressure. Tests to obtain information on fission-gas release during pressure cycling, fission product decay heating in the charcoal trap, and iodine deposition in the trap have also been made.

### 11.1.1 Effluent Sweep Line Activity

Two radiation monitors on the effluent sweep line (see *RE* locations in Fig. 11.3) provide a sensitive indication of changes in operating conditions. Figure 11.4 shows the response of the ionization chamber on the high-pressure section of effluent sweep line during a period in which the sweep pressure control system was functioning improperly and cycling the sweep pressure over a ±0.2-psi range. The cycling started during unattended operation and lasted 28 hr before the situation was detected and corrected. The sweep flow was across the top of the trap during this time. The activity release is much more sensitive to pressure

changes with the sweep flowing across the top of the trap than through the trap. The reason for this behavior is that a relatively large volume of gas (~68 cm<sup>3</sup>) is trapped in the lower inlet sweep line (which extends about 80 ft back to a valve box) when the sweep is directed across the top of the trap. This trapped gas expands and contracts during pressure fluctuations and creates gas flow in the charcoal trap.

The response of the effluent sweep line monitor during a typical steady-state sampling period is shown in Fig. 11.5. At this time, the capsule had been at full power a total of 82 days.

The behavior of the effluent sweep line activity during typical reactor shutdown and startup periods is shown in Fig. 11.6. Upon shutdown there is an inflow of clean gas into the rod; at the same time, gaseous activity is swept out of the sweep line, leaving only deposited activity, which gradually decays off. Following startup, there is a rapid initial buildup of the activity release rate which takes about 8 to 10 hr after a long shutdown period.

### 11.1.2 Steady-State Fission-Gas Release vs Burnup

The results of gas release measurements made under the steady-state operating conditions (Table 11.1) during the first 220 days of full-power operation are shown for the two sweep flow cases in Figs. 11.7 and 11.8. The fractional release values (*R/B*) showed a general increase up to about 10,000 MWd/metric ton of heavy metal burnup (~88 days) and since then have remained about constant to the present burnup of 51,000 MWd/metric ton. The effectiveness of the charcoal trap in reducing the steady-state fission-gas release rates is a function of the half-life of the isotopes as expected. The trap reduction values (Table 11.2) are reasonably close to those predicted.

### 11.1.3 Fission-Gas Release during Slow Pressure Cycling

The results of several slow pressure cycling tests conducted in June and July 1970 (burnup level of about 7500 MWd/metric ton) are summarized in Fig. 11.9. Each of these tests was conducted with the sweep flow across the top of the trap at all times. Several days were allowed before the start of each test for fission products to reach steady-state levels. During each of the depressurizations, the volumetric flow rate (actual cm<sup>3</sup>/min) of sweep gas past the radiation monitor (on the high-pressure section of effluent line) was approximately constant at 19 cm<sup>3</sup>/min. This was a consequence of the manner in which the depressurizations

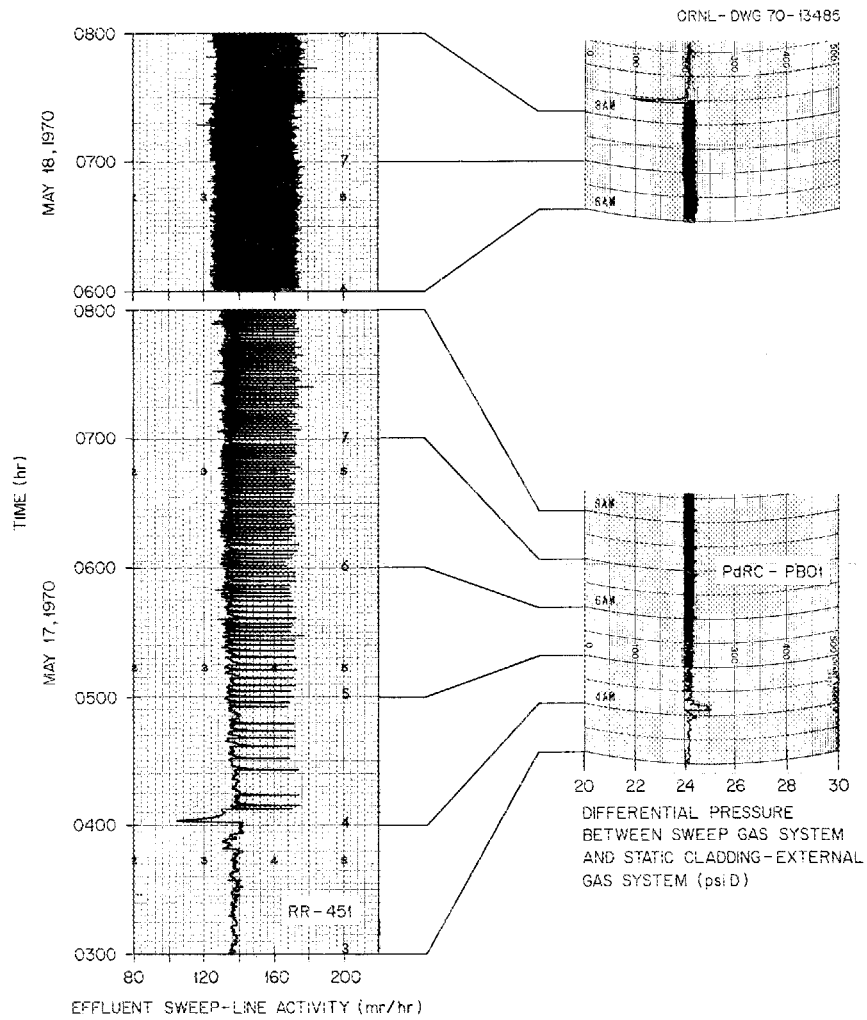


Fig. 11.4. Effluent sweep line activity during inadvertent cycling of the capsule GB-9 pressure control valve on May 17-18, 1970.

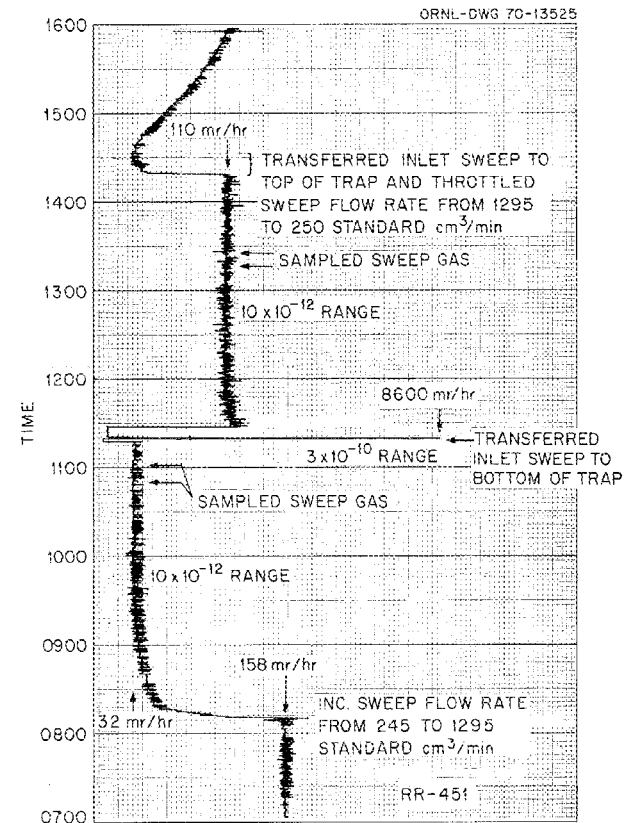


Fig. 11.5. Effluent sweep line activity while sampling capsule GB-9 sweep gas on July 9, 1970.

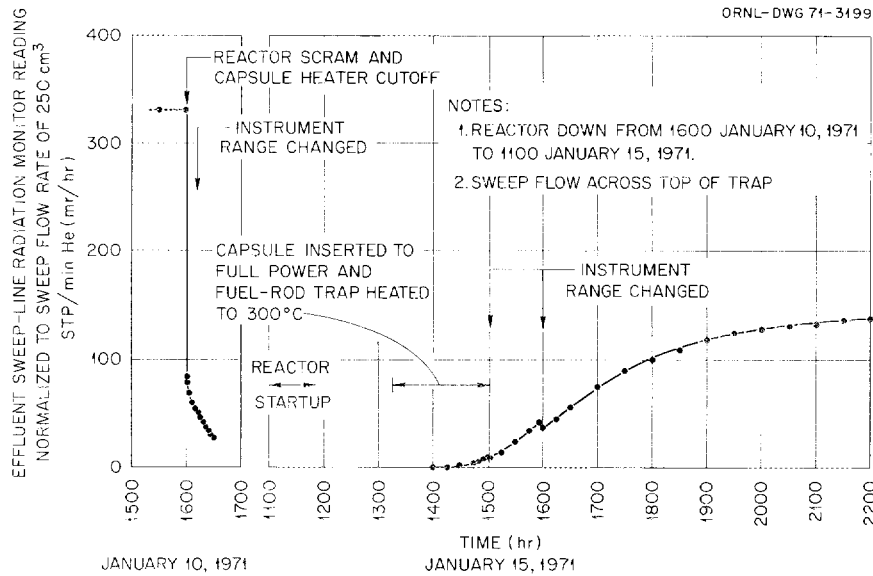


Fig. 11.6. GCFBR-ORR capsule GB-9 sweep line activity following reactor shutdown on January 10, 1971, and startup on January 15, 1971.

Table 11.2. Effectiveness of fuel-rod trap in reducing the steady-state fission-gas release from GCFBR-ORR capsule GB-9

Time at full power (days)	Ratio of fission-gas release rate with sweep flow across top of trap to that with sweep flow through trap							
	4.4-hr <sup>85m</sup> Kr	2.8-hr <sup>88</sup> Kr	1.3-hr <sup>87</sup> Kr	3.2-min <sup>89</sup> Kr	5.27-day <sup>133</sup> Xe	9.13-hr <sup>135</sup> Xe	17.0-min <sup>138</sup> Xe	15.3-min <sup>135m</sup> Xe
3	0.54	0.71	0.47		0.79	0.38		
4	0.74	0.72	0.43		0.71	0.41	0.036	0.038
6	0.53	0.53	0.44		0.81	0.30		
10	0.69		0.74		0.99	0.30		
18	0.68	0.58	0.52			0.37		
24	0.52	0.61	0.58		0.73	0.30		
32	0.76		0.68		1.0	0.41		
40	0.85	0.65	0.48		0.97	0.44		
46	0.95	0.72	0.51		1.0	0.35	0.040	
82	0.74	0.65	0.48		1.1	0.50		
105	0.75	0.73	0.49		1.1	0.49		
121	0.73	0.79	0.45		1.0	0.46		
134	0.59	0.70	0.51		0.89	0.43		0.082
158	0.54	0.61	0.41		0.85	0.41		0.030
171	0.53	0.66	0.51		0.91	0.59		0.025
184	0.75	0.64	0.39		0.46	0.34		0.054
192	0.49	0.60	0.48			0.37		0.034
216	0.59	0.49	0.50		0.69	0.39		
218	0.86	0.70	0.53		0.80	0.38		0.065
Average	0.68	0.65	0.51		0.87	0.40	0.038	0.047
Predicted <sup>a</sup>	0.71	0.60	0.38	10 <sup>-4</sup>	0.98	0.81	0.10	0.10

<sup>a</sup>J. R. Lindgren et al., *Planned Thermal Irradiation of Manifolder-Vented (U,Pu)O<sub>2</sub>-Fueled Rod in Capsule P-9*, GA-9896 (Mar. 15, 1970).

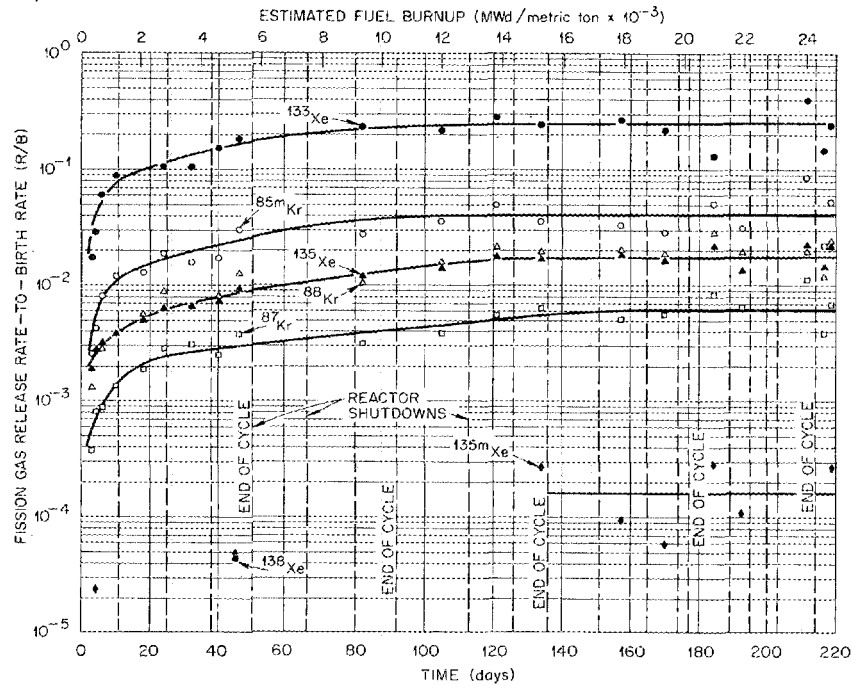


Fig. 11.7. Steady-state fission-gas release from GCFBR-ORR capsule GB-9 vs time at full power for case of sweep flow across top of trap.

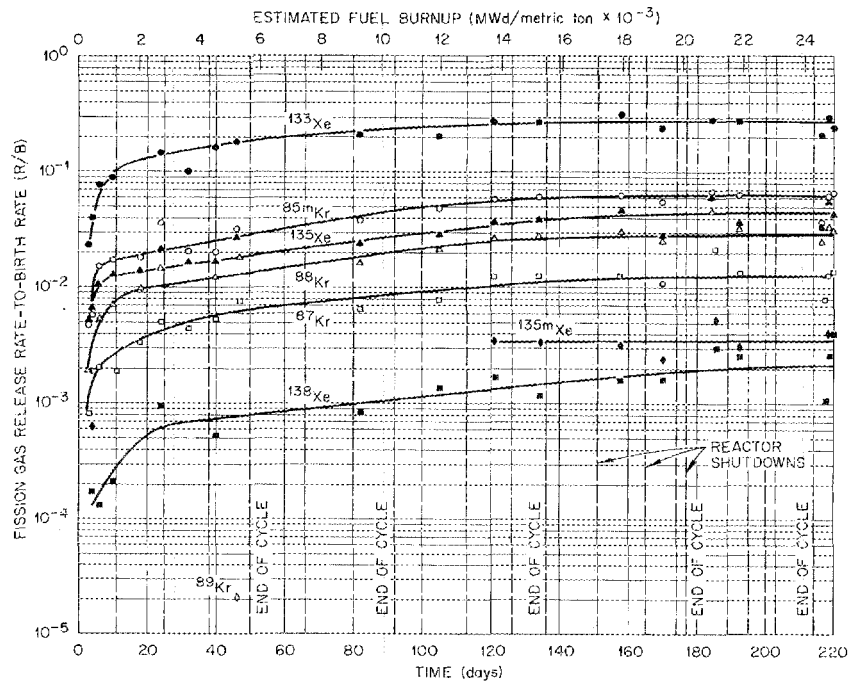


Fig. 11.8. Steady-state fission-gas release from GCFBR-ORR capsule GB-9 vs time at full power for case of sweep flow through trap.

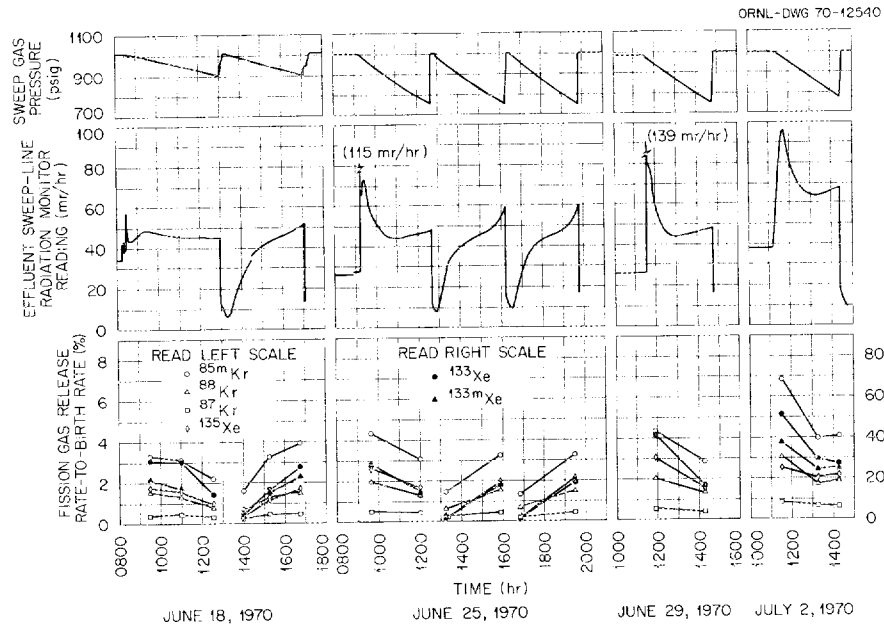


Fig. 11.9. Activity release from GCFBR-ORR capsule GB-9 during slow pressure cycling tests conducted on June 18, 25, and 29 and July 2, 1970.

were conducted (approximately exponential decay of pressure at pressure decay half-lives of 23.4 and 8.5 hr for the two different depressurization rates respectively). The response of the radiation monitor can therefore be interpreted, without flow rate corrections, as changes in the gross gamma activity release rate from the fuel rod, provided deposition activity on the sweep line is small compared with the gaseous activity.

The release behavior during these tests was discussed in detail previously.<sup>4</sup> However, in that preliminary analysis of the test data, the effect on release behavior of trapped gas in the lower inlet sweep line to the bottom of the trap was not taken into account. The activity peaking that occurred early in the first cycle of each of the four tests was attributed at that time to dumping of a portion of the fission-gas inventory contained in the charcoal as a consequence of the increased gas flow rate through the trap with decreasing pressure. It now appears that the activity peaking was associated primarily with displacement of the concentrated gaseous activity in the trap at the start of depressurization by a mixture of the gas expanding from the lower inlet sweep line ( $\sim 68 \text{ cm}^3$ ) and from the fuel rod free volume below the trap ( $\sim 2.4 \text{ cm}^3$ ). The activity spikes at the start of the first three tests were caused by small pressure fluctuations that occurred while attempting to start the pressure decay smoothly. In general, the release behavior during these

slow pressure cycling tests with the sweep flowing across the top of the trap agreed with expectations once the flow conditions within the rod were properly evaluated.

#### 11.1.4 Correlation of Effluent Sweep Line Activity Data and Sweep-Gas Sample Data

A limited number of dose-rate calculations were made in an attempt to correlate the radiation monitor data and the sweep-gas sample data and to determine what the radiation monitors on the effluent sweep line are seeing under the various capsule operating conditions. In these calculations, the gas sample release-rate data were used to estimate dose rates at the radiation monitor for comparison with its actual response. Such calculations were made with the gas sample results obtained during the slow pressure cycling tests (Fig. 11.9). The calculated dose rates, normalized to the radiation monitor reading at the time of the first sample set, are shown by the starred points in Fig. 11.10. The gas sample data were found to be consistent with the radiation monitor data except for the third set of  $R/B$  results. Since no error could be found in the  $R/B$  calculations for that sample, an error in sampling or counting is suspected.

Similar dose rate calculations made for the case of sweep flow across the top of the trap under the

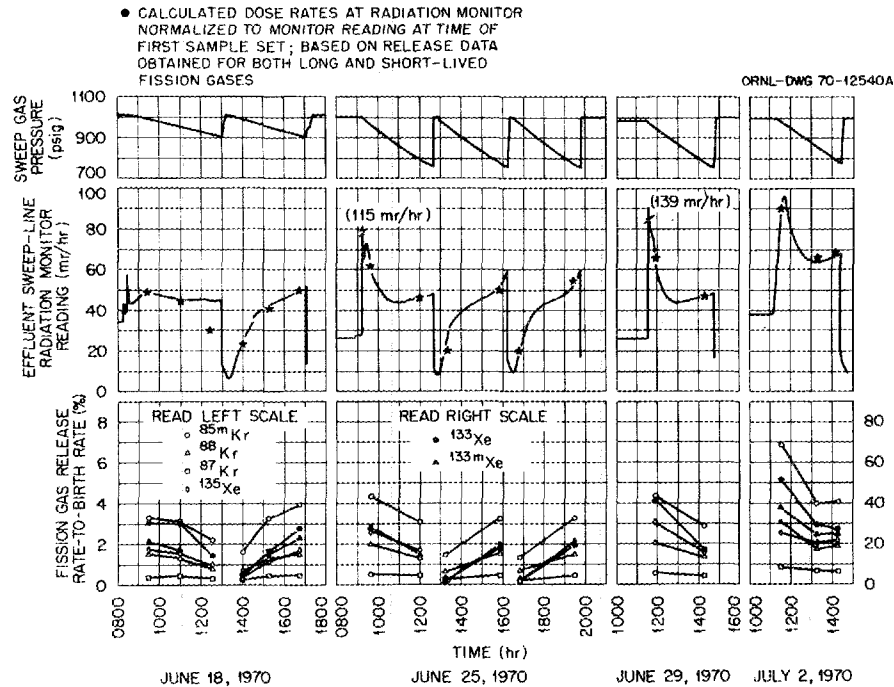


Fig. 11.10. Activity release from GCFBR-ORR capsule GB-9 during slow pressure cycling tests conducted on June 18, 25, and 29 and July 2, 1970.

steady-state design conditions have indicated the isotopic contributions to the total radiation monitor readings under these conditions to be roughly as follows:  $^{88}\text{Kr}$ ,  $\sim 58\%$ ;  $^{88}\text{Rb}$  deposition,  $\sim 13\%$ ;  $^{87}\text{Kr}$ ,  $\sim 8\%$ ;  $^{135}\text{Xe}$ ,  $\sim 8\%$ ;  $^{85\text{m}}\text{Kr}$ ,  $\sim 4\%$ ; and lesser percentages for  $^{135\text{m}}\text{Xe}$ ,  $^{138}\text{Cs}$  deposition,  $^{133}\text{Xe}$ , and  $^{133\text{m}}\text{Xe}$ . In the case of sweep flow through the trap, the release of short-lived fission gases is much higher, and calculations indicate that  $^{138}\text{Cs}$  deposition alone accounts for about one-third of the total monitor reading.

As can be seen in Figs. 11.7 and 11.8, there is significant scatter in the gas sample  $R/B$  data obtained as a function of time at normal design operating conditions. For comparison with Fig. 11.7, values of effluent sweep line activity immediately preceding the steady-state gas sampling periods are shown plotted in Fig. 11.11. These data show about the same scatter as the  $R/B$  results and indicate that most of the scatter in the  $R/B$  results is not associated with experimental measurement error, but rather with relatively small variations in the normal operating conditions. To better understand the release behavior, special tests were conducted to measure the steady-state release as a function of the temperature level of the electrically heated charcoal trap and upper blanket region and as a

function of fuel region power temperature. The results of these special tests are summarized in the next two sections.

### 11.1.5 Fission-Gas Release vs Charcoal Trap Temperature

A special test was conducted the week of May 10, 1971 (burnup level of  $\sim 35,000$  MWd/metric ton) to determine the effect of temperature level of the charcoal trap and upper blanket region on fission-gas release. In this test, steady-state fission-gas release rates were measured at charcoal trap temperatures of 200, 300, and  $400^\circ\text{C}$  while holding the fuel region peak power constant at 16 kW/ft. The estimated temperature profiles existing along the hot side of the rod (side toward reactor) during the test are shown in Fig. 11.12. Such cladding temperature profiles are obtained by applying appropriate temperature corrections (based on two-dimensional neutron flux and heat transfer calculations) to the readings of nearby thermocouples spaced along the length of the rod. The results of the gas release measurements are shown in Fig. 11.13. The effluent sweep line activity levels indicated by the radiation monitors were reasonably consistent with the

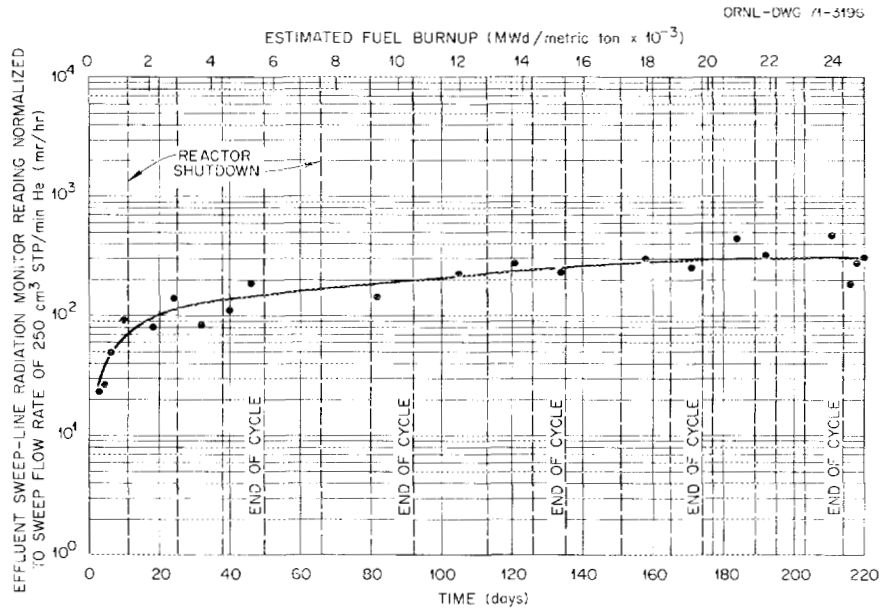


Fig. 11.11. GCFBR-ORR capsule GB-9 effluent sweep line activity preceding steady-state gas sampling periods.

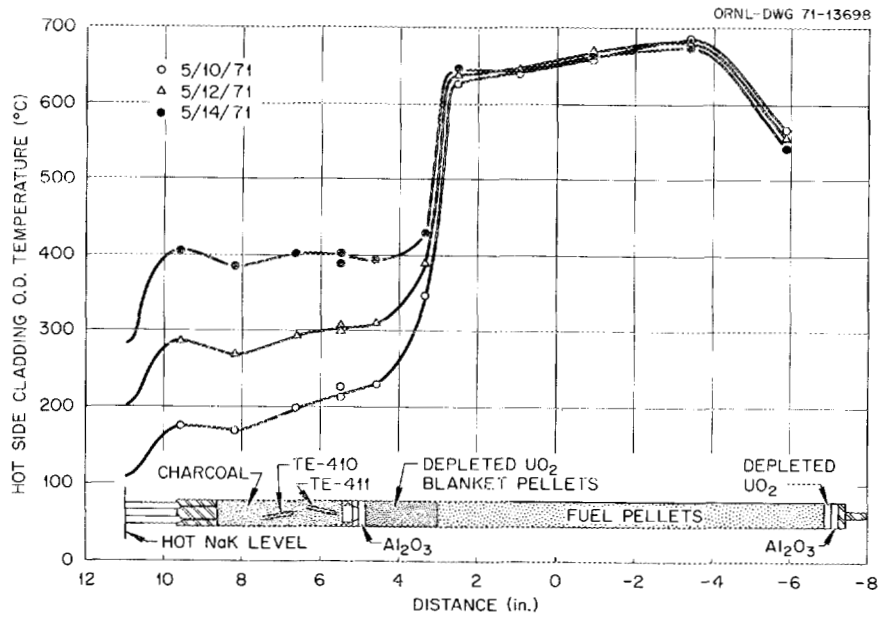


Fig. 11.12. Axial temperature profiles during capsule GB-9 release vs trap temperature test conducted May 10-14, 1971.

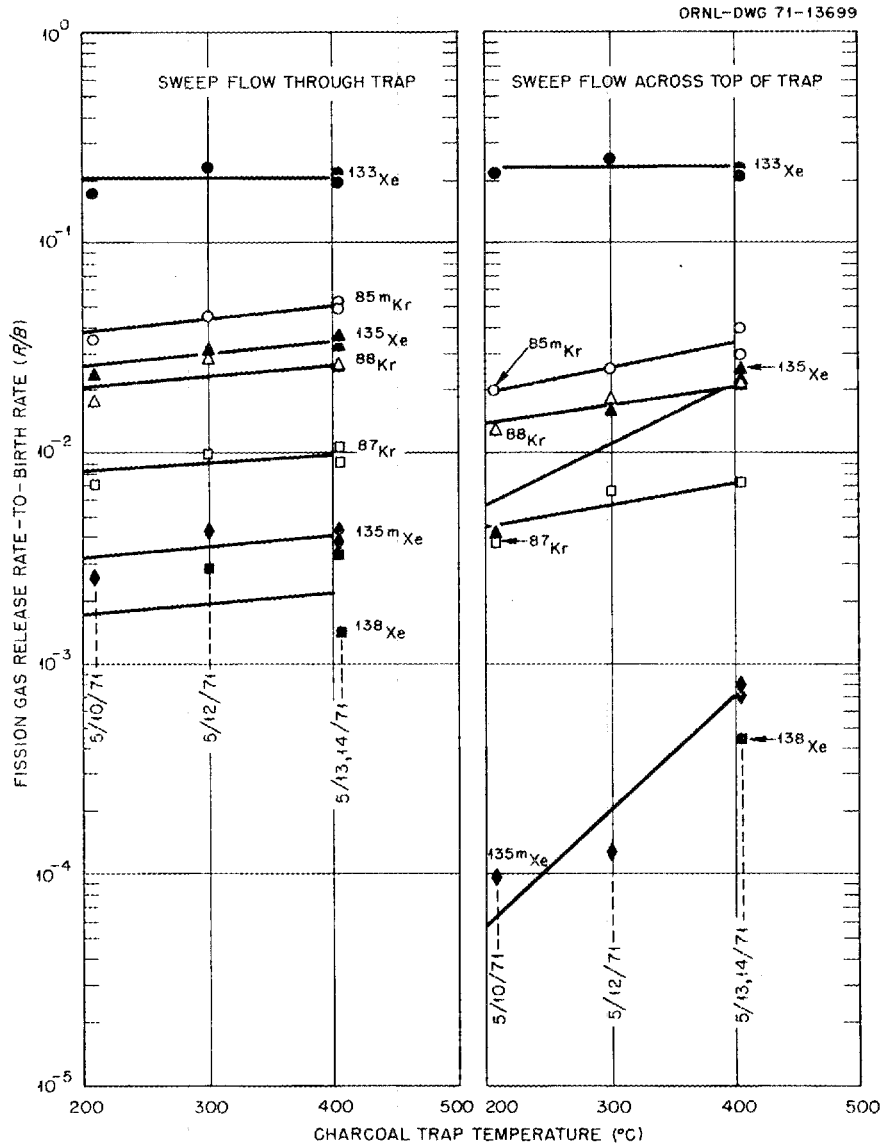


Fig. 11.13. Steady-state fission-gas release from GCFBR-ORR capsule GB-9 during release vs trap temperature test conducted May 10-14, 1971.

gas sample results; in going from 200 to 400°C trap temperature, the line activity increased by a factor of 2 for the case of sweep flow across the top of trap and by only 25% for the case of sweep flow through the trap.

### 11.1.6 Fission-Gas Release vs Fuel Rod Power Temperature

Steady-state fission-gas release was measured as a function of fuel rod power temperature in special tests conducted May 19-25, 1971 (burnup level of ~36,000

MWd/metric ton) and July 26-August 2, 1971 (burnup level of ~43,000 MWd/metric ton). These tests were conducted at peak cladding OD temperatures ranging from 550 to 685°C (fuel rod total power ranging from 9.8 to 12.4 kW) while holding the charcoal trap temperature constant at 300°C. The cladding temperature profiles corrected to those along the hot side of the rod (side toward reactor) during the tests are shown in Figs. 11.14 and 11.15. It is important to note the difference between the temperature patterns of the two tests. The temperature of the upper portion of the fuel

region relative to the peak temperature was lower in the first test than in the second. During normal operation, there are changes in the temperature profile that are associated with movement of the reactor control rods. Usually, as the rods are gradually withdrawn during a reactor core life and small capsule position adjustments

are made to maintain the peak cladding temperature at  $685 \pm 15^\circ\text{C}$ , the cladding temperature near the top end of the fuel column increases by about  $50^\circ\text{C}$ .

The gas sample results and the indicated sweep line activity levels were consistent in these tests, and both showed an increase in fission-gas release of a factor of

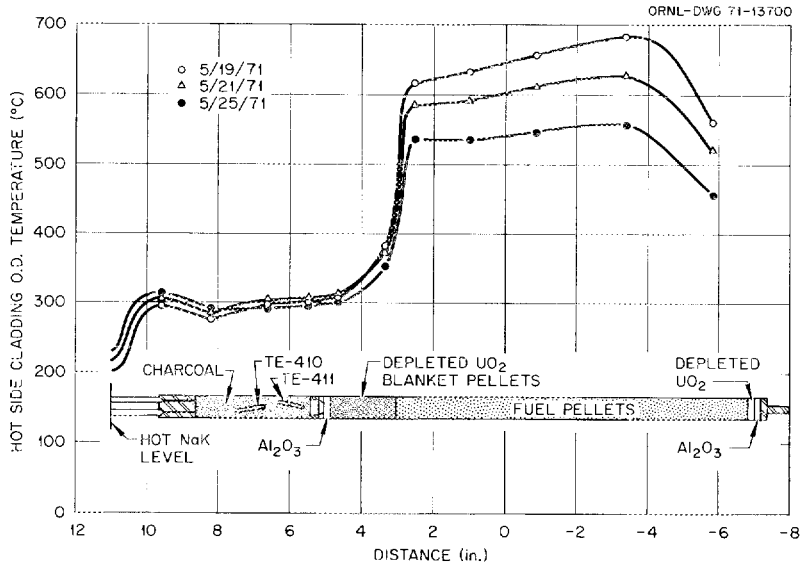


Fig. 11.14. Axial temperature profiles during capsule GB-9 release vs fuel rod power-temperature test conducted May 19-25, 1971.

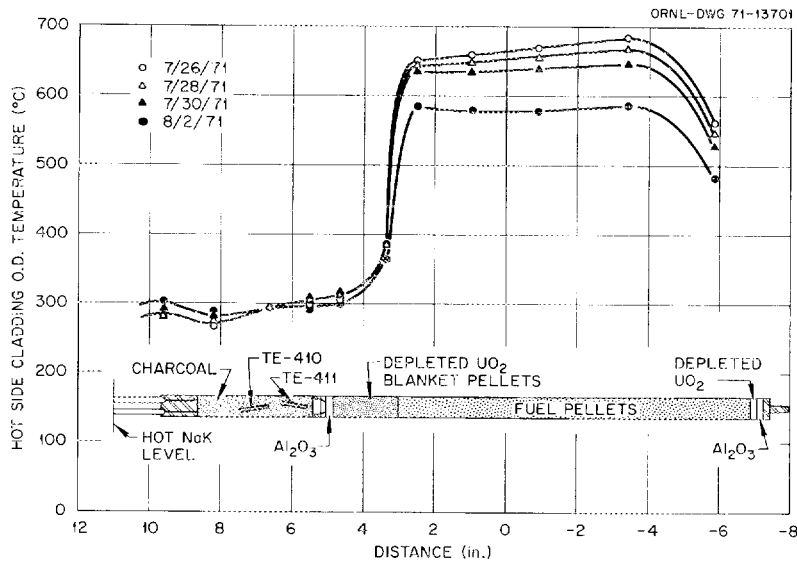


Fig. 11.15. Axial temperature profiles during capsule GB-9 release vs fuel rod power-temperature test conducted July 26-August 2, 1971.

10 in going from a peak cladding temperature of 550 to 685°C. The gas sample  $R/B$  data from each test yielded smooth curves when plotted vs peak cladding temperature; however, attempts to correlate the combined data of the two tests with temperature indicated the release to be more dependent on the overall temperature profile than on the local peak cladding temperature. When the  $R/B$  data were plotted vs peak cladding temperature, the data points of the second tests were noticeably higher

than those of the first test, and two curves were required to fit the combined test data for each isotope. Correlation with average cladding temperature yielded better results. The best fit, however, was obtained when the  $R/B$  data were plotted vs the cladding temperatures near the top of the fuel column. In Figs. 11.16 and 11.17 the  $R/B$  data for the two flow cases are shown plotted vs the estimated cladding temperature at a point 2 in. below the top of the fuel column. A more logical

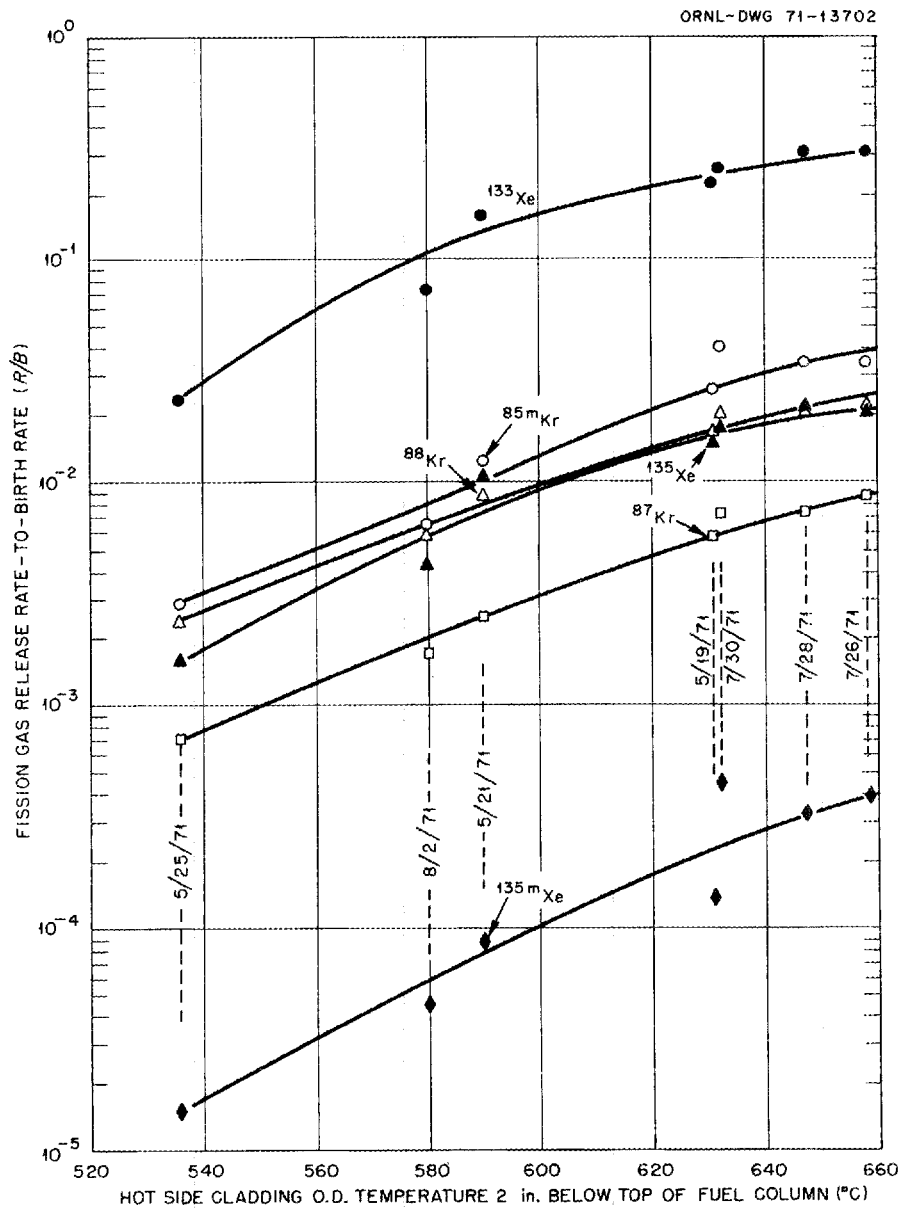


Fig. 11.16. Steady-state fission-gas release from GCFBR-ORR capsule GB-9 during release vs fuel rod power-temperature tests conducted May 19-25 and July 26-August 2, 1971, for case of sweep flow across top of trap.

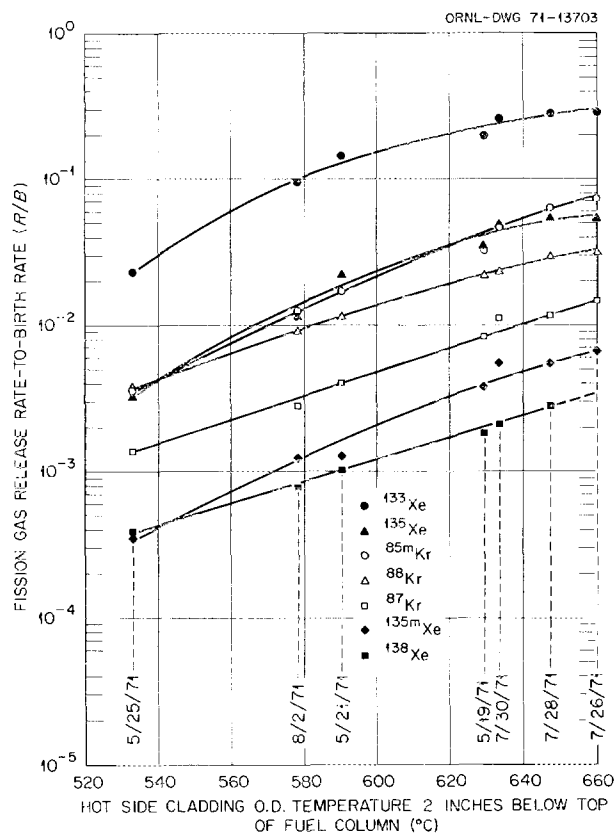


Fig. 11.17. Steady-state fission-gas release from GCFBR-ORR capsule GB-9 during release vs fuel rod power-temperature tests conducted May 19--25 and July 26--August 2, 1971, for case of sweep flow through trap.

parameter would be the volume-averaged fuel temperature. Values of this parameter are currently being estimated on the basis of the temperature profiles shown in Figs. 11.14 and 11.15.

The results of these tests, together with the results of the trap temperature test, show the fission-gas release from the rod to be much more sensitive to cladding temperature changes and temperature profile changes over the fuel region than to temperature changes of the charcoal trap and blanket region of the rod.

#### 11.1.7 Decay Heating in Charcoal Trap

Following several reactor shutdowns (at burnup levels of 23,000, 28,000, and 32,000 MWd/metric ton), the temperature decay indicated by thermocouples internal and external to the charcoal trap was followed for a period of several hours in an attempt to detect fission product decay heating in the trap. The electrical heaters used to maintain the trap at 300°C during normal

operation were shut off immediately following reactor shutdown so that the only heat source would be decay heat. These tests indicated little or no residual fission product heating in the trap following shutdown and suggest that volatile fission products are not migrating to the trap in appreciable quantities during steady-state operation.

#### 11.1.8 Iodine Deposition in Charcoal Trap

A series of gas samples were taken following a reactor shutdown when the fuel burnup level was ~24,000 MWd/metric ton in an attempt to determine the equilibrium deposition of  $^{133}\text{I}$  and  $^{135}\text{I}$  in the charcoal trap during the preceding period of steady-state operation. From the amount of  $^{133}\text{Xe}$  and  $^{135}\text{Xe}$  found in the samples, which were taken under carefully controlled pressure and flow conditions, the parent iodine deposition activities at the time of shutdown were deduced. Although there was considerable scatter in the data, the data indicated no appreciable iodine deposition on the effluent sweep line; the trap contained less than 1.5% of the total shutdown inventory of  $^{133}\text{I}$  (~775 Ci) and less than 0.5% of the  $^{135}\text{I}$  inventory (~650 Ci). These values of iodine deposition represent upper limits; actual deposition may be considerably less.

#### 11.1.9 Neutron Radiography

Neutron radiographs of the capsule were taken at fuel burnup levels of 20,000 and 44,000 MWd/metric ton. Examination of the radiographs showed no unexpected changes in the fuel rod appearance. In both sets of radiographs, the individual fuel pellets and most of the other fuel rod and capsule parts could be seen. The charcoal bed at the top of the fuel rod did not show up as well as components with higher neutron absorption cross sections, but it appeared in both sets of radiographs that the top of the bed was about 0.6 in. below the top end plug of the rod. Some settling of the bed was expected because the charcoal as loaded in the rod was at a lower density than the normal charcoal bulk density in unrestricted geometry. In the latter set of radiographs, the central hole of the fuel pellets was distinct, and several cracks in the fuel pellets were visible. The central hole appeared to have shifted about 0.013 in. from the geometric center of the pellets toward the hot side of the rod. Over most of the fuel column length the central hole appeared to be close to its original size (0.060 in. in diameter) or slightly larger; however, the hole reduced to about half this size in the lowermost two or three mixed oxide pellets. A slight

enlargement of the central hole could be seen in the upper half of the top mixed oxide pellet.

### 11.1.10 Fission-Gas Release vs Sweep Pressure

The GB-9 capsule is currently being operated at a reduced sweep pressure of 500 psig (475 psig cladding external pressure) to determine the effect of pressure on steady-state fission-gas release. Before returning to the design sweep pressure of 1000 psig, release data will also be obtained at 250 psig sweep pressure.

The release data obtained to date at 500 psig sweep pressure show no significant change in the release rates of the longer-lived fission gases from their release rates at 1000 psig. There are some indications that the release rates of very short-lived fission gases (e.g., 3.2-min  $^{89}\text{Kr}$ ) have increased, but additional results at 250, 500, and 1000 psig will be required before the effect of pressure on their release rates can be fully evaluated.

## 11.2 DESIGN OF GCFBR-ORR CAPSULE GB-10

A. W. Longest J. A. Conlin

Design of the tenth capsule experiment in the series of GCFBR fuel rod irradiation tests in the ORR

poolside facility was initiated during this report period. This experiment, designated capsule GB-10, will be similar to the currently operating capsule GB-9 experiment described in the preceding section. With the experience gained in the design and operation of capsule GB-9, capsule GB-10 has been designed with increased capability to measure fission product release and transport.<sup>7</sup> As in the previous tests, the GB-10 experiment is a joint effort of GGA and ORNL.

The design of the fuel rod to be irradiated in capsule GB-10 is shown in Fig. 11.18. This rod is similar to the GB-9 fuel rod, but it has a roughened outer surface and contains solid instead of hollow  $(\text{U,Pu})\text{O}_2$  fuel pellets. The fuel stack height is slightly less than in the GB-9 rod, the upper blanket region of depleted  $\text{UO}_2$  pellets is one pellet longer, and the charcoal trap is 1 in. long instead of 3 in. The charcoal trap was shortened to 1 in. in GB-10 to provide the same potential fission product loading as the rod trap in the reference GCFBR plant;<sup>2</sup> that is, the trap will contain the same ratio of charcoal mass to power generated within the rod. The design of the capsule itself is similar to the GB-9 capsule design (see Fig. 11.1) except for additional sweep-gas lines.

The sweep-gas lines and valving arrangement for capsule GB-10 are shown in Fig. 11.19. The three sweep

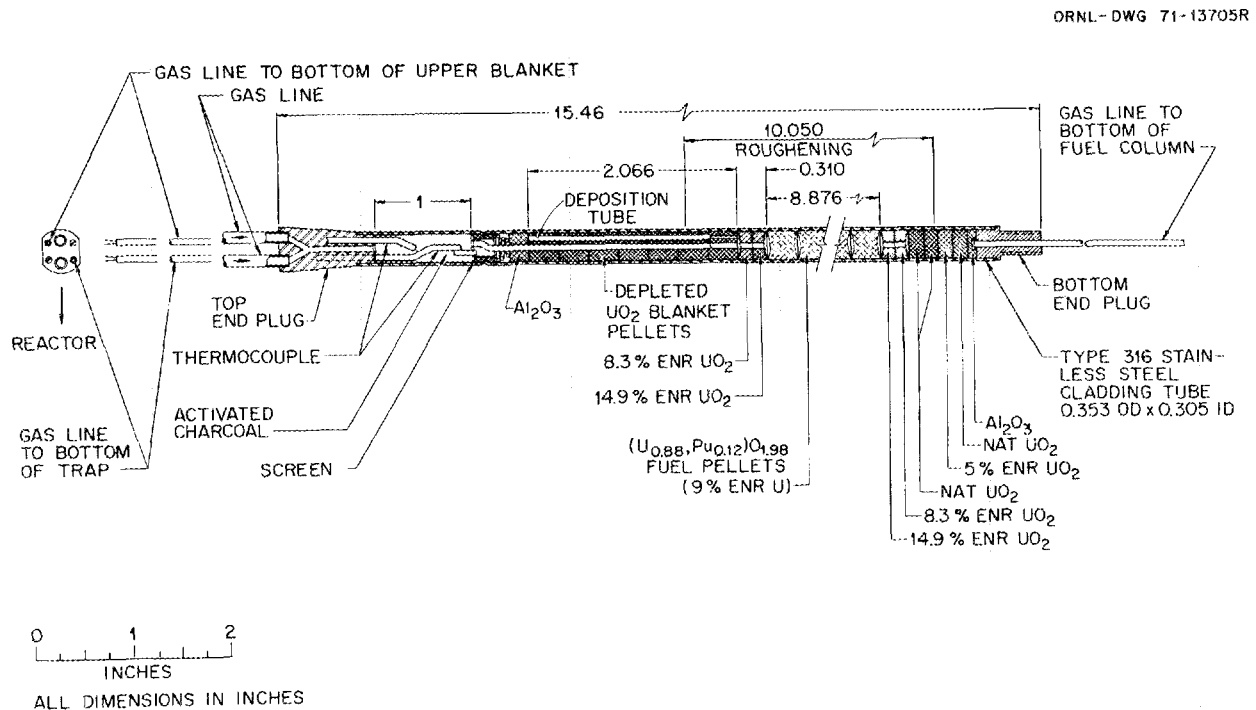


Fig. 11.18. Fuel rod specimen for irradiation in GCFBR-ORR capsule GB-10. Specimen designed by GGA.

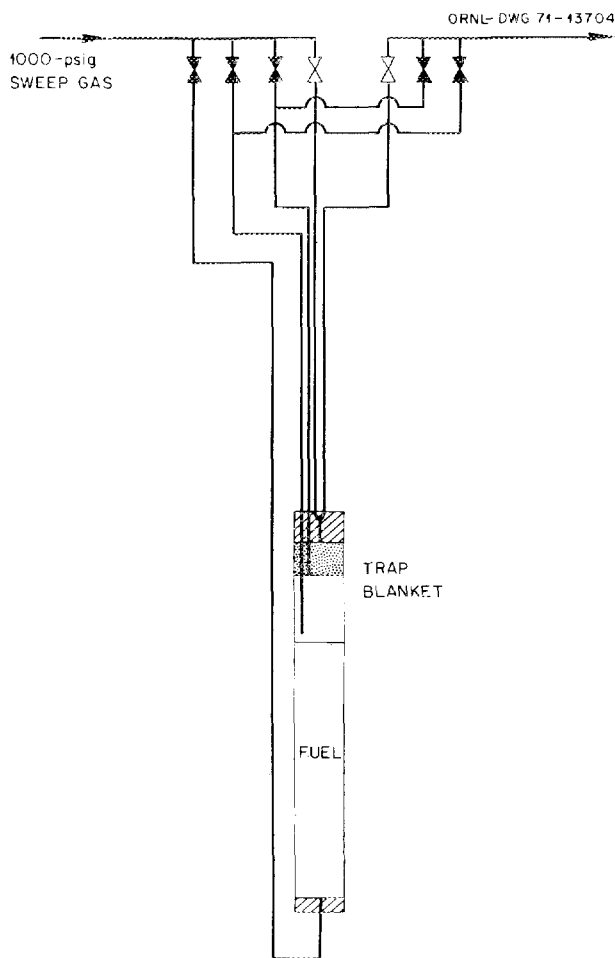


Fig. 11.19. Sweep lines for GCFBR-ORR capsule GB-10.

line connections to the trap are essentially the same as those in capsule GB-9. Two additional sweep lines have been added to GB-10, one to the bottom of the blanket region and one to the bottom of the fuel region. With these connections and valving, it will be possible to measure fission-gas release from each of the three main regions of the rod (trap, blanket, and fuel). This increased capability for measuring fission product release and transport will permit study of release mechanisms and transport times in greater detail than is possible with capsule GB-9. By directing the sweep through the fuel region, for example, fission-gas release rates from the oxide fuel matrix can be determined. This flow condition also simulates a leak in the cladding of a GCFBR rod, and resulting effects such as fission product decay heating in the charcoal trap can be observed.

The planned operating conditions for capsule GB-10 are the same as those listed in Table 11.1 for capsule GB-9.

The construction drawings for capsule GB-10 have been completed, and procurement activities are under way. As set forth in the quality assurance program plan for capsule GB-10, fabrication of the capsule is scheduled to be completed by April 1, 1972. Installation, preoperational testing, and startup will follow termination of the GB-9 irradiation, so that the existing GB-9 sweep and cladding external gas systems (Fig. 11.3) and associated equipment can be used. Some modification of the sweep system will be required to accommodate the more complex valving arrangement for GB-10 and the higher levels of radioactivity expected under some of the planned sweep flow modes.

### 11.3 ANALYSIS OF IRRADIATION CONDITIONS

J. D. Jenkins

A continuing difficulty in the physics analysis of the ORR irradiation capsules has been a lack of ability to predict absolute power generation rates and detailed power distributions in GCFBR fuel capsules. This information is necessary both to set initial fuel enrichments needed to achieve the desired heat rates and to aid in postirradiation analysis.

In irradiation capsule calculations one is looking for extremely detailed information about the neutron flux over a small region, of the order of several square centimeters. However, the flux in the region of interest is strongly influenced by the surrounding reactor configuration and by the perturbing effect of the capsule itself. Conventional reactor computational tools are designed to give accurate results in the large — that is, full core diffusion theory techniques — or in the small — that is, integral transport or discrete ordinates cell calculational techniques. Neither method performs both functions well and efficiently in a single calculation.

A technique has now been implemented which allows detailed calculations of the irradiation capsules using both techniques appropriately. The method consists in coupling a full core diffusion theory calculation to a detailed two-dimensional transport theory calculation of a subregion of the reactor containing the capsule through appropriate boundary conditions. The technique uses the existing reactor programs CITATION<sup>8</sup>

8. T. B. Fowler and D. R. Vondy, *Nuclear Reactor Core Analysis Code: CITATION*, ORNL-TM-2496, Rev. 2 (July 1971).

and DOT.<sup>9</sup> The coupling is achieved with the program SCID,<sup>10</sup> which digests CITATION flux output and calculates appropriate boundary conditions for the subregion DOT calculations.

---

9. F. R. Mynatt, *A Users Manual for DOT*, K-1694 (1968).

10. J. D. Jenkins and O. W. Hermann, *A Technique for Calculating In Pile Irradiation Experiments*, ORNL-TM report, in preparation.

Capsule GB-10 has been analyzed with the technique to determine the power asymmetry across the fuel pellets and the effect of this asymmetry on thermocouple readings at different azimuthal positions around the capsule.

A report describing the method and the SCID program is being written.

## 12. GCFBR Fuel Fabrication

J. D. Sease R. A. Bradley

The fuel for capsule GB-10 and for the F-1 replacement pins for an assembly in EBR-II is being fabricated at ORNL. We will load the GB-10 fuel into a fuel pin fabricated by Gulf General Atomic (GGA) and transfer it to the Reactor Division for encapsulation. The F-1 replacement pins and capsules will be fabricated and loaded at ORNL from hardware supplied by GGA.

### 12.1 REPLACEMENT FUEL FOR THE F-1 IRRADIATION EXPERIMENT

The fuel requirements for the GCFBR F-1 irradiation experiment<sup>1,2</sup> replacement pins are summarized in Table 12.1. The mixed (U,Pu)O<sub>2</sub> powder for making these pellets was prepared by the sol-gel process, described previously.<sup>2</sup> Sintering conditions that would yield the required pellet densities were established in a series of sintering tests.

The 88%-dense solid pellets were made from calcined powder by pressing at 40,000 psi and sintering in Ar-8% H<sub>2</sub> at 1550°C for 14 hr. The 92%-dense annular pellets were made from the same calcined powder after it had been ball-milled 5 hr. The pellets were pressed at 30,000 psi and sintered by heating to 1425°C in argon and then to 1550°C in Ar-8% H<sub>2</sub> for 15 hr. Argon was used in the initial stage of the sintering cycle because sintering tests showed that the ball-milled powder produced 95%-dense pellets when sintered in a reducing

atmosphere. The higher oxygen-to-metal ratio maintained by sintering in argon led to trapped porosity through enhanced grain growth, thus yielding pellets with the required density of 92% of theoretical. The densities and oxygen-to-metal ratios achieved are summarized in Table 12.1. An oxygen-to-metal ratio of  $1.98 \pm 0.01$  was achieved during the sintering treatment by reduction in Ar-8% H<sub>2</sub> for the length of time calculated from the kinetic reduction model of Lindemer and Bradley.<sup>3</sup> Pellets were heat treated in graphite boats in Ar-10% CO at 1550°C for 20 hr to obtain an oxygen-to-metal ratio of  $1.94 \pm 0.01$ .

These pellets will be loaded into fuel pins fabricated at ORNL from hardware supplied by GGA. The weld development and qualification are complete, and fuel pin fabrication will begin in the near future.

### 12.2 FUEL FOR GB-10 CAPSULE

The fuel pin for the GB-10 capsule will contain 8.8 in. of nominally 87.5%-dense solid dish-ended pellets with an oxygen-to-metal ratio of 1.97. The smear density of the fuel pin is required to be  $84.0 \pm 1.0\%$  of theoretical. The (U<sub>0.88</sub>,Pu<sub>0.12</sub>)O<sub>2</sub> powder, with the uranium containing 9% <sup>235</sup>U, was prepared by the sol-gel process.<sup>2</sup> The powder is presently being calcined.

We expect to fabricate these pellets in a manner similar to that used for the 88%-dense pellets for the F-1 replacement pins.

1. T. N. Washburn, "F-1 Irradiation Capsules for EBR-II," *GCR-TU Programs Semiannu. Progr. Rep. Sept. 30, 1970*, ORNL-4637, pp. 47-49.

2. R. A. Bradley and J. D. Sease, "Fuel Fabrication," *ibid.*, p. 49.

3. T. B. Lindemer and R. A. Bradley, "Kinetic Models for the Synthesis of (U,Pu)O<sub>2-y</sub> by Hydrogen-Reduction and Carbothermic Techniques," accepted for publication in *Journal of Nuclear Materials*.

Table 12.1. Densities and oxygen-to-metal ratios of pellets fabricated for GCFBR F-1 replacement pins

Fuel design requirements			Results		
Type <sup>a</sup>	Density <sup>b</sup> (% of theoretical)	Oxygen-to-metal ratio	Batch No.	Average density (% of theoretical)	Oxygen-to-metal ratio
Annular	92.3 ± 1.0	1.98 ± 0.01	1	92.1	1.967
			2	92.2	1.969
			3	92.3	1.968
			4	91.8	1.967
			5	91.8	1.967
Annular	92.3 ± 1.0	1.94 ± 0.1	1	92.4	1.944
			2	93.1	1.948
			3	93.0	1.937
Solid	88.6 ± 1.0	1.98 ± 0.01	1	88.9	1.978
			2	87.2	1.975
			3	87.8	1.975
			4	87.9	1.972
			5	90.1	1.972

<sup>a</sup>All pellets have dished ends.

<sup>b</sup>Pellet densities required to yield fuel column smear density of 84.0 ± 1.0% of theoretical.



## Part IV. Associated USAEC Exchange Programs

---

### 13. Exchange Programs

J. H. Coobs

There are currently two exchange programs in effect that concern high-temperature reactor research. The first and older of these is the USAEC/Dragon HTGR Agreement, which primarily concerns the exchange of information on the properties and performance of fuels and core materials. The second is the USAEC/KFA Exchange Arrangement, which was negotiated during this year, under which information on fuel reprocessing as well as on fuel preparation and testing is exchanged.

#### 13.1 USAEC/DAGON HTGR EXCHANGE

Arrangements were made with the Dragon Project for return shipment to ORNL of selected fuel compacts from the two Dragon fuel elements that contained ORNL fuel. These two elements, 413 and 443, contained (Th,U)O<sub>2</sub> and sol-gel microspheres that were prepared and coated at ORNL. The coated particles were overcoated and compacted at the Project. These two elements were irradiated for about 450 days in the Dragon Reactor. About half of the fuel compacts from each element were returned during September 1971 for examination and use in head-end reprocessing studies.

Other activities under this Agreement include the routine exchange of reports and visits of personnel. During a visit of Dragon Project representatives to

ORNL, we discussed the design and specifications of a cooperative irradiation experiment in HFIR to test overcoated samples. Such an experiment would contain inert coated particles prepared at ORNL and overcoated and compacted at the Dragon Project. A proposed design for the experiment was prepared.

#### 13.2 USAEC/KFA EXCHANGE ARRANGEMENT

The new exchange arrangement was implemented by visits, correspondence, and exchange of reports. Lists of reports proposed for exchange were prepared. The list proposed by KFA was reviewed, and an order of priority for translation of the documents was recommended. Discussions were held relative to the assignment of personnel to work in the field of fuel reprocessing. In addition, a member of the AVR group visited ORNL for several weeks so as to complete a series of reactor physics calculations for the AVR using an ORNL program. Assistance by ORNL personnel consisted of consultations on the planning and performance of the calculations. Results of the calculations indicate that the AVR core can be loaded and operated with slightly enriched uranium fuel so as to give helium outlet temperatures of 900°C, which would make it compatible with a direct-cycle system.



GAS-COOLED REACTOR-THORIUM UTILIZATION PROGRAMS

SEPTEMBER 1972

